BARYONIC FORCES AND HYPERONS IN NUCLEAR MATTER FROM SU(3) CHIRAL EFFECTIVE FIELD THEORY

Stefan Petschauer
December, 2015

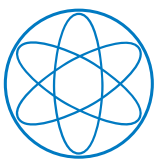

Technische Universität München

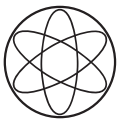

Technische Universität München
Physik Department
Institut für Theoretische Physik T39

Baryonic forces and hyperons in nuclear matter from SU(3) chiral effective field theory

Stefan Karl Petschauer

Vollständiger Abdruck der von der Fakultät für Physik der Technischen Universität München zur Erlangung des akademischen Grades eines

Doktors der Naturwissenschaften (Dr. rer. nat.)

genehmigten Dissertation.

Vorsitzender:		Univ.-Prof. Dr. Stephan Paul
Prüfer der Dissertation:	1.	apl. Prof. Dr. Norbert Kaiser
	2.	Univ.-Prof. Dr. Nora Brambilla
	3.	Univ.-Prof. Evgeny Epelbaum, Ph.D. Ruhr-Universität Bochum (nur schriftliche Beurteilung)

Die Dissertation wurde am 10.12.2015 bei der Technischen Universität München eingereicht und durch die Fakultät für Physik am 12.02.2016 angenommen.

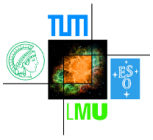

This work has been supported in part by the DFG and the NSFC through funds provided to the Sino-German CRC 110 “Symmetries and the Emergence of Structure in QCD”, the BMBF, the Excellence Cluster “Origin and Structure of the Universe”, the TUM Graduate School, and the Wilhelm und Else Heraeus-Stiftung.

ABSTRACT

In this work the baryon-baryon interaction is studied at next-to-leading order in SU(3) chiral effective field theory and applied to hyperon-nucleon scattering. Using the constructed YN potentials, the properties of hyperons in isospin-symmetric as well as asymmetric nuclear matter are calculated within the Bruecker-Hartree-Fock formalism. Moreover, the leading three-baryon interaction is derived and its low-energy constants are estimated from decuplet intermediate states. We conclude, that chiral effective field theory is a well-suited tool to describe the baryonic forces, leading to good agreement with the experimental data.

ZUSAMMENFASSUNG

In dieser Arbeit untersuchen wir die Baryon-Baryon-Wechselwirkung in nächst-führender Ordnung in der SU(3) chiralen effektiven Feldtheorie und wenden diese auf die Hyperon-Nukleon-Streuung an. Ausgehend von den konstruierten Potentialen werden die Eigenschaften von Hyperonen in isospin-symmetrischer sowie isospin-asymmetrischer Kernmaterie mittels des Brueckner-Hartree-Fock-Formalismus berechnet. Schließlich wird die führende Drei-Baryon-Wechselwirkung abgeleitet und ihre Niedrigenergiekonstanten durch Beiträge von Dekuplettbaryonen in Zwischenzuständen abgeschätzt. Wir stellen fest, dass die chirale effektive Feldtheorie ein gut geeignetes Werkzeug zur Beschreibung der baryonischen Kräfte ist, und dass sie zu einer guten Übereinstimmung mit den experimentellen Daten führt.

PUBLICATIONS

The text of this thesis contains material which has previously been published in the articles listed below.

S. Petschauer, "SU(3) chiral dynamics and baryon-baryon interactions", *Nucl. Phys. A* **914** (2013) 238-242, arXiv:1309.5529,

J. Haidenbauer, S. Petschauer, N. Kaiser, U.-G. Meißner, A. Nogga, W. Weise, "Hyperon-nucleon interaction at next-to-leading order in chiral effective field theory", *Nucl. Phys. A* **915** (2013) 24-58, arXiv:1304.5339,

S. Petschauer, N. Kaiser, "Relativistic SU(3) chiral baryon-baryon Lagrangian up to order q^2", *Nucl. Phys. A* **916** (2013) 1-29, arXiv:1305.3427,

N. Kaiser, S. Petschauer, "Radiative corrections to the charged pion-pair production process $\pi^-\gamma \to \pi^+\pi^-\pi^-$ at low energies", *Eur. Phys. J. A* **49** (2013) 159, arXiv:1312.0517,

S. Petschauer, "Hyperon-nucleon interaction and baryonic contact terms in SU(3) chiral effective field theory", Chiral Symmetry in Hadrons and Nuclei: Proceedings of the Seventh International Symposium, World Scientific, Singapore, 2014, pp. 177-180, arXiv:1312.4467,

S. Petschauer, "Chiral effective field theory description of the hyperon-nucleon interaction at next-to-leading order", *EPJ Web Conf.* **73** (2014) 05012,

J. Haidenbauer, U.-G. Meißner, S. Petschauer, "Do ΞΞ bound states exist?", *Eur. Phys. J. A* **51** (2015) 17, arXiv:1412.2991,

S. Petschauer, J. Haidenbauer, N. Kaiser, U.-G. Meißner, W. Weise, "Hyperons in nuclear matter from SU(3) chiral effective field theory", *Eur. Phys. J. A* **52** (2016) 15, Topical Issue "Exotic Matter in Neutron Stars", arXiv:1507.08808,

S. Petschauer, N. Kaiser, J. Haidenbauer, U.-G. Meißner, W. Weise, "Leading three-baryon forces from SU(3) chiral effective field theory", *Phys. Rev. C* **93** (2016) 014001, arXiv:1511.02095,

J. Haidenbauer, U.-G. Meißner, S. Petschauer, "Strangeness $S = -2$ baryon-baryon interaction at next-to-leading order in chiral effective field theory", *Nucl. Phys. A*, in print, arXiv:1511.05859.

CONTENTS

1

INTRODUCTION

Nuclear physics deals with the properties of atomic nuclei, built up of protons and neutrons, which are collectively referred to as nucleons. The understanding of the strong forces which bind nuclei and nuclear matter is a central topic in nuclear physics and it has consequences for astrophysics. With the discovery of "strange" particles, such as the Λ hyperon, in the early 1950s, a whole new branch of nuclear physics emerged: *strangeness nuclear physics*. It concerns the various facets of nuclear many-body systems involving the new quantum number *strangeness*, ranging from light hypernuclei to exotic neutron star matter. Hyperons and nucleons belong to the general class of particles called *baryons*. As the interaction among nucleons (N) is essential for a microscopic understanding of nuclear matter, the interactions among hyperons (Y) and nucleons is essential, not only for YN scattering but also for the description of nuclear many-body systems with strangeness. This thesis is concerned with the general low-energy interaction among octet baryons (N, Λ, Σ, Ξ) and the resulting properties of hyperons in infinite nuclear matter.

Nuclear many-body systems are (mainly) governed by the strong interaction, described at the fundamental level by *quantum chromodynamics* (QCD). QCD possesses quarks and gluons as elementary degrees of freedom. However, in the low-energy regime of QCD quarks and gluons are confined into colorless hadrons. This is actually the region, where (hyper-)nuclear systems are formed. In this region QCD can not be solved in a perturbative way. Lattice QCD is approaching this problem via purely numerical simulations: the space-time is discretized and QCD is applied on a finite grid [1, 2, 3]. Since the seminal work of Weinberg [4, 5] *chiral effective field theory* (χEFT) has become a powerful tool for calculating systematically the strong interaction dynamics for low-energy hadronic processes [6, 7, 8]. Chiral EFT employs the same symmetries and symmetry breaking patterns at low-energy as QCD, but it used the proper degrees of freedom, namely hadrons instead of quarks and gluons. In combination with an appropriate expansion in small external momenta, the results can be improved systematically, by going to higher order in the power counting, and at the same time theoretical errors can be estimated. Furthermore, two- and three-baryon forces can be constructed in a consistent fashion. The unresolved short-distance dynamics is encoded in χEFT in contact terms, with a priori unknown low-energy constants (LECs).

The NN interaction is experimentally known to very high precision. Corresponding two-nucleon potentials have been derived to high accuracy in phenomenological approaches [9, 10, 11], but nowadays the systematic theory to construct nuclear forces is χEFT [12, 13]. Note that there are still debates about the Weinberg power counting scheme, that is employed in practice [14, 15]. The YN interaction is presently not known in such detail. The scarce experimental data (about 35 data points for low-energy total cross sections) do not allow for a unique determination of the hyperon-nucleon interaction. The limited accuracy of the YN scattering data does not permit a unique phase shift analysis. However, at new

experimental facilities, such as J-PARC in Japan or FAIR in Germany, a significant amount of beam time will be devoted to strangeness nuclear physics. Various phenomenological approaches have been employed to describe the YN interaction, in particular one-boson-exchange models [16, 17, 18, 19, 20] or quark models [21, 22]. However, given the poor experimental data base, these interactions differ considerably from each other. Obviously there is a need for a more systematic investigation based on the underlying theory of the strong interaction, QCD. Some aspects of YN scattering and hyperon mass shifts in nuclear matter using EFT methods have been covered in Refs. [23, 24]. The YN interaction has been investigated at leading order (LO) in SU(3) χEFT [25] by extending the very successful χEFT framework for the nucleonic sector [12, 13] to the strangeness $S = -1$ sector. Already at LO in the chiral expansion, good results have been obtained. Also the YY interaction between all members of the baryon octet has been studied at LO [26, 27].

Numerous advanced few- and many-body techniques have been developed to employ such phenomenological or chiral interactions, in order to calculate the properties of nuclear systems with and without strangeness. For example, systems with three or four particles can be reliably treated by Faddeev-Yakubovsky theory [28, 29]. In the nucleonic sector many-body approaches such as Quantum Monte Carlo calculations [30, 31, 32], or nuclear lattice simulations [33, 34, 35] have been successfully applied and can be extended to the strangeness sector. Furthermore, nuclear matter is well described by many-body perturbation theory with chiral low-momentum interactions [36, 37, 38]. Concerning Λ and Σ hyperons in nuclear matter, specific long-range processes related to two-pion exchange between hyperons and nucleons in the nuclear medium have been studied in Refs. [39, 40]. Conventional Brueckner theory [41, 42, 43] at first order in the hole-line expansion, the so-called Bruecker-Hartree-Fock approximation, has been widely applied to calculations of hypernuclear matter [18, 21, 44, 45] employing phenomenological two-body potentials. This approach is also used in investigations of neutron star matter [46, 47, 48]. Recently, corresponding calculations of the properties of hyperons in nuclear matter have been also performed with a chiral YN interaction [49].

Employing the high precision NN interactions described above, already nuclear systems such as the triton cannot be described satisfactorily with two-body interactions alone. The introduction of three-nucleon forces (3NF) substantially improves this situation [50, 51] and also in the context of infinite nuclear matter 3NF are essential to achieve saturation of nuclear matter. These 3NF are introduced either phenomenologically, such as the families of Tuscon-Melbourne [52, 53], Brazilian [54] or Urbana-Illinois [55, 56] 3NF, or constructed according to the basic principles of χEFT [51, 57, 58, 59, 60, 61, 62, 63, 64, 65]. Within an EFT approach, 3NF arise naturally and consistently together with two-nucleon forces. Chiral three-nucleon forces are important in order to get saturation of nuclear matter from chiral low-momentum two-body interactions treated in many-body perturbation theory [37]. In the strangeness sectors the situation is similar: Three-baryon forces (3BF), especially the ΛNN interaction, seem to be important for a satisfactorily description of hypernuclei and hypernuclear matter [32, 66, 67, 68, 69, 70, 71, 72, 73]. Especially in the context of neutron stars, 3BF are often discussed. The observation of two-solar-mass neutron stars [74, 75] sets strong constraints on the stiffness of the equation-of-state (EoS) of dense baryonic matter [76, 77, 78, 79]. A naive introduction of Λ-hyperons as an additional baryonic degree of freedom would soften the EoS such that it is not possible to stabilize a two-solar-mass neutron star against gravitational collapse [80]. To solve this so-called *hyperon puzzle*, several ad-hoc mechanisms have so far been

invoked, e.g., through vector meson exchange [81, 82], multi-Pomeron exchange [83] or a suitably adjusted repulsive ΛNN three-body interaction [84, 85, 86]. Clearly, a more systematic approach to the three-baryon interaction within χEFT is needed, to estimate whether the 3BF can provide the necessary repulsion and thus keep the equation-of-state sufficiently stiff.

In this work, the aforementioned topics are addressed within the SU(3) χEFT approach: the interaction between hyperons and nucleons is derived at next-to-leading order (NLO) and applied to YN scattering and the hyperon mean-field potentials in nuclear matter by employing the self-consistent Bruecker-Hartree-Fock formalism. The leading three-baryon interaction is derived systematically, and its LECs are estimated via decuplet intermediate states. It is demonstrated, that SU(3) χEFT is a well-suited tool to describe the interaction among baryons. The present thesis is organized as follows. In *Chapter 2* we give a brief introduction to QCD, where we focus on its symmetries and symmetry breaking patterns. Then, the principles of χEFT and the construction principles for chiral Lagrangians are outlined. The Weinberg power counting scheme is introduced for the two- and three-baryon potentials. In *Chapter 3* the construction of the effective Lagrangian in the baryon-number-two sector is described in detail up to order $\mathcal{O}(q^2)$. The pure baryon-baryon contact terms encode the unresolved short-distance dynamics and their corresponding (a priori unknown) constants have to be fitted to experimental data. The contact terms involving pseudoscalar Goldstone-boson fields or electroweak gauge bosons are included as well. These come into play in the description of chiral many-body forces and exchange-currents in few-baryon systems. In *Chapter 4*, the baryon-baryon interaction from χEFT is considered at NLO. Contributions from baryon-baryon contact terms as well as one-meson and two-meson exchange diagrams are derived. As a first application of the potentials, YN scattering is treated by solving the coupled-channel Lippmann-Schwinger equation. Hyperon mean fields in nuclear matter, employing the YN chiral potentials, are examined in *Chapter 5*. We briefly review the basic concepts of Bruecker theory and and the approximations going into the Brueckner-Hartree-Fock formalism. Single-particle potentials for Λ and Σ hyperons are calculated in homogeneous isospin-symmetric nuclear matter as well as isospin-asymmetric nuclear matter and pure neutron matter. Furthermore, the Λ-nuclear spin-orbit coupling is computed. In *Chapter 6* the leading three-baryon forces from χEFT are studied. We show in detail the construction of the contact terms and the evaluation of the one-meson and two-meson exchange diagrams. The terms required in a minimal effective Lagrangian are derived. In *Chapter 7* we estimate the LECs of the leading 3BF via decuplet intermediate states. Finally, we summarize our results in *Chapter 8*.

2

SU(3) CHIRAL EFFECTIVE FIELD THEORY

All forces in nature can be reduced to only four fundamental interactions: gravity, electromagnetism, the weak and the strong interaction. The last three of these interactions, are theoretically described in the so-called standard model of particle physics. The structures and interactions of hadrons is mainly governed by the strong interaction, which is described in the standard model by quantum chromodynamics. However, the impossibility to apply QCD in a perturbative way to the low-energy regime, makes different approaches necessary to explore hadronic physics, in particular nuclear and hypernuclear physics. One of the most successful approaches, based on the symmetry properties of QCD, is chiral effective field theory.

In this chapter, we give a short introduction to QCD, with a special focus on the underlying symmetries and their breaking pattern. The basic concepts of χEFT are explained, especially the explicit degrees of freedom and the connection to the symmetries of QCD. We state in more detail how the chiral Lagrangian can be constructed from basic principles. Finally, it is shown how the interactions between baryons can be organized according to their strength in a systematic way. We follow Refs. [8, 12, 13, 87, 88] and refer the reader for more details to these references (and references therein).

2.1 QUANTUM CHROMODYNAMICS

Quantum chromodynamics is formulated with *quarks and gluons* as fundamental degrees of freedom, and it is a non-Abelian quantum field theory based on the (local) *color gauge symmetry* $\mathrm{SU(3)_C}$. Quarks are spin-1/2 fermions and can appear in six different flavors, $f = \text{up}\,(u)$, down (d), strange (s), charm (c), bottom (b), top (t), and for each flavor in three possible colors, $c =$ red, green, blue. The quarks are described by the four-component Dirac fields $q_f^c(x)$ and the masses of the quarks are denoted by m_f. The QCD Lagrangian, invariant under local transformations in color space, reads[1]

$$\mathscr{L}_{\mathrm{QCD}} = \sum_{f=u,d,s,c,b,t} \bar{q}_f \left(\mathrm{i}\not{D} - m_f\right) q_f - \frac{1}{4} G_{\mu\nu,a} G_a^{\mu\nu} \,. \tag{2.1}$$

with $q_f(x) = \left(q_f^{\text{red}}(x), q_f^{\text{green}}(x), q_f^{\text{blue}}(x)\right)^\top$. The gauge covariant derivative D_μ is given by

$$D_\mu = \mathbb{1}\partial_\mu - \mathrm{i}g A_\mu^a \frac{\lambda_a}{2} \,, \tag{2.2}$$

1 We omit the so-called θ term of QCD, which introduces strong CP violation. This term is, for example, related to the neutron electric dipole moment, which has so far not been observed [89].

where the gluon fields $A^a_\mu(x)$ are eight independent vector bosons belonging to the adjoint representation of $\mathrm{SU}(3)_\mathrm{C}$ to fulfill local gauge invariance. The eight generators of $\mathrm{SU}(3)_\mathrm{C}$ are denoted by $\{\mathrm{i}\lambda_a/2\}$. The gluonic *field-strength tensor* $G_{\mu\nu,a}(x)$ is given by

$$G_{\mu\nu,a} = \partial_\mu A_{\nu,a} - \partial_\nu A_{\mu,a} + g f_{abc} A_{\mu,b} A_{\nu,c}\,, \tag{2.3}$$

with f_{abc} the structure constants of the Lie algebra $\mathfrak{su}(3)$. The non-Abelian nature of QCD gives rise to gluon self interactions.

QCD is characterized by two important properties. For high energies the (running) coupling strength of QCD becomes weak, hence a perturbative approach in the high-energy regime of QCD is possible. This famous feature is called *asymptotic freedom* of QCD and originates from the non-Abelian structure of QCD. However, at low energies and momenta the coupling strength of QCD is of order one, and a perturbative approach is no longer possible. This is the region of *non-perturbative QCD*. Several strategies to approach this regime have been developed, such as lattice simulations, Dyson-Schwinger equations, QCD sum rules or chiral perturbation theory. In the present work, we will focus on the latter approach. The second important feature of QCD is the so-called *color confinement*: isolated quarks and gluons are not observed in nature, but only color-singlet objects. Such color-neutral particles consist of quarks and gluons and are called hadrons (strongly interacting particles).

2.1.1 *Symmetries of QCD*

The Lagrangian of QCD is constructed to be invariant under local $\mathrm{SU}(3)_\mathrm{C}$ gauge transformations, and under global Lorentz transformations. Furthermore, it obeys the *discrete symmetries*

- parity $P\colon\ (t,\vec{x}\,) \to (t,-\vec{x}\,)\,,$
- charge conjugation C and
- time reversal $T\colon\ (t,\vec{x}\,) \to (-t,\vec{x}\,)\,.$

Due to the CPT theorem, the time reversal symmetry is automatically fulfilled if C and P are symmetries of the Lagrangian. The quark fields transform under parity and charge conjugation as

$$P\colon\ q_f\,(t,\vec{x}\,) \to \gamma^0 q_f\,(t,-\vec{x}\,)\ , \qquad C\colon\ q_{\alpha,f} \to C_{\alpha\beta}\bar{q}_{\beta,f}\ ,\ \bar{q}_{\alpha,f} \to -q_{\beta,f}C^{-1}_{\beta\alpha}\,, \tag{2.4}$$

with the flavor index f, the Dirac-spinor indices α,β and with $C = \mathrm{i}\gamma^2\gamma^0$. The conventional gamma matrices $\{\gamma^0,\gamma^1,\gamma^2,\gamma^3\}$ can be found in Appendix A.1.

In the following we will introduce the so-called *chiral symmetry*, a global continuous symmetry of the QCD Lagrangian. The chiral symmetry is essential for chiral effective field theory. In view of the application to low energies, we divide the quarks into three light quarks u,d,s and three heavy quarks c,b,t, since the quark masses fulfill a hierarchical ordering:

$$m_u, m_d, m_s \ll 1\ \mathrm{GeV} \leq m_c, m_b, m_t\,. \tag{2.5}$$

At energies and momenta well below 1 GeV, the heavy quarks can be treated effectively as static. Therefore, the light quarks are the only active degrees of freedom of QCD for

the low-energy region we are interested in. In the following we approximate the QCD Lagrangian by using only the three light quarks. Compared to characteristic hadronic scales, such as the nucleon mass ($M_N \approx 939$ MeV), the light quark masses are small. Therefore, a good starting point for our discussion of low-energy QCD are massless quarks $m_u = m_d = m_s = 0$, which is referred to as the *chiral limit*. The QCD Lagrangian becomes in the chiral limit

$$\mathscr{L}^0_{\mathrm{QCD}} = \sum_{f=u,d,s} \bar{q}_f \mathrm{i} \not{D} q_f - \frac{1}{4} G_{\mu\nu,a} G^{\mu\nu}_a \,. \tag{2.6}$$

Now each quark field $q_f(x)$ is decomposed into its *chiral components*

$$q_{f,\mathrm{L}} = P_{\mathrm{L}}\, q_f \,, \qquad q_{f,\mathrm{R}} = P_{\mathrm{R}}\, q_f \,. \tag{2.7}$$

using the left- and right-handed projection operators

$$P_{\mathrm{L}} = \frac{1}{2}\left(1 - \gamma_5\right) \,, \qquad P_{\mathrm{R}} = \frac{1}{2}\left(1 + \gamma_5\right) \,, \tag{2.8}$$

with the chirality matrix γ_5. These projectors are called left- and right-handed since in the chiral limit they project the free quark fields on helicity eigenstates, $\hat{h}\, q_{L,R} = \pm\, q_{L,R}$, with $\hat{h} = \vec{\sigma} \cdot \vec{p} \,/\, |\vec{p}|$. For massless free fermions helicity is equal to chirality.

Collecting the three quark-flavor fields,

$$q = \begin{pmatrix} q_u \\ q_d \\ q_s \end{pmatrix} \,, \quad q_{\mathrm{L}} = \begin{pmatrix} q_{u,\mathrm{L}} \\ q_{d,\mathrm{L}} \\ q_{s,\mathrm{L}} \end{pmatrix} \,, \quad q_{\mathrm{R}} = \begin{pmatrix} q_{u,\mathrm{R}} \\ q_{d,\mathrm{R}} \\ q_{s,\mathrm{R}} \end{pmatrix} \,, \tag{2.9}$$

we can express the QCD Lagrangian in the chiral limit as

$$\mathscr{L}^0_{\mathrm{QCD}} = \bar{q}_{\mathrm{R}} \mathrm{i} \not{D} q_{\mathrm{R}} + \bar{q}_{\mathrm{L}} \mathrm{i} \not{D} q_{\mathrm{L}} - \frac{1}{4} G_{\mu\nu,a} G^{\mu\nu}_a \,. \tag{2.10}$$

Obviously the right- and left-handed components of the massless quarks are separated. The Lagrangian is invariant under a global transformation

$$q_{\mathrm{L}} \to L\, q_{\mathrm{L}} \,, \quad q_{\mathrm{R}} \to R\, q_{\mathrm{R}} \,, \tag{2.11}$$

with *independent* unitary 3×3 matrices L and R acting in flavor space. These can be expressed as

$$L = \exp\left(-\mathrm{i} \sum_{a=1}^{8} \theta^{\mathrm{L}}_a \frac{\lambda_a}{2}\right) \exp\left(-\mathrm{i}\theta^{\mathrm{L}}\right) \,, \quad R = \exp\left(-\mathrm{i} \sum_{a=1}^{8} \theta^{\mathrm{R}}_a \frac{\lambda_a}{2}\right) \exp\left(-\mathrm{i}\theta^{\mathrm{R}}\right) \,, \tag{2.12}$$

with 18 real parameters θ. This means that $\mathscr{L}^0_{\mathrm{QCD}}$ possesses (at the classical, unquantized level) a global $\mathrm{U}(3)_{\mathrm{L}} \times \mathrm{U}(3)_{\mathrm{R}}$ symmetry, isomorphic to a global $\mathrm{SU}(3)_{\mathrm{L}} \times \mathrm{U}(1)_{\mathrm{L}} \times \mathrm{SU}(3)_{\mathrm{R}} \times \mathrm{U}(1)_{\mathrm{R}}$ symmetry. The included symmetry group $\mathrm{SU}(3)_{\mathrm{L}} \times \mathrm{SU}(3)_{\mathrm{R}}$ refers to *chiral symmetry*. Noether's theorem states, that for every continuous symmetry generator there exists a conserved current. These 18 classically conserved currents associated with unitary transformations of left- or right-handed quarks are

$$\begin{aligned} J^{\mu,a}_{\mathrm{L}} &= \bar{q}_{\mathrm{L}} \gamma^\mu \frac{\lambda^a}{2} q_{\mathrm{L}} \,, \qquad & J^{\mu,a}_{\mathrm{R}} &= \bar{q}_{\mathrm{R}} \gamma^\mu \frac{\lambda^a}{2} q_{\mathrm{R}} \,, \\ J^{\mu}_{\mathrm{L}} &= \bar{q}_{\mathrm{L}} \gamma^\mu q_{\mathrm{L}} \,, & J^{\mu}_{\mathrm{R}} &= \bar{q}_{\mathrm{R}} \gamma^\mu q_{\mathrm{R}} \,. \end{aligned} \tag{2.13}$$

The divergence of all 18 currents is zero, $\partial_\mu J^\mu = 0$. It is convenient to introduce the *vector and axial-vector currents*

$$\begin{aligned} J^{\mu,a}_{\mathrm{V}} &= J^{\mu,a}_{\mathrm{R}} + J^{\mu,a}_{\mathrm{L}} = \bar{q}\gamma^\mu \frac{\lambda^a}{2} q\,, & J^{\mu,a}_{\mathrm{A}} &= J^{\mu,a}_{\mathrm{R}} - J^{\mu,a}_{\mathrm{L}} = \bar{q}\gamma^\mu\gamma_5 \frac{\lambda^a}{2} q\,, \\ J^{\mu}_{\mathrm{V}} &= J^{\mu}_{\mathrm{R}} + J^{\mu}_{\mathrm{L}} = \bar{q}\gamma^\mu q\,, & J^{\mu}_{\mathrm{A}} &= J^{\mu}_{\mathrm{R}} - J^{\mu}_{\mathrm{L}} = \bar{q}\gamma^\mu\gamma_5 q\,, \end{aligned} \tag{2.14}$$

since these have a definite transformation behavior under parity. The flavor-singlet vector current J^μ_{V} originates from rotations of the left- and right-handed quark fields with the same phase and the corresponding conserved charge is the *baryon number*. After quantization of the Dirac fermions, the conservation of the flavor-singlet axial vector current J^μ_{A} gets broken due to the so-called Adler-Bell-Jackiw anomaly [90, 91].

After the introduction of small *non-vanishing quark masses*, the quark mass term of the QCD Lagrangian can be expressed as

$$\mathscr{L}_M = -\bar{q}Mq = -\left(\bar{q}_{\mathrm{R}} M q_{\mathrm{L}} + \bar{q}_{\mathrm{L}} M q_{\mathrm{R}}\right)\,, \tag{2.15}$$

with the diagonal quark mass matrix $M = \mathrm{diag}(m_u, m_d, m_s)$. Left- and right-handed quark fields are mixed in $\mathscr{L}_M$ and the chiral symmetry is explicitly broken. The baryon number is still conserved, but for the flavor-octet vector and axial-vector currents one obtains

$$\partial_\mu J^{\mu,a}_{\mathrm{V}} = \mathrm{i}\bar{q}\left[M, \frac{\lambda_a}{2}\right] q\,, \qquad \partial_\mu J^{\mu,a}_{\mathrm{A}} = \mathrm{i}\bar{q}\left\{M, \frac{\lambda_a}{2}\right\}\gamma_5 q\,. \tag{2.16}$$

The axial-vector current is not conserved for any small quark masses. However, the vector current remains conserved, if the quark masses are equal, $m_u = m_d = m_s$, referred to as the *(flavor) SU(3) limit*.

Another crucial aspect of QCD is the so-called *spontaneous chiral symmetry breaking*. The chiral symmetry of the Lagrangian is not necessarily a symmetry of the ground state of the system, the QCD vacuum. Assuming the ground state would be chirally invariant (called the *Wigner-Weyl realization*), there should exist degenerate multiplets of opposite parity. This feature is not observed in the hadron spectrum. For example, the mass of the ρ meson ($J^P = 1^-$), $m_\rho \approx 0.77$ GeV, is much smaller than the mass of the a_1 meson ($J^P = 1^+$), $m_{a_1} \approx 1.23$ GeV. From such considerations and the approximate flavor SU(3) symmetry of the hadron spectrum, one concludes that chiral symmetry $\mathrm{SU}(3)_{\mathrm{L}} \times \mathrm{SU}(3)_{\mathrm{R}}$ is spontaneously broken to its vectorial subgroup $\mathrm{SU}(3)_{\mathrm{V}}$. This corresponds to the so-called *Nambu-Goldstone realization* of chiral symmetry. The spontaneous breaking of chiral symmetry can be characterized by a non-vanishing *chiral quark condensate* $\langle\bar{q}q\rangle \neq 0$, i.e., the vacuum involves strong correlations of scalar quark-antiquark pairs.

Goldstone's theorem states that for each spontaneously broken global symmetry, there is a corresponding massless particle, called a *Goldstone boson*. Hence, the spontaneous symmetry breaking, as described above, leads to eight Goldstone bosons. These have to be pseudoscalar particles, due to the parity transformation behavior of the axial vector currents. The Goldstone bosons are identified with the eight lightest hadrons, the pseudoscalar mesons ($\pi^\pm, \pi^0, K^\pm, K^0, \bar{K}^0, \eta$). The explicit chiral symmetry breaking due to non-vanishing quark masses leads to non-zero masses of the pseudoscalar mesons. However, there is a substantial mass gap, between the masses of the pseudoscalar mesons and the lightest hadrons of the remaining hadronic spectrum. This can be considered as another evidence for the Nambu-Goldstone realization of chiral symmetry in QCD. For

non-vanishing but equal quark masses, $\mathrm{SU}(3)_\mathrm{V}$ remains a symmetry of the ground state. In this context $\mathrm{SU}(3)_\mathrm{V}$ is often called the flavor group SU(3), which provides the basis for the classification of low-lying hadrons in multiplets. In the following chapters we will consider the so-called *isospin symmetric limit*, with $m_u = m_d \neq m_s$. The remaining symmetry is the SU(2) isospin symmetry. An essential feature of low-energy QCD is, that the pseudoscalar mesons *interact weakly* at low energies. This is a direct consequence of their Goldstone-boson nature. This feature allows for the construction of a low-energy effective field theory enabling a systematic expansion in small momenta and quark masses.

2.1.2 *External-field method*

In the following, we introduce the external-field method as a tool for the systematic development of χEFT. The chiral symmetry gives rise to so-called *chiral Ward identities*: relations between the divergence of Green functions that include a symmetry current (vector or axial-vector currents) to linear combinations of Green functions. Even if the symmetry is explicitly broken, Ward identities related to the symmetry breaking term exist. The chiral Ward identities do not rely on perturbation theory, but are also valid in the non-perturbative region of QCD. The external-field method is an elegant way to formally combine all chiral Ward identities in terms of invariance properties of a generating functional. We follow the procedure of Gasser and Leutwyler [6, 92] and introduce (color neutral) *external fields*, $s(x)$, $p(x)$, $v_\mu(x)$, $a_\mu(x)$, of the form of Hermitian 3×3 matrices that couple to scalar, pseudoscalar, vector and axial-vector currents of quarks:

$$\mathscr{L} = \mathscr{L}^0_\mathrm{QCD} + \mathscr{L}_\mathrm{ext} = \mathscr{L}^0_\mathrm{QCD} + \bar{q}\gamma^\mu(v_\mu + \gamma_5 a_\mu)q - \bar{q}(s - \mathrm{i}\gamma_5 p)q\,. \tag{2.17}$$

Note that the physical three-flavor QCD Lagrangian can be obtained by setting:

$$v^\mu(x) = a^\mu(x) = p(x) = 0 \quad \text{and} \quad s(x) = M = \mathrm{diag}\,(m_u, m_d, m_s)\ . \tag{2.18}$$

The corresponding generating functional in path-integral representation is given by

$$\mathrm{e}^{\mathrm{i}\mathcal{Z}[v,a,s,p]} = \int \mathscr{D}A^a_\mu \mathscr{D}q \mathscr{D}\bar{q}\, \exp\left[\mathrm{i}\int \mathrm{d}^4x\, \mathscr{L}\left(q, \bar{q}, A^a_\mu; v, a, s, p\right)\right]\ , \tag{2.19}$$

and is related to the vacuum-to-vacuum transition amplitude in the presence of external fields,

$$\mathrm{e}^{\mathrm{i}\mathcal{Z}[v,a,s,p]} = \langle 0; \mathrm{out}|0; \mathrm{in}\rangle_{v,a,s,p}\ . \tag{2.20}$$

The essential point is now, that *all* chiral Ward identities are encoded in the generating functional, if the global chiral symmetry $\mathrm{SU}(3)_\mathrm{L} \times \mathrm{SU}(3)_\mathrm{R}$ of $\mathscr{L}^0_\mathrm{QCD}$ is promoted to a *local gauge symmetry* of $\mathscr{L}$ [93]. Since $\mathscr{L}^0_\mathrm{QCD}$ is only invariant under the global chiral symmetry, the external fields have to fulfill a suitable transformation behavior:

$$\begin{aligned}
v_\mu + a_\mu &\to R(v_\mu + a_\mu)R^\dagger + \mathrm{i}\, R\partial_\mu R^\dagger\,,\\
v_\mu - a_\mu &\to L(v_\mu - a_\mu)L^\dagger + \mathrm{i}\, L\partial_\mu L^\dagger\,,\\
s + \mathrm{i}\, p &\to R\,(s + \mathrm{i}\, p)\, L^\dagger\,,\\
s - \mathrm{i}\, p &\to L\,(s - \mathrm{i}\, p)\, R^\dagger\,,
\end{aligned} \tag{2.21}$$

	v^μ	a^μ	s	p
P	${P^\mu}_\nu v^\nu$	$-{P^\mu}_\nu a^\nu$	s	$-p$
C	$-{v^\mu}^\top$	${a^\mu}^\top$	$s^\top$	$p^\top$

TABLE 2.1: Transformation properties of the external fields under parity and charge conjugation. For P a change of the spatial arguments $(t, \vec{x}) \to (t, -\vec{x})$ is implied and we defined the matrix ${P^\mu}_\nu = \mathrm{diag}(+1, -1, -1, -1)$.

where $L(x)$ and $R(x)$ are (independent) space-time-dependent elements of $\mathrm{SU}(3)_\mathrm{L}$ and $\mathrm{SU}(3)_\mathrm{R}$.

Furthermore, we still require the full Lagrangian $\mathscr{L}$ to be invariant under P, C and T. With the transformation properties of the quarks in Eq. (2.4) we obtain the transformation behavior of the external fields given in Tab. 2.1. Time reversal symmetry will not be considered explicitly, since it is automatically fulfilled due to the CPT theorem.

Another central aspect of the external-field method is the addition of terms to the three-flavor QCD Lagrangian in the chiral limit, $\mathscr{L}^0_\mathrm{QCD}$. Non-vanishing current quark masses and therefore the *explicit breaking* of chiral symmetry can be introduced by setting the scalar field equal to the quark mass matrix, $s(x) = M$. In the same way *electroweak interactions* get included through appropriate external vector and axial vector fields. For example in the case of the electromagnetic interaction we use $v_\mu(x) = -eQA_\mu(x)$, with the quark charge matrix $Q = \mathrm{diag}(2/3, -1/3, -1/3)$ and with $A_\mu(x)$ the photon field. This results in an additional term of the Lagrangian

$$-eA_\mu J^\mu_\mathrm{em} = -eA_\mu \left(\frac{2}{3}\bar{u}\gamma^\mu u - \frac{1}{3}\bar{d}\gamma^\mu d - \frac{1}{3}\bar{s}\gamma^\mu s \right) . \tag{2.22}$$

This feature is important, to systematically include explicit chiral symmetry breaking or couplings to electroweak gauge fields into the chiral effective Lagrangian.

2.2 PRINCIPLES OF CHIRAL EFFECTIVE FIELD THEORY

An *effective field theory* (EFT) is a low-energy approximation to a more fundamental theory. Physical quantities can be calculated in terms of a low-energy expansion in powers of small energies and momenta over some characteristic large scale. The basic idea of an EFT is to include the relevant degrees of freedom explicitly, while heavier (frozen) degrees of freedom are integrated out. An effective Lagrangian is obtained by constructing the most general Lagrangian including the active degrees of freedom, that is consistent with the symmetries of the underlying fundamental theory [5]. At a given order in the expansion, the theory is characterized by a finite number of coupling constants, called *low-energy constants* (LECs). The LECs encode the unresolved short-distance dynamics and furthermore allow for an order-by-order renormalization of the theory. These constants are a priori unknown, but once determined from one experiment or from the underlying theory, predictions for physical observables can be made. However, due to the low-energy expansion and the truncation of degrees of freedom, an EFT has only a limited range of validity.

The underlying theory of *chiral effective field theory* is quantum chromodynamics. But already before QCD was established, the ideas of an effective field theory were used in

the context of the strong interaction. In the sixties the Ward identities related to spontaneously broken chiral symmetry were explored by using current algebra methods, e.g., by Adler and Dashen [94]. The group-theoretical foundations for constructing phenomenological Lagrangians in the presence of spontaneous symmetry breaking have been developed by Weinberg [4] and Callan, Coleman, Wess and Zumino [95, 96]. With Weinberg's seminal paper [5] it became clear how to systematically construct an EFT and generate loop corrections to tree level results. This method was improved later by Gasser and Leutwyler [6, 92]. A systematic introduction of nucleons as degrees of freedom was done by Gasser, Sainio and Svarc [7]. They showed that a fully relativistic treatment of nucleons is problematic, as the nucleon mass does not vanish in the chiral limit and thus adds an extra scale. A solution for this problem was proposed by Jenkins and Manohar [97] by considering baryons as heavy static sources. The nucleon-nucleon interaction and related topics were considered by Weinberg in Ref. [57]. Nowadays χEFT is used as a powerful tool for calculating systematically the strong interaction dynamics of hadronic processes, such as the accurate description of nuclear forces [12, 13].

In the low-energy regime of QCD, hadrons are the observable states. The active degrees of freedom of χEFT are identified as the pseudoscalar Goldstone-boson octet. The soft scale of the low-energy expansion is given by the small external momenta and the small masses of the pseudo-Goldstone bosons, while the large scale is a typical hadronic scale of about 1 GeV. The QCD generating functional of Eq. (2.19) is approximated by that following from an effective chiral Lagrangian

$$\mathrm{e}^{\mathrm{i}\mathcal{Z}[v,a,s,p]} = \int \mathscr{D}U \, \exp\left[\mathrm{i}\int \mathrm{d}^4x \, \mathscr{L}_{\mathrm{eff}}\left(U;v,a,s,p\right)\right] , \tag{2.23}$$

where the SU(3)-matrix U contains the pseudoscalar mesons. The effective Lagrangian has to fulfill the same symmetry properties as QCD: invariance under Lorentz and parity transformations, charge conjugation and time reversal symmetry. Especially the chiral symmetry and its spontaneous symmetry breaking has to be incorporated. As described in the last section, the Green functions calculated from this generating functional automatically obey the pertinent Ward identities, if we promote the global chiral symmetry to a local one. The *same* external fields v, a, s, p as in Eq. (2.17), with the same transformation behavior as in QCD, are included in the effective Lagrangian. This allows us to include electroweak gauge bosons in the chiral Lagrangian as well as to consider explicit chiral symmetry breaking through finite quark masses in a perturbative fashion. The introduction of the baryon octet and decuplet in the chiral Lagrangian is done in the same way. However, since the baryon mass is not vanishing even in the chiral limit, special care has to be taken.

As the QCD vacuum is approximately invariant under the flavor symmetry group SU(3), one expects the hadrons to organize themselves in multiplets of irreducible representations of SU(3). The pseudoscalar mesons form an octet, Fig. 2.1. The members of the octet are characterized by the strangeness quantum number S and the third component I_3 of the isospin. The symbol η stands for the octet component (η_8). As an approximation we identify η_8 with the physical η, ignoring possible mixing with the singlet state η_1. For the lowest-lying baryons one finds an octet and a decuplet, Fig. 2.2. In the following we summarize how these explicit degrees of freedom are included in the chiral Lagrangian in the standard non-linear realization of chiral symmetry [95, 96].

The chiral symmetry group $\mathrm{SU}(3)_\mathrm{L} \times \mathrm{SU}(3)_\mathrm{R}$ is spontaneously broken to its diagonal subgroup $\mathrm{SU}(3)_\mathrm{V}$. The *Goldstone-boson octet* should transform under $\mathrm{SU}(3)_\mathrm{L} \times \mathrm{SU}(3)_\mathrm{R}$

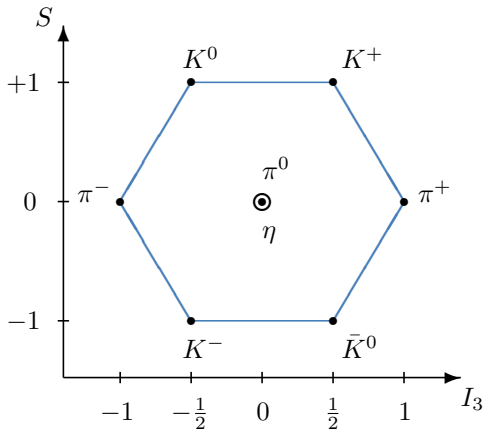

FIGURE 2.1: Pseudoscalar meson octet ($J^P = 0^-$).

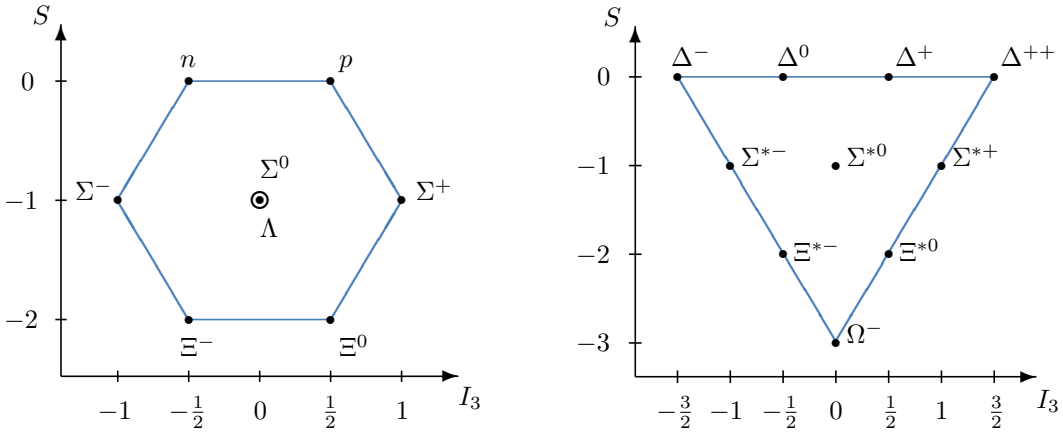

FIGURE 2.2: Baryon octet ($J^P = 1/2^+$) and baryon decuplet ($J^P = 3/2^+$).

such that an irreducible **8**-representation results for $\mathrm{SU}(3)_\mathrm{V}$. A convenient choice to describe the pseudoscalar mesons under these conditions is a unitary 3×3 matrix $U(x)$ in flavor space, which fulfills

$$U^\dagger U = 1\,, \qquad \det U = 1\,. \tag{2.24}$$

The transformation behavior under chiral symmetry reads

$$U \to RUL^\dagger\,, \tag{2.25}$$

where $L(x)$, $R(x)$ are elements of $\mathrm{SU}(3)_{L,R}$. An explicit parametrization of $U(x)$ in terms of the pseudoscalar mesons is given by

$$U(x) = \exp\left[\mathrm{i}\,\phi(x)/f_0\right]\,, \tag{2.26}$$

with the traceless Hermitian matrix

$$\phi(x) = \sum_{a=1}^{8} \phi_a(x)\lambda_a = \begin{pmatrix} \pi^0 + \frac{1}{\sqrt{3}}\eta & \sqrt{2}\pi^+ & \sqrt{2}K^+ \\ \sqrt{2}\pi^- & -\pi^0 + \frac{1}{\sqrt{3}}\eta & \sqrt{2}K^0 \\ \sqrt{2}K^- & \sqrt{2}\bar{K}^0 & -\frac{2}{\sqrt{3}}\eta \end{pmatrix}\,. \tag{2.27}$$

The constant f_0 is the *decay constant* of the pseudoscalar Goldstone bosons in the chiral limit, defined by

$$\left\langle 0 \left| J_{\mathrm{A}}^{\mu,a}(x) \right| \phi^b(p) \right\rangle = \mathrm{i}\, p_\mu f_0 \delta^{ab} e^{-ip\cdot x} \,. \tag{2.28}$$

For a transformation of the subgroup $\mathrm{SU(3)_V}$ with $L = R = V$, the meson matrix U transforms as

$$U \to V U V^\dagger \,, \tag{2.29}$$

i.e., the mesons $\phi_a(x)$ transform in the adjoint (irreducible) **8**-representation of SU(3). The parity transformation behavior of the pseudoscalar mesons is $\phi_a(t,\vec{x}\,) \xrightarrow{P} -\phi_a(t,-\vec{x}\,)$ or, equivalently, $U(t,\vec{x}\,) \xrightarrow{P} U^\dagger(t,-\vec{x}\,)$. Under charge conjugation the particle fields are mapped to antiparticle fields, leading to $U \xrightarrow{C} U^\top$.

The *octet baryons* are described by Dirac spinor fields and represented in a traceless 3×3 matrix $B(x)$ in flavor space,

$$B = \sum_{a=1}^{8} \frac{B_a \lambda_a}{\sqrt{2}} = \begin{pmatrix} \frac{1}{\sqrt{2}}\Sigma^0 + \frac{1}{\sqrt{6}}\Lambda & \Sigma^+ & p \\ \Sigma^- & -\frac{1}{\sqrt{2}}\Sigma^0 + \frac{1}{\sqrt{6}}\Lambda & n \\ \Xi^- & \Xi^0 & -\frac{2}{\sqrt{6}}\Lambda \end{pmatrix} . \tag{2.30}$$

We use the convenient [98] non-linear realization of chiral symmetry for the baryons, which lifts the well-known flavor transformations to the chiral symmetry group. The matrix $B(x)$ transforms under the chiral symmetry group $\mathrm{SU(3)_L} \times \mathrm{SU(3)_R}$ as

$$B \to K B K^\dagger \,, \tag{2.31}$$

with the SU(3)-valued compensator field

$$K\,(L,R,U) = \sqrt{L U^\dagger R^\dagger} R \sqrt{U} \,. \tag{2.32}$$

Note that $K\,(L,R,U)$ also depends on the meson matrix U. The square root of the meson matrix,

$$u = \sqrt{U} \,, \tag{2.33}$$

transforms as $u \to \sqrt{RUL^\dagger} = RuK^\dagger = KuL^\dagger$. For transformations under the subgroup $\mathrm{SU(3)_V}$ the baryons transform as an octet, i.e., the adjoint representation of SU(3):

$$B \to V B V^\dagger \,. \tag{2.34}$$

The transformation behavior of the octet-baryon fields under parity and charge conjugation is the same as for the quark fields in Eq. (2.4).

A natural choice to represent the *decuplet baryons* is a totally symmetric three-index tensor T. It transforms under the chiral symmetry $\mathrm{SU(3)_L} \times \mathrm{SU(3)_R}$ as

$$T_{abc} \to K_{ad} K_{be} K_{cf} T_{def} \,, \tag{2.35}$$

with the compensator field $K(L,R,U)$ of Eq. (2.32). For an $\mathrm{SU(3)_V}$ transformation the decuplet fields transform as an irreducible representation of SU(3):

$$T_{abc} \to V_{ad} V_{be} V_{cf} T_{def} \,. \tag{2.36}$$

The physical fields are assigned to the following components of the totally antisymmetric tensor:

$$
\begin{aligned}
&T^{111} = \Delta^{++}\,, && T^{112} = \tfrac{1}{\sqrt{3}}\Delta^{+}\,, && T^{122} = \tfrac{1}{\sqrt{3}}\Delta^{0}\,, && T^{222} = \Delta^{-}\,,\\
&T^{113} = \tfrac{1}{\sqrt{3}}\Sigma^{*+}\,, && T^{123} = \tfrac{1}{\sqrt{6}}\Sigma^{*0}\,, && T^{223} = \tfrac{1}{\sqrt{3}}\Sigma^{*-}\,,\\
&T^{133} = \tfrac{1}{\sqrt{3}}\Xi^{*0}\,, && T^{233} = \tfrac{1}{\sqrt{3}}\Xi^{*-}\,,\\
&T^{333} = \Omega^{-}\,.
\end{aligned}
\tag{2.37}
$$

Since decuplet baryons are spin-3/2 particles, each component is expressed through *Rarita-Schwinger fields*. However, we will only use decuplet baryons in Chapter 7 for estimating LECs via decuplet resonance saturation. It is sufficient to treat them in their non-relativistic form, where no complications with the Rarita-Schwinger formalism arise.

Now the representation of the explicit degrees of freedom and their transformation behavior are established. Together with the external fields the construction of the chiral effective Lagrangian is straightforward.

2.3 CONSTRUCTION OF CHIRAL LAGRANGIAN

The chiral Lagrangian can be ordered according to the number of baryon fields:

$$
\mathscr{L}_{\text{eff}} = \mathscr{L}_{\phi} + \mathscr{L}_{B} + \mathscr{L}_{BB} + \dots\,,
\tag{2.38}
$$

where $\mathscr{L}_{\phi}$ denotes the purely mesonic part of the Lagrangian. Each part is organized in the number of small momenta (i.e., derivatives) or small meson masses, e.g.,

$$
\mathscr{L}_{\phi} = \mathscr{L}_{\phi}^{(2)} + \mathscr{L}_{\phi}^{(4)} + \mathscr{L}_{\phi}^{(6)} + \dots\,.
\tag{2.39}
$$

$\mathscr{L}_{\phi}$ has been constructed to $\mathcal{O}(q^6)$ in Refs. [99, 100]. The meson-baryon interaction Lagrangian $\mathscr{L}_{B}$ has been derived to $\mathcal{O}(q^3)$ in Refs. [101, 102].

As already published in Ref. [103], we summarize the basic procedure for constructing systematically the three-flavor chiral effective Lagrangian [95, 96] with the inclusion of external fields [6, 92]. The effective chiral Lagrangian has to fulfill all discrete and continuous symmetries of the strong interaction. Therefore it has to be invariant under parity (P), charge conjugation (C), Hermitian conjugation (H) and the proper, orthochronous Lorentz transformations. Time reversal symmetry is then automatically fulfilled via the CPT theorem. Especially *local* chiral symmetry has to be fulfilled. A common way to construct the chiral Lagrangian is to define so-called *building blocks*, from which the effective Lagrangian can be determined as an invariant polynomial. With respect to the chiral transformation properties, the most convenient choice for the building blocks is given by

$$
\begin{aligned}
u_{\mu} &= \mathrm{i}\left[u^{\dagger}\left(\partial_{\mu} - \mathrm{i}\,r_{\mu}\right)u - u\left(\partial_{\mu} - \mathrm{i}\,l_{\mu}\right)u^{\dagger}\right]\,,\\
\chi_{\pm} &= u^{\dagger}\chi u^{\dagger} \pm u\chi^{\dagger}u\,,\\
f_{\mu\nu}^{\pm} &= u f_{\mu\nu}^{\mathrm{L}} u^{\dagger} \pm u^{\dagger} f_{\mu\nu}^{\mathrm{R}} u\,,
\end{aligned}
\tag{2.40}
$$

with the combination

$$
\chi = 2B_0\,(s + \mathrm{i}\,p)\,,
\tag{2.41}
$$

of the external scalar and pseudoscalar field and a new parameter B_0. The external field strength tensors are defined by

$$f^{\mathrm{R}}_{\mu\nu} = \partial_\mu r_\nu - \partial_\nu r_\mu - \mathrm{i}\,[r_\mu, r_\nu]\,, \qquad f^{\mathrm{L}}_{\mu\nu} = \partial_\mu l_\nu - \partial_\nu l_\mu - \mathrm{i}\,[l_\mu, l_\nu]\,, \tag{2.42}$$

where

$$r_\mu = v_\mu + a_\mu\,, \quad l_\mu = v_\mu - a_\mu\,, \tag{2.43}$$

denote right handed and left handed external vector fields. In the absence of flavor singlet couplings we can assume $\langle a_\mu \rangle = \langle v_\mu \rangle = 0$, where $\langle \dots \rangle$ stands for the flavor trace. Hence, the fields u_μ and $f^{\pm}_{\mu\nu}$ in Eq. (2.40) are all traceless.

Using the *transformation behavior* of the pseudoscalar mesons and octet baryons in Eq. (2.25) and Eq. (2.31), and the transformation properties of the external fields in Eq. (2.21), one can determine the transformation behavior of the building blocks. All building blocks A, and therefore all products of these, transform according to the adjoint (octet) representation of SU(3), i.e., $A \to KAK^\dagger$. Note that traces of products of such building blocks are invariant under local chiral symmetry, since $K^\dagger K = \mathbb{1}$. The chiral covariant derivative of such a building block A is defined by

$$D_\mu A = \partial_\mu A + [\Gamma_\mu, A]\,, \tag{2.44}$$

with the chiral connection

$$\Gamma_\mu = \frac{1}{2}\left[u^\dagger\,(\partial_\mu - \mathrm{i}\,r_\mu)\,u + u\,(\partial_\mu - \mathrm{i}\,l_\mu)\,u^\dagger\right]\,. \tag{2.45}$$

The covariant derivative transforms homogeneously under the chiral group as $D_\mu A \to K\,(D_\mu A)\,K^\dagger$. The chiral covariant derivative of the baryon field B is given by Eq. (2.44) as well.

We use the Lorentz-covariant *power counting scheme*, introduced by Krause in Ref. [104]. Because of the large baryon mass M_0 in the chiral limit, a time-derivative acting on a baryon field B cannot be counted as small. Only baryon three-momenta can be small on a typical chiral scale. One has the following counting rules for baryon fields and their covariant derivatives,

$$B\,,\ \bar{B}\,,\ D_\mu B \sim \mathcal{O}(q^0)\,, \qquad (\mathrm{i}\not{D} - M_0)\,B \sim \mathcal{O}\,(q)\,. \tag{2.46}$$

The chiral dimension of the chiral building blocks and baryon bilinears $\bar{B}\Gamma B$ are given in Tab. 2.2. A covariant derivative acting on a building block (but not on B) raises the chiral dimension by one.

The transformation behavior of a building block A under parity, charge conjugation and Hermitian conjugation is

$$A^P = (-1)^p A\,, \quad A^C = (-1)^c A^\top\,, \quad A^\dagger = (-1)^h A\,, \tag{2.47}$$

with the exponents (modulo two) $p, c, h \in \{0, 1\}$ given in Tab. 2.2(a), and $\top$ denotes the transpose of a (flavor) matrix. In the case of parity P, a sign change of the spatial argument, $(t, \vec{x}) \to (t, -\vec{x})$, is implied in the fields. Lorentz indices transform with the matrix $P^\mu{}_\nu = \mathrm{diag}(+1, -1, -1, -1)$ under the parity transformation, e.g., $(u^\mu)^P = (-1)^p P^\mu{}_\nu u^\nu$.

	p	c	h	$\mathcal{O}$
u_μ	1	0	0	$\mathcal{O}(q^1)$
$f^+_{\mu\nu}$	0	1	0	$\mathcal{O}(q^2)$
$f^-_{\mu\nu}$	1	0	0	$\mathcal{O}(q^2)$
χ_+	0	0	0	$\mathcal{O}(q^2)$
χ_-	1	0	1	$\mathcal{O}(q^2)$

(a) Chiral building blocks

Γ	p	c	h	$\mathcal{O}$
$\mathbb{1}$	0	0	0	$\mathcal{O}(q^0)$
γ_5	1	0	1	$\mathcal{O}(q^1)$
γ_μ	0	1	0	$\mathcal{O}(q^0)$
$\gamma_5\gamma_\mu$	1	0	0	$\mathcal{O}(q^0)$
$\sigma_{\mu\nu}$	0	1	0	$\mathcal{O}(q^0)$

(b) Baryon bilinears $\bar{B}\Gamma B$

TABLE 2.2: Behavior under parity, charge conjugation and Hermitian conjugation as well as the chiral dimensions of chiral building blocks and baryon bilinears $\bar{B}\Gamma B$ [101].

Commutators and anticommutators of two building blocks A_1, A_2 have the same transformation behavior and therefore should be used instead of simple products, e.g.,

$$[A_1, A_2]^C_\pm = (-1)^{c_1+c_2}(A_1^\top A_2^\top \pm A_2^\top A_1^\top) = \pm(-1)^{c_1+c_2}[A_1, A_2]^\top_\pm \,.$$

For Hermitian conjugation the behavior is the same. The basis elements of the Dirac algebra forming the baryon bilinears have the transformation behavior

$$\gamma_0\Gamma\gamma_0 = (-1)^{p_\Gamma}\Gamma\,, \quad C^{-1}\Gamma C = (-1)^{c_\Gamma}\Gamma^\top\,, \quad \gamma_0\Gamma^\dagger\gamma_0 = (-1)^{h_\Gamma}\Gamma\,, \tag{2.48}$$

where the exponents $p_\Gamma, c_\Gamma, h_\Gamma \in \{0,1\}$ can be found in Tab. 2.2(b). Again, Lorentz indices of baryon bilinears transform under parity with the matrix $P^\mu{}_\nu$.

Because of the relation

$$[D_\mu, D_\nu]\,A = \frac{1}{4}\left[[u_\mu, u_\nu], A\right] - \frac{\mathrm{i}}{2}\left[f^+_{\mu\nu}, A\right] \tag{2.49}$$

for any building block A (or baryon field B), it is sufficient to use only totally symmetrized products of covariant derivatives, $D^{\alpha\beta\gamma\cdots}A$. Furthermore, because of the identity

$$D_\nu u_\mu - D_\mu u_\nu = f^-_{\mu\nu}\,, \tag{2.50}$$

one needs to consider only the symmetrized covariant derivative acting on u_μ,

$$h_{\mu\nu} = D_\mu u_\nu + D_\nu u_\mu\,. \tag{2.51}$$

Finally, the chiral effective Lagrangian can be constructed by taking traces (and products of traces) of different polynomials in the building blocks, so that they are invariant under chiral symmetry, Lorentz transformations, C and P.

2.3.1 *Leading-order meson Lagrangian*

As a first example, we show the leading-order purely mesonic Lagrangian. From the general construction principles discussed above, one obtains for the leading-order effective Lagrangian

$$\mathscr{L}^{(2)}_\phi = \frac{f_0^2}{4}\langle u_\mu u^\mu + \chi_+\rangle\,. \tag{2.52}$$

Note that there is no contribution of order $\mathcal{O}(q^0)$. This is consistent with the vanishing interaction of the Goldstone bosons in the chiral limit at zero momenta.

Before we continue with the meson-baryon interaction Lagrangian, let us elaborate on the leading chiral Lagrangian in the purely mesonic sector without external fields, but with non-vanishing quark masses in the isospin limit: $v^\mu(x) = a^\mu(x) = p(x) = 0$ and $s(x) = M = \mathrm{diag}\,(m, m, m_s)$. Inserting the definitions of the building blocks, Eq. (2.52) becomes with these restrictions:

$$\mathscr{L}_\phi^{(2)} = \frac{f_0^2}{4}\langle \partial_\mu U \partial^\mu U^\dagger \rangle + \frac{1}{2} B_0 f_0^2 \langle M U^\dagger + U M \rangle \,. \tag{2.53}$$

The scale f_0 is the decay constant of the pseudoscalar Goldstone bosons in the chiral limit. The axial-vector currents determined from $\mathscr{L}_\phi^{(2)}$ after expanding the meson matrix $U(x)$ read $J_\mathrm{A}^{\mu,a} = -f_0 \partial^\mu \phi^a + \ldots$ and are consistent with the definition of f_0 in Eq. (2.28). The physical decay constants $f_\pi \neq f_K \neq f_\eta$ differ in terms of order (m, m_s): $f_\phi = f_0 \{1 + \mathcal{O}(m, m_s)\}$. The constant B_0 is related to the chiral quark condensate. Since $\partial H_\mathrm{QCD}/\partial m_q = \bar{q}q$ it follows from Eq. (2.53) with $U = \mathbb{1}$, that

$$\langle \bar{q}q \rangle = \langle 0|\bar{u}u|0\rangle = \langle 0|\bar{d}d|0\rangle = \langle 0|\bar{s}s|0\rangle = -f_0^2 B_0 \{1 + \mathcal{O}(m, m_s)\} \,. \tag{2.54}$$

Rewriting the mass term of Eq. (2.53) in terms of the physical meson fields by expanding the matrix $U(x)$, relations between meson masses an quark masses can be established. Together with Eq. (2.54) the famous leading-order *Gell-Mann–Oakes–Renner relations* are obtained[2]

$$\begin{aligned} m_\pi^2 f_\pi^2 &= -2\, m \,\langle \bar{q}q \rangle + \mathcal{O}(m_q^2) \,, \\ m_K^2 f_K^2 &= -\,(m + m_s)\,\langle \bar{q}q \rangle + \mathcal{O}(m_q^2) \,, \\ m_\eta^2 f_\eta^2 &= -\frac{2}{3}\,(m + 2m_s)\,\langle \bar{q}q \rangle + \mathcal{O}(m_q^2) \,. \end{aligned} \tag{2.55}$$

In the chiral limit, i.e., for vanishing quark masses, the masses of the mesons vanish as expected from Goldstone's theorem. By elimination of m, m_s the relations in Eq. (2.55) lead to the Gell-Mann–Okubo mass formula

$$4m_K^2 = 3m_\eta^2 + m_\pi^2 \,. \tag{2.56}$$

2.3.2 *Leading-order meson-baryon interaction Lagrangian*

The leading-order meson-baryon interaction Lagrangian $\mathscr{L}_\mathrm{B}^{(1)}$ is of order $\mathcal{O}(q)$ and reads[3]

$$\mathscr{L}_\mathrm{B}^{(1)} = \langle \bar{B}\,(i\not{D} - M_\mathrm{B})\,B \rangle + \frac{D}{2}\langle \bar{B}\gamma^\mu\gamma_5 \{u_\mu, B\} \rangle + \frac{F}{2}\langle \bar{B}\gamma^\mu\gamma_5\,[u_\mu, B] \rangle \,. \tag{2.57}$$

The constant M_B is the mass of the baryon octet in the chiral limit. The two new constants D and F are called axial-vector coupling constants. Their values can be obtained from semi-leptonic hyperon decays and are roughly $D \approx 0.8$ and $F \approx 0.5$. The sum of the two constants is related to the axial-vector coupling constant of nucleons, $g_\mathrm{A} = D + F = 1.27$, obtained from neutron beta decay. At lowest order the pion-nucleon coupling constant $g_{\pi N}$ is connected to the axial-vector coupling constant by the Goldberger-Treiman relation,

2 These relations were first obtained by Gell-Mann, Oakes and Renner [105], using current algebra, especially the so-called partially conserved axial-vector current (PCAC) method.

3 Note that an overall plus sign in front of the constants D and F is chosen, consistent with the conventions in SU(2) χEFT [12].

$g_{\pi N} f_\pi = g_{\rm A} M_N$. The covariant derivative in Eq. (2.57) includes the field Γ_μ, which leads to a vertex between two octet baryons and two mesons, whereas the terms containing u_μ lead to a vertex between two octet baryons and one meson. Different octet-baryon masses appear first in $\mathscr{L}_{\rm B}^{(2)}$ due to explicit chiral symmetry breaking and renormalization and lead to corrections linear in the quark masses:

$$M_i = M_{\rm B} + \mathcal{O}(m, m_s)\,. \tag{2.58}$$

2.4 WEINBERG POWER COUNTING SCHEME

As stated before, an effective field theory has an infinite number of terms in the effective Lagrangian and for a fixed process an infinite number of diagrams contribute. Therefore, it is crucial to have a power counting scheme, to assign the importance of a term. Then, to a certain order in the power counting, only a *finite number* of terms contribute and the observables can be calculated to a given accuracy.

First, let us discuss the power counting scheme of χEFT in the pure meson sector, i.e., only the pseudoscalar Goldstone bosons are explicit degrees of freedom. The *chiral dimension* ν of a Feynman diagram represents the order in the low-momentum expansion, $(q/\Lambda_\chi)^\nu$. The symbol q is generic for a small external meson momentum or a small meson mass. The scale of chiral symmetry breaking Λ_χ is often estimated as $4\pi f_\pi \approx 1$ GeV or as the mass of the lowest-lying resonance, $M_\rho \approx 770$ MeV. A simple dimensional analysis leads to the following expression for the chiral dimension of a connected Feynman diagram [5]:

$$\nu = 2 + 2L + \sum_i v_i \Delta_i\,, \qquad \Delta_i = d_i - 2\,. \tag{2.59}$$

The number of Goldstone boson loops is denoted by L and v_i is the number of vertices with vertex dimension Δ_i. The symbol d_i stands for the number of derivatives or meson mass insertions at the vertex, i.e., the vertex originates from a term of the Lagrangian of the order $\mathcal{O}(q^{d_i})$.

With the introduction of baryons in the chiral effective Lagrangian, the power counting is more complicated. The large baryon mass comes as an extra scale and destroys the one-to-one correspondence between the loop and the small momentum expansion. Jenkins and Manohar used methods from heavy-quark effective field theory to solve this problem [97]. Basically they considered baryons as heavy, static sources. This leads to a description of the baryons in the extreme non-relativistic limit with an expansion in powers of the inverse baryon mass, called heavy-baryon chiral perturbation theory. Furthermore, in the two-baryon sector, additional features arise. The reducible Feynman diagrams are enhanced due to the presence of small kinetic energy denominators resulting from purely nucleonic intermediate states. These graphs hint at the non-perturbative aspects in few-body problems, such as the existence of shallow bound states, and must be summed up to all orders. As suggested by Weinberg [57, 58], we treat the baryons non-relativistically and apply the power counting scheme to an effective potential V, that contains only the irreducible Feynman diagrams. This effective potential is then the input for quantum mechanical few-body calculations. In case of the baryon-baryon interaction the effective potential is inserted into the Lippmann-Schwinger equation and solved for bound and scattering states. This is graphically shown in Fig. 2.3. The T-matrix is obtained from

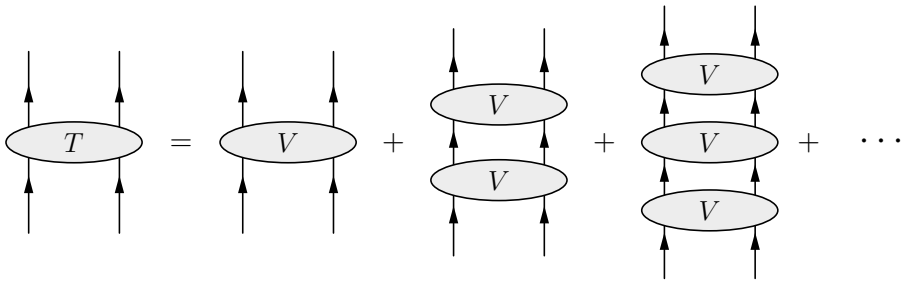

FIGURE 2.3: Graphical representation of the Lippmann-Schwinger equation.

the infinite series of ladder diagrams with the effective potential V. In this way the omitted reducible diagrams are regained. As argued in Refs. [57, 58] the baryon mass M_{B} is counted as

$$\frac{q}{M_{\mathrm{B}}} \propto \left(\frac{q}{\Lambda_\chi}\right)^2 . \tag{2.60}$$

After these considerations, a consistent power counting scheme for the effective potential V is possible. The soft scale q in the low-momentum expansion $(q/\Lambda_\chi)^\nu$ denotes now small external meson four-momenta, small external baryon three-momenta or the small meson masses. Naive dimensional analysis leads to the generalization of Eq. (2.59):

$$\nu = 2 - B + 2L + \sum_i v_i \Delta_i \,, \qquad \Delta_i = d_i + \frac{1}{2} b_i - 2 \,, \tag{2.61}$$

where B is the number of external baryons and b_i is the number of internal baryon lines at the considered vertex. However, Eq. (2.61) has an unwanted dependence on the baryon number, due to the normalization of baryon states. Such an effect can be avoided by assigning the chiral dimension to the transition operator instead of the matrix elements. This leads to the addition of $3B - 6$ to the formula for the chiral dimension, which leaves the $B = 2$ case unaltered, and one obtains

$$\nu = -4 + 2B + 2L + \sum_i v_i \Delta_i \,, \qquad \Delta_i = d_i + \frac{1}{2} b_i - 2 \,. \tag{2.62}$$

Following this scheme one arrives at the hierarchy of baryonic forces shown in Fig. 2.4. The leading-order ($\nu = 0$) potential is given by one-meson-exchange diagrams and non-derivative four-baryon contact terms. At next-to-leading order ($\nu = 2$) higher order contact terms and two-meson-exchange diagrams with intermediate octet baryons contribute. Finally, at next-to-next-to-leading order ($\nu = 3$) the three-baryon forces start to contribute. Diagrams that lead to mass and coupling constant renormalization are not shown.

2.5 APPLICATION: RADIATIVE CORRECTIONS TO PION-PAIR PRODUCTION

As an application of chiral perturbation theory in the mesonic sector, we briefly review our calculation in Ref. [106] concerning the QED radiative corrections to the charged pion-pair production process $\pi^-\gamma \to \pi^+\pi^-\pi^-$ at low energies. This process is measured with high statistics in the COMPASS experiment at CERN. Here, the Primakoff scattering of high-energetic pions in the Coulomb field of a heavy nucleus is used to extract cross sections

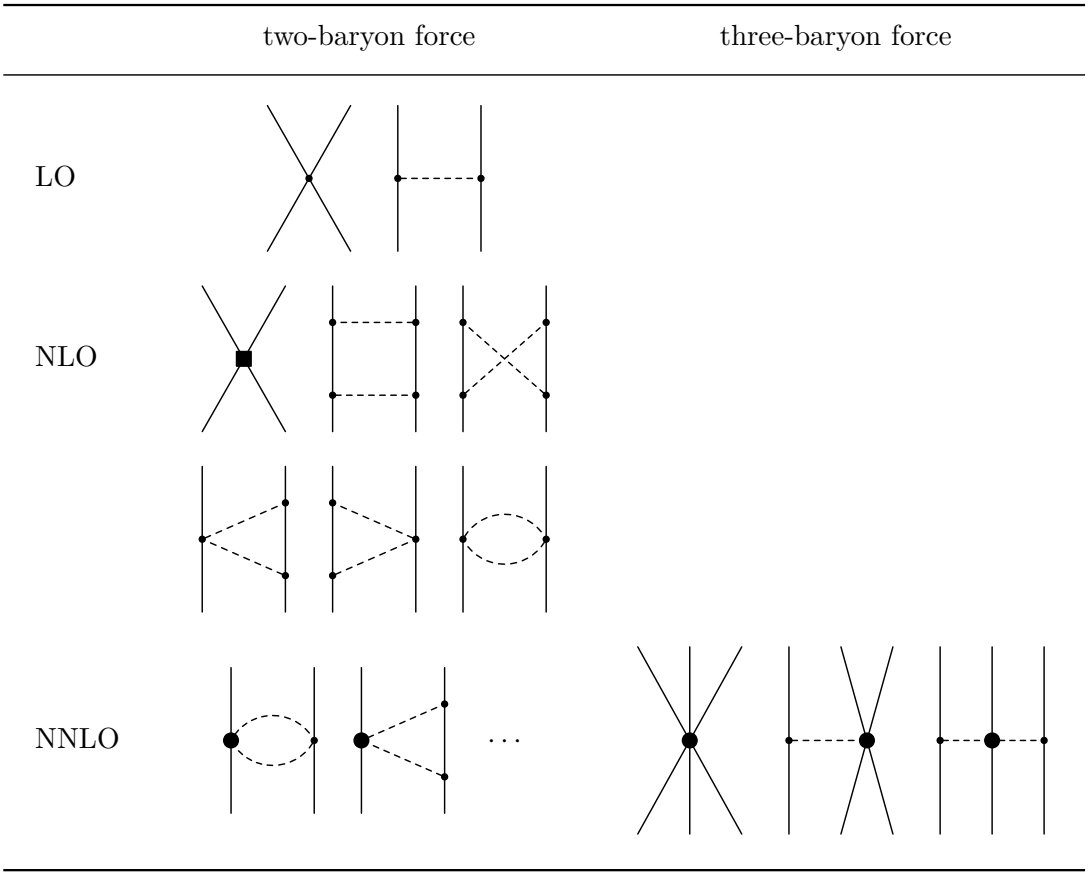

FIGURE 2.4: Hierarchy of baryonic forces. Solid lines are baryons, dashed lines are pseudoscalar mesons. Solid dots, filled circles and squares denote vertices with $\Delta_i = 0, 1$ and 2, respectively.

for low-energy $\pi^-\gamma$ reactions. The total cross sections for the reactions $\pi^-\gamma \to 3\pi$ in the low-energy region serve as a good testing ground for chiral perturbation theory, since it involves all the chiral dynamics of $\pi\pi$ scattering, in a reaction induced by a photon. In contrast to the baryonic sector, a purely perturbative approach can be used for pion-interactions in the low-energy regime. Total cross sections for the process $\pi^-\gamma \to \pi^+\pi^-\pi^-$ in the energy region from threshold up to a total center-of-mass energy $\sqrt{s}$ of about $5m_\pi$ have been published by the COMPASS collaboration in Ref. [107]. Good agreement has been found with the leading-order prediction of chiral perturbation theory, which can be obtained from the tree-level Feynman diagrams shown in Fig. 2.5. However, for the analysis of future high statistics experiments at COMPASS, a higher theoretical precision is desirable. The chiral corrections to $\pi^-\gamma \to 3\pi$ processes at low energies have already been calculated in Ref. [108]. It has been found that the total cross sections of neutral pion pair production $\pi^-\gamma \to \pi^-\pi^0\pi^0$ get enhanced by a factor 1.5–1.8 in the low-energy region up to $\sqrt{s} = 7m_\pi$. On the other hand, the total cross sections of the charged pion pair production process $\pi^-\gamma \to \pi^+\pi^-\pi^-$ remain almost unchanged in this region by the inclusion of higher-order corrections. The QED radiative corrections of order $\mathcal{O}(e^2p^2)$ to the neutral pion production process $\pi^-\gamma \to \pi^-\pi^0\pi^0$ have been derived in Ref. [109], where 12 relevant Feynman diagrams contribute. The radiative corrections to the total cross section vary between -2% and 2% in the low-energy region.

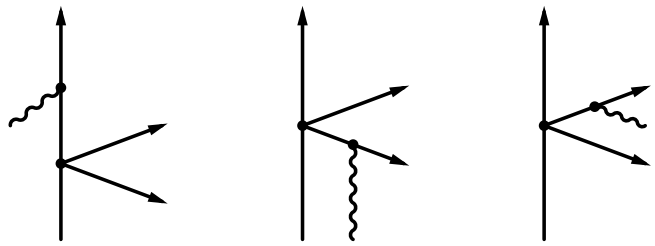

FIGURE 2.5: Leading-order contributions to the process $\pi^-\gamma \to \pi^+\pi^-\pi^-$.

In Ref. [106] we have considered the QED radiative corrections to the more complex process $\pi^-\gamma \to \pi^+\pi^-\pi^-$, which involves in total 110 relevant Feynman diagrams. Isospin breaking effects (proportional to $m_{\pi^\pm} - m_{\pi^0} \propto \alpha$) in pion loops which count also as $\mathcal{O}(e^2p^2)$ have been neglected. The various contributions to the radiative corrections of relative order $\alpha = e^2/4\pi$ consist of purely electromagnetic interactions of the charged pions mediated by (tree-level) one-photon exchange (10 diagrams) and of one-photon-loop corrections to the leading-order diagrams in Fig. 2.5. The loop diagrams fall into three classes: self-energy corrections on external pion-lines (12 diagrams), which give only ultraviolet and infrared divergences, vertex corrections to the pion-photon coupling (12 diagrams), which sum to zero, and "irreducible" photon loop diagrams (42 diagrams), which produce the finite contribution of interest. Ultraviolet as well as infrared divergences in loop diagrams are treated with the use of dimensional regularization. In order to achieve ultraviolet finiteness, electromagnetic counterterms need to be included (22 diagrams). Furthermore, infrared divergences are canceled by including soft-photon bremsstrahlung off the in- and out-going charged pions below an energy cut-off $\lambda \approx 5$ MeV (12 diagrams). The calculation of the difficult 42 irreducible diagrams was done by using the packages FeynCalc [110] and LoopTools [111]. The results for all other diagrams can be given in concise analytical formulas.

In general the radiative corrections to the total cross sections and dipion mass spectra are of the order of a few percent, as assumed in the analysis of the COMPASS data in Ref. [107]. In Fig. 2.6 the resulting radiative corrections (in percent) to the total cross sections of the process $\pi^-\gamma \to \pi^+\pi^-\pi^-$ are presented as a function of the total center-of-mass energy $\sqrt{s}$. The largest contribution is given by the one-photon exchange, which gives a correction of about 8% close to threshold. However, it is partly compensated by the leading isospin-breaking correction from the mass difference between neutral and charged pions. The horizontal gray band represents the contribution from the electromagnetic counterterms and it is obtained by varying the corresponding LECs in a natural range. Surprisingly, the contribution from the irreducible loop diagrams is almost constant in the region $3.5m_\pi < \sqrt{s} < 7m_\pi$. Another feature of the radiative corrections is, that the Coulomb singularity of the final state interaction leads to a kink in the dipion invariant mass spectra. This can be seen exemplary in Fig. 2.7, which shows the radiative corrections to $\pi^-\pi^-$ mass spectrum. With these results, the radiative corrections can be consistently taken into account in the analysis of a future high statistics experiment of COMPASS.

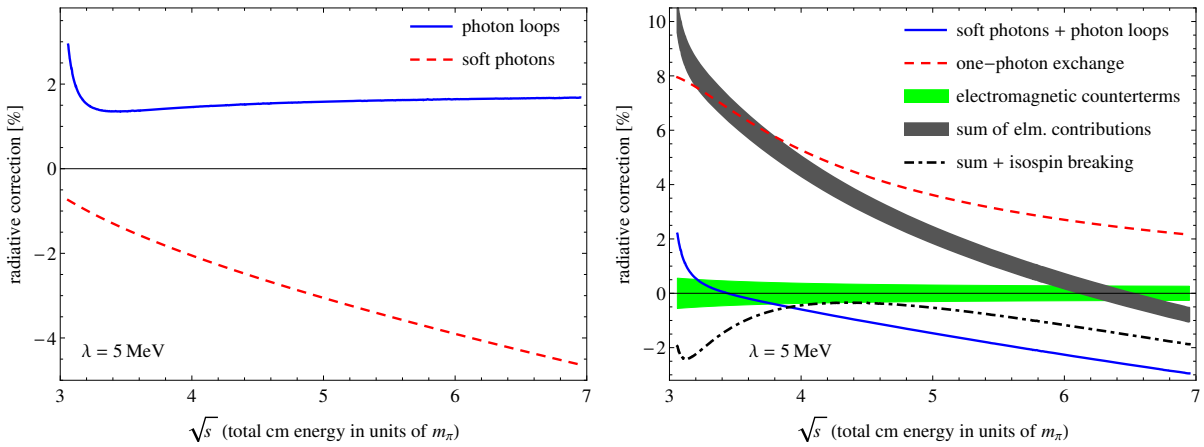

FIGURE 2.6: Radiative corrections to the total cross sections of the process $\pi^-\gamma \to \pi^+\pi^-\pi^-$.

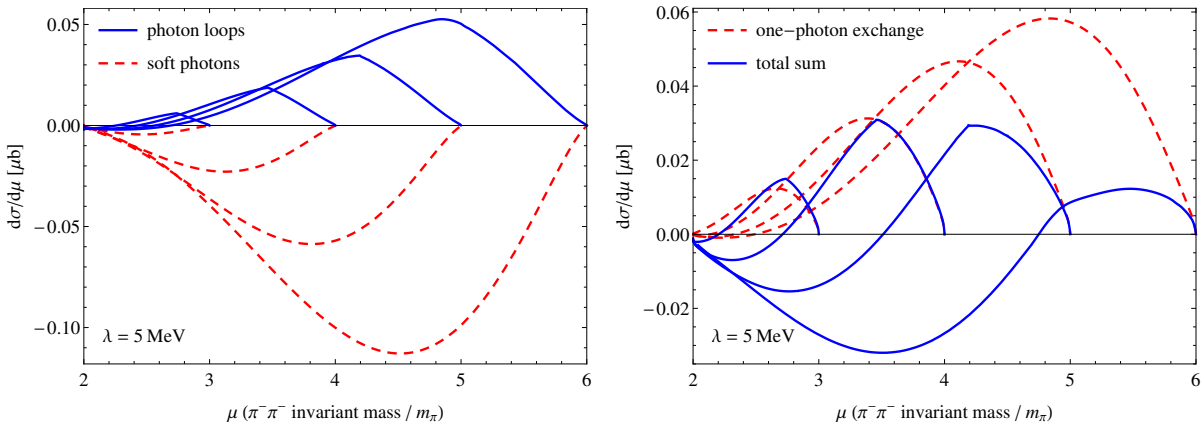

FIGURE 2.7: Radiative corrections the the $\pi^-\pi^-$ mass spectrum of the process $\pi^-\gamma \to \pi^+\pi^-\pi^-$ for $\sqrt{s} = (4, 5, 6, 7)m_\pi$.

3

RELATIVISTIC BARYON-NUMBER-TWO CHIRAL LAGRANGIAN

In this somewhat technical chapter, we construct the most general chiral effective Lagrangian in flavor SU(3) up to order q^2 in the baryon-number-two sector, using a covariant power counting. The resulting Lagrangian leads in the absence of external fields to the baryon-baryon contact terms up to $\mathcal{O}(q^2)$, which are an important ingredient for complete calculations of the baryon-baryon interaction beyond leading order, as they encode the unresolved short-distance dynamics. The corresponding low-energy constants have to be fitted to experimental data. By introducing external fields of scalar, pseudoscalar, vector and axial-vector type, the contact terms (linear in the quark masses) that break explicitly chiral symmetry, emerge as a particular subset. Additional types of four-baryon contact vertices including, e.g., pseudoscalar Goldstone bosons, weak gauge bosons or photons are obtained by this method as well. A small subset of the constructed vertices is shown in Fig. 3.1. Especially the four-baryon vertex with one Goldstone boson is important for meson-production processes and the construction of three-baryon forces with one-meson exchange, as explained in Chapter 6. Parts of the present chapter have been previously published in Ref. [103].

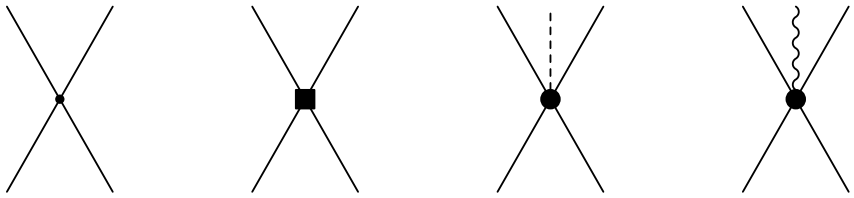

FIGURE 3.1: Examples for baryon-baryon contact vertices. Solid lines, dashed lines and wavy lines are baryons, pseudoscalar mesons and photons. Solid dots, filled circles and squares denote vertices with $\Delta_i = 0, 1$ and 2, respectively.

The chiral Lagrangian for the baryon-number-one sector has been investigated in various works. The chiral effective pion-nucleon Lagrangian of order $\mathcal{O}(q^4)$ has been constructed in Ref. [112]. The three-flavor Lorentz invariant chiral meson-baryon Lagrangians at order $\mathcal{O}(q^2)$ and $\mathcal{O}(q^3)$ have been first formulated in Ref. [104] and were later completed in Refs. [101] and [102]. In these papers the external field method has been used and a locally chiral invariant relativistic Lagrangian has been derived. Concerning the nucleon-nucleon contact terms, the relativistically invariant contact Lagrangian at order $\mathcal{O}(q^2)$ for two flavors (without any external fields) has been constructed in Ref. [113]. In this chapter we extend the framework to construct the general baryon-baryon contact terms up to order $\mathcal{O}(q^2)$ for three flavors using the external field method. At lowest order $\mathcal{O}(q^0)$ this Lagrangian has been given in Refs. [23, 25]. The three-flavor chiral Lagrangian for the baryon-number-two sector is constructed such that each individual term fulfills the

invariance under charge conjugation, parity transformation, Hermitian conjugation and local chiral symmetry $\mathrm{SU}(3)_\mathrm{L} \times \mathrm{SU}(3)_\mathrm{R}$. In order to eliminate linearly dependent terms, we use the Fierz identities, the equations of motion, the cyclic property of the trace and a Cayley-Hamilton relation for SU(3). As one might expect, we find that the number of terms in the Lagrangian and associated low-energy constants is very large. This is due to the fact, that many possible orderings of the flavor matrices including external fields give rise to invariant terms. In addition, the particle content is considerably larger than for flavor SU(2). However, many physical processes such as baryon-baryon scattering are sensitive to only a small fraction of these terms and their associated low-energy constants. By employing the non-relativistic reduction we show that many of the relativistic $\mathcal{O}(q^2)$-terms actually contribute at higher order and thus can be discarded in non-relativistic calculations up to order $\mathcal{O}(q^2)$.

3.1 CONSTRUCTION OF CHIRAL BARYON-BARYON LAGRANGIAN

For the construction of all terms in the Lagrangian, invariance under local chiral transformations, proper Lorentz transformations, parity, charge conjugation and Hermitian conjugation has to be fulfilled. Since the baryon field B and all building blocks A (cf. Eq. (2.40)) transform under the chiral symmetry group in the same way, $A \to KAK^\dagger$, the invariant terms for the Lagrangians are constructed by traces over products of these, or by products of such traces. Note that $K^\dagger K = \mathbb{1}$. The baryon-baryon contact terms include two baryon fields B and two adjoint baryon fields $\bar{B}$. The different arrangements of these four baryon fields (exploiting the cyclic property of the trace) are of the schematic form:

$$\begin{aligned}
&\langle \bar{B}B\bar{B}B\rangle\,,\ \langle \bar{B}\bar{B}BB\rangle\,,\\
&\langle \bar{B}B\rangle\langle \bar{B}B\rangle\,,\ \langle \bar{B}\rangle\langle B\bar{B}B\rangle\,,\ \langle \bar{B}\bar{B}\rangle\langle BB\rangle\,,\ \langle \bar{B}B\bar{B}\rangle\langle B\rangle\,,\\
&\langle \bar{B}B\rangle\langle \bar{B}\rangle\langle B\rangle\,,\ \langle \bar{B}\rangle\langle \bar{B}\rangle\langle BB\rangle\,,\ \langle \bar{B}\bar{B}\rangle\langle B\rangle\langle B\rangle\,,\\
&\langle \bar{B}\rangle\langle B\rangle\langle \bar{B}\rangle\langle B\rangle\,.
\end{aligned} \tag{3.1}$$

Chiral building blocks and Dirac operators have to be supplemented appropriately. By using the Fierz identity, a product of two baryon bilinears can be rearranged

$$(\bar{\Psi}^{(1)}\Gamma^A\Psi^{(2)})(\bar{\Psi}^{(3)}\Gamma^B\Psi^{(4)}) = -\sum_{C,D} \mathcal{C}^{AB}_{CD}(\bar{\Psi}^{(1)}\Gamma^C\Psi^{(4)})(\bar{\Psi}^{(3)}\Gamma^D\Psi^{(2)})\,, \tag{3.2}$$

where $\mathcal{C}^{AB}_{CD}$ are the well-known Fierz transformation coefficients. This allows one to fix and label the fields $\bar{B}$ and B which form the first and second baryon bilinear, respectively. The other arrangement can be expressed as a linear combination of the chosen type.

One arrives at the following list of general flavor structures for contact terms to arbitrary chiral order:

$$\begin{aligned}
X^1 &:= \hat{D}_2^k\,\langle \bar{B}_1 A_a \Theta_1 B_1 A_b \bar{B}_2 A_c \Theta_2 B_2 A_d\rangle,\\
X^2 &:= \hat{D}_2^k\,\langle \bar{B}_1 A_a \bar{B}_2 A_b \Theta_1 B_1 A_c \Theta_2 B_2 A_d\rangle,\\
X^3 &:= \hat{D}_2^k\,\langle \bar{B}_1 A_a \Theta_1 B_1 A_b\rangle\,\langle \bar{B}_2 A_c \Theta_2 B_2 A_d\rangle,\\
X^4 &:= \hat{D}_2^k\,\langle \bar{B}_1 A_a\rangle\,\langle \Theta_1 B_1 A_b \bar{B}_2 A_c \Theta_2 B_2 A_d\rangle,\\
X^5 &:= \hat{D}_2^k\,\langle \bar{B}_1 A_a \Theta_1 B_1 A_b\rangle\,\langle \bar{B}_2 A_c\rangle\,\langle \Theta_2 B_2 A_d\rangle,
\end{aligned}$$

$$
\begin{aligned}
X^6 &:= \hat{D}_2^k \, \langle \bar{B}_1 A_a \rangle \, \langle \bar{B}_2 A_b \rangle \, \langle \Theta_1 B_1 A_c \Theta_2 B_2 A_d \rangle , \\
X^7 &:= \hat{D}_2^k \, \langle \bar{B}_1 A_a \rangle \, \langle \Theta_1 B_1 A_b \rangle \, \langle \bar{B}_2 A_c \rangle \, \langle \Theta_2 B_2 A_d \rangle , \\
&\quad \text{and all terms of the form: } X^i \cdot \langle A_e \rangle \cdot \langle A_f \rangle \, \dots \, ,
\end{aligned} \tag{3.3}
$$

where the A are either $\mathbb{1}$ or the building blocks (u_μ, $f^\pm_{\mu\nu}$, $\chi_\pm$), covariant derivatives thereof, and commutators or anticommutators of these. We have omitted their Lorentz indices for the sake of notational simplicity. The operators $\Theta_{1,2}$ consist of basis elements of the Dirac algebra (in order to get the complete set of baryon bilinears) and products of the metric tensor $g_{\mu\nu}$ and the Levi-Civita tensor $\epsilon_{\mu\nu\rho\lambda}$. They include also an arbitrary number ($n_{1,2}$) of totally symmetrized covariant derivatives acting on the baryon field B to the right: $\Theta_1 := \Gamma_1 D^{n_1}$, $\Theta_2 := \Gamma_2 D^{n_2}$, $\Gamma_i \in \{\mathbb{1}, \gamma_5, \gamma_\mu, \gamma_5\gamma_\mu, \sigma_{\mu\nu}\}$. The indices 1,2 of the baryon fields and Θ's indicate to which baryon bilinear they belong, e.g., $(\dots \bar{B}_1 \dots \Theta_1 B_1 \dots)$ means $(\dots \bar{B}_\alpha \dots \Theta^{\alpha\beta} B_\beta \dots)$ with α, β being spinor indices. The operator $\hat{D}_2^k$ is defined such, that it acts only on the baryon field indexed by 2, e.g., $\hat{D}_2(\dots \bar{B}_2 \dots B_2 \dots)$ means $(\dots (D\bar{B}_2) \dots B_2 \dots) + (\dots \bar{B}_2 \dots (DB_2) \dots)$. Furthermore, these k covariant derivatives are totally symmetrized. Each operator $\hat{D}_2$ raises the chiral power of the monomial by one.

Obviously, a total derivative term ∂X can be omitted from the Lagrangian. In our case this gives, by the use of the product rule[1],

$$
\partial X = DX = \hat{D}_1 X + \hat{D}_2 X + \sum (\dots DA \dots) \, , \tag{3.4}
$$

where $(\dots DA \dots)$ denotes a term including the covariant derivatives of a chiral building block. Since DA is by definition a chiral building block, the corresponding term is already included in the construction of the most general Lagrangian. As a consequence of Eq. (3.4) there is no need to consider the operator $\hat{D}_1^k$ since it can be replaced by $-\hat{D}_2^k$. In a similar way we do not need to consider covariant derivatives of $\bar{B}$, since these can be expressed by higher order terms and terms that are already included in the list $X^1, \dots, X^7$ of Eq. (3.3). This property follows from the definition of $\hat{D}_2$,

$$
\hat{D}_2(\dots \bar{B}_2 \dots B_2 \dots) = (\dots (D\bar{B}_2) \dots B_2 \dots) + (\dots \bar{B}_2 \dots (DB_2) \dots) \, . \tag{3.5}
$$

The arrangement $\langle \bar{B}\bar{B} \rangle \langle BB \rangle$ of baryon fields under the flavor traces, which stands for a general term $\hat{D}_2^k \, \langle \bar{B}_1 A_a \bar{B}_2 A_b \rangle \, \langle \Theta_1 B_1 A_c \Theta_2 B_2 A_d \rangle$, can be expressed by other arrangements, using the Fierz identity together with the SU(3) Cayley-Hamilton relation (cf. Refs. [100, 102, 114])

$$
\begin{aligned}
0 = &\sum_{6 \text{ perm}} \langle M_1 M_2 M_3 M_4 \rangle - \sum_{8 \text{ perm}} \langle M_1 M_2 M_3 \rangle \langle M_4 \rangle - \sum_{3 \text{ perm}} \langle M_1 M_2 \rangle \langle M_3 M_4 \rangle \\
&+ \sum_{6 \text{ perm}} \langle M_1 M_2 \rangle \langle M_3 \rangle \langle M_4 \rangle - \langle M_1 \rangle \langle M_2 \rangle \langle M_3 \rangle \langle M_4 \rangle \, ,
\end{aligned} \tag{3.6}
$$

with $M_1 = \bar{B}_1 A_a$, $M_2 = \bar{B}_2 A_b$, $M_3 = \Theta_1 B_1 A_c$, $M_4 = \Theta_2 B_2 A_d$. The arrangements $\langle \bar{B}\bar{B}B \rangle \langle B \rangle$ and $\langle \bar{B}\bar{B} \rangle \langle B \rangle \langle B \rangle$ arise by charge conjugation from the monomials X^4 and X^6 and therefore do not need to be included explicitly.

1 The product rule reads $D^\mu(A_a A_b) = A_a (D^\mu A_b) + (A_a \overleftarrow{D}^\mu) A_b$ with $A \overleftarrow{D}^\mu := D^\mu A$. We also use the relation $\partial_\mu \langle \dots \rangle = \langle D_\mu (\dots) \rangle$ for trace terms.

Transformation behavior of monomials X^i under parity

Each monomial X^i in the list of Eq. (3.3) transforms under parity as

$$(X^i)^P = (-1)^{p_A + p_{\Gamma_1} + p_{\Gamma_2} + n_\epsilon} X^i = (-1)^p X^i \,, \tag{3.7}$$

where p_A is the sum of parity exponents of the external fields $p_A = \sum_{j=a,b,c,d,\ldots} p_{A_j}$ (cf. Tab. 2.2(a)). Likewise, p_{Γ_i} is the parity exponent of the Dirac algebra element in Θ_i (cf. Tab. 2.2(b)), deduced from the transformation $\bar\Psi\Gamma\Phi \xrightarrow{P} \bar\Psi\gamma_0\Gamma\gamma_0\Phi$, and n_ϵ counts the number of Levi-Civita tensors in the monomial X^i . The counting rule for the sign in Eq. (3.7) holds, because all Lorentz indices of the building blocks and also of the Dirac algebra basis elements transform as $I_\mu^P = \pm {P^\nu}_\mu I_\nu$ with $({P^\nu}_\mu) = \mathrm{diag}(+1,-1,-1,-1)$ and therefore[2]

$$I_\mu^P J^{\mu,P} = \pm I_\rho {P^\rho}_\mu {P^\mu}_\nu J^\nu = \pm I_\mu J^\mu \,. \tag{3.8}$$

With inclusion of the Lorentz indices we have the tensorial structures $A_{\mu(\nu)}$, D_μ, $\Gamma_{\mu(\nu)}$, $g_{\mu\nu}$, $\epsilon_{\mu\nu\rho\sigma}$, where the metric $g_{\mu\nu}$ can be dropped, since it merely raises or lowers indices. Because of the relation

$${P^\mu}_{\mu'} {P^\nu}_{\nu'} {P^\rho}_{\rho'} {P^\sigma}_{\sigma'} \epsilon^{\mu'\nu'\rho'\sigma'} = \det(P)\epsilon^{\mu\nu\rho\sigma} = -\epsilon^{\mu\nu\rho\sigma} \,, \tag{3.9}$$

one gets a minus sign for each ϵ-tensor that appears in a monomial term.

Transformation behavior of monomials X^i under charge conjugation

Here, we analyze the transformation behavior of the monomials X^i listed in Eq. (3.3) under charge conjugation. The symbol $\top$ denotes transposition of matrices in Dirac space as well as in flavor space. For the first monomial X^1 one gets

$$\begin{aligned}
(X^1)^C &= \Big(\hat D_2^k \,\langle \bar B_1 A_a \Theta_1 B_1 A_b \bar B_2 A_c \Theta_2 B_2 A_d\rangle\Big)^C \\
&= (-1)^{c_A + c_{\Gamma_1} + c_{\Gamma_2}} \hat D_2^k \,\langle B_1^\top A_a^\top (\bar B_1 \overleftarrow{\Theta}_1)^\top A_b^\top B_2^\top A_c^\top (\bar B_2 \overleftarrow{\Theta}_2)^\top A_d^\top\rangle \\
&= (-1)^{c_A + c_{\Gamma_1} + c_{\Gamma_2}} \hat D_2^k \,\langle A_d \bar B_2 \overleftarrow{\Theta}_2 A_c B_2 A_b \bar B_1 \overleftarrow{\Theta}_1 A_a B_1\rangle \\
&= (-1)^{c} \hat D_2^k \,\langle \bar B_1 \overleftarrow{\Theta}_1 A_a B_1 A_d \bar B_2 \overleftarrow{\Theta}_2 A_c B_2 A_b\rangle \\
&= (-1)^{c+n_1+n_2} X^1_{b\leftrightarrow d} + \text{h.o.} \,,
\end{aligned} \tag{3.10}$$

where we have used in the first step $B^C = C\bar B^\top$ and $\bar B^C = -B^\top C^{-1}$, with $C = \mathrm{i}\gamma^2\gamma^0$, cf. Eq. (2.4). The relations $C^{-1}\Gamma_i C = (-1)^{c_{\Gamma_i}}\Gamma_i^\top$, $A_i^C = (-1)^{c_i} A_i^\top$ and $D_\mu^C A^\top = (D_\mu A)^\top$ give the charge conjugation for Dirac matrices, external fields and covariant derivatives, cf. Eqs. (2.47) and (2.48). One obtains the exponents $c_A = \sum_{j=a,b,c,d,\ldots} c_{A_j}$ and $c = c_A + c_{\Gamma_1} + c_{\Gamma_2} \in \{0,1\}$. In the step from the second to the third line one uses the relation $\Psi^\top \Gamma^\top \bar\Phi^\top = \Psi_\alpha \Gamma_{\beta\alpha} \bar\Phi_\beta = -\bar\Phi\Gamma\Psi$ for bilinears in Dirac space and the relation $(A^\top B^\top C^\top \ldots) = (\ldots CBA)^\top$ for flavor matrices, together with $\langle A^\top\rangle = \langle A\rangle$. The notation $\overleftarrow{\Theta}_i = \overleftarrow{D}^{n_i}\Gamma_i$ indicates that the covariant derivatives act on the baryon field to the left. For the last equality we used the product rule Eq. (3.5) and the abbreviation h.o. denotes higher order terms.

2 Covariant derivatives transform as four-vectors under parity, $(D^\mu A)^P = {P^\mu}_\nu (D^\nu A^P)$.

Similarly, one finds for the monomials X^2, X^3 and X^4:

$$\begin{aligned}(X^2)^C &= (-1)^c \hat{D}_2^k \langle \bar{B}_2 \overleftarrow{\Theta}_2 A_c \bar{B}_1 \overleftarrow{\Theta}_1 A_b B_2 A_a B_1 A_d \rangle \\ &= (-1)^{c+n_1+n_2+k} X^2{}_{\substack{a\leftrightarrow c \\ \Gamma_1\leftrightarrow\Gamma_2 \\ n_1\leftrightarrow n_2}} + \text{h.o.}\,, \end{aligned} \tag{3.11}$$

$$\begin{aligned}(X^3)^C &= (-1)^c \hat{D}_2^k \langle \bar{B}_1 \overleftarrow{\Theta}_1 A_a B_1 A_b \rangle \langle \bar{B}_2 \overleftarrow{\Theta}_2 A_c B_2 A_d \rangle \\ &= (-1)^{c+n_1+n_2} X^3 + \text{h.o.}\,, \end{aligned} \tag{3.12}$$

$$(X^4)^C = (-1)^c \hat{D}_2^k \langle \bar{B}_2 \overleftarrow{\Theta}_2 A_c B_2 A_b \bar{B}_1 \overleftarrow{\Theta}_1 A_d \rangle \langle B_1 A_a \rangle\,. \tag{3.13}$$

At this point one can see that every term of the schematic form $\langle \bar{B}B\bar{B}\rangle\langle B\rangle$ can be written as the charge-conjugate of a term of the form $\langle \bar{B}\rangle\langle B\bar{B}B\rangle$ (and vice versa). Since only charge conjugation invariant terms $X + X^C$ are allowed, it is sufficient to consider only the form $\langle \bar{B}\rangle\langle B\bar{B}B\rangle$, i.e., terms of the type X^4. We continue with the charge conjugation properties of the monomials X^5 and X^6:

$$\begin{aligned}(X^5)^C &= (-1)^c \hat{D}_2^k \langle \bar{B}_1 \overleftarrow{\Theta}_1 A_a B_1 A_b \rangle \langle \bar{B}_2 \overleftarrow{\Theta}_2 A_d \rangle \langle B_2 A_c \rangle \\ &= (-1)^{c+n_1+n_2} X^5_{c\leftrightarrow d} + \text{h.o.}\,, \end{aligned} \tag{3.14}$$

$$(X^6)^C = (-1)^c \hat{D}_2^k \langle \bar{B}_2 \overleftarrow{\Theta}_2 A_c \bar{B}_1 \overleftarrow{\Theta}_1 A_d \rangle \langle B_2 A_b \rangle \langle B_1 A_a \rangle\,. \tag{3.15}$$

As before, the schematic forms $\langle \bar{B}\bar{B}\rangle\langle B\rangle\langle B\rangle$ and $\langle \bar{B}\rangle\langle \bar{B}\rangle\langle BB\rangle$ are connected by charge conjugation. Therefore it is sufficient to consider only $\langle \bar{B}\bar{B}\rangle\langle B\rangle\langle B\rangle$, i.e., terms of the type X^6. Finally, the charge conjugation property of X^7 is

$$\begin{aligned}(X^7)^C &= (-1)^c \hat{D}_2^k \langle \bar{B}_1 \overleftarrow{\Theta}_1 A_b \rangle \langle B_1 A_a \rangle \langle \bar{B}_2 \overleftarrow{\Theta}_2 A_d \rangle \langle B_2 A_c \rangle \\ &= (-1)^{c+n_1+n_2} X^7{}_{\substack{a\leftrightarrow b \\ c\leftrightarrow d}} + \text{h.o.}\,. \end{aligned} \tag{3.16}$$

For terms with additional traces multiplied to X^i (see Eq. (3.3)) the behavior under charge conjugation follows as

$$(X^i \cdot \langle A_e\rangle \cdot \langle A_f\rangle \cdot \ldots)^C = (-1)^{c_e+c_f+\cdots} (X^i)^C \cdot \langle A_e\rangle \cdot \langle A_f\rangle \cdot \ldots\,. \tag{3.17}$$

Transformation behavior of monomials X^i under Hermitian conjugation

Now we consider the transformation behavior of the monomials X^i listed in Eq. (3.3) under Hermitian conjugation. For the first monomial X^1 we have

$$\begin{aligned}(X^1)^* &= \hat{D}_2^k \langle \bar{B}_1 A_a \Theta_1 B_1 A_b \bar{B}_2 A_c \Theta_2 B_2 A_d \rangle^* \\ &= \hat{D}_2^k \langle A_d^\dagger B_2^\dagger \overleftarrow{\Theta}_2^\dagger A_c^\dagger \bar{B}_2^\dagger A_b^\dagger B_1^\dagger \overleftarrow{\Theta}_1^\dagger A_a^\dagger \bar{B}_1^\dagger \rangle \\ &= (-1)^{h_A+h_{\Gamma_1}+h_{\Gamma_2}} \hat{D}_2^k \langle A_d \bar{B}_2 \overleftarrow{\Theta}_2 A_c B_2 A_b \bar{B}_1 \overleftarrow{\Theta}_1 A_a B_1 \rangle \\ &= (-1)^h \hat{D}_2^k \langle \bar{B}_1 \overleftarrow{\Theta}_1 A_a B_1 A_d \bar{B}_2 \overleftarrow{\Theta}_2 A_c B_2 A_b \rangle \\ &= (-1)^{h+n_1+n_2} X^1_{b\leftrightarrow d} + \text{h.o.}\,, \end{aligned} \tag{3.18}$$

where we used in the first step the relations $\langle A^* \rangle = \langle A^\dagger \rangle$, $(ABC\dots)^\dagger = (\dots C^\dagger B^\dagger A^\dagger)$ for flavor matrices and the relation $(\bar\Psi \Gamma \Phi)^* = (\bar\Psi \Gamma \Phi)^\dagger = \Phi^\dagger \Gamma^\dagger \bar\Psi^\dagger$ for (mixed) baryon bilinears. Covariant derivatives follow the rule $(D^\mu A)^\dagger = A^\dagger \overleftarrow{D}^\mu$, and the notation $\overleftarrow{\Theta}_i^\dagger = \overleftarrow{D}^{n_i} \Gamma_i^\dagger$ means that the Hermitian conjugate of Θ_i acts only on the Dirac matrix. In the second step we used the properties $A_i^\dagger = (-1)^{h_i} A_i$ and $\gamma_0 \Gamma_i^\dagger \gamma_0 = (-1)^{h_{\Gamma_i}} \Gamma_i$, cf. Eqs. (2.47) and (2.48). One obtains the exponents $h_A = \sum_{j=a,b,c,d,\dots} h_{A_j}$ and $h = h_A + h_{\Gamma_1} + h_{\Gamma_2} \in \{0, 1\}$. In the last step the product rule Eq. (3.5) has been employed.

Just as for the monomial X^1, the transformation behavior under Hermitian conjugation of the other monomials X^i is given by the replacement of the exponents $c \to h$ in the transformation under charge conjugation.

3.2 RESULTS FOR CHIRAL CONTACT TERMS

In this section we apply the rules for constructing a chiral Lagrangian to obtain a complete set of three-flavor contact terms up to order $\mathcal{O}(q^2)$. We define for an arbitrary monomial X the charge conjugation invariant combination $Y = X + X^C$. It transforms under parity as $(Y)^P = (-1)^p Y$, since X and X^C transform into themselves up to a sign factor $(-1)^{p_X}$. The behavior under Hermitian conjugation is $Y^* = (-1)^{c+h} Y$, since

$$(X + X^C)^* = X^* + X^{C*} = (-1)^{c+h}(X^C + X)\,. \tag{3.19}$$

Here the similar transformation behavior under charge conjugation and Hermitian conjugation led to the relation $X^* = (-1)^{c+h} X^C$. If Y transforms under Hermitian conjugation into its negative, one has to multiply it with a factor i. In the cases where $X^C = -X + \text{h.o.}$ one can drop these monomials, since Y is then zero to the considered order.

At a given order there are arbitrarily many terms with pairwise contracted covariant derivatives of the form

$$Y(\Theta_1 = \dots \cdot D_{\mu_1 \mu_2 \dots \mu_n}\,,\ \Theta_2 = \dots \cdot D^{\mu_1 \mu_2 \dots \mu_n})\,. \tag{3.20}$$

Following an argument of Ref. [113], one needs to take into account values for n only up to a finite number for the Lagrangian to order $\mathcal{O}(q^2)$. A term of the form in Eq. (3.20) gives rise to a matrix element $(\bar u_3 \Theta_1 u_1)(\bar u_4 \Theta_2 u_2)$, where every contracted pair of D's produces a factor $p_1 \cdot p_2$. Up to $\mathcal{O}(q^2)$ one can approximate its n-th power as

$$(p_1 \cdot p_2)^n \approx (M_0)^{2n} \left[1 + \frac{n}{2M_0^2}(\vec p_1 - \vec p_2)^2\right]\,, \tag{3.21}$$

and therefore all n larger than 1 do not give rise to new structures. Because of the field Γ_μ (which is of $\mathcal{O}(q)$) in the covariant derivative one needs to go one order higher. At $\mathcal{O}(q^0)$ terms with $n = 0, 1, 2$ are needed, at $\mathcal{O}(q)$ terms with $n = 0, 1$ can contribute and at $\mathcal{O}(q^2)$ only terms with $n = 0$ need to be considered.

In order to avoid the construction of redundant terms, one uses the lowest-order equation of motion fulfilled by the baryon field

$$\not{D} B = -\mathrm{i} M_0 B + \mathcal{O}(q)\,, \tag{3.22}$$

and its Dirac conjugated. Up to higher order corrections one can replace $\not{D} B$ by $-\mathrm{i} M_0 B$ and $\bar B \overleftarrow{\not{D}}$ by $\mathrm{i} M_0 \bar B$. Beyond the obvious replacements one can bring terms not containing

$\not{D}B$ into a form where they do. Following closely Ref. [112], where this method has been applied to the πN Lagrangian, a systematic use of the equation of motion can be summarized by the following restrictions for remaining independent terms, where Θ^i is a general Dirac operator in the baryon bilinear i:

- Γ of Θ^i is a matrix from the set $\{\mathbb{1}, \gamma_5\gamma_\mu, \sigma_{\mu\nu}\}$ with possible additional $g_{\mu\nu}$ and $\epsilon_{\mu\nu\rho\tau}$ factors,
- Lorentz indices within Θ^i must not be contracted, with the exception of one index of an $\epsilon_{\mu\nu\rho\tau}$-tensor, which has then to be contracted with $D^n_{\mu\ldots}$.
- $\hat{D}^\mu_2$ must not be contracted with any $D^n_{\mu\ldots}$ or with $\sigma_{\mu\nu}$.

The generalized proof for these rules can be found in our work Ref. [103].

Furthermore, by using the lowest-order equation of motion satisfied by the mesons,

$$D_\mu u^\mu = \frac{\mathrm{i}}{2}\left(\chi_- - \frac{1}{3}\langle\chi_-\rangle\right) , \tag{3.23}$$

one can get rid of terms including $h_\mu{}^\mu = D_\mu u^\mu + D^\mu u_\mu$ (see Eq. (2.51)).

Via the Feynman rules the baryon-baryon contact terms get translated into matrix elements of the form $(\bar{u}_3\Gamma_1 u_1)(\bar{u}_4\Gamma_2 u_2)$ with additional momentum factors from derivatives, with u the well-known free Dirac spinors. Let us now comment on the non-relativistic reduction, where one expands the baryon bilinears in the inverse large baryon mass. A derivative acting on a baryon field, $D_\mu B$, is counted of order $\mathcal{O}(q^0)$ for $\mu = 0$ and of order $\mathcal{O}(q^1)$ for $\mu = 1, 2, 3$. If a derivative D_μ is contracted with one of the Dirac matrices $\gamma_5\gamma^\mu$ or $\sigma^{\mu\nu}$ the matrix element has no order $\mathcal{O}(q^0)$ contribution, since $\bar{u}_i\gamma_5\gamma^0 u_j = \mathcal{O}(q^1)$ and $\bar{u}_i\sigma^{0\nu}u_j = \mathcal{O}(q^1)$ (see Appendix A.1). The corresponding term starts in the non-relativistic power counting at least one order higher than in the covariant power counting, proportional to q/M_0. The same argument holds for the product operator $\epsilon^{\mu\nu\rho\tau}\mathbb{1}D_\rho \otimes \mathbb{1}D_\tau$ sandwiched between Dirac spinors. The leading components from the index combination $\rho = \tau = 0$ gets nullified by the antisymmetric ϵ-tensor. In the following tables we will label such suppressed terms by an asterisk $\star$. It is still possible that independent terms in the covariant power counting become equal in the non-relativistic power counting, even though none of them is suppressed. This leads to a further reduction of independent terms and associated low-energy constants.

3.2.1 *Baryon-baryon contact terms of* $\mathcal{O}(q^0)$

At order $\mathcal{O}(q^0)$ only terms of the type $X^{1,2,3}$ contribute, since there are no external fields present, and $\langle B\rangle = \langle\bar{B}\rangle = 0$. The leading-order three-flavor contact Lagrangian has 15 terms and is given by

$$\mathscr{L}^{(0)}_{BB} = \sum_{i=1}^{5}\left(a_{1,i}\hat{\mathcal{A}}^1_i + a_{2,i}\hat{\mathcal{A}}^2_i + a_{3,i}\hat{\mathcal{A}}^3_i\right) , \tag{3.24}$$

with the flavor structures

$$\begin{aligned}
\hat{\mathcal{A}}^1_i &= \langle\bar{B}_1\theta^i B_1\bar{B}_2\xi^i B_2\rangle + \langle\bar{B}_1\overleftarrow{\theta}^i B_1\bar{B}_2\overleftarrow{\xi}^i B_2\rangle\,,\\
\hat{\mathcal{A}}^2_i &= \langle\bar{B}_1\bar{B}_2\theta^i B_1\xi^i B_2\rangle + \langle\bar{B}_1\overleftarrow{\xi}^i\bar{B}_2\overleftarrow{\theta}^i B_1 B_2\rangle\,,\\
\hat{\mathcal{A}}^3_i &= \langle\bar{B}_1\theta^i B_1\rangle\langle\bar{B}_2\xi^i B_2\rangle + \langle\bar{B}_1\overleftarrow{\theta}^i B_1\rangle\langle\bar{B}_2\overleftarrow{\xi}^i B_2\rangle\,,
\end{aligned} \tag{3.25}$$

θ^i	ξ^i	NR	contributes to $\hat{\mathcal{A}}^j$
$\mathbb{1}$	$\mathbb{1}$		$1,2,3$
$\gamma_5\gamma^\mu$	$\gamma_5\gamma_\mu$		$1,2,3$
$\gamma_5\gamma^\mu D^\nu$	$\gamma_5\gamma_\nu D_\mu$	$\star$	$1,2,3$
$\sigma^{\mu\nu}$	$\sigma_{\mu\nu}$		$1,2,3$
$\sigma^{\mu\nu}D^\rho$	$\sigma_{\mu\rho}D_\nu$	$\star$	$1,2,3$

TABLE 3.1: Dirac operators θ^i and ξ^i for contact terms of $\mathcal{O}(q^0)$. An asterisk $\star$ in the column NR denotes structures which contribute at higher order in the non-relativistic expansion. The last column shows, to which flavor structures these operators contribute.

and the operators θ^i, ξ^i given in Tab. 3.1. The real parameters $a_{j,i}$ are the associated low-energy constants. As in Ref. [101] we choose the terms to be exactly invariant under charge and Hermitian conjugation, and not just invariant to leading order. Therefore both summands in Eq. (3.25) are needed. As stated above additionally the Dirac operators in Tab. 3.1 with one contracted pair of covariant derivatives (e.g. $\sigma^{\mu\nu}D^\rho \otimes \sigma_{\mu\nu}D_\rho$) and with two contracted pairs (e.g. $\sigma^{\mu\nu}D^{\rho\tau} \otimes \sigma_{\mu\nu}D_{\rho\tau}$) have to be included.

Considering this Lagrangian in the non-relativistic approximation for baryon-baryon scattering, we recover the results of Ref. [25]. Dirac operators such as $\sigma^{\mu\nu}\partial^\rho \otimes \sigma_{\mu\nu}\partial_\rho$ give in leading order the same contribution as the ones without contracted derivatives, but differ at higher order. To leading order in the non-relativistic expansion the only contributions come from the Dirac operators $\mathbb{1} \otimes \mathbb{1}$ and $\gamma_5\gamma^\mu \otimes \gamma_5\gamma_\mu$. The others are either of higher order or give contributions equal to these two. As a result one has six independent non-relativistic contact terms at leading order. This is consistent with group theoretical considerations, where the product of two (baryon) octets is decomposed into a sum of six irreducible SU(3) representations, $\mathbf{8} \otimes \mathbf{8} = \mathbf{27}_s \oplus \mathbf{10}_a \oplus \mathbf{10}^*{}_a \oplus \mathbf{8}_s \oplus \mathbf{8}_a \oplus \mathbf{1}_s$. The symmetric and antisymmetric flavor representation are combined with the spin singlet and spin triplet states, respectively. The parameters of the leading order Lagrangian $\mathscr{L}^{(0)}_{BB}$ can be combined to the low-energy constants for irreducible SU(3) representations and spin multiplets, which will be used in Tab. 4.2 of Chapter 4. The corresponding relations read:

$$
\begin{aligned}
\tilde{c}^{27}_{{}^1S_0} &= 8\pi\left[2(a_{1,1}+3a_{1,2})+2(a_{3,1}+3a_{3,2})\right] , \\
\tilde{c}^{8s}_{{}^1S_0} &= 8\pi\left[-\frac{4}{3}(a_{1,1}+3a_{1,2})-\frac{5}{3}(a_{2,1}+3a_{2,2})+2(a_{3,1}+3a_{3,2})\right] , \\
\tilde{c}^{1}_{{}^1S_0} &= 8\pi\left[-\frac{2}{3}(a_{1,1}+3a_{1,2})-\frac{16}{3}(a_{2,1}+3a_{2,2})+2(a_{3,1}+3a_{3,2})\right] , \\
\tilde{c}^{8a}_{{}^3S_1} &= 8\pi\left[3(a_{2,1}-a_{2,2})+2(a_{3,1}-a_{3,2})\right] , \\
\tilde{c}^{10}_{{}^3S_1} &= 8\pi\left[-2(a_{1,1}-a_{1,2})+2(a_{3,1}-a_{3,2})\right] , \\
\tilde{c}^{10^*}_{{}^3S_1} &= 8\pi\left[2(a_{1,1}-a_{1,2})+2(a_{3,1}-a_{3,2})\right] .
\end{aligned}
\tag{3.26}
$$

3.2.2 *Baryon-baryon contact terms of* $\mathcal{O}(q^1)$

The Lagrangian of order $\mathcal{O}(q^1)$ can be constructed by including a covariant derivative $\hat{D}^\alpha_2$ or a field u^α, but not both. When including the covariant derivative, one needs to consider again only terms of the type $X^{1,2,3}$, due to the tracelessness of the baryon fields. However,

the restrictions through the equation of motion and the special structure of the monomials X^1 and X^3 allow in the end for only two terms of type X^2. They read

$$\begin{aligned}\mathscr{L}^{(1)}_{BB} = \quad & b_1\big(\hat{D}^\alpha_2\langle\bar{B}_1\bar{B}_2(\gamma_5\gamma_\alpha D_\mu B_1)(\gamma_5\gamma^\mu B_2)\rangle \\ & \qquad + \hat{D}^\alpha_1\langle(\bar{B}_1\gamma_5\gamma^\mu)(\bar{B}_2\overleftarrow{D}_\mu\gamma_5\gamma_\alpha)B_1B_2\rangle\big) \\ & + b_2\big(\hat{D}^\alpha_2\langle\bar{B}_1\bar{B}_2(\gamma_5\gamma_\alpha D_{\mu\nu} B_1)(\gamma_5\gamma^\mu D^\nu B_2)\rangle \\ & \qquad + \hat{D}^\alpha_1\langle(\bar{B}_1\overleftarrow{D}_\nu\gamma_5\gamma^\mu)(\bar{B}_2\overleftarrow{D}_{\mu\nu}\gamma_5\gamma_\alpha)B_1B_2\rangle\big)\,, \end{aligned} \tag{3.27}$$

with b_1 and b_2 new low-energy constants. In the non-relativistic approximation these terms start to contribute at $\mathcal{O}(q^2)$. This behavior agrees with the fact, that parity conservation excludes any pure baryon-baryon contact terms at order $\mathcal{O}(q^1)$. The second term differs only from the first term, if additional mesons are involved.

The other possibility to obtain terms at order $\mathcal{O}(q^1)$ is to include the chiral building block u^α. The corresponding terms can be of the type $X^{1,2,3,4}$ with less than three flavor traces. They describe baryon-baryon contact interactions including additional Goldstone-boson fields. In total one can construct 67 terms for the Lagrangian,

$$\begin{aligned}\mathscr{L}^{(1)}_{BB} = & \sum_{i=1}^{3} c_{1,i}\hat{\mathcal{C}}^1_i + \sum_{i=1}^{7} c_{2,i}\hat{\mathcal{C}}^2_i + \sum_{i=1}^{3} c_{3,i}\hat{\mathcal{C}}^3_i + \sum_{i=1}^{7} c_{4,i}\hat{\mathcal{C}}^4_i + \sum_{i=1}^{7} c_{5,i}\hat{\mathcal{C}}^5_i \\ & + \sum_{i=1}^{7} c_{6,i}\hat{\mathcal{C}}^6_i + \sum_{i=1}^{7} c_{7,i}\hat{\mathcal{C}}^7_i + \sum_{i=1}^{3} c_{8,i}\hat{\mathcal{C}}^8_i + \sum_{i=1}^{3} c_{9,i}\hat{\mathcal{C}}^9_i + \sum_{i=1}^{3} c_{10,i}\hat{\mathcal{C}}^{10}_i \\ & + \sum_{i=1}^{3} c_{11,i}\hat{\mathcal{C}}^{11}_i + \sum_{i=1}^{7} c_{12,i}\hat{\mathcal{C}}^{12}_i + \sum_{i=1}^{7} c_{13,i}\hat{\mathcal{C}}^{13}_i\,. \end{aligned} \tag{3.28}$$

The general flavor structures for terms with one chiral building block A inserted are

$$\begin{aligned}
\hat{\mathcal{C}}^1_i &= \langle\bar{B}_1\,A\,\theta^i B_1\bar{B}_2\xi^i B_2\rangle + (-1)^{c_i}\langle\bar{B}_1\overleftarrow{\theta}^i\,A\,B_1\bar{B}_2\overleftarrow{\xi}^i B_2\rangle,\\
\hat{\mathcal{C}}^2_i &= \langle\bar{B}_1\theta^i B_1\,A\,\bar{B}_2\xi^i B_2\rangle + (-1)^{c_i}\langle\bar{B}_1\overleftarrow{\theta}^i B_1\bar{B}_2\overleftarrow{\xi}^i B_2\,A\,\rangle,\\
\hat{\mathcal{C}}^3_i &= \langle\bar{B}_1\,A\,\xi^i B_1\bar{B}_2\theta^i B_2\rangle + (-1)^{c_i}\langle\bar{B}_1\overleftarrow{\xi}^i\,A\,B_1\bar{B}_2\overleftarrow{\theta}^i B_2\rangle,\\
\hat{\mathcal{C}}^4_i &= \langle\bar{B}_1\,A\,\bar{B}_2\theta^i B_1\xi^i B_2\rangle + (-1)^{c_i}\langle\bar{B}_1\overleftarrow{\xi}^i\bar{B}_2\overleftarrow{\theta}^i B_1\,A\,B_2\rangle,\\
\hat{\mathcal{C}}^5_i &= \langle\bar{B}_1\bar{B}_2\,A\,\theta^i B_1\xi^i B_2\rangle + (-1)^{c_i}\langle\bar{B}_1\overleftarrow{\xi}^i\bar{B}_2\overleftarrow{\theta}^i\,A\,B_1B_2\rangle,\\
\hat{\mathcal{C}}^6_i &= \langle\bar{B}_1\,A\,\bar{B}_2\xi^i B_1\theta^i B_2\rangle + (-1)^{c_i}\langle\bar{B}_1\overleftarrow{\theta}^i\bar{B}_2\overleftarrow{\xi}^i B_1\,A\,B_2\rangle,\\
\hat{\mathcal{C}}^7_i &= \langle\bar{B}_1\bar{B}_2\theta^i B_1\xi^i B_2\,A\,\rangle + (-1)^{c_i}\langle\bar{B}_1\overleftarrow{\xi}^i\bar{B}_2\overleftarrow{\theta}^i B_1B_2\,A\,\rangle,\\
\hat{\mathcal{C}}^8_i &= \langle\bar{B}_1\,A\,\theta^i B_1\rangle\langle\bar{B}_2\xi^i B_2\rangle + (-1)^{c_i}\langle\bar{B}_1\overleftarrow{\theta}^i\,A\,B_1\rangle\langle\bar{B}_2\overleftarrow{\xi}^i B_2\rangle,\\
\hat{\mathcal{C}}^9_i &= \langle\bar{B}_1\theta^i B_1\,A\,\rangle\langle\bar{B}_2\xi^i B_2\rangle + (-1)^{c_i}\langle\bar{B}_1\overleftarrow{\theta}^i B_1\,A\,\rangle\langle\bar{B}_2\overleftarrow{\xi}^i B_2\rangle,\\
\hat{\mathcal{C}}^{10}_i &= \langle\bar{B}_1\,A\,\xi^i B_1\rangle\langle\bar{B}_2\theta^i B_2\rangle + (-1)^{c_i}\langle\bar{B}_1\overleftarrow{\xi}^i\,A\,B_1\rangle\langle\bar{B}_2\overleftarrow{\theta}^i B_2\rangle,\\
\hat{\mathcal{C}}^{11}_i &= \langle\bar{B}_1\xi^i B_1\,A\,\rangle\langle\bar{B}_2\theta^i B_2\rangle + (-1)^{c_i}\langle\bar{B}_1\overleftarrow{\xi}^i B_1\,A\,\rangle\langle\bar{B}_2\overleftarrow{\theta}^i B_2\rangle\\
\hat{\mathcal{C}}^{12}_i &= \langle\bar{B}_1\,A\,\rangle\langle\theta^i B_1\bar{B}_2\xi^i B_2\rangle + (-1)^{c_i}\langle\bar{B}_2\overleftarrow{\xi}^i B_2\bar{B}_1\overleftarrow{\theta}^i\rangle\langle B_1\,A\,\rangle,\\
\hat{\mathcal{C}}^{13}_i &= \langle\bar{B}_1\,A\,\rangle\langle\xi^i B_1\bar{B}_2\theta^i B_2\rangle + (-1)^{c_i}\langle\bar{B}_2\overleftarrow{\theta}^i B_2\bar{B}_1\overleftarrow{\xi}^i\rangle\langle B_1\,A\,\rangle,
\end{aligned}$$

$$\hat{\mathcal{C}}_i^{14} = \langle \bar{B}_1 \theta^i B_1 \bar{B}_2 \xi^i B_2 \rangle \langle A \rangle + (-1)^{c_i} \langle \bar{B}_1 \overleftarrow{\theta}^i B_1 \bar{B}_2 \overleftarrow{\xi}^i B_2 \rangle \langle A \rangle,$$
$$\hat{\mathcal{C}}_i^{15} = \langle \bar{B}_1 \bar{B}_2 \theta^i B_1 \xi^i B_2 \rangle \langle A \rangle + (-1)^{c_i} \langle \bar{B}_1 \overleftarrow{\xi}^i \bar{B}_2 \overleftarrow{\theta}^i B_1 B_2 \rangle \langle A \rangle,$$
$$\hat{\mathcal{C}}_i^{16} = \langle \bar{B}_1 \theta^i B_1 \rangle \langle \bar{B}_2 \xi^i B_2 \rangle \langle A \rangle + (-1)^{c_i} \langle \bar{B}_1 \overleftarrow{\theta}^i B_1 \rangle \langle \bar{B}_2 \overleftarrow{\xi}^i B_2 \rangle \langle A \rangle \,. \tag{3.29}$$

In the present case $A = u^\alpha$, and the operators θ^i, ξ^i and the corresponding exponents c_i are given in Tab. 3.2. Not all operators contribute to each flavor structure, e.g., if $X^C = -X + \text{h.o.}$, or if one flavor structure is equal to another one up to higher order terms. For the same reasons, the exchanged combinations with $\theta^i \leftrightarrow \xi^i$ need not to be considered for all flavor structures. The flavor structures $\hat{\mathcal{C}}_i^{14-16}$ do not appear, since u^α is traceless. All Dirac operators in Tab. 3.2, except the combinations $\mathbb{1} \otimes \gamma_5\gamma_\alpha$ and $\gamma_5\gamma^\mu \otimes \sigma_{\alpha\mu}$, contribute in the non-relativistic expansion first at $\mathcal{O}(q^2)$. These criteria lead to 20 terms in the non-relativistic power counting. It is worth to note that in the two-flavor case (with pions and nucleons only) one gets from this list of terms the frequently used $4N\pi$ contact vertex proportional to the low-energy constant c_D. It determines the mid-range 1π-exchange component of the leading-order chiral three-nucleon interaction (see Chapter 6).

If more mesons are involved in addition to the Dirac operators in Tab. 3.2 the same operators with one contracted pair of covariant derivatives have to be included, e.g., $\mathbb{1} \cdot D_\alpha{}^{\mu\nu} \otimes \gamma_5\gamma_\mu D_\nu$. Their properties ($c_i$, NR, $\hat{\mathcal{C}}^j$) are the same as for the ones without the contracted pair in Tab. 3.2.

θ^i	ξ^i	c_i	NR	contributes to $\hat{\mathcal{C}}^j$ with $A = u^\alpha$
$\mathbb{1} \cdot D_\alpha{}^\mu$	$\gamma_5\gamma_\mu$	0	$\star$	1-13
$\mathbb{1} \cdot D^\mu$	$\gamma_5\gamma_\mu D_\alpha$	0	$\star$	1-13
$\mathbb{1}$	$\gamma_5\gamma_\alpha$	0		1-13
i $\gamma_5\gamma^\mu D_\alpha{}^\nu$	$\sigma_{\mu\nu}$	1	$\star$	2,4,5,6,7,12,13
i $\gamma_5\gamma^\mu$	$\sigma_{\alpha\mu}$	1		2,4,5,6,7,12,13
i $\gamma_5\gamma^\mu D^\nu$	$\sigma_{\alpha\nu} D_\mu$	1	$\star$	2,4,5,6,7,12,13
i $\gamma_5\gamma^\mu D^\nu$	$\sigma_{\mu\nu} D_\alpha$	1	$\star$	2,4,5,6,7,12,13

TABLE 3.2: Dirac operators θ^i and ξ^i for contact terms of $\mathcal{O}(q^1)$ with one field u^α, and associated charge conjugation exponents c_i. An asterisk $\star$ in the column NR denotes structures which are of higher order in the non-relativistic power counting. The last column shows, to which flavor structures these operators contribute.

3.2.3 *Baryon-baryon contact terms of $\mathcal{O}(q^2)$*

In the following we construct the baryon-baryon contact Lagrangian at $\mathcal{O}(q^2)$. In the non-relativistic limit the terms including Dirac operators marked by $\star$ do not contribute in a calculation up to $\mathcal{O}(q^2)$. Nevertheless, we have decided to include these terms for the sake of completeness and in order to give a complete description of the contact terms in the covariant power counting.

θ^i	ξ^i	NR	contributes to $\hat{\mathcal{D}}^j$
$g_{\alpha\beta}\mathbb{1}$	$\mathbb{1}$		1,2,3
$g_{\alpha\beta}\gamma_5\gamma^\mu$	$\gamma_5\gamma_\mu$		1,2,3
$g_{\alpha\beta}\gamma_5\gamma^\mu D^\nu$	$\gamma_5\gamma_\nu D_\mu$	$\star$	1,2,3
$g_{\alpha\beta}\sigma^{\mu\nu}$	$\sigma_{\mu\nu}$		1,2,3
$g_{\alpha\beta}\sigma^{\mu\nu}D^\rho$	$\sigma_{\mu\rho}D_\nu$	$\star$	1,2,3
$\gamma_5\gamma_\alpha$	$\gamma_5\gamma_\beta$		1,2,3

TABLE 3.3: Dirac operators θ^i and ξ^i for contact terms of $\mathcal{O}(q^2)$ without external fields. An asterisk $\star$ in the column NR indicates structures which are at higher order in non-relativistic power counting. The last column shows, to which flavor structures these operators contribute.

Terms without external fields

The first contributions to the Lagrangian of $\mathcal{O}(q^2)$ comes from terms with two derivatives of baryon bilinears and no external fields. They contribute to the pure baryon-baryon interaction. One obtains 18 such terms:

$$\mathscr{L}^{(2)}_{BB} = \sum_{i=1}^{6} \left(d_{1,i}\hat{\mathcal{D}}^1_i + d_{2,i}\hat{\mathcal{D}}^2_i + d_{3,i}\hat{\mathcal{D}}^3_i \right) , \tag{3.30}$$

which are similar to the $\mathcal{O}(q^0)$ terms,

$$\begin{aligned}
\hat{\mathcal{D}}^1_i &= \hat{D}_2^{\alpha\beta}\langle \bar{B}_1\theta^i B_1 \bar{B}_2 \xi^i B_2\rangle + \hat{D}_2^{\alpha\beta}\langle \bar{B}_1 \overleftarrow{\theta}^i B_1 \bar{B}_2 \overleftarrow{\xi}^i B_2\rangle, \\
\hat{\mathcal{D}}^2_i &= \hat{D}_2^{\alpha\beta}\langle \bar{B}_1\bar{B}_2\theta^i B_1 \xi^i B_2\rangle + \hat{D}_1^{\alpha\beta}\langle \bar{B}_1 \overleftarrow{\xi}^i \bar{B}_2 \overleftarrow{\theta}^i B_1 B_2\rangle, \\
\hat{\mathcal{D}}^3_i &= \hat{D}_2^{\alpha\beta}\langle \bar{B}_1\theta^i B_1\rangle\langle \bar{B}_2 \xi^i B_2\rangle + \hat{D}_2^{\alpha\beta}\langle \bar{B}_1 \overleftarrow{\theta}^i B_1\rangle\langle \bar{B}_2 \overleftarrow{\xi}^i B_2\rangle ,
\end{aligned} \tag{3.31}$$

with the operators θ^i, ξ^i given in Tab. 3.3. The structures $g_{\alpha\beta}\gamma_5\gamma^\mu D^\nu \otimes \gamma_5\gamma_\nu D_\mu$ and $g_{\alpha\beta}\sigma^{\mu\nu}D^\rho \otimes \sigma_{\mu\rho}D_\nu$ contribute in the non-relativistic counting at $\mathcal{O}(q^3)$ or higher. Therefore, one obtains at order $\mathcal{O}(q^2)$ 12 relevant terms in the non-relativistic power counting.

Terms including the external fields $\chi_\pm$

The terms including the external fields $\chi_\pm$ are similar to the $\mathcal{O}(q^1)$ terms including the field u_μ. When setting the external scalar field equal to the quark mass matrix, these terms describe chiral symmetry breaking four-baryon contact interactions. For χ_+ one finds in total 55 terms and for χ_- one has in total 24 terms. The Lagrangians for both cases read,

$$\mathscr{L}^{(2)}_{BB} = \sum_{i,j} c^+_{j,i}\hat{\mathcal{C}}^j_i(A \to \chi_+) , \qquad \mathscr{L}^{(2)}_{BB} = \sum_{i,j} c^-_{j,i}\hat{\mathcal{C}}^j_i(A \to \chi_-) , \tag{3.32}$$

with the flavor structures $\hat{\mathcal{C}}^j$ given in Eqs. (3.29). The operators θ^i and ξ^i for one insertion of χ_+ and χ_- are given in Tab. 3.4 and Tab. 3.5, respectively. In the non-relativistic power counting the number of χ_+ terms reduces to 33 and all χ_- terms are at least of order $\mathcal{O}(q^3)$.

θ^i	ξ^i	c_i	NR	contributes to $\hat{\mathcal{C}}^j$ with $A = \chi_+$
$\mathbb{1}$	$\mathbb{1}$	0		1,2,4,5,7,8,9,12,14,15,16
$\gamma_5\gamma^\mu$	$\gamma_5\gamma_\mu$	0		1,2,4,5,7,8,9,12,14,15,16
$\gamma_5\gamma^\mu D^\nu$	$\gamma_5\gamma_\nu D_\mu$	0	$\star$	1,2,4,5,7,8,9,12,14,15,16
$\sigma^{\mu\nu}$	$\sigma_{\mu\nu}$	0		1,2,4,5,7,8,9,12,14,15,16
$\sigma^{\mu\nu}D^\rho$	$\sigma_{\mu\rho}D_\nu$	0	$\star$	1,2,4,5,7,8,9,12,14,15,16

TABLE 3.4: Dirac operators θ^i and ξ^i for contact terms of $\mathcal{O}(q^2)$ with χ_+. An asterisk $\star$ in the column NR indicates structures which are at higher order in non-relativistic power counting. The last column shows, to which flavor structures these operators contribute.

θ^i	ξ^i	c_i	NR	contributes to $\hat{\mathcal{C}}^j$ with $A = \chi_-$
$\mathrm{i}\mathbb{1}\cdot D^\mu$	$\gamma_5\gamma_\mu$	0	$\star$	2,4,5,6,7,12,13,15
$\gamma_5\gamma^\mu D^\nu$	$\sigma_{\mu\nu}$	1	$\star$	1-16

TABLE 3.5: Dirac structures θ^i and ξ^i for contact terms of $\mathcal{O}(q^2)$ with χ_-. An asterisk $\star$ in the column NR indicates structures which are at higher order in non-relativistic power counting. The last column shows, to which flavor structures these operators contribute.

Terms including the fields $f_{\alpha\beta}^\pm$ and $h_{\alpha\beta}$

When using the traceless chiral building blocks $f_\pm^{\alpha\beta}$ and $h^{\alpha\beta}$, which count of order $\mathcal{O}(q^2)$, one obtains for each a contact Lagrangian,

$$\mathscr{L}_{BB}^{(2)} = \sum_{i,j} c'_{j,i}\hat{\mathcal{C}}_i^j\,, \tag{3.33}$$

with the (first thirteen) flavor structures $\hat{\mathcal{C}}^j$ $(j = 1,\ldots,13)$ listed in Eq. (3.29) and the substitution $A \to f_+^{\alpha\beta}, f_-^{\alpha\beta}, h^{\alpha\beta}$. The Dirac operators θ^i and ξ^i for $A = f_+^{\alpha\beta}$ are given in Tab. 3.7. Column 4 in that table gives the additional factor i, if it is necessary for recovering hermiticity. Column 5 gives the corresponding charge conjugation exponent c_i and column 6 shows the flavor structures to which the occurring Dirac operators can contribute. Table 3.6 gives the same information for the cases $A = f_-^{\alpha\beta}$ and $A = h^{\alpha\beta}$. One obtains in total 127, 137 and 139 terms with one external field $f_+^{\alpha\beta}$, $f_-^{\alpha\beta}$ and $h^{\alpha\beta}$, respectively. Many of the Dirac operators in Tab. 3.7 and Tab. 3.6 contribute in the non-relativistic counting first at $\mathcal{O}(q^3)$, and these are indicated by an asterisk $\star$ in the column NR. Examples for these are $\gamma_5\gamma_\alpha D^\mu \otimes \sigma_{\beta\mu}$ and $\epsilon_{\alpha\beta}{}^{\delta\rho}\mathbb{1}D_\delta \otimes \mathbb{1}D_\rho$. The number of $\mathcal{O}(q^2)$ terms in non-relativistic counting reduces then to 33, 40 and 40 terms with one external field $f_+^{\alpha\beta}$, $f_-^{\alpha\beta}$ and $h^{\alpha\beta}$, respectively. The terms with the field $h_{\alpha\beta}$ lead, e.g., to four-baryon vertices involving two pseudoscalar mesons, whereas the terms including the fields $f_{\alpha\beta}^\pm$ are for example important for four-baryon vertices involving photons.

Terms with one field u_μ

The terms of order $\mathcal{O}(q^2)$ with one field u^α and hence with an additional covariant derivative $\hat{D}_2^\beta$, have the same flavor structure as the $\mathcal{O}(q^1)$ terms with one field u^α. The pertinent part of the contact Lagrangian is

$$\mathscr{L}_{BB}^{(2)} = \sum_{i,j} e_{j,i} \hat{\mathcal{E}}_i^j \,, \tag{3.34}$$

with the flavor structures

$$\begin{aligned}
\hat{\mathcal{E}}_i^1 &= \hat{D}_2^\beta \langle \bar{B}_1 u^\alpha \theta^i B_1 \bar{B}_2 \xi^i B_2 \rangle + (-1)^{c_i} \hat{D}_2^\beta \langle \bar{B}_1 \overleftarrow{\theta}^i u^\alpha B_1 \bar{B}_2 \overleftarrow{\xi}^i B_2 \rangle, \\
\hat{\mathcal{E}}_i^2 &= \hat{D}_2^\beta \langle \bar{B}_1 \theta^i B_1 u^\alpha \bar{B}_2 \xi^i B_2 \rangle + (-1)^{c_i} \hat{D}_2^\beta \langle \bar{B}_1 \overleftarrow{\theta}^i B_1 \bar{B}_2 \overleftarrow{\xi}^i B_2 u^\alpha \rangle, \\
\hat{\mathcal{E}}_i^3 &= \hat{D}_2^\beta \langle \bar{B}_1 u^\alpha \xi^i B_1 \bar{B}_2 \theta^i B_2 \rangle + (-1)^{c_i} \hat{D}_2^\beta \langle \bar{B}_1 \overleftarrow{\xi}^i u^\alpha B_1 \bar{B}_2 \overleftarrow{\theta}^i B_2 \rangle, \\
\hat{\mathcal{E}}_i^4 &= \hat{D}_2^\beta \langle \bar{B}_1 u^\alpha \bar{B}_2 \theta^i B_1 \xi^i B_2 \rangle + (-1)^{c_i} \hat{D}_1^\beta \langle \bar{B}_1 \overleftarrow{\xi}^i \bar{B}_2 \overleftarrow{\theta}^i B_1 u^\alpha B_2 \rangle, \\
\hat{\mathcal{E}}_i^5 &= \hat{D}_2^\beta \langle \bar{B}_1 \bar{B}_2 u^\alpha \theta^i B_1 \xi^i B_2 \rangle + (-1)^{c_i} \hat{D}_1^\beta \langle \bar{B}_1 \overleftarrow{\xi}^i \bar{B}_2 \overleftarrow{\theta}^i u^\alpha B_1 B_2 \rangle, \\
\hat{\mathcal{E}}_i^6 &= \hat{D}_2^\beta \langle \bar{B}_1 u^\alpha \bar{B}_2 \xi^i B_1 \theta^i B_2 \rangle + (-1)^{c_i} \hat{D}_1^\beta \langle \bar{B}_1 \overleftarrow{\theta}^i \bar{B}_2 \overleftarrow{\xi}^i B_1 u^\alpha B_2 \rangle, \\
\hat{\mathcal{E}}_i^7 &= \hat{D}_2^\beta \langle \bar{B}_1 \bar{B}_2 \theta^i B_1 \xi^i B_2 u^\alpha \rangle + (-1)^{c_i} \hat{D}_1^\beta \langle \bar{B}_1 \overleftarrow{\xi}^i \bar{B}_2 \overleftarrow{\theta}^i B_1 B_2 u^\alpha \rangle, \\
\hat{\mathcal{E}}_i^8 &= \hat{D}_2^\beta \langle \bar{B}_1 u^\alpha \theta^i B_1 \rangle \langle \bar{B}_2 \xi^i B_2 \rangle + (-1)^{c_i} \hat{D}_2^\beta \langle \bar{B}_1 \overleftarrow{\theta}^i u^\alpha B_1 \rangle \langle \bar{B}_2 \overleftarrow{\xi}^i B_2 \rangle, \\
\hat{\mathcal{E}}_i^9 &= \hat{D}_2^\beta \langle \bar{B}_1 \theta^i B_1 u^\alpha \rangle \langle \bar{B}_2 \xi^i B_2 \rangle + (-1)^{c_i} \hat{D}_2^\beta \langle \bar{B}_1 \overleftarrow{\theta}^i B_1 u^\alpha \rangle \langle \bar{B}_2 \overleftarrow{\xi}^i B_2 \rangle, \\
\hat{\mathcal{E}}_i^{10} &= \hat{D}_2^\beta \langle \bar{B}_1 u^\alpha \xi^i B_1 \rangle \langle \bar{B}_2 \theta^i B_2 \rangle + (-1)^{c_i} \hat{D}_2^\beta \langle \bar{B}_1 \overleftarrow{\xi}^i u^\alpha B_1 \rangle \langle \bar{B}_2 \overleftarrow{\theta}^i B_2 \rangle, \\
\hat{\mathcal{E}}_i^{11} &= \hat{D}_2^\beta \langle \bar{B}_1 \xi^i B_1 u^\alpha \rangle \langle \bar{B}_2 \theta^i B_2 \rangle + (-1)^{c_i} \hat{D}_2^\beta \langle \bar{B}_1 \overleftarrow{\xi}^i B_1 u^\alpha \rangle \langle \bar{B}_2 \overleftarrow{\theta}^i B_2 \rangle, \\
\hat{\mathcal{E}}_i^{12} &= \hat{D}_2^\beta \langle \bar{B}_1 u^\alpha \rangle \langle \theta^i B_1 \bar{B}_2 \xi^i B_2 \rangle + (-1)^{c_i} \hat{D}_2^\beta \langle \bar{B}_2 \overleftarrow{\xi}^i B_2 \bar{B}_1 \overleftarrow{\theta}^i \rangle \langle B_1 u^\alpha \rangle, \\
\hat{\mathcal{E}}_i^{13} &= \hat{D}_2^\beta \langle \bar{B}_1 u^\alpha \rangle \langle \xi^i B_1 \bar{B}_2 \theta^i B_2 \rangle + (-1)^{c_i} \hat{D}_2^\beta \langle \bar{B}_2 \overleftarrow{\theta}^i B_2 \bar{B}_1 \overleftarrow{\xi}^i \rangle \langle B_1 u^\alpha \rangle \,.
\end{aligned} \tag{3.35}$$

The allowed Dirac operators θ^i and ξ^i are given in columns 10-12 of Tab. 3.6. One obtains 82 such terms in covariant power counting out of which 14 remain in non-relativistic power counting.

Terms with two fields u_μ in the combination $[u_\alpha, u_\beta]_\pm$

When considering terms with two adjacent fields u_α and u_β as the building block A to be inserted into the flavor structures $\hat{\mathcal{C}}_i^j$ (see Eq. (3.29)), the two combinations $A = \{u_\alpha, u_\beta\}$ and $A = [u_\alpha, u_\beta]$ are to be considered separately. The pertinent part of the contact Lagrangian is,

$$\mathscr{L}_{BB}^{(2)} = \sum_{i,j} c''_{j,i} \hat{\mathcal{C}}_i^j \,, \tag{3.36}$$

with the allowed Dirac operators θ^i and ξ^i given in Tab. 3.7. The columns 7-9 give the possibilities for the anticommutator $A = \{u_\alpha, u_\beta\}$ and the columns 10-12 for the commutator $A = [u_\alpha, u_\beta]$. In total there are 303 terms for $A = \{u_\alpha, u_\beta\}$ and 127 terms for $A = [u_\alpha, u_\beta]$. In the non-relativistic power counting the number of such terms reduces to 125 terms for $A = \{u_\alpha, u_\beta\}$ and 33 terms for $A = [u_\alpha, u_\beta]$. Such terms with two fields u_μ lead to four-baryon vertices involving at least two pseudoscalar mesons.

Terms with two fields u_μ at non-neighboring positions

The last possibility is to have two fields u^α and u^β at non-neighboring positions in the flavor traces. This allows for a large number of new flavor structures $\hat{\mathcal{F}}_i^j$ with up to three flavor traces. The pertinent part of the contact Lagrangian reads

$$\mathscr{L}_{BB}^{(2)} = \sum_{i,j} f_{j,i} \hat{\mathcal{F}}_i^j \,, \tag{3.37}$$

with the flavor structures

$$\begin{aligned}
\hat{\mathcal{F}}_i^1 &= \langle \bar{B}_1 u^\alpha \theta^i B_1 u^\beta \bar{B}_2 \xi^i B_2 \rangle + (-1)^{c_i} \langle \bar{B}_1 \overleftarrow{\theta}^i u^\alpha B_1 \bar{B}_2 \overleftarrow{\xi}^i B_2 u^\beta \rangle, \\
\hat{\mathcal{F}}_i^2 &= \langle \bar{B}_1 u^\alpha \theta^i B_1 \bar{B}_2 u^\beta \xi^i B_2 \rangle + (-1)^{c_i} \langle \bar{B}_1 \overleftarrow{\theta}^i u^\alpha B_1 \bar{B}_2 \overleftarrow{\xi}^i u^\beta B_2 \rangle, \\
\hat{\mathcal{F}}_i^3 &= \langle \bar{B}_1 \theta^i B_1 u^\alpha \bar{B}_2 u^\beta \xi^i B_2 \rangle + (-1)^{c_i} \langle \bar{B}_1 \overleftarrow{\theta}^i B_1 \bar{B}_2 \overleftarrow{\xi}^i u^\beta B_2 u^\alpha \rangle, \\
\hat{\mathcal{F}}_i^4 &= \langle \bar{B}_1 \theta^i B_1 u^\alpha \bar{B}_2 \xi^i B_2 u^\beta \rangle + (-1)^{c_i} \langle \bar{B}_1 \overleftarrow{\theta}^i B_1 u^\beta \bar{B}_2 \overleftarrow{\xi}^i B_2 u^\alpha \rangle, \\
\hat{\mathcal{F}}_i^5 &= \langle \bar{B}_1 u^\alpha \bar{B}_2 u^\beta \theta^i B_1 \xi^i B_2 \rangle + (-1)^{c_i} \langle \bar{B}_1 \overleftarrow{\xi}^i \bar{B}_2 \overleftarrow{\theta}^i u^\beta B_1 u^\alpha B_2 \rangle, \\
\hat{\mathcal{F}}_i^6 &= \langle \bar{B}_1 u^\alpha \bar{B}_2 \theta^i B_1 u^\beta \xi^i B_2 \rangle + (-1)^{c_i} \langle \bar{B}_1 \overleftarrow{\xi}^i u^\beta \bar{B}_2 \overleftarrow{\theta}^i B_1 u^\alpha B_2 \rangle, \\
\hat{\mathcal{F}}_i^7 &= \langle \bar{B}_1 u^\alpha \bar{B}_2 \theta^i B_1 \xi^i B_2 u^\beta \rangle + (-1)^{c_i} \langle \bar{B}_1 \overleftarrow{\xi}^i \bar{B}_2 \overleftarrow{\theta}^i B_1 u^\alpha B_2 u^\beta \rangle, \\
\hat{\mathcal{F}}_i^8 &= \langle \bar{B}_1 \bar{B}_2 u^\alpha \theta^i B_1 u^\beta \xi^i B_2 \rangle + (-1)^{c_i} \langle \bar{B}_1 \overleftarrow{\xi}^i u^\beta \bar{B}_2 \overleftarrow{\theta}^i u^\alpha B_1 B_2 \rangle, \\
\hat{\mathcal{F}}_i^9 &= \langle \bar{B}_1 \bar{B}_2 u^\alpha \theta^i B_1 \xi^i B_2 u^\beta \rangle + (-1)^{c_i} \langle \bar{B}_1 \overleftarrow{\xi}^i \bar{B}_2 \overleftarrow{\theta}^i u^\alpha B_1 B_2 u^\beta \rangle, \\
\hat{\mathcal{F}}_i^{10} &= \langle \bar{B}_1 u^\alpha \theta^i B_1 u^\beta \rangle \langle \bar{B}_2 \xi^i B_2 \rangle + (-1)^{c_i} \langle \bar{B}_1 \overleftarrow{\theta}^i u^\alpha B_1 u^\beta \rangle \langle \bar{B}_2 \overleftarrow{\xi}^i B_2 \rangle, \\
\hat{\mathcal{F}}_i^{11} &= \langle \bar{B}_1 u^\alpha \theta^i B_1 \rangle \langle \bar{B}_2 u^\beta \xi^i B_2 \rangle + (-1)^{c_i} \langle \bar{B}_1 \overleftarrow{\theta}^i u^\alpha B_1 \rangle \langle \bar{B}_2 \overleftarrow{\xi}^i u^\beta B_2 \rangle, \\
\hat{\mathcal{F}}_i^{12} &= \langle \bar{B}_1 u^\alpha \theta^i B_1 \rangle \langle \bar{B}_2 \xi^i B_2 u^\beta \rangle + (-1)^{c_i} \langle \bar{B}_1 \overleftarrow{\theta}^i u^\alpha B_1 \rangle \langle \bar{B}_2 \overleftarrow{\xi}^i B_2 u^\beta \rangle, \\
\hat{\mathcal{F}}_i^{13} &= \langle \bar{B}_1 \theta^i B_1 u^\alpha \rangle \langle \bar{B}_2 \xi^i B_2 u^\beta \rangle + (-1)^{c_i} \langle \bar{B}_1 \overleftarrow{\theta}^i B_1 u^\alpha \rangle \langle \bar{B}_2 \overleftarrow{\xi}^i B_2 u^\beta \rangle, \\
\hat{\mathcal{F}}_i^{14} &= \langle \bar{B}_1 u^\alpha \rangle \langle \theta^i B_1 u^\beta \bar{B}_2 \xi^i B_2 \rangle + (-1)^{c_i} \langle \bar{B}_2 \overleftarrow{\xi}^i B_2 u^\beta \bar{B}_1 \overleftarrow{\theta}^i \rangle \langle B_1 u^\alpha \rangle, \\
\hat{\mathcal{F}}_i^{15} &= \langle \bar{B}_1 u^\alpha \rangle \langle \theta^i B_1 \bar{B}_2 u^\beta \xi^i B_2 \rangle + (-1)^{c_i} \langle \bar{B}_2 \overleftarrow{\xi}^i u^\beta B_2 \bar{B}_1 \overleftarrow{\theta}^i \rangle \langle B_1 u^\alpha \rangle, \\
\hat{\mathcal{F}}_i^{16} &= \langle \bar{B}_1 u^\alpha \rangle \langle \theta^i B_1 \bar{B}_2 \xi^i B_2 u^\beta \rangle + (-1)^{c_i} \langle \bar{B}_2 \overleftarrow{\xi}^i B_2 \bar{B}_1 \overleftarrow{\theta}^i u^\beta \rangle \langle B_1 u^\alpha \rangle, \\
\hat{\mathcal{F}}_i^{17} &= \langle \bar{B}_1 \xi^i B_1 \rangle \langle \bar{B}_2 u^\alpha \rangle \langle \theta^i B_2 u^\beta \rangle + (-1)^{c_i} \langle \bar{B}_1 \overleftarrow{\xi}^i B_1 \rangle \langle \bar{B}_2 \overleftarrow{\theta}^i u^\beta \rangle \langle B_2 u^\alpha \rangle, \\
\hat{\mathcal{F}}_i^{18} &= \langle \bar{B}_1 u^\alpha \rangle \langle \bar{B}_2 u^\beta \rangle \langle \theta^i B_1 \xi^i B_2 \rangle + (-1)^{c_i} \langle \bar{B}_2 \overleftarrow{\theta}^i \bar{B}_1 \overleftarrow{\xi}^i \rangle \langle B_2 u^\beta \rangle \langle B_1 u^\alpha \rangle,
\end{aligned} \tag{3.38}$$

and the corresponding primed structures

$$\hat{\mathcal{F}}_i^{j'} = \hat{\mathcal{F}}_i^j |_{\theta^i \leftrightarrow \xi^i} \,. \tag{3.39}$$

The Dirac operators θ^i and ξ^i are given in columns 13-15 of Tab. 3.7. One counts in total 817 such terms. In the non-relativistic power counting their number reduces to 276. A further reduction of the flavor structures might be possible when applying the Lagrangian to definite processes.

			$\hat{\mathcal{C}}^j$ with $A = f_-^{\alpha\beta}$			$\hat{\mathcal{C}}^j$ with $A = h^{\alpha\beta}$			$\hat{\mathcal{E}}^j$		
θ^i	ξ^i	NR	factor	c_i	$\hat{\mathcal{C}}^j$	factor	c_i	$\hat{\mathcal{C}}^j$	factor	c_i	$\hat{\mathcal{E}}^j$
$g_{\alpha\beta}\mathbb{1}D^\mu$	$\gamma_5\gamma_\mu$	$\star$							1	0	2,4,5,6, 7,12,13
$\mathbb{1}D_{\alpha\beta}{}^\mu$	$\gamma_5\gamma_\mu$	$\star$				1	0	2,4,5,6, 7,12,13			
$\mathbb{1}D_\alpha$	$\gamma_5\gamma_\beta$		1	0	2,4,5,6, 7,12,13	1	0	2,4,5,6, 7,12,13	1	0	2,4,5,6, 7,12,13
$\mathbb{1}D_\alpha{}^\mu$	$\gamma_5\gamma_\mu D_\beta$	$\star$	1	0	2,4,5,6, 7,12,13	1	0	2,4,5,6, 7,12,13			
$\mathbb{1}$	$\gamma_5\gamma_\alpha D_\beta$		1	0	2,4,5,6, 7,12,13	1	0	2,4,5,6, 7,12,13			
$\mathbb{1}D^\mu$	$\gamma_5\gamma_\mu D_{\alpha\beta}$	$\star$				1	0	2,4,5,6, 7,12,13			
$\mathbb{1}$	$\gamma_5\gamma_\beta D_\alpha$								1	0	2,4,5,6, 7,12,13
$g_{\alpha\beta}\gamma_5\gamma^\mu D^\nu$	$\sigma_{\mu\nu}$	$\star$							i	1	1-13
$\gamma_5\gamma_\alpha D^\mu$	$\sigma_{\beta\mu}$	$\star$	i	1	1-13	i	1	1-13			
$\gamma_5\gamma^\mu D_{\alpha\beta}{}^\nu$	$\sigma_{\mu\nu}$	$\star$				i	1	1-13			
$\gamma_5\gamma^\mu D_\alpha$	$\sigma_{\beta\mu}$		i	1	1-13	i	1	1-13			
$\gamma_5\gamma^\mu D^{\alpha\nu}$	$\sigma^\beta{}_\nu D_\mu$	$\star$	i	1	1-13	i	1	1-13			
$\gamma_5\gamma^\mu D_\alpha{}^\nu$	$\sigma_{\mu\nu}D_\beta$	$\star$	i	1	1-13	i	1	1-13			
$\gamma_5\gamma^\mu$	$\sigma_{\alpha\beta}D_\mu$	$\star$	i	1	1-13						
$\gamma_5\gamma^\mu$	$\sigma_{\alpha\mu}D_\beta$		i	1	1-13	i	1	1-13			
$\gamma_5\gamma^\mu D^\nu$	$\sigma_{\alpha\nu}D_{\beta\mu}$	$\star$	i	1	1-13	i	1	1-13			
$\gamma_5\gamma^\mu D^\nu$	$\sigma_{\mu\nu}D_{\alpha\beta}$	$\star$				i	1	1-13			
$\gamma_5\gamma_\beta D^\mu$	$\sigma_{\alpha\mu}$	$\star$							i	1	1-13
$\epsilon_{\alpha\beta}{}^{\delta\rho}\mathbb{1}D_\delta$	$\mathbb{1}D_\rho$	$\star$	1	0	1,4,8, 9,12				1	0	1,4,5,7, 8,9,12
$\epsilon_{\alpha\beta}{}^{\delta\rho}\gamma_5\gamma^\mu D_\delta$	$\gamma_5\gamma_\mu D_\rho$	$\star$	1	0	1,4,8, 9,12				1	0	1,4,5,7, 8,9,12
$\epsilon_{\alpha\beta}{}^{\delta\rho}\gamma_5\gamma^\mu D^\nu{}_\delta$	$\gamma_5\gamma_\nu D_{\mu\rho}$	$\star$	1	0	1,4,8, 9,12				1	0	1,4,5,7, 8,9,12
$\epsilon_{\alpha\beta}{}^{\delta\rho}\sigma^{\mu\nu}D_\delta$	$\sigma_{\mu\nu}D_\rho$	$\star$	1	0	1,4,8, 9,12				1	0	1,4,5,7, 8,9,12
$\epsilon_{\alpha\beta}{}^{\delta\rho}\sigma^{\mu\nu}D^\xi{}_\delta$	$\sigma_{\mu\xi}D_{\nu\rho}$	$\star$	1	0	1,4,8, 9,12				1	0	1,4,5,7, 8,9,12

TABLE 3.6: Dirac operators θ^i and ξ^i for contact terms of $\mathcal{O}(q^2)$ with odd-parity external fields carrying two Lorentz indices. The sets of flavor structures $\hat{\mathcal{C}}^j$ and $\hat{\mathcal{E}}^j$ are listed in Eqs. (3.29) and (3.35). Combinations that contribute in non-relativistic power counting at $\mathcal{O}(q^3)$ or higher are marked by an asterisk $\star$. The columns "factor" indicate the cases where a prefactor i is necessary for Hermitian conjugation invariance. The columns "c_i" give the charge conjugation exponent c_i. The allowed flavor structures $\hat{\mathcal{C}}^j, \hat{\mathcal{E}}^j$ are given by listing the indices j of the corresponding subset.

TABLE 3.7: Dirac operators θ^i and ξ^i for contact terms of $\mathcal{O}(q^2)$ with even-parity external fields carrying two Lorentz indices. The sets of flavor structures $\hat{\mathcal{C}}^j$ and $\hat{\mathcal{F}}^j$ are listed in Eqs. (3.29) and (3.38). Combinations that contribute in the non-relativistic power counting at $\mathcal{O}(q^3)$ or higher are marked by an asterisk $\star$. The columns "factor" indicate the cases where a prefactor i is necessary for Hermitian conjugation invariance. The columns "c_i" give the charge conjugation exponent c_i. The allowed flavor structures $\hat{\mathcal{C}}^j, \hat{\mathcal{F}}^j$ are given by listing the indices j of the corresponding subset.

			$\hat{\mathcal{C}}^j$ with $A = f_+^{\alpha\beta}$			$\hat{\mathcal{C}}^j$ with $A = \{u^\alpha, u^\beta\}$			$\hat{\mathcal{C}}^j$ with $A = [u^\alpha, u^\beta]$			$\hat{\mathcal{F}}^j$		
θ^i	ξ^i	NR	factor	c_i	$\hat{\mathcal{C}}^j$	factor	c_i	$\hat{\mathcal{C}}^j$	factor	c_i	$\hat{\mathcal{C}}^j$	factor	c_i	$\hat{\mathcal{F}}^j$
$g_{\alpha\beta}\mathbb{1}$	$\mathbb{1}$					1	0	1,2,4,5,7,8, 9,12,14,15,16				1	0	1-18
$\mathbb{1}D_{\alpha\beta}$	$\mathbb{1}$					1	0	1-16				1	0	$1\text{-}18, 7', 10', 12', 14'\text{-}16', 17'$
$\mathbb{1}D_\alpha$	$\mathbb{1}D_\beta$		i	1	2,4,5, 7,12	1	0	1,2,4,5,7,8, 9,12,14,15,16	1	1	2,4,5, 7,12	1	0	$1, 2, 4\text{-}7, 9\text{-}18, 1', 2', 5'\text{-}7', 10'\text{-}18'$
$\mathbb{1}D_\alpha{}^\mu$	$\sigma_{\beta\mu}$	$\star$	1	0	1-13	i	1	2,4,5,6,7, 12,13,15	i	0	1-13	i	1	$1, 3\text{-}9, 14\text{-}18, 1', 3', 5'\text{-}8', 14'\text{-}18'$
$\mathbb{1}$	$\sigma_{\alpha\beta}$		1	0	1-13				i	0	1-13	i	1	$1, 3\text{-}9, 14\text{-}18, 7', 14'\text{-}17'$
$\mathbb{1}D^\mu$	$\sigma_{\alpha\mu}D_\beta$	$\star$	1	0	1-13	i	1	2,4,5,6,7, 12,13,15	i	0	1-13	i	1	$1, 3\text{-}9, 14\text{-}18, 1', 3', 5'\text{-}8', 14'\text{-}18'$
$\mathbb{1}D_\beta{}^\mu$	$\sigma_{\alpha\mu}$	$\star$										i	1	$7, 9, 14\text{-}17, 7', 14'\text{-}17'$
$\mathbb{1}D^\mu$	$\sigma_{\beta\mu}D_\alpha$	$\star$										i	1	$7, 9, 14\text{-}17, 7', 14'\text{-}17'$
$g_{\alpha\beta}\gamma_5\gamma^\mu$	$\gamma_5\gamma_\mu$					1	0	1,2,4,5,7,8, 9,12,14,15,16				1	0	1-18
$g_{\alpha\beta}\gamma_5\gamma^\mu D^\nu$	$\gamma_5\gamma_\nu D_\mu$	$\star$				1	0	1,2,4,5,7,8, 9,12,14,15,16				1	0	1-18
$\gamma_5\gamma_\alpha D_\beta{}^\mu$	$\gamma_5\gamma_\mu$	$\star$	i	1	2,4,5,6, 7,12,13	1	0	1-16	1	1	2,4,5,6, 7,12,13	1	0	$1\text{-}18, 1'\text{-}3', 5'\text{-}8', 10'\text{-}18'$
$\gamma_5\gamma_\alpha$	$\gamma_5\gamma_\beta$		i	1	2,4,5, 7,12	1	0	1,2,4,5,7,8, 9,12,14,15,16	1	1	2,4,5, 7,12	1	0	$1, 2, 4\text{-}7, 9\text{-}18, 1', 2', 5'\text{-}7', 10'\text{-}18'$
$\gamma_5\gamma_\alpha D^\mu$	$\gamma_5\gamma_\mu D_\beta$	$\star$	i	1	2,4,5,6, 7,12,13	1	0	1-16	1	1	2,4,5,6, 7,12,13	1	0	$1\text{-}18, 1'\text{-}3', 5'\text{-}8', 10'\text{-}18'$
$\gamma_5\gamma^\mu D_{\alpha\beta}$	$\gamma_5\gamma_\mu$					1	0	1-16				1	0	$1\text{-}18, 7', 10', 12', 14'\text{-}16', 17'$
$\gamma_5\gamma^\mu D_\alpha{}_\beta{}^\nu$	$\gamma_5\gamma_\nu D_\mu$	$\star$				1	0	1-16				1	0	$1\text{-}18, 7', 10', 12', 14'\text{-}16', 17'$

. . . continues on next page

TABLE 3.7: (. . . continued)

			$\hat{\mathcal{C}}^j$ with $A = f_+^{\alpha\beta}$			$\hat{\mathcal{C}}^j$ with $A = \{u^\alpha, u^\beta\}$			$\hat{\mathcal{C}}^j$ with $A = [u^\alpha, u^\beta]$			$\hat{\mathcal{F}}^j$		
θ^i	ξ^i	NR	factor	c_i	$\hat{\mathcal{C}}^j$	factor	c_i	$\hat{\mathcal{C}}^j$	factor	c_i	$\hat{\mathcal{C}}^j$	factor	c_i	$\hat{\mathcal{F}}^j$
$\gamma_5\gamma^\mu D_\alpha$	$\gamma_5\gamma_\mu D_\beta$		i	1	2,4,5, 7,12	1	0	1,2,4,5,7,8, 9,12,14,15,16	1	1	2,4,5, 7,12	1	0	$1, 2, 4\text{-}7, 9\text{-}18, 1', 2', 5'\text{-}7', 10'\text{-}18'$
$\gamma_5\gamma^\mu D_\alpha{}^\nu$	$\gamma_5\gamma_\nu D_{\beta\mu}$	$\star$	i	1	2,4,5, 7,12	1	0	1,2,4,5,7,8, 9,12,14,15,16	1	1	2,4,5, 7,12	1	0	$1, 2, 4\text{-}7, 9\text{-}18, 1', 2', 5'\text{-}7', 10'\text{-}18'$
$\gamma_5\gamma^\mu D_\alpha$	$\gamma_5\gamma_\beta D_\mu$	$\star$										1	0	$1\text{-}18, 1'\text{-}3', 5'\text{-}8', 10'\text{-}18'$
$\gamma_5\gamma_\beta D_\alpha{}^\mu$	$\gamma_5\gamma_\mu$	$\star$										1	0	$7, 9, 10, 12, 14\text{-}17, 7', 10', 12', 14'\text{-}17'$
$g_{\alpha\beta}\sigma^{\mu\nu}$	$\sigma_{\mu\nu}$					1	0	1,2,4,5,7,8, 9,12,14,15,16				1	0	1-18
$g_{\alpha\beta}\sigma^{\mu\nu}D^\rho$	$\sigma_{\mu\rho}D_\nu$	$\star$				1	0	1,2,4,5,7,8, 9,12,14,15,16				1	0	1-18
$\sigma_\alpha{}^\mu D_\beta{}^\nu$	$\sigma_{\mu\nu}$	$\star$	i	1	2,4,5,6, 7,12,13	1	0	1-16	1	1	2,4,5,6, 7,12,13	1	0	$1\text{-}18, 1'\text{-}3', 5'\text{-}8', 10'\text{-}18'$
$\sigma_\alpha{}^\mu$	$\sigma_{\beta\mu}$		i	1	2,4,5, 7,12	1	0	1,2,4,5,7,8, 9,12,14,15,16	1	1	2,4,5, 7,12	1	0	$1, 2, 4\text{-}7, 9\text{-}18, 1', 2', 5'\text{-}7', 10'\text{-}18'$
$\sigma_\alpha{}^\mu D^\nu$	$\sigma_{\beta\nu}D_\mu$	$\star$	i	1	2,4,5, 7,12	1	0	1,2,4,5,7,8, 9,12,14,15,16	1	1	2,4,5, 7,12	1	0	$1, 2, 4\text{-}7, 9\text{-}18, 1', 2', 5'\text{-}7', 10'\text{-}18'$
$\sigma_\alpha{}^\mu D^\nu$	$\sigma_{\mu\nu}D_\beta$	$\star$	i	1	2,4,5,6, 7,12,13	1	0	1-16	1	1	2,4,5,6, 7,12,13	1	0	$1\text{-}18, 1'\text{-}3', 5'\text{-}8', 10'\text{-}18'$
$\sigma^{\mu\nu}D_{\alpha\beta}$	$\sigma_{\mu\nu}$					1	0	1-16				1	0	$1\text{-}18, 7', 10', 12', 14'\text{-}16', 17'$
$\sigma^{\mu\nu}D^\rho{}_{\alpha\beta}$	$\sigma_{\mu\rho}D_\nu$	$\star$				1	0	1-16				1	0	$1\text{-}18, 7', 10', 12', 14'\text{-}16', 17'$
$\sigma^{\mu\nu}D_\alpha$	$\sigma_{\beta\mu}D_\nu$											1	0	$1\text{-}18, 1'\text{-}3', 5'\text{-}8', 10'\text{-}18'$
$\sigma^{\mu\nu}D_\alpha$	$\sigma_{\mu\nu}D_\beta$	$\star$	i	1	2,4,5, 7,12	1	0	1,2,4,5,7,8, 9,12,14,15,16	1	1	2,4,5, 7,12	1	0	$1, 2, 4\text{-}7, 9\text{-}18, 1', 2', 5'\text{-}7', 10'\text{-}18'$
$\sigma^{\mu\nu}D^\rho{}_\alpha$	$\sigma_{\mu\rho}D_{\nu\beta}$	$\star$	i	1	2,4,5, 7,12	1	0	1,2,4,5,7,8, 9,12,14,15,16	1	1	2,4,5, 7,12	1	0	$1, 2, 4\text{-}7, 9\text{-}18, 1', 2', 5'\text{-}7', 10'\text{-}18'$
$\sigma_\beta{}^\mu D_\alpha{}^\nu$	$\sigma_{\mu\nu}$	$\star$										1	0	$7, 9, 10, 12, 14\text{-}17, 7', 10', 12', 14'\text{-}17'$
$\epsilon_{\alpha\beta}{}^{\delta\rho}\mathbb{1}D_\delta{}^\mu$	$\gamma_5\gamma_\mu D_\rho$	$\star$	i	1	1-13				1	1	1-13	1	0	$1, 3\text{-}9, 14\text{-}18, 7', 14'\text{-}17'$
$\epsilon_{\alpha\beta}{}^{\delta\rho}\gamma_5\gamma^\mu D_\delta{}^\nu$	$\sigma_{\mu\nu}D_\rho$	$\star$	1	0	2,4,5,6, 7,12,13				i	0	2,4,5,6, 7,12,13	i	1	$1\text{-}3, 5\text{-}16, 18, 7', 10', 12', 14'\text{-}16'$

4

BARYON-BARYON INTERACTION UP TO NLO

In this chapter we apply chiral effective field theory to the baryon-baryon interaction up to next-to-leading order, as shown in Fig. 2.4. The constructed potentials serve not only as input for the description of baryon-baryon scattering, but are also basis for few- and many-body calculations ranging from light hypernuclei to exotic neutron star matter. The potentials due to the four-baryon contact terms are derived from the chiral Lagrangian constructed in Chapter 3. The contributions from Feynman diagrams involving one or two Goldstone-boson exchanges are given at LO and NLO. Finally, results for the hyperon-nucleon interaction, using these chiral YN potentials, are shown. An excellent description of the YN scattering data is obtained, comparable to that of most advanced phenomenological models.

4.1 PURE BARYON-BARYON CONTACT TERMS

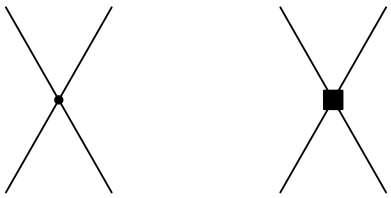

FIGURE 4.1: Leading-order and next-to-leading-order baryon-baryon contact vertices.

In the following we use the chiral Lagrangian constructed in Chapter 3 in order to derive the baryon-baryon contact potentials, Fig. 4.1, relevant for the (two-body) baryon-baryon scattering process. Parts of this section have been published previously in Ref. [103]. Since no pseudoscalar mesons are involved almost all external fields can be dropped and covariant derivatives D_μ reduce to ordinary derivatives ∂_μ. The only surviving external field is χ_+, which is responsible for the inclusion of quark masses into the chiral Lagrangian:

$$\frac{\chi_+}{2} = \chi = 2B_0 \begin{pmatrix} m_u & 0 & 0 \\ 0 & m_d & 0 \\ 0 & 0 & m_s \end{pmatrix} \approx \begin{pmatrix} m_\pi^2 & 0 & 0 \\ 0 & m_\pi^2 & 0 \\ 0 & 0 & 2m_K^2 - m_\pi^2 \end{pmatrix} , \tag{4.1}$$

where in the last step the Gell-Mann–Oakes–Renner relations, Eq. (2.55), have been used. The corresponding terms provide the explicit SU(3) symmetry breaking contact potentials linear in the quark masses. The subset of contact terms proportional to $\langle \chi_+ \rangle = 4B_0(m_u + m_d + m_s)$ can be absorbed in the leading order terms, since the corresponding low-energy constants merely get shifted by a correction linear in the sum of the three quark masses.

After a non-relativistic expansion up to $\mathcal{O}(q^2)$ the four-baryon contact Lagrangian leads to potentials in spin and momentum space. We use the operator basis of Ref. [25]:

$$\begin{aligned} P_1 &= 1\,, & P_2 &= \vec{\sigma}_1\cdot\vec{\sigma}_2\,, \\ P_3 &= (\vec{\sigma}_1\cdot\vec{q})(\vec{\sigma}_2\cdot\vec{q}) - \frac{1}{3}(\vec{\sigma}_1\cdot\vec{\sigma}_2)\vec{q}^{\,2}\,, & P_4 &= \frac{\mathrm{i}}{2}(\vec{\sigma}_1+\vec{\sigma}_2)\cdot\vec{n}\,, \\ P_5 &= (\vec{\sigma}_1\cdot\vec{n})(\vec{\sigma}_2\cdot\vec{n})\,, & P_6 &= \frac{\mathrm{i}}{2}(\vec{\sigma}_1-\vec{\sigma}_2)\cdot\vec{n}\,, \\ P_7 &= (\vec{\sigma}_1\cdot\vec{k})(\vec{\sigma}_2\cdot\vec{q}) + (\vec{\sigma}_1\cdot\vec{q})(\vec{\sigma}_2\cdot\vec{k})\,, & P_8 &= (\vec{\sigma}_1\cdot\vec{k})(\vec{\sigma}_2\cdot\vec{q}) - (\vec{\sigma}_1\cdot\vec{q})(\vec{\sigma}_2\cdot\vec{k})\,, \end{aligned} \tag{4.2}$$

with $\vec{\sigma}_{1,2}$ the Pauli spin matrices and with the vectors

$$\vec{k} = \frac{1}{2}(\vec{p}_f+\vec{p}_i)\,, \quad \vec{q} = \vec{p}_f-\vec{p}_i\,, \quad \vec{n} = \vec{p}_i\times\vec{p}_f\,. \tag{4.3}$$

The momenta $\vec{p}_f$ and $\vec{p}_i$ are the initial and final state momenta in the center-of-mass frame. For convenience we introduce additionally the combination $P_9 = \vec{\sigma}_1\cdot\vec{k}\,\vec{\sigma}_2\cdot\vec{k} = (\frac{n^2}{q^2}-\frac{1}{3}k^2)P_2 - \frac{k^2}{q^2}P_3 - \frac{1}{q^2}P_5 + \frac{p_f^2-p_i^2}{2q^2}P_7$. In order to obtain a minimal set of Lagrangian terms in the non-relativistic power counting, we have decomposed the emerging potentials into partial waves. The formulas for the partial wave projection of a general interaction $V = \sum_{j=1}^{8} V_j P_j$ can be found in the appendix of Ref. [25]. For each partial wave one produces a non-square matrix which connects the Lagrangian constants with the different baryon-baryon channels. Lagrangian terms are considered as redundant if their omission does not lower the rank of this matrix. In the case of the SU(3)-breaking terms we have done this reduction together with the leading SU(3) symmetric terms, since here we are not interested in the quark-mass dependence of the contact potential. Using the results of Chapter 3, one obtains the relevant linearly independent Lagrangians displayed in Tab. 4.1, which contribute in the non-relativistic power counting up to $\mathcal{O}(q^2)$. The first 28 terms contain only baryon fields and derivatives, and are therefore SU(3) symmetric. The other 12 terms include the diagonal matrix χ and produce explicit SU(3) symmetry breaking. As in Chapter 3, the operator $\hat{\partial}_i$ means, that the derivative acts only on baryon fields in the baryon bilinear i. Furthermore, Tab. 4.1 shows to which of the basis element P_i the terms in the Lagrangian contribute. Note, that these are only the direct contributions. Additional structures are obtained from contributions with exchanged final state baryons, where the negative spin-exchange operator $-P^{(\sigma)} = -\frac{1}{2}\,(\mathbb{1}+\vec{\sigma}_1\cdot\vec{\sigma}_2)$ is applied.

An interesting feature of the baryon-baryon interaction at NLO is the transition between spin-singlet and spin-triplet states, for instance ${}^1P_1 \leftrightarrow {}^3P_1$. Such a spin singlet-triplet transition arises from the spin operators P_6 and P_8. It originates solely from the term 28 in Tab. 4.1, which gives rise to the antisymmetric spin-orbit operator P_6 and its Fierz-transformed counterpart $P_8 = 2\,P^{(\sigma)}P_6\big|_{\vec{p}_f\to-\vec{p}_f}$. Therefore, only a single low-energy constant is present for the singlet-triplet mixing. In case of the NN interaction such transitions are forbidden by isospin symmetry. Note that the singlet-triplet transition is possible for certain two-baryon channels even in the limit of exact SU(3) symmetry.

In Tab. 4.2 we present the non-vanishing transitions projected onto partial waves and express them in the isospin basis. One recovers the SU(3) relations of Refs. [25, 26, 27]. The pertinent constants are redefined according to the relevant irreducible SU(3) representations. This comes about in the following way. Baryons form a flavor octet and the tensor product of two baryons decomposes into irreducible representations as follows:

$$\mathbf{8}\otimes\mathbf{8} = \mathbf{27}_s \oplus \mathbf{10}_a \oplus \mathbf{10}^*_a \oplus \mathbf{8}_s \oplus \mathbf{8}_a \oplus \mathbf{1}_s\,, \tag{4.4}$$

where the irreducible representations $\mathbf{27}_s$, $\mathbf{8}_s$, $\mathbf{1}_s$ are symmetric and $\mathbf{10}_a$, $\mathbf{10}^*_a$, $\mathbf{8}_a$ are antisymmetric with respect to the exchange of both baryons. Due to the generalized Pauli principle, the symmetric flavor representations $\mathbf{27}_s$, $\mathbf{8}_s$, $\mathbf{1}_s$ have to combine with the space-spin antisymmetric partial waves ${}^1S_0$, ${}^3P_0$, ${}^3P_1$, ${}^3P_2$, ... ($L+S$ even). The antisymmetric flavor representations $\mathbf{10}_a$, $\mathbf{10}^*_a$, $\mathbf{8}_a$ combine with the space-spin symmetric partial waves ${}^3S_1$, ${}^1P_1$, ${}^3D_1 \leftrightarrow {}^3S_1$, ... ($L+S$ odd). Transitions can only occur between equal irreducible representations. Hence, transitions between space-spin antisymmetric partial waves up to $\mathcal{O}(q^2)$ involve the 15 constants $\tilde{c}^{27,8s,1}_{{}^1S_0}$, $c^{27,8s,1}_{{}^1S_0}$, $c^{27,8s,1}_{{}^3P_0}$, $c^{27,8s,1}_{{}^3P_1}$ and $c^{27,8s,1}_{{}^3P_2}$, whereas transitions between space-spin symmetric partial waves involve the 12 constants $\tilde{c}^{8a,10,10^*}_{{}^3S_1}$, $c^{8a,10,10^*}_{{}^3S_1}$, $c^{8a,10,10^*}_{{}^1P_1}$ and $c^{8a,10,10^*}_{{}^3D_1\text{-}{}^3S_1}$. The constants with a tilde denote leading-order constants, whereas the ones without tilde are at NLO. The spin singlet-triplet transitions ${}^1P_1 \leftrightarrow {}^3P_1$ (induced by the Lagrangian term #28 in Tab. 4.1) is perfectly allowed by SU(3) symmetry since it is related to transitions between the irreducible representations $\mathbf{8}_a$ and $\mathbf{8}_s$. The corresponding low-energy constant is denoted by c^{8as}. The constants $\tilde{c}^{27,8s,1}_{{}^1S_0}$ and $\tilde{c}^{8a,10,10^*}_{{}^3S_1}$ fulfill the same SU(3) relations as the constants $c^{27,8s,1}_{{}^1S_0}$ and $c^{8a,10,10^*}_{{}^3S_1}$ in Tab. 4.2. SU(3) breaking terms linear in the quark masses appears only in the S-waves, ${}^1S_0$, ${}^3S_1$, and are proportional $m_K^2 - m_\pi^2$. The corresponding 12 constants are $c^{1,\ldots,12}_\chi$. The SU(3) symmetry relations in Tab. 4.2 can also be derived by group theoretical considerations [25, 115, 116, 117]. Clearly, for the SU(3)-breaking part this is not possible and these contributions have to be derived from the chiral Lagrangian.

In order to obtain the complete partial-wave projected potentials, some entries in Tab. 4.2 have to be multiplied with additional momentum factors. The leading order constants $\tilde{c}^i_j$ receive no further factor. For the next-to-leading-order constants (without tilde and without χ) the contributions to the partial waves ${}^1S_0$, ${}^3S_1$ have to be multiplied with a factor $p_i^2 + p_f^2$. The contribution to the partial waves ${}^1S_0$, ${}^3S_1$ from constants c^j_χ has to be multiplied with $(m_K^2 - m_\pi^2)$. The partial waves ${}^3P_0$, ${}^3P_1$, ${}^3P_2$, ${}^1P_1$, ${}^1P_1 \leftrightarrow {}^3P_1$ get multiplied with the factor $p_i p_f$. The entries for ${}^3S_1 \to {}^3D_1$ and ${}^3D_1 \to {}^3S_1$ have to be multiplied with p_i^2 and p_f^2, respectively. For example, one obtains for the NN interaction in the ${}^1S_0$ partial wave:

$$\langle NN, {}^1S_0|\hat{V}|NN, {}^1S_0\rangle = \tilde{c}^{27}_{{}^1S_0} + c^{27}_{{}^1S_0}(p_i^2 + p_f^2) + \frac{1}{2}c^1_\chi(m_K^2 - m_\pi^2)\,, \tag{4.5}$$

or for the $\Xi N \to \Sigma\Sigma$ interaction with total isospin $I = 0$ in the ${}^1P_1 \to {}^3P_1$ partial wave:

$$\langle \Sigma\Sigma, {}^3P_1|\hat{V}|\Xi N, {}^1P_1\rangle = 2\sqrt{3}c^{8as}p_i p_f\,. \tag{4.6}$$

When restricting to the NN channel we recover the well-known two leading and seven next-to-leading order low-energy constants of Ref. [118] contributing to the partial waves ${}^1S_0$, ${}^3S_1$, ${}^1P_1$, ${}^3P_0$, ${}^3P_1$, ${}^3P_2$, ${}^3S_1 \leftrightarrow {}^3D_1$.

Note, that the SU(3) relations in Tab. 4.2 are general relations that have to be fulfilled by the baryon-baryon potential in the SU(3) limit, i.e., $m_\pi = m_K = m_\eta$. This feature serves as a great check for the inclusion of the loop diagrams. Moreover, the SU(3) relations contain only a few constants in each partial wave. For example, in the ${}^1S_0$ partial wave only the constants $\tilde{c}^{27}_{{}^1S_0}$, $\tilde{c}^{8s}_{{}^1S_0}$, $\tilde{c}^1_{{}^1S_0}$ are present. If these constants are fixed in some of the baryons channels, predictions for other channels can be made. This has, for instance, been used in Ref. [119], where the existence of $\Sigma\Sigma$, $\Sigma\Xi$ and $\Xi\Xi$ bound states has been studied within SU(3) χEFT.

#	$\mathscr{L}$	contributes to
1	$\langle \bar{B}_1 B_1 \bar{B}_2 B_2 \rangle$	P_1, P_4
2	$\langle \bar{B}_1 (\partial^\mu B)_1 \bar{B}_2 (\partial_\mu B)_2 \rangle + \langle (\partial^\mu \bar{B})_1 B_1 (\partial_\mu \bar{B})_2 B_2 \rangle$	P_1, P_4
3	$\langle \bar{B}_1 (\gamma_5 \gamma^\mu B)_1 \bar{B}_2 (\gamma_5 \gamma_\mu B)_2 \rangle$	P_2, P_3, P_4, P_9
4	$\langle \bar{B}_1 (\gamma_5 \gamma^\mu \partial^\nu B)_1 \bar{B}_2 (\gamma_5 \gamma_\mu \partial_\nu B)_2 \rangle + \langle (\partial^\nu \bar{B})_1 (\gamma_5 \gamma^\mu B)_1 (\partial_\nu \bar{B})_2 (\gamma_5 \gamma_\mu B)_2 \rangle$	P_2, P_3, P_4, P_9
5	$\langle \bar{B}_1 (\gamma_5 \gamma^\mu \partial^\nu B)_1 \bar{B}_2 (\gamma_5 \gamma_\nu \partial_\mu B)_2 \rangle + \langle (\partial^\nu \bar{B})_1 (\gamma_5 \gamma^\mu B)_1 (\partial_\mu \bar{B})_2 (\gamma_5 \gamma_\nu B)_2 \rangle$	P_2, P_3, P_9
6	$\langle \bar{B}_1 (\sigma^{\mu\nu} B)_1 \bar{B}_2 (\sigma_{\mu\nu} B)_2 \rangle$	P_1, P_2, P_3, P_4, P_9
7	$\hat{\partial}_2^2 \langle \bar{B}_1 B_1 \bar{B}_2 B_2 \rangle$	P_1
8	$\hat{\partial}_2^2 \langle \bar{B}_1 (\gamma_5 \gamma^\mu B)_1 \bar{B}_2 (\gamma_5 \gamma_\mu B)_2 \rangle$	P_2
9	$\hat{\partial}_2^\alpha \hat{\partial}_2^\beta \langle \bar{B}_1 (\gamma_5 \gamma_\alpha B)_1 \bar{B}_2 (\gamma_5 \gamma_\beta B)_2 \rangle$	P_2, P_3
10	$\langle \bar{B}_1 \bar{B}_2 B_1 B_2 \rangle$	P_1, P_4
11	$\langle \bar{B}_1 \bar{B}_2 (\partial^\mu B)_1 (\partial_\mu B)_2 \rangle + \langle (\partial^\mu \bar{B})_1 (\partial_\mu \bar{B})_2 B_1 B_2 \rangle$	P_1, P_4
12	$\langle \bar{B}_1 \bar{B}_2 (\gamma_5 \gamma^\mu B)_1 (\gamma_5 \gamma_\mu B)_2 \rangle$	P_2, P_3, P_4, P_9
13	$\langle \bar{B}_1 \bar{B}_2 (\gamma_5 \gamma^\mu \partial^\nu B)_1 (\gamma_5 \gamma_\mu \partial_\nu B)_2 \rangle + \langle (\partial^\nu \bar{B})_1 (\partial_\nu \bar{B})_2 (\gamma_5 \gamma^\mu B)_1 (\gamma_5 \gamma_\mu B)_2 \rangle$	P_2, P_3, P_4, P_9
14	$\langle \bar{B}_1 \bar{B}_2 (\gamma_5 \gamma^\mu \partial^\nu B)_1 (\gamma_5 \gamma_\nu \partial_\mu B)_2 \rangle + \langle (\partial^\nu \bar{B})_1 (\partial_\mu \bar{B})_2 (\gamma_5 \gamma^\mu B)_1 (\gamma_5 \gamma_\nu B)_2 \rangle$	P_2, P_3, P_9
15	$\langle \bar{B}_1 \bar{B}_2 (\sigma^{\mu\nu} B)_1 (\sigma_{\mu\nu} B)_2 \rangle$	P_1, P_2, P_3, P_4, P_9
16	$(\hat{\partial}_2^2 + \hat{\partial}_1^2) \langle \bar{B}_1 \bar{B}_2 B_1 B_2 \rangle$	P_1
17	$(\hat{\partial}_2^2 + \hat{\partial}_1^2) \langle \bar{B}_1 \bar{B}_2 (\gamma_5 \gamma^\mu B)_1 (\gamma_5 \gamma_\mu B)_2 \rangle$	P_2
18	$(\hat{\partial}_2^\alpha \hat{\partial}_2^\beta + \hat{\partial}_1^\alpha \hat{\partial}_1^\beta) \langle \bar{B}_1 \bar{B}_2 (\gamma_5 \gamma_\alpha B)_1 (\gamma_5 \gamma_\beta B)_2 \rangle$	P_2, P_3
19	$\langle \bar{B}_1 B_1 \rangle \langle \bar{B}_2 B_2 \rangle$	P_1, P_4
20	$\langle \bar{B}_1 (\partial^\mu B)_1 \rangle \langle \bar{B}_2 (\partial_\mu B)_2 \rangle + \langle (\partial^\mu \bar{B})_1 B_1 \rangle \langle (\partial_\mu \bar{B})_2 B_2 \rangle$	P_1, P_4
21	$\langle \bar{B}_1 (\gamma_5 \gamma^\mu B)_1 \rangle \langle \bar{B}_2 (\gamma_5 \gamma_\mu B)_2 \rangle$	P_2, P_3, P_4, P_9
22	$\langle \bar{B}_1 (\gamma_5 \gamma^\mu \partial^\nu B)_1 \rangle \langle \bar{B}_2 (\gamma_5 \gamma_\mu \partial_\nu B)_2 \rangle + \langle (\partial^\nu \bar{B})_1 (\gamma_5 \gamma^\mu B)_1 \rangle \langle (\partial_\nu \bar{B})_2 (\gamma_5 \gamma_\mu B)_2 \rangle$	P_2, P_3, P_4, P_9
23	$\langle \bar{B}_1 (\gamma_5 \gamma^\mu \partial^\nu B)_1 \rangle \langle \bar{B}_2 (\gamma_5 \gamma_\nu \partial_\mu B)_2 \rangle + \langle (\partial^\nu \bar{B})_1 (\gamma_5 \gamma^\mu B)_1 \rangle \langle (\partial_\mu \bar{B})_2 (\gamma_5 \gamma_\nu B)_2 \rangle$	P_2, P_3, P_9
24	$\langle \bar{B}_1 (\sigma^{\mu\nu} B)_1 \rangle \langle \bar{B}_2 (\sigma_{\mu\nu} B)_2 \rangle$	P_1, P_2, P_3, P_4, P_9
25	$\hat{\partial}_2^2 \langle \bar{B}_1 B_1 \rangle \langle \bar{B}_2 B_2 \rangle$	P_1
26	$\hat{\partial}_2^2 \langle \bar{B}_1 (\gamma_5 \gamma^\mu B)_1 \rangle \langle \bar{B}_2 (\gamma_5 \gamma_\mu B)_2 \rangle$	P_2
27	$\hat{\partial}_2^\alpha \hat{\partial}_2^\beta \langle \bar{B}_1 (\gamma_5 \gamma_\alpha B)_1 \rangle \langle \bar{B}_2 (\gamma_5 \gamma_\beta B)_2 \rangle$	P_2, P_3
28	$\hat{\partial}_2^\alpha \langle \bar{B}_1 \bar{B}_2 (\gamma_5 \gamma_\alpha \partial_\mu B)_1 (\gamma_5 \gamma^\mu B)_2 \rangle + \hat{\partial}_1^\alpha \langle \bar{B}_1 (\partial_\mu \bar{B})_2 (\gamma_5 \gamma^\mu B)_1 (\gamma_5 \gamma_\alpha B)_2 \rangle$	P_2, P_3, P_8
29	$\langle \bar{B}_1 \chi B_1 \bar{B}_2 B_2 \rangle$	P_1
30	$\langle \bar{B}_1 \chi (\gamma_5 \gamma^\mu B)_1 \bar{B}_2 (\gamma_5 \gamma_\mu B)_2 \rangle$	P_2
31	$\langle \bar{B}_1 B_1 \chi \bar{B}_2 B_2 \rangle$	P_1
32	$\langle \bar{B}_1 (\gamma_5 \gamma^\mu B)_1 \chi \bar{B}_2 (\gamma_5 \gamma_\mu B)_2 \rangle$	P_2
33	$\langle \bar{B}_1 \chi \bar{B}_2 B_1 B_2 \rangle + \langle \bar{B}_1 \bar{B}_2 B_1 \chi B_2 \rangle$	P_1
34	$\langle \bar{B}_1 \chi \bar{B}_2 (\gamma_5 \gamma^\mu B)_1 (\gamma_5 \gamma_\mu B)_2 \rangle + \langle \bar{B}_1 \bar{B}_2 (\gamma_5 \gamma^\mu B)_1 \chi (\gamma_5 \gamma_\mu B)_2 \rangle$	P_2
35	$\langle \bar{B}_1 \bar{B}_2 \chi B_1 B_2 \rangle$	P_1
36	$\langle \bar{B}_1 \bar{B}_2 \chi (\gamma_5 \gamma^\mu B)_1 (\gamma_5 \gamma_\mu B)_2 \rangle$	P_2
37	$\langle \bar{B}_1 \bar{B}_2 B_1 B_2 \chi \rangle$	P_1
38	$\langle \bar{B}_1 \bar{B}_2 (\gamma_5 \gamma^\mu B)_1 (\gamma_5 \gamma_\mu B)_2 \chi \rangle$	P_2
39	$\langle \bar{B}_1 \chi B_1 \rangle \langle \bar{B}_2 B_2 \rangle$	P_1
40	$\langle \bar{B}_1 \chi (\gamma_5 \gamma^\mu B)_1 \rangle \langle \bar{B}_2 (\gamma_5 \gamma_\mu B)_2 \rangle$	P_2

TABLE 4.1: Linearly independent Lagrangian terms up to $\mathcal{O}(q^2)$ for pure baryon-baryon interaction in non-relativistic power counting and their contribution in spin-space.

S	I	transition	$j \in \{^1S_0, ^3P_0, ^3P_1, ^3P_2\}$	$j \in \{^3S_1, ^1P_1, ^3S_1 \leftrightarrow {}^3D_1\}$	$^1P_1 \to {}^3P_1$	$^3P_1 \to {}^1P_1$	$^1S_0\ \chi$	$^3S_1\ \chi$
0	0	$NN \to NN$	0	$c_j^{10^*}$	0	0	0	$\frac{c_\chi^7}{2}$
	1	$NN \to NN$	c_j^{27}	0	0	0	$\frac{c_\chi^1}{2}$	0
-1	$\frac{1}{2}$	$\Lambda N \to \Lambda N$	$\frac{1}{10}(9c_j^{27} + c_j^{8s})$	$\frac{1}{2}(c_j^{10^*} + c_j^{8a})$	$-c^{8as}$	$-c^{8as}$	c_χ^2	c_χ^8
	$\frac{1}{2}$	$\Lambda N \to \Sigma N$	$-\frac{3}{10}(c_j^{27} - c_j^{8s})$	$\frac{1}{2}(c_j^{10^*} - c_j^{8a})$	$-3c^{8as}$	c^{8as}	$-c_\chi^3$	$-c_\chi^9$
	$\frac{1}{2}$	$\Sigma N \to \Sigma N$	$\frac{1}{10}(c_j^{27} + 9c_j^{8s})$	$\frac{1}{2}(c_j^{10^*} + c_j^{8a})$	$3c^{8as}$	$3c^{8as}$	c_χ^4	c_χ^{10}
	$\frac{3}{2}$	$\Sigma N \to \Sigma N$	c_j^{27}	c_j^{10}	0	0	$\frac{c_\chi^1}{4}$	$-\frac{c_\chi^7}{4}$
-2	0	$\Lambda\Lambda \to \Lambda\Lambda$	$\frac{1}{40}(5c_j^1 + 27c_j^{27} + 8c_j^{8s})$	0	0	0	$\frac{c_\chi^5}{2}$	0
	0	$\Lambda\Lambda \to \Xi N$	$\frac{1}{20}(5c_j^1 - 9c_j^{27} + 4c_j^{8s})$	0	0	$2c^{8as}$	$\frac{3c_\chi^1}{4} - 3c_\chi^2 - c_\chi^3 + \frac{3c_\chi^5}{4}$	0
	0	$\Lambda\Lambda \to \Sigma\Sigma$	$-\frac{\sqrt{3}}{40}(5c_j^1 + 3c_j^{27} - 8c_j^{8s})$	0	0	0	0	0
	0	$\Xi N \to \Xi N$	$\frac{1}{10}(5c_j^1 + 3c_j^{27} + 2c_j^{8s})$	c_j^{8a}	$2c^{8as}$	$2c^{8as}$	$\frac{2c_\chi^1}{3} - 3c_\chi^2 + \frac{c_\chi^4}{3} + \frac{9c_\chi^5}{8}$	c_χ^{11}
	0	$\Xi N \to \Sigma\Sigma$	$\frac{\sqrt{3}}{20}(-5c_j^1 + c_j^{27} + 4c_j^{8s})$	0	$2\sqrt{3}c^{8as}$	0	$-\frac{c_\chi^1}{4\sqrt{3}} + \sqrt{3}c_\chi^3 + \frac{c_\chi^4}{\sqrt{3}}$	0
	0	$\Sigma\Sigma \to \Sigma\Sigma$	$\frac{1}{40}(15c_j^1 + c_j^{27} + 24c_j^{8s})$	0	0	0	0	0
	1	$\Xi N \to \Xi N$	$\frac{1}{5}(2c_j^{27} + 3c_j^{8s})$	$\frac{1}{3}(c_j^{10} + c_j^{10^*} + c_j^{8a})$	$-2c^{8as}$	$-2c^{8as}$	c_χ^6	c_χ^{12}
	1	$\Xi N \to \Sigma\Sigma$	0	$\frac{1}{3\sqrt{2}}(c_j^{10} + c_j^{10^*} - 2c_j^{8a})$	0	$2\sqrt{2}c^{8as}$	0	$\sqrt{2}c_\chi^{10} - \frac{c_\chi^7}{2\sqrt{2}} - \sqrt{2}c_\chi^9$
	1	$\Xi N \to \Sigma\Lambda$	$\frac{\sqrt{6}}{5}(c_j^{27} - c_j^{8s})$	$\frac{1}{\sqrt{6}}(c_j^{10} - c_j^{10^*})$	$2\sqrt{\frac{2}{3}}c^{8as}$	0	$-\frac{1}{3}\sqrt{\frac{2}{3}}c_\chi^1 + \sqrt{\frac{3}{2}}c_\chi^2 - \frac{c_\chi^4}{3\sqrt{6}} - \sqrt{\frac{2}{3}}c_\chi^6$	$\frac{c_\chi^{10}}{\sqrt{6}} + \sqrt{\frac{2}{3}}c_\chi^{12} + \frac{c_\chi^7}{2\sqrt{6}} - \sqrt{\frac{3}{2}}c_\chi^8 + \sqrt{\frac{2}{3}}c_\chi^9$
	1	$\Sigma\Lambda \to \Sigma\Lambda$	$\frac{1}{5}(3c_j^{27} + 2c_j^{8s})$	$\frac{1}{2}(c_j^{10} + c_j^{10^*})$	0	0	$-\frac{c_\chi^1}{9} + \frac{4c_\chi^3}{3} + \frac{4c_\chi^4}{9} + \frac{2c_\chi^6}{3}$	$\frac{4c_\chi^{10}}{3} + \frac{2c_\chi^{12}}{3} - \frac{c_\chi^7}{3} - \frac{4c_\chi^9}{3}$
	1	$\Sigma\Lambda \to \Sigma\Sigma$	0	$\frac{1}{2\sqrt{3}}(c_j^{10} - c_j^{10^*})$	0	$\frac{4}{\sqrt{3}}c^{8as}$	0	0
	1	$\Sigma\Sigma \to \Sigma\Sigma$	0	$\frac{1}{6}(c_j^{10} + c_j^{10^*} + 4c_j^{8a})$	0	0	0	0
	2	$\Sigma\Sigma \to \Sigma\Sigma$	c_j^{27}	0	0	0	0	0
-3	$\frac{1}{2}$	$\Xi\Lambda \to \Xi\Lambda$	$\frac{1}{10}(9c_j^{27} + c_j^{8s})$	$\frac{1}{2}(c_j^{10} + c_j^{8a})$	$-c^{8as}$	$-c^{8as}$	$-\frac{55c_\chi^1}{72} + 2c_\chi^2 + \frac{7c_\chi^3}{6} + \frac{c_\chi^4}{18} + \frac{3c_\chi^5}{32} + \frac{c_\chi^6}{12}$	$\frac{11c_\chi^{10}}{12} + \frac{3c_\chi^{11}}{4} + \frac{25c_\chi^{12}}{12} + \frac{5c_\chi^7}{24} - \frac{7c_\chi^8}{4} - \frac{c_\chi^9}{6}$
	$\frac{1}{2}$	$\Xi\Lambda \to \Xi\Sigma$	$-\frac{3}{10}(c_j^{27} - c_j^{8s})$	$\frac{1}{2}(c_j^{10} - c_j^{8a})$	$-3c^{8as}$	c^{8as}	$\frac{11c_\chi^1}{24} - \frac{3c_\chi^2}{2} - \frac{c_\chi^3}{2} - \frac{c_\chi^4}{3} + \frac{9c_\chi^5}{32} + \frac{c_\chi^6}{4}$	$\frac{9c_\chi^{10}}{4} - \frac{3c_\chi^{11}}{4} + \frac{5c_\chi^{12}}{4} - \frac{c_\chi^7}{8} - \frac{3c_\chi^8}{4} - \frac{c_\chi^9}{2}$
	$\frac{1}{2}$	$\Xi\Sigma \to \Xi\Sigma$	$\frac{1}{10}(c_j^{27} + 9c_j^{8s})$	$\frac{1}{2}(c_j^{10} + c_j^{8a})$	$3c^{8as}$	$3c^{8as}$	$\frac{11c_\chi^1}{24} - 3c_\chi^2 + \frac{5c_\chi^3}{2} + \frac{c_\chi^4}{6} + \frac{27c_\chi^5}{32} + \frac{3c_\chi^6}{4}$	$\frac{5c_\chi^{10}}{4} + \frac{3c_\chi^{11}}{4} + \frac{3c_\chi^{12}}{4} - \frac{c_\chi^7}{8} - \frac{3c_\chi^8}{4} - \frac{3c_\chi^9}{2}$
	$\frac{3}{2}$	$\Xi\Sigma \to \Xi\Sigma$	c_j^{27}	$c_j^{10^*}$	0	0	$-\frac{2c_\chi^1}{3} + \frac{3c_\chi^2}{2} + c_\chi^3 + \frac{c_\chi^4}{6}$	$\frac{3c_\chi^{10}}{2} - c_\chi^7 + \frac{3c_\chi^8}{2} - 3c_\chi^9$
-4	0	$\Xi\Xi \to \Xi\Xi$	0	c_j^{10}	0	0	0	$5c_\chi^{10} + 4c_\chi^{12} - 3c_\chi^8 - 2c_\chi^9$
	1	$\Xi\Xi \to \Xi\Xi$	c_j^{27}	0	0	0	$-\frac{4c_\chi^1}{3} + 3c_\chi^2 + 2c_\chi^3 + \frac{c_\chi^4}{3}$	0

TABLE 4.2: SU(3) relations of pure baryon-baryon contact terms in non-vanishing partial waves up to $\mathcal{O}(q^2)$ with non-relativistic power counting. The channels are described by strangeness S and total isospin I.

4.2 ONE- AND TWO-MESON-EXCHANGE CONTRIBUTIONS

In the last section, we have addressed the short-range part of the baryon-baryon interaction via contact terms. Let us now analyze the long- and mid-range part of the interaction, generated by one- and two-meson-exchange. The contributing diagrams up to NLO are shown in Fig. 2.4, which displays the hierarchy of baryonic forces.

The vertices, necessary for the construction of these diagrams stem from the leading-order meson-baryon interaction Lagrangian $\mathscr{L}_{\mathrm{B}}^{(1)}$ in Eq. (2.57). The vertex between two baryons and one meson emerges from the part

$$\begin{aligned}&\frac{D}{2}\langle\bar{B}\gamma^\mu\gamma_5\{u_\mu,B\}\rangle+\frac{F}{2}\langle\bar{B}\gamma^\mu\gamma_5\left[u_\mu,B\right]\rangle\\&=-\frac{1}{2f_0}\sum_{i,j,k=1}^{8}N_{B_iB_j\phi_k}(\bar{B}_i\gamma^\mu\gamma_5B_j)(\partial_\mu\phi_k)+\mathcal{O}(\phi^3)\,,\end{aligned}\tag{4.7}$$

where we have used $u_\mu=-\frac{1}{f_0}\partial_\mu\phi+\mathcal{O}(\phi^3)$ and have rewritten the pertinent part of the Lagrangian in terms of the physical meson and baryon fields

$$\phi_i\in\left\{\pi^0,\pi^+,\pi^-,K^+,K^-,K^0,\bar{K}^0,\eta\right\}\,,\quad B_i\in\left\{n,p,\Sigma^0,\Sigma^+,\Sigma^-,\Lambda,\Xi^0,\Xi^-\right\}\,.\tag{4.8}$$

The factors $N_{B_iB_j\phi_k}$ are linear combinations of the axial vector coupling constants D and F with certain SU(3) coefficients. These factors vary for different combinations of the involved baryons and mesons and can be obtained easily by multiplying out the baryon and meson flavor matrices. In a similar way, we obtain the (Weinberg-Tomozawa) vertex between two baryons and two mesons from the covariant derivative in $\mathscr{L}_{\mathrm{B}}^{(1)}$, leading to

$$\langle\bar{B}\mathrm{i}\gamma^\mu\left[\Gamma_\mu,B\right]\rangle=\frac{\mathrm{i}}{8f_0^2}\sum_{i,j,k,l=1}^{8}N_{B_i\phi_kB_j\phi_l}(\bar{B}_i\gamma^\mu B_j)(\phi_k\partial_\mu\phi_l)+\mathcal{O}(\phi^4)\,,\tag{4.9}$$

where $\Gamma_\mu=\frac{1}{8f_0^2}[\phi,\partial_\mu\phi]+\mathcal{O}(\phi^4)$ was used.

The calculation of the baryon-baryon potentials is done in the center-of-mass frame and in the isospin limit $m_u=m_d$. To obtain the contribution of the Feynman diagrams to the non-relativistic potential, we perform an expansion in the inverse baryon mass $1/M_{\mathrm{B}}$. If loops are involved, the integrand is expanded before integrating over the loop momenta. This produces results that are equivalent to the usual heavy-baryon formalism. In the case of the two-meson-exchange diagrams at one-loop level, ultraviolet divergences are treated by dimensional regularization, which introduces a scale λ. In dimensional regularization divergences are isolated as terms proportional to

$$R=\frac{2}{d-4}+\gamma_{\mathrm{E}}-1-\ln\left(4\pi\right)\,,\tag{4.10}$$

with $d\neq4$ the space-time dimension and the Euler-Mascheroni constant $\gamma_{\mathrm{E}}\approx0.5772$. These terms can be absorbed by the contact terms.

According to Eqs. (4.7) and (4.9) the vertices have the same form for different combinations of baryons and mesons, just their prefactors change. Therefore, the one- and two-pseudoscalar-meson exchange potentials can be given by a master formula, where the proper masses of the exchanged mesons have to be inserted, and which has to be multiplied with an appropriate SU(3) factor N. In the following we will present the analytic

formulas for the one- and two-meson-exchange diagrams, which we have derived already in Ref. [120]. The pertinent SU(3) factors will be displayed next to the considered Feynman diagram. The results will be given in terms of a central potential (V_C), a spin-spin potential ($\vec{\sigma}_1 \cdot \vec{\sigma}_2\, V_S$) and a tensor-type potential ($\vec{\sigma}_1 \cdot \vec{q}\, \vec{\sigma}_2 \cdot \vec{q}\, V_T$). The momentum transfer is $q = |\vec{p}_f - \vec{p}_i\,|$, with $\vec{p}_i$ and $\vec{p}_f$ the initial and final state momenta in the center-of-mass frame.

Note that the presented results apply only to direct diagrams. This is for example the case for the leading-order one-eta exchange in the Λn interaction, i.e., for $\Lambda(\vec{p}_i)n(-\vec{p}_i) \xrightarrow{\eta} \Lambda(\vec{p}_f)n(-\vec{p}_f)$. An example of a crossed diagram is the one-kaon exchange in the process $\Lambda(\vec{p}_i)n(-\vec{p}_i) \xrightarrow{K} n(-\vec{p}_f)\Lambda(\vec{p}_f)$, where the nucleon and the hyperon in the final state are interchanged and strangeness is exchanged. In such cases, $\vec{p}_f$ is replaced by $-\vec{p}_f$ and the momentum transfer in the potentials is $q = |\vec{p}_f + \vec{p}_i\,|$. Due to the exchange of fermions in the final states a minus sign arises, and additionally the spin-exchange operator $P^{(\sigma)} = \frac{1}{2}(\mathbb{1} + \vec{\sigma}_1 \cdot \vec{\sigma}_2)$ has to be applied. The remaining structure of the potentials stays the same. More details about crossed diagrams can be found in Chapter 6.

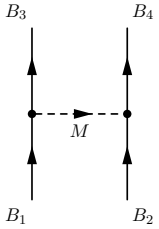

$$N = N_{B_3 B_1 \bar{M}} N_{B_4 B_2 M}$$

FIGURE 4.2: One-meson exchange

The leading-order contribution comes from the *one-meson exchange* diagram in Fig. 4.2. It contributes only to the tensor-type potential:

$$V_{\mathrm{T}}^{\mathrm{ome}}(q) = -\frac{N}{4f_0^2}\frac{1}{q^2 + m^2 - \mathrm{i}\epsilon}\,. \tag{4.11}$$

The symbol $\bar{M}$ in the SU(3) coefficient N denotes the charge-conjugated meson of meson M in particle basis (e.g., $\pi^+ \leftrightarrow \pi^-$). In the following we will omit NLO effects of the one-meson exchange diagrams, that stem, e.g., from corrections to the coupling constants. This is in accordance with our assumption of SU(3) symmetry in Sec. 4.3.

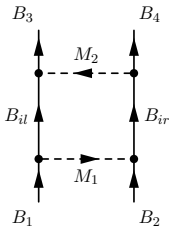

$$N = N_{B_{il} B_1 \bar{M}_1} N_{B_3 B_{il} M_2} N_{B_{ir} B_2 M_1} N_{B_4 B_{ir} \bar{M}_2}$$

FIGURE 4.3: Planar box

At next-to-leading order the two-meson exchange diagrams start to contribute. The *planar box* in Fig. 4.3 contains an irreducible part and a reducible part coming from the iteration of the one-meson exchange to second order. Inserting the potential into the Lippmann-Schwinger equation generates the reducible part; it is therefore not part of the potential. The irreducible part is obtained from the residues at the poles of the meson propagators,

disregarding the poles of the baryon propagators. With the masses of the two exchanged mesons set to m_1 and m_2, the irreducible potentials can be written in closed analytical form,

$$\begin{aligned} V_{\text{irr, C}}^{\text{planar box}}(q) = \frac{N}{3072\pi^2 f_0^4}\Bigg\{ & \frac{5}{3}q^2 + \frac{\left(m_1^2-m_2^2\right)^2}{q^2} + 16\left(m_1^2+m_2^2\right) \\ & + \left[23q^2 + 45\left(m_1^2+m_2^2\right)\right]\left(R + 2\ln\frac{\sqrt{m_1 m_2}}{\lambda}\right) \\ & + \frac{m_1^2-m_2^2}{q^4}\left[12q^4 + \left(m_1^2-m_2^2\right)^2 - 9q^2\left(m_1^2+m_2^2\right)\right]\ln\frac{m_1}{m_2} \\ & + \frac{2}{w^2(q)}\Bigg[23q^4 - \frac{\left(m_1^2-m_2^2\right)^4}{q^4} + 56\left(m_1^2+m_2^2\right)q^2 + 8\frac{m_1^2+m_2^2}{q^2}\left(m_1^2-m_2^2\right)^2 \\ & \qquad + 2\left(21m_1^4 + 22m_1^2m_2^2 + 21m_2^4\right)\Bigg] L(q)\Bigg\}, \end{aligned} \tag{4.12}$$

$$\begin{aligned} V_{\text{irr, T}}^{\text{planar box}}(q) &= -\frac{N}{128\pi^2 f_0^4}\left[L(q) - \frac{1}{2} - \frac{m_1^2-m_2^2}{2q^2}\ln\frac{m_1}{m_2} + \frac{R}{2} + \ln\frac{\sqrt{m_1 m_2}}{\lambda}\right] \\ &= -\frac{1}{q^2}V_{\text{irr, S}}^{\text{planar box}}(q), \end{aligned} \tag{4.13}$$

where we have defined the functions

$$\begin{aligned} w(q) &= \frac{1}{q}\sqrt{\left(q^2+(m_1+m_2)^2\right)\left(q^2+(m_1-m_2)^2\right)}, \\ L(q) &= \frac{w(q)}{2q}\ln\frac{\left[qw(q)+q^2\right]^2 - \left(m_1^2-m_2^2\right)^2}{4m_1m_2q^2}. \end{aligned} \tag{4.14}$$

The relation between the spin-spin and tensor-type potential follows from the identity $(\vec{\sigma}_1\times\vec{q})\cdot(\vec{\sigma}_2\times\vec{q}) = q^2\vec{\sigma}_1\cdot\vec{\sigma}_2 - (\vec{\sigma}_1\cdot\vec{q})(\vec{\sigma}_2\cdot\vec{q})$.

One should note that all potentials shown above are finite also in the limit $q\to 0$. Terms proportional to $1/q^2$ or $1/q^4$ are canceled by opposite terms in the functions $L(q)$ and $w(q)$ in the limit of small q. For numerical calculations it is advantageous to perform an expansion of the potentials in a power series for small q in order to implement directly this cancellation. For equal meson masses the expressions for the potentials reduce to the results in Refs. [121]. This is the case for the NN interaction of Refs. [118, 122, 123, 124] based on χEFT, where only contributions from two-pion exchange need to be taken into account.

In the actual calculations only the non-polynomial part of Eqs. (4.12) and (4.13) is taken into account, i.e., the pieces proportional to $L(q)$ and to $1/q^2$ and $1/q^4$. The polynomial part is equivalent to the LO and NLO contact terms and, therefore, does not need to be considered. The contributions proportional to the divergence R are likewise omitted. Their effect is absorbed by the contact terms or a renormalization of the coupling constants, see, e.g., the corresponding discussion in Appendix A of Ref. [122] for the NN case.

These statements above apply also to the other contributions to the potential described below.

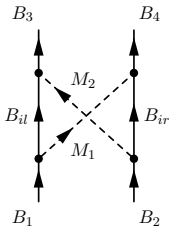

$$N = N_{B_{il}B_1\bar{M}_1}N_{B_3B_{il}M_2}N_{B_{ir}B_2\bar{M}_2}N_{B_4B_{ir}M_1}$$

FIGURE 4.4: Crossed box

The *crossed box* diagrams in Fig. 4.4 contribute to the central, spin-spin, and tensor-type potentials. The similar structure with some differences in the kinematics of the planar and crossed box diagram leads to relations between them. Obviously, the crossed box has no iterated part. The potentials of the crossed box are equal to the potentials of the irreducible part of the planar box, up to a sign in the central potential:

$$\begin{aligned} V_{\mathrm{C}}^{\text{crossed box}}(q) &= -V_{\mathrm{C,\,irr}}^{\text{planar box}}(q)\,, \\ V_{\mathrm{T}}^{\text{crossed box}}(q) &= -\frac{1}{q^2}V_{\mathrm{S}}^{\text{crossed box}}(q) = V_{\mathrm{T,\,irr}}^{\text{planar box}}(q)\,. \end{aligned} \tag{4.15}$$

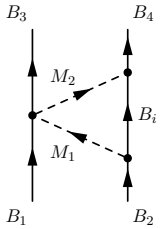

FIGURE 4.5: Left triangle

$$N = N_{B_3\bar{M}_2B_1M_1}N_{B_iB_2\bar{M}_1}N_{B_4B_iM_2}$$

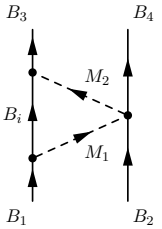

FIGURE 4.6: Right triangle

$$N = N_{B_iB_1\bar{M}_1}N_{B_3B_iM_2}N_{B_4\bar{M}_2B_2M_1}$$

The two *triangle* diagrams, Figs. 4.5 and 4.6, constitute potentials, that are of equal form with different SU(3) factors N. The corresponding central potential reads

$$\begin{aligned} V_{\mathrm{C}}^{\text{triangle}}(q) = -\frac{N}{3072\pi^2 f_0^4}\Bigg\{ & -2\left(m_1^2+m_2^2\right) + \frac{\left(m_1^2-m_2^2\right)^2}{q^2} - \frac{13}{3}q^2 \\ & + \left[8\left(m_1^2+m_2^2\right) - \frac{2\left(m_1^2-m_2^2\right)^2}{q^2} + 10q^2\right] L\left(q\right) \\ & + \frac{m_1^2-m_2^2}{q^4}\left[\left(m_1^2-m_2^2\right)^2 - 3\left(m_1^2+m_2^2\right)q^2\right]\ln\frac{m_1}{m_2} \\ & + \left[9\left(m_1^2+m_2^2\right)+5q^2\right]\left(R + 2\ln\frac{\sqrt{m_1m_2}}{\lambda}\right)\Bigg\}\,. \end{aligned} \tag{4.16}$$

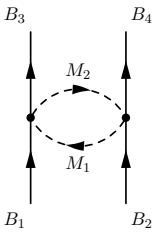

$$N = N_{B_3\bar{M}_2B_1M_1}N_{B_4\bar{M}_1B_2M_2}$$

FIGURE 4.7: Football diagram

The *football* diagrams in Fig. 4.7 contributes only to the central potential. One finds

$$V_{\rm C}^{\rm football}(q) = \frac{N}{3072\pi^2 f_0^4}\Bigg\{ -2\left(m_1^2+m_2^2\right) - \frac{\left(m_1^2-m_2^2\right)^2}{2q^2} - \frac{5}{6}q^2 + w^2(q)\,L(q) + \frac{1}{2}\left[3\left(m_1^2+m_2^2\right)+q^2\right]\left(R + 2\ln\frac{\sqrt{m_1 m_2}}{\lambda}\right) - \frac{m_1^2-m_2^2}{2q^4}\left[\left(m_1^2-m_2^2\right)^2 + 3\left(m_1^2+m_2^2\right)q^2\right]\ln\frac{m_1}{m_2}\Bigg\}. \tag{4.17}$$

4.3 HYPERON-NUCLEON SCATTERING

Using the potentials derived in Secs. 4.1 and 4.2, the hyperon-nucleon interaction at NLO can now be investigated. The very successful approach to the nucleon-nucleon interaction of Ref. [118, 122, 123] within SU(2) χEFT, has been extended to the leading-order baryon-baryon interaction in Refs. [25, 26, 27] by the Bonn-Jülich group. In the following we present our joint results of Ref. [125], where the hyperon-nucleon interaction is extended to next-to-leading order in SU(3) chiral effective field theory.

As mentioned in Sec. 2.4 the chiral power counting is applied to the potential, where only two-particle irreducible diagrams contribute. These potentials are then inserted into a regularized Lippmann-Schwinger equation to obtain the reaction amplitude (or T-matrix). In contrast to the NN interaction, the Lippmann-Schwinger equation for the YN interaction involves not only coupled partial waves, but also coupled two-baryon channels. The coupled-channel Lippmann-Schwinger equation in the particle basis reads after partial-wave decomposition

$$T_{\nu''\nu'}^{\rho''\rho',J}(k'',k';\sqrt{s}) = V_{\nu''\nu'}^{\rho''\rho',J}(k'',k') + \sum_{\rho,\nu}\int_0^\infty \frac{{\rm d}k\,k^2}{(2\pi)^3}\,V_{\nu''\nu}^{\rho''\rho,J}(k'',k)\frac{2\mu_\nu}{k_\nu^2-k^2+{\rm i}\epsilon}T_{\nu\nu'}^{\rho\rho',J}(k,k';\sqrt{s})\,, \tag{4.18}$$

where J denotes the conserved total angular momentum. The coupled two-particle channels $(\Lambda p, \Sigma^+ n, \Sigma^0 p, \ldots)$ are labeled by ν, and the partial waves $({}^1S_0, {}^3P_0, \ldots)$ by ρ. Furthermore, μ_ν is the reduced baryon mass in channel ν. We have chosen a non-relativistic scattering equation to ensure that the potential can also be applied consistently to Faddeev and Faddeev-Yakubovsky calculations in the few-body sector, and to (hyper) nuclear matter calculations within the conventional Brueckner-Hartree-Fock formalism (see Chapter 5). Nevertheless, the relativistic relation between the on-shell momentum k_ν and the center-of-mass energy has been used, $\sqrt{s} = \sqrt{M_{B_{1,\nu}}^2 + k_\nu^2} + \sqrt{M_{B_{2,\nu}}^2 + k_\nu^2}$, in order to get the two-particle thresholds at their correct positions. Note that we use the physical baryon masses in the Lippmann-Schwinger equation, which introduces some additional SU(3) symmetry breaking. Relativistic kinematics has also been used to relate the laboratory momentum $p_{\rm lab}$ of the hyperon to the center-of-mass energy $\sqrt{s}$. The Coulomb interaction is implemented by the use of the Vincent-Phatak method [118, 126]. Similar to the nucleonic sector at NLO [118], a regulator function of the form $f_R(\Lambda) = \exp[-(k'^4+k^4)/\Lambda^4]$ is employed to cut off the high-energy components of the potential. For higher orders in the chiral power counting, higher powers than 4 in the exponent of f_R have to be used. This ensures that the regulator introduces only contributions, that are beyond the given order. The cutoff Λ is varied in the range $(500\ldots700)$ MeV, i.e., comparable to what was used

for the NN interaction in Ref. [118]. The resulting bands represent the cutoff dependence, after readjusting the contact parameters, and thus could be viewed as a lower bound on the theoretical uncertainty. Recently, improved schemes to estimate the theoretical error were proposed and applied to the NN interaction [127, 128, 129]. However, such schemes require higher orders in the chiral power counting and are therefore not performed in a NLO calculation.

Let us now give some further remarks on the hyperon-nucleon potential. The partial-wave contributions of the meson-exchange diagrams are obtained by employing the partial-wave decomposition formulas of Ref. [25]. Given the sparse experimental information on YN scattering, SU(3) flavor symmetric LECs have been used, while SU(3) symmetry breaking is incorporated through the physical masses of the exchanged pseudoscalar mesons (π, K, η). This means, that the SU(3) symmetry breaking contact terms c_χ^i of Tab. 4.2 are set to zero. The polynomial part of the two-meson exchange amplitudes are absorbed in the contact terms. The majority of those terms involve the masses of the pseudoscalar mesons and, therefore, generate some SU(3) symmetry breaking. Thus, the SU(3) symmetry imposed on our contact interaction is understood as one that is fulfilled on the level of the renormalized coupling constants. Furthermore, the constant c^{8as}, responsible for singlet-triplet mixing, is set to zero. The effect of this constant is described in more detail in Chapter 5. For the one-meson exchange, diagrams with π, K or η exchange are possible. For the two meson exchange, all combinations $\pi\pi$, πK, $\pi\eta$, KK, $K\eta$, $\eta\eta$ can occur, with intermediate baryons from the full octet, N, Λ, Σ and even Ξ. The contributions of such diagrams do not involve any free parameters. The pseudoscalar-meson decay constant is set to $f_0 = 93$ MeV and for the axial-vector coupling constants the values $D = 0.76$ and $F = 0.50$ have been used. Small changes in these parameters lead to a comparable description of the YN scattering data, if the LECs are refitted accordingly.

As can be seen in Tab. 4.2, one gets for the YN contact terms five independent LO constants, acting in the S-waves, eight additional constants at NLO in the S-waves, and nine NLO constant acting in the P-waves. The contact terms represent the unresolved short-distance dynamics, and the corresponding low-energy constants are fitted to empirical data. The "standard" set of 36 YN data points has been used. It includes low-energy total cross sections for the reactions: $\Lambda p \to \Lambda p$ from Ref. [130] (6 data points) and Ref. [131] (6 data points), $\Sigma^- p \to \Lambda n$ [132] (6 data points), $\Sigma^- p \to \Sigma^0 n$ [132] (6 data points), $\Sigma^- p \to \Sigma^- p$ [133] (7 data points), $\Sigma^+ p \to \Sigma^+ p$ [133] (4 data points), and the inelastic capture ratio at rest [134, 135]. The hypertriton ($^3_\Lambda$H) binding energy is chosen as a further input. It determines the relative strength of the spin-singlet and spin-triplet S-wave contributions of the Λp interaction. The experimental total cross sections for $\Sigma^+ p \to \Sigma^+ p$ and $\Sigma^- p \to \Sigma^- p$ were obtained with an incomplete angular coverage [133]:

$$\sigma = \frac{2}{\cos\theta_{\rm max} - \cos\theta_{\rm min}} \int_{\cos\theta_{\rm min}}^{\cos\theta_{\rm max}} \frac{{\rm d}\sigma(\theta)}{{\rm d}\cos\theta}\, {\rm d}\cos\theta \ . \tag{4.19}$$

Following Ref. [18], $\cos\theta_{\rm min} = -0.5$ and $\cos\theta_{\rm max} = 0.5$ has been used for the cross sections in these two channels, in order to stay as close as possible to the experimental situation. The total cross sections for the other channels are evaluated by integrating the differential cross sections over the whole angular region.

The χ^2 fits to the cross sections were done for a cutoff $\Lambda = 600$ MeV. For other values of the cutoff, the LECs were varied so that the result stays as close as possible to the result for $\Lambda = 600$ MeV. Note, that due to the sparse and inaccurate experimental data,

Λ [MeV]		450	500	550	600	650	700
$^1S_0$	$\tilde{C}^{27}_{^1S_0}$	−0.0893	−0.0672	0.00648	0.1876	0.6140	1.145
	$\tilde{C}^{8_s}_{^1S_0}$	0.2000	0.1970	0.1930	0.1742	0.1670	0.1730
	$C^{27}_{^1S_0}$	1.500	1.800	2.010	2.200	2.400	2.410
	$C^{8_s}_{^1S_0}$	−0.200	−0.200	−0.206	−0.0816	−0.0597	0.1000
$^3S_1$-$^3D_1$	$\tilde{C}^{10^*}_{^3S_1}$	0.104	0.541	1.490	3.440	4.990	5.600
	$\tilde{C}^{10}_{^3S_1}$	0.171	0.209	0.635	1.420	2.200	2.960
	$\tilde{C}^{8_a}_{^3S_1}$	0.0218	0.00715	−0.0143	−0.0276	−0.0269	0.00173
	$C^{10^*}_{^3S_1}$	2.240	2.310	2.450	2.740	2.530	2.030
	$C^{10}_{^3S_1}$	0.310	0.143	0.741	1.090	1.150	1.120
	$C^{8_a}_{^3S_1}$	0.373	0.469	0.627	0.775	0.854	0.964
	$C^{10^*}_{^3S_1-^3D_1}$	−0.360	−0.429	−0.428	−0.191	−0.191	−0.122
	$C^{10}_{^3S_1-^3D_1}$	−0.300	−0.300	−0.356	−0.380	−0.380	−0.228
	$C^{8_a}_{^3S_1-^3D_1}$	0.0356	0.0475	0.0453	−0.00621	−0.00621	−0.0497

TABLE 4.3: The YN contact terms for the $^1S_0$ and $^3S_1$-$^3D_1$ partial waves for various cutoffs Λ. The values of the $\tilde{C}$'s are in 10^4 GeV^{-2} the ones of the C's in 10^4 GeV^{-4}.

the obtained fit of the low-energy constants is not unique. For instance, the YN data can be described equally well with a repulsive or an attractive interaction in the $^3S_1$ partial wave of the ΣN interaction with isospin $I = 3/2$. However, recent calculations from lattice QCD [3] suggest a repulsive $^3S_1$ phase shift in the ΣN $I = 3/2$ channel, hence the repulsive solution has been adopted. Furthermore, this is consistent with empirical information from Σ^--production on nuclei, which point to a repulsive Σ-nucleus potential. This is discussed in more detail in Chapter 5, where the properties of hyperons in nuclear matter are studied. The determination of the P-wave amplitudes is even more problematic, as there are mostly total cross sections at low energies given, which are dominated by the S-wave amplitudes. Only a limited number of differential cross sections and no polarization observables are available. Therefore parts, of the low-energy constants, present in the P-waves of the YN potentials, are determined in the NN sector with the use of SU(3) symmetry. However, a simultaneous description of the NN and YN interactions with SU(3) symmetric LECs is not possible at NLO, due to the strong correlation between the $^1S_0$ partial wave in the NN $(I = 1)$ and ΣN $(I = 3/2)$ channels imposed by SU(3) symmetry, cf. Tab. 4.2.

In the following we present the results obtained under these restrictions with the fitting procedure to the YN sector described above. Other scenarios, such as the inclusion of SU(3) symmetry breaking in the decay constant f_0, or including only two-meson-exchange diagrams that involve pions, lead to a comparable description of the empirical YN data. The values of the LECs, obtained with the procedure described above, are given in Tabs. 4.3 and 4.4 for the cutoff region $\Lambda = (450 \ldots 700)$ MeV. The best χ^2 values for the fit were obtained in the region $\Lambda = (500 \ldots 650)$ MeV. In this plateau region the χ^2 has only a small cutoff dependence, with a excellent total χ^2 of about 16. This is comparable to what can be obtained with the most advanced phenomenological YN models. Note that at LO a χ^2-value of about 28 was obtained [25], therefore, going to higher order in the chiral power

Λ [MeV]		450	500	550	600	650	700
${}^3P_0$	$C^{27}_{{}^3P_0}$	1.47	1.49	1.51	1.55	1.60	1.71
	$C^{8_s}_{{}^3P_0}$	2.50	2.50	2.50	2.50	2.50	2.50
${}^3P_1$	$C^{27}_{{}^3P_1}$	−0.43	−0.43	−0.43	−0.43	−0.43	−0.43
	$C^{8_s}_{{}^3P_1}$	0.65	0.65	0.65	0.65	0.65	0.65
${}^3P_2$	$C^{27}_{{}^3P_2}$	−0.096	−0.063	−0.041	−0.025	−0.012	0.000
	$C^{8_s}_{{}^3P_2}$	1.00	1.00	1.00	1.00	1.00	1.00
${}^1P_1$	$C^{10}_{{}^1P_1}$	0.49	0.49	0.49	0.49	0.49	0.49
	$C^{10^*}_{{}^1P_1}$	−0.14	−0.14	−0.14	−0.14	−0.14	−0.14
	$C^{8_a}_{{}^1P_1}$	−0.65	−0.60	−0.58	−0.56	−0.54	−0.52
${}^1P_1$-${}^3P_1$	$C^{8_s 8_a}_{{}^1P_1-{}^3P_1}$	0	0	0	0	0	0

TABLE 4.4: The YN contact terms for the P-waves for various cutoffs Λ. The values of the LECs are in 10^4 GeV^{-4}.

counting leads to a significant improvement. In the following figures the bands of the NLO results correspond to the cutoff range $\Lambda = (500 \ldots 650)$ MeV. Furthermore, results for the leading-order calculation of Ref. [25] are displayed. Here the bands correspond to the cutoff region $\Lambda = (550 \ldots 700)$ MeV. For comparison, results of the Jülich '04 meson-exchange model [19] are also shown in the following figures.

In Fig. 4.8 the total cross sections (as defined in Eq. (4.19)) as functions of p_{lab} for various YN interactions are presented. The experimental data is well reproduced at NLO. Especially the results in the Λp channel are in line with the data points (also at higher energies) and the energy dependence in the $\Sigma^+ p$ channel is significantly improved at NLO. It is also interesting to note that the NLO results are now closer to the phenomenological Jülich '04 model than at LO. One expects the theoretical uncertainties to become smaller, when going to higher order in the chiral power counting. This is reflected in the fact, that the bands at NLO are considerably smaller than at LO. These bands represent only the cutoff dependence and therefore constitute a lower bound on the theoretical error. Similar features can be seen in Fig. 4.9, where the differential cross section is presented as a function of $\cos\theta$. The shown data points were not included directly in the fitting routine and the predicted curves of the χEFT interaction agree mostly with the trend of these data.

In Tab. 4.5 the scattering lengths and effective range parameters for the Λp and $\Sigma^+ p$ interactions in the ${}^1S_0$ and ${}^3S_1$ partial waves are given. Result for LO [25] and NLO χEFT [125], for the Jülich '04 model [19] and for the Nijmegen NSC97f potential [18] are shown. The NLO Λp scattering lengths are larger than for the LO calculation, and closer to the values obtained by the meson-exchange models. The triplet $\Sigma^+ p$ scattering length is positive in the LO as well as the NLO calculation, which indicates a repulsive interaction in this channel. Also given in Tab. 4.5 is the hypertriton binding energy, calculated with the corresponding chiral potentials. As stated before, the hypertriton binding energy was part of the fitting procedure and values close to the experimental value could be achieved. The predictions for the ${}^3_\Lambda H$ binding energy are based on the

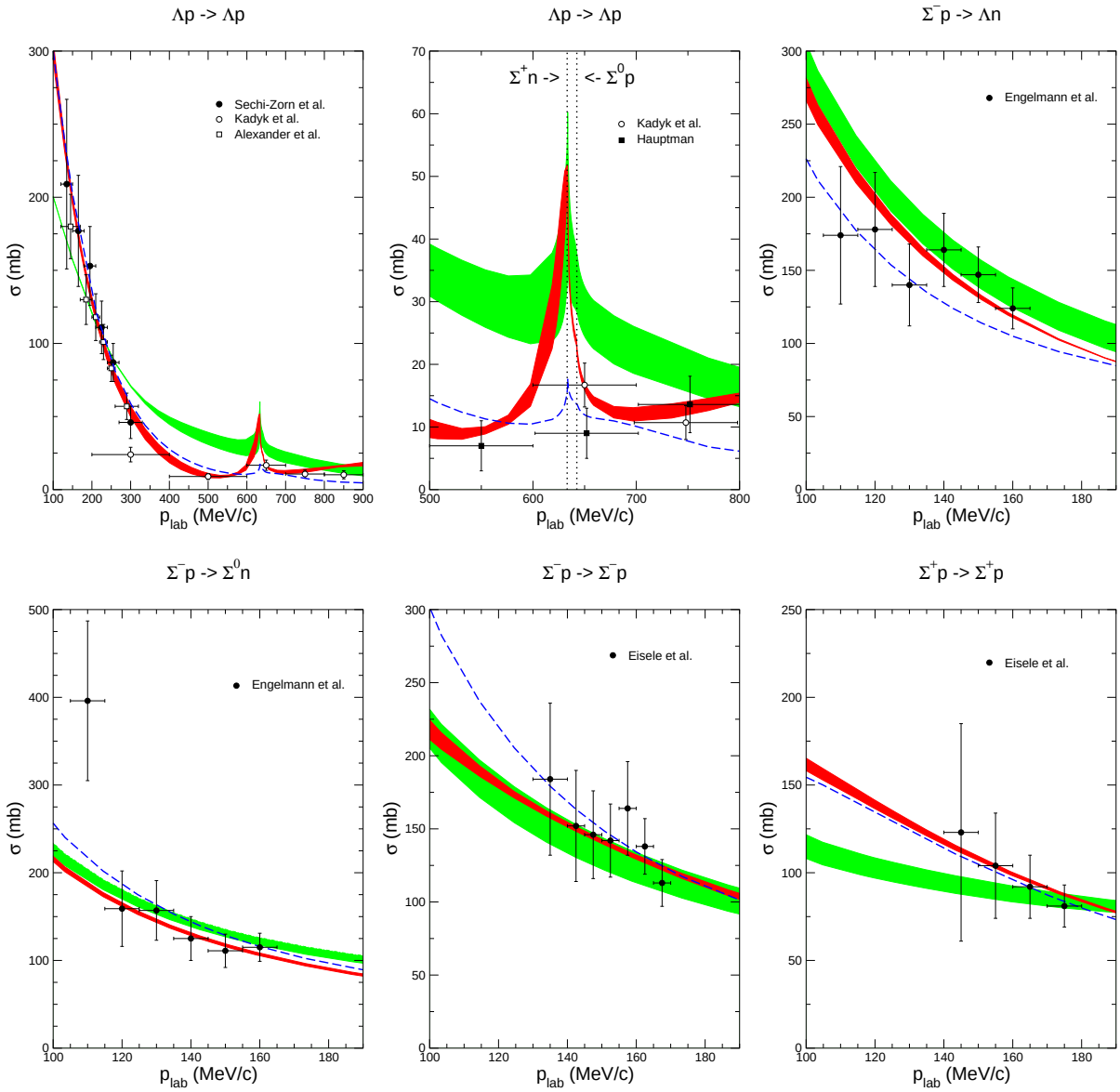

FIGURE 4.8: "Total" cross section σ as a function of $p_{\rm lab}$ [125]. The experimental cross sections are taken from Refs. [130] (filled circles), [131] (open squares), [136] (open circles), and [137] (filled squares) ($\Lambda p \to \Lambda p$), from [132] ($\Sigma^- p \to \Lambda n$, $\Sigma^- p \to \Sigma^0 n$) and from [133] ($\Sigma^- p \to \Sigma^- p$, $\Sigma^+ p \to \Sigma^+ p$). The red (dark) band shows the chiral EFT results to NLO for variations of the cutoff in the range $\Lambda = (500 \ldots 650)$ MeV, while the green (light) band are results to LO for $\Lambda = (550 \ldots 700)$ MeV [25]. The dashed curve is the result of the Jülich '04 meson-exchange potential [19].

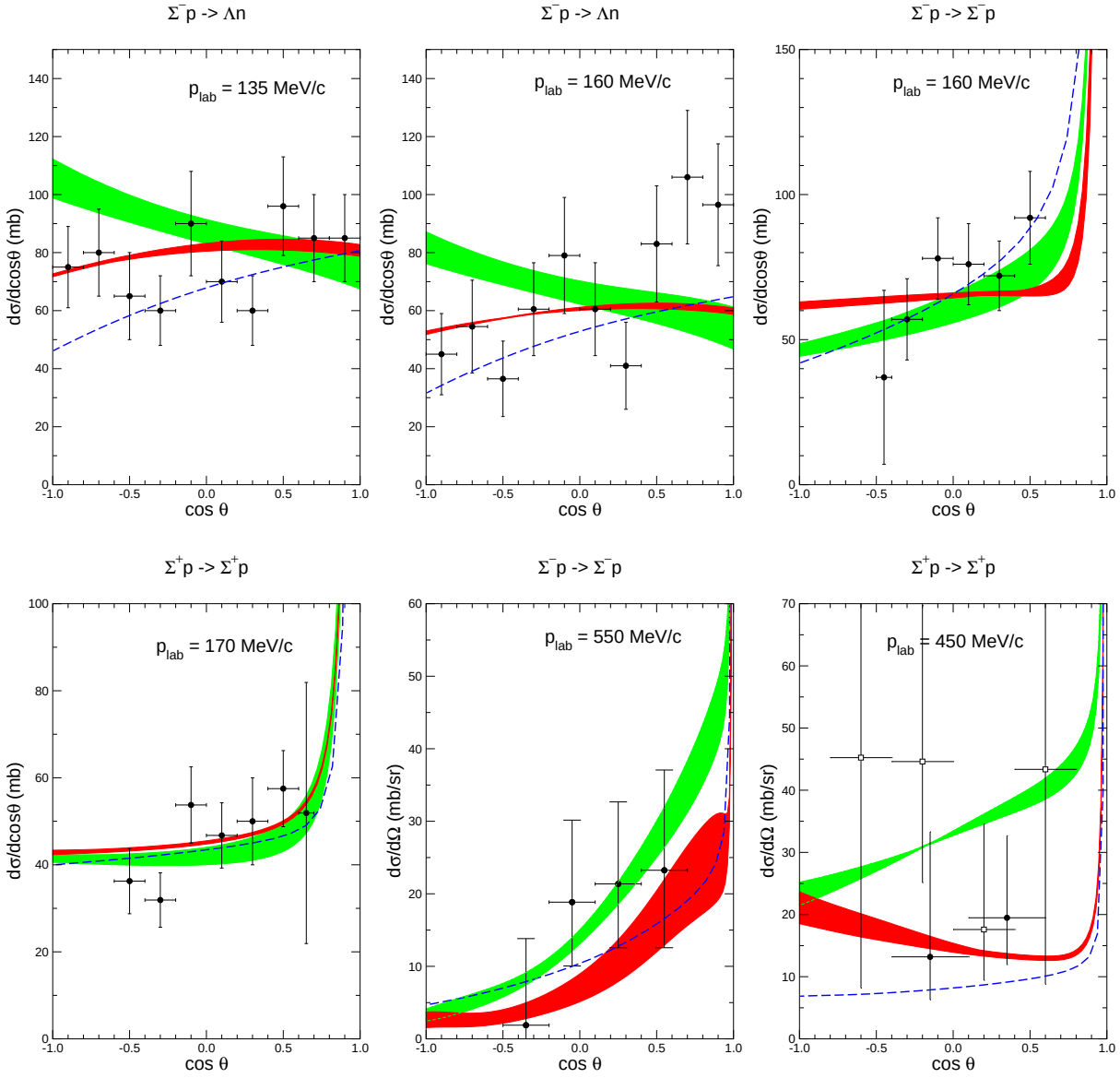

FIGURE 4.9: Differential cross section $\mathrm{d}\sigma/\mathrm{d}\cos\theta$ as a function of $\cos\theta$ [125], where θ is the c.m. scattering angle, at various values of p_{lab}. The experimental differential cross sections are taken from Refs. [132] ($\Sigma^- p \to \Lambda n$), [133] ($\Sigma^- p \to \Sigma^- p$, $\Sigma^+ p \to \Sigma^+ p$), [138] ($\Sigma^- p \to \Sigma^- p$), and from [139] (filled circles) and [140] (open circles) ($\Sigma^+ p \to \Sigma^+ p$). Same description of curves as in Fig. 4.8.

	NLO						LO	Jül '04	NSC97f
Λ [MeV]	450	500	550	600	650	700	600		
$a_s^{\Lambda p}$	−2.90	−2.91	−2.91	−2.91	−2.90	−2.90	−1.91	−2.56	−2.60
$r_s^{\Lambda p}$	2.64	2.86	2.84	2.78	2.65	2.56	1.40	2.74	3.05
$a_t^{\Lambda p}$	−1.70	−1.61	−1.52	−1.54	−1.51	−1.48	−1.23	−1.67	−1.72
$r_t^{\Lambda p}$	3.44	3.05	2.83	2.72	2.64	2.62	2.13	2.93	3.32
$a_s^{\Sigma^+ p}$	−3.58	−3.59	−3.60	−3.56	−3.46	−3.49	−2.32	−3.60	−4.35
$r_s^{\Sigma^+ p}$	3.49	3.59	3.56	3.54	3.53	3.45	3.60	3.24	3.16
$a_t^{\Sigma^+ p}$	0.48	0.49	0.49	0.49	0.48	0.49	0.65	0.31	−0.25
$r_t^{\Sigma^+ p}$	−4.98	−5.18	−5.03	−5.08	−5.41	−5.18	−2.78	−12.2	−28.9
$({}^3_\Lambda\mathrm{H})$ E_B	−2.39	−2.33	−2.30	−2.30	−2.30	−2.32	−2.34	−2.27	−2.30

TABLE 4.5: The YN singlet (s) and triplet (t) scattering length a and effective range r (in fm) and the hypertriton binding energy E_B (in MeV) [125]. The binding energies for the hypertriton are calculated using the Idaho-N3LO NN potential [124]. The experimental value for the ${}^3_\Lambda$H binding energy is -2.354(50) MeV.

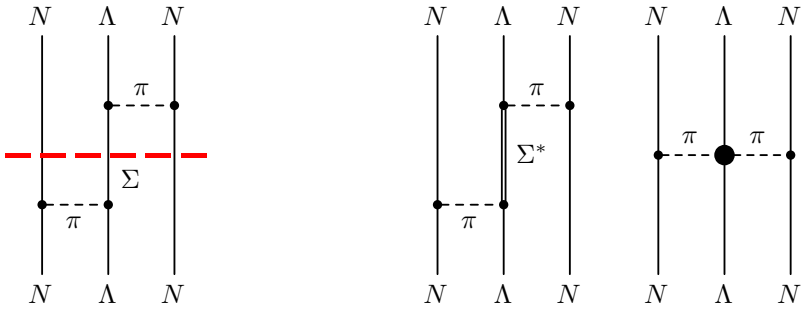

FIGURE 4.10: Examples for reducible (left) and irreducible (right) three-baryon interactions for ΛNN. The red dashed line cuts the reducible diagram in two two-body interaction parts.

Faddeev equations in momentum space, as described in Refs. [29, 141]. Note that genuine (irreducible) three-baryon interactions were not included in this calculation. However, in the employed coupled-channel formalism, effects like the important Λ-Σ conversion process are naturally included. One should distinguish such iterated two-body interactions, from irreducible three-baryon forces, as exemplified in Fig. 4.10. The leading irreducible three-baryon forces will be discussed in Chapter 6.

To end this section, predictions for S- and P-wave phase shifts δ as a function of $p_{\rm lab}$ for Λp and $\Sigma^+ p$ scattering are shown in Fig. 4.11. The ${}^1S_0$ Λp phase shift from the NLO χEFT calculation is closer to the phenomenological Jülich '04 model than the LO result. It points to moderate attraction at low momenta and strong repulsion at higher momenta. At NLO the phase shift has a stronger downward bending at higher momenta compared to LO or the Jülich '04 model. As stated before, more repulsion at higher energies is a welcome feature in view of neutron star matter with Λ-hyperons as additional baryonic degree of freedom. The ${}^3S_1$ Λp phase shift, part of the S-matrix for the coupled ${}^3S_1$-${}^3D_1$ system, changes qualitatively from LO to NLO. The ${}^3S_1$ phase shift of the NLO interaction passes through 90° slightly below the ΣN threshold, which indicates the presence of an unstable bound state in the ΣN system. For the LO interaction and the Jülich '04 model

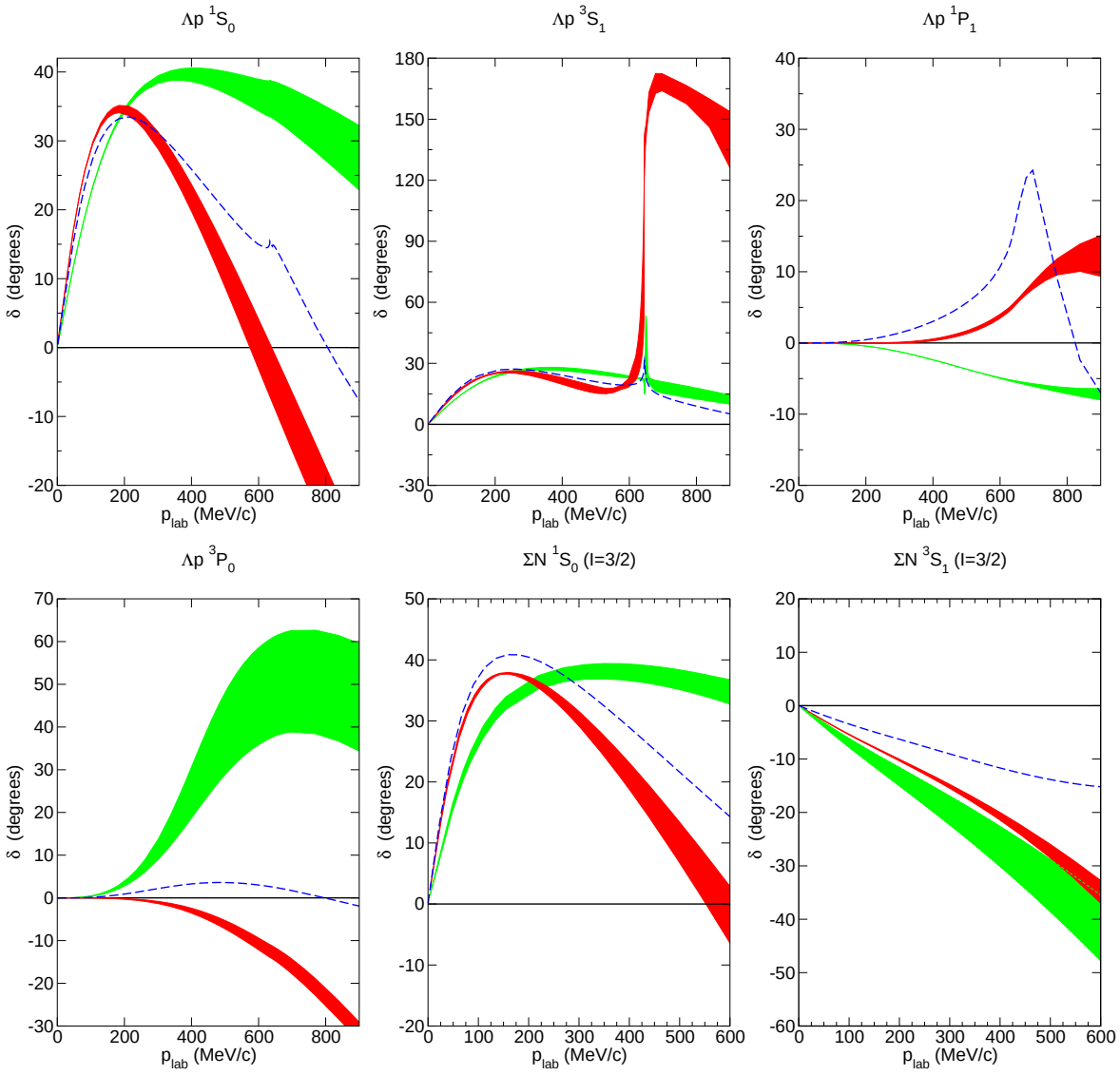

FIGURE 4.11: Various S- and P-wave phase shifts δ as a function of $p_{\rm lab}$ for the Λp and $\Sigma^+ p$ interaction [125]. Same description of curves as in Fig. 4.8.

no passing through 90° occurs and a cusp is predicted, that is caused by an inelastic virtual state in the ΣN system. These effects are also reflected by a strong increase of the Λp cross section close to the ΣN threshold, see Fig. 4.8. For illustrative purposes the presented phase shifts of the $\Sigma^+ p$ interaction are obtained from a calculation without Coulomb interaction, and these correspond to the ΣN $I = 3/2$ channel. As stated before, we have chosen a repulsive $^3S_1$ ΣN interaction in order to be consistent with recent experimental information, cf. Chapter 5. The phase shift for the NLO interaction is moderately repulsive and comparable to the LO phase shift.

5

HYPERONS IN NUCLEAR MATTER

Experimental investigations of nuclear many-body systems including strange baryons, for instance, the spectroscopy of hypernuclei, provide important constraints on the underlying hyperon-nucleon interaction. The analysis of data for single Λ-hypernuclei over a wide range in mass number leads to the result, that the attractive Λ single-particle potential is about half as deep (≈ -28 MeV) as the one for nucleons. At the same time the Λ-nuclear spin-orbit interaction is found to be exceptionally weak [142, 143]. Recently, the repulsive nature of the Σ-nuclear potential has been experimentally established in Σ^--formation reactions on heavy nuclei. In this chapter we connect such observables with the baryon-baryon potentials derived within χEFT as presented in Chapter 4. We calculate the properties of hyperons in infinite homogeneous nuclear matter, with the baryon-baryon interaction as a microscopic input. For the description of hyperons in nuclear matter, first-order Brueckner theory is used to treat the many-body problem. It is beyond the scope of this thesis to give a complete introduction to Brueckner theory. But for orientation we give a brief introduction to the basic concepts of Brueckner theory, as far as they are needed for the further analysis. We follow the presentation in Refs. [43, 144] and refer the reader for more details to Ref. [145]. The relevant formulas concerning baryonic matter treated within first-order Brueckner theory are stated explicitly. We present results for hyperon single-particle potentials, i.e., the mean fields experienced by hyperons, in isospin symmetric and asymmetric nuclear matter. Parts of this chapter have been previously published in Ref. [146].

5.1 CONCEPTS OF BRUECKNER THEORY

Brueckner theory is founded on the so-called *Goldstone expansion*, a linked-cluster perturbation series for the ground state energy of a fermionic many-body system. Let us consider a system of A identical fermions, described by the Hamiltonian

$$H = T + V\,, \tag{5.1}$$

where T is the kinetic part and V corresponds to the two-body interaction. The goal is to calculate the ground state energy of this interacting A-body system. It is advantageous to introduced a so-called *auxiliary potential*, or single-particle potential, U. The Hamiltonian is then split into two parts

$$H = (T + U) + (V - U) = H_0 + H_1\,, \tag{5.2}$$

the unperturbed part H_0 and the perturbed part H_1. One expects the perturbed part to be small, if the single particle potential describes well the averaged effect of the medium

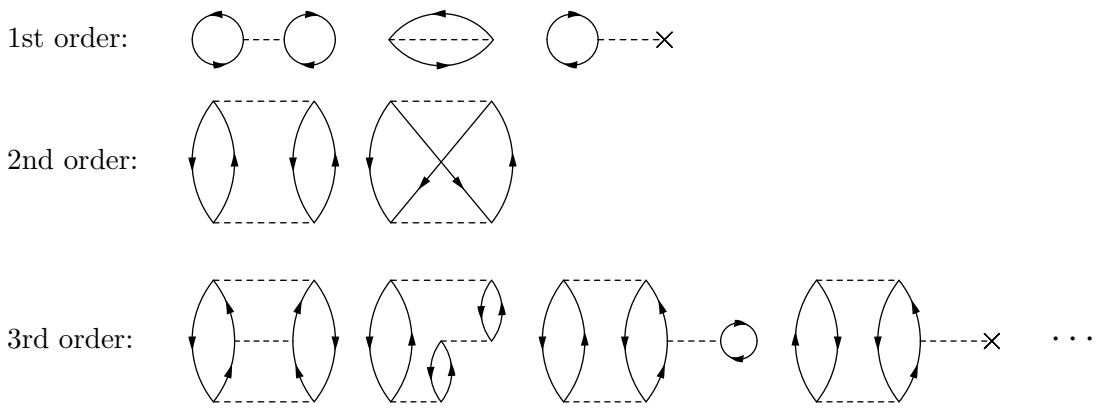

FIGURE 5.1: Goldstone expansion with first, second and some third order contributions.

on the particle. In fact, the proper introduction of the auxiliary potential is crucial for the convergence of Brueckner theory.

The unperturbed one-particle solutions $|n\rangle$ (in the homogeneous medium) fulfill the non-relativistic Schrödinger equation

$$H_0|n\rangle = \epsilon_n|n\rangle\,, \tag{5.3}$$

with the one-particle energies ϵ_n. The momentum eigenstates $|n\rangle$ are assumed to form a complete orthonormal set. The unperturbed ground state of the many-body system is then represented by a Slater determinant $|\Phi_0\rangle$ formed by the A one-particle eigenstates with lowest energy. This represents the so-called filled *Fermi sea*. Due to translation invariance, the one-particle states in a homogeneous medium (e.g., infinite nuclear matter) are given by *plane waves*. The unperturbed ground state $|\Phi_0\rangle$ fulfills the equation

$$H_0|\Phi_0\rangle = E_0|\Phi_0\rangle\,, \tag{5.4}$$

where the *unperturbed ground-state energy* is given by

$$E_0 = \sum_{n\leq A}\epsilon_n = \sum_{n\leq A}\langle n|T|n\rangle + \sum_{n\leq A}\langle n|U|n\rangle\,. \tag{5.5}$$

The sum $\sum_{n\leq A}$ symbolizes a sum over A single-particle states with lowest energies ϵ_n.

The exact ground state $|\Psi_0\rangle$ of the correlated many-body system obeys the eigenvalue equation

$$H|\Psi_0\rangle = E|\Psi_0\rangle\,. \tag{5.6}$$

Goldstone used diagrammatic techniques to derive the linked-cluster perturbation formula [147] for the *ground-state energy shift* $\Delta E = E - E_0$:

$$\Delta E = \langle\Phi_0|H_1\sum_{n=0}^{\infty}\left(\frac{1}{E_0 - H_0}H_1\right)^n|\Phi_0\rangle_{\rm L}\,, \tag{5.7}$$

where the index L means, that only *connected* graphs representing expectation values in Φ_0 have to be included. In Fig. 5.1 various contributions up to third order ($n = 0, 1, 2$) in this expansion are shown. Diagrams which vanish in nuclear matter due to momentum conservation are omitted. Upward directed lines denote particles (excited states above the

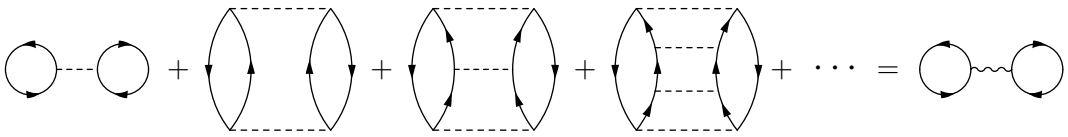

FIGURE 5.2: Example for resummation of the interaction.

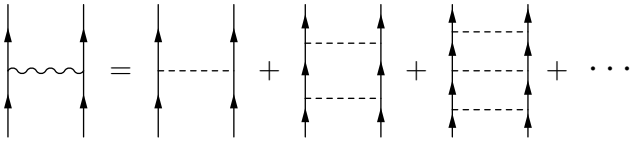

FIGURE 5.3: Definition of the G-matrix.

Fermi sea), whereas downward directed lines denote holes (vacancies in the Fermi sea). Dashed lines represent an interaction via the perturbation H_1 and the order of a certain diagram is given by the number of such interactions. The interaction H_1 occurs either between two particles or holes via the V part of H_1 or between a particle/hole and the auxiliary field U, denoted by the crosses.

The three first-order contributions are given by

$$\Delta E = \frac{1}{2}\sum_{m,n\leq A}\langle mn|V|mn\rangle - \frac{1}{2}\sum_{m,n\leq A}\langle mn|V|nm\rangle - \sum_{n\leq A}\langle n|U|n\rangle\,, \tag{5.8}$$

following the ordering in Fig. 5.1. Therefore, the first-order ground state energy is given by

$$E = E_0 + \Delta E = \sum_{n\leq A}\langle n|T|n\rangle + \frac{1}{2}\sum_{m,n\leq A}\langle mn|V|mn\rangle_{\mathcal{A}}\,, \tag{5.9}$$

where Eq. (5.5) was inserted for E_0 and the index $\mathcal{A}$ denotes an antisymmetrized state. Note that the explicit contribution of the auxiliary potential U drops out at first order. However, the results still depends on U, since the one-particle wave-functions $|n\rangle$ depend on U.

Conventional nucleon-nucleon potentials exhibit a strong short-range repulsion that leads to very large matrix elements. Hence, the Goldstone expansion in the form described above will not converge for such hard-core potentials. One way to approach this problem is the introduction of the so-called *Brueckner reaction matrix*, or G-matrix. The idea behind it is illustrated in Fig. 5.2. Instead of only using the leading Hartree diagram, an infinite number of diagrams with increasing number of interactions is summed up. This defines the G-matrix interaction (wiggly line), which is, in contrast to the bare potential, weak and of reasonable range. In a more general way, the reaction matrix is defined by the *Bethe-Goldstone equation*:

$$G(\omega) = V + V\frac{Q}{\omega - H_0 + \mathrm{i}\epsilon}G(\omega)\,, \tag{5.10}$$

with the so-called starting energy ω. The Pauli operator Q ensures, that the intermediate states are from outside the Fermi sea. As shown in Fig. 5.3 this equation represents a resummation of the ladder diagrams to all orders. The arising G-matrix interaction is an effective interaction of two particles in the presence of the medium. The medium

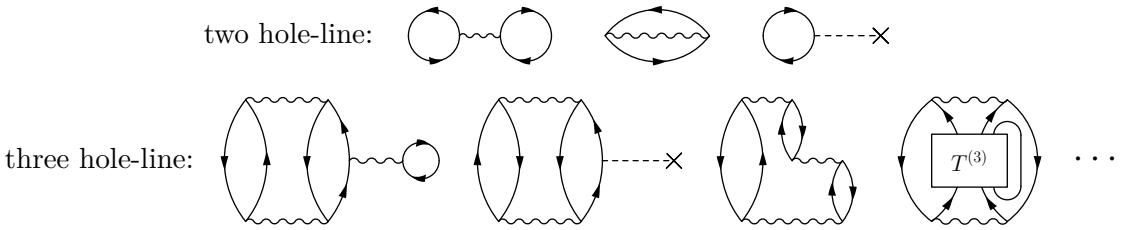

FIGURE 5.4: Brueckner-Bethe-Goldstone expansion with one hole-line and some three hole-line contributions.

effects come in solely through the Pauli operator and the energy denominator via the single-particle potentials. If we set the single-particle potentials to zero and omit the Pauli operator ($Q = 1$), we recover the usual Lippmann-Schwinger equation for two-body scattering in vacuum.

The idea is now to replace all interactions V (dashed lines) by G-matrix interactions (wiggly lines). One has to make sure, that no double counting is involved. For example, the two second order diagrams in Fig. 5.1 are already included in the resummation of the first-order diagrams, and thus have to be excluded. However, it was found that the size of the contribution of a diagram is not determined by the number of G-matrix interactions, but rather by the number of hole-lines. This leads to the Bethe-Brueckner-Goldstone expansion, or *hole-line expansion*. The two hole-line and some three hole-line contributions are displayed in Fig. 5.4. The symbol $T^{(3)}$ in the last contribution of Fig. 5.4 represents a resummation of all two-body interactions between three particles, similar to the resummation in Fig. 5.3 for two particles, and is obtained by the so-called Bethe-Faddeev equation. The free space analogon are the well-known Faddeev equations.

The physical idea behind the hole-line expansion is as follows. Assume that two particles are "strongly correlated" only if their separation distance is smaller than a core radius c. Within a sphere of radius r_0 centered about any particle, on average one other particle is present, where r_0 is determined from the density by $4\pi r_0^3/3 = \rho^{-1}$. The probability p for two particles to be strongly correlated can be roughly estimated as the ratio between the volume occupied by the core and the on average available volume per particle, $p \approx (c/r_0)^3$. Then the power p^n measures the probability for n particles to be all at a relative distance less than c. If p is now small, an expansion of the energy shift ΔE can be done in powers of p, i.e., the density plays the role of the small parameter. This is the type of expansion obtained by grouping the diagrams according to the number of hole lines: diagrams with n independent hole lines stand for the energy arising from n-body correlations. For nuclear matter this expansion should converge well, since the core radius of the nucleon-nucleon interaction is small compared to the typical interparticle spacing, and the nuclear attraction is weak enough so that the range of strong correlations is dominated by the repulsive core.

Finally, we have to choose the form of the *auxiliary potential* U. As can be seen from Eq. (5.2), the introduction of U should not have an effect on the final result if we include all orders of the perturbation series. However, at a finite order of the expansion, the result depends on the choice of U. This choice is important for the convergence of the hole-line expansion. The diagrams at higher orders involving U (crosses), should cancel important higher-order contributions from diagrams without U. Bethe, Brandow and Petschek [148]

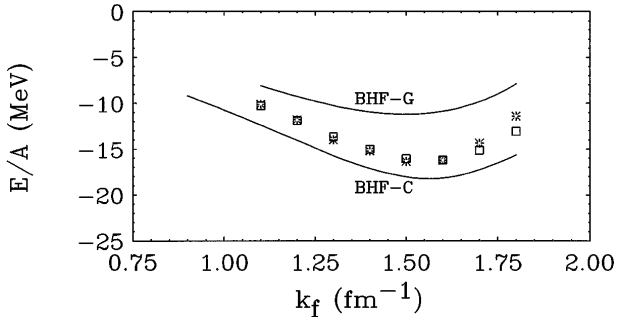

FIGURE 5.5: Equation of state of symmetric nuclear matter. Full lines include two-hole line contributions with the gap (BHF-G) and continuous (BHF-C) choice. Squares and stars include two and three hole-line contributions with the gap and continuous choice, respectively. Figure taken from Ref. [149].

showed for nuclear matter that this is the case if the auxiliary potential is taken as

$$U_m = \mathrm{Re} \sum_{n \leq A} \langle mn|G(\omega = \epsilon_m + \epsilon_n)|mn\rangle_{\mathcal{A}} \,, \tag{5.11}$$

where the Brueckner reaction matrix is evaluated *on-shell*, i.e., the starting energy is equal to the energy of the two particles in the initial state. Note that this implies a non-trivial self-consistency problem. On the one hand, U is calculated from the G-matrix elements via Eq. (5.11), and on the other hand the starting energy of the G-matrix elements depends on U through the single-particle energies ϵ_n.

At the level of two hole-lines, called *Brueckner-Hartree-Fock approximation* (BHF), the total energy is given by

$$\begin{aligned} E &= \sum_{n \leq A} \langle n|T|n\rangle + \frac{1}{2} \sum_{m,n \leq A} \langle mn|G|mn\rangle_{\mathcal{A}} \\ &= \sum_{n \leq A} \langle n|T|n\rangle + \frac{1}{2} \sum_{n \leq A} \langle n|U|n\rangle \,, \end{aligned} \tag{5.12}$$

i.e., the ground-state energy E can be calculated directly after the single-particle potential has been determined.

The definition of U in Eq. (5.11) applies only to occupied states within the Fermi sea. For intermediate-state energies above the Fermi sea, typically two choices for the single-particle potential are employed. In the so-called *gap choice*, the single-particle potential is given by Eq. (5.11) for $k \leq k_F$ and set to zero for $k > k_F$, implying a "gap" (discontinuity) in the single-particle potential. Only the free particle energies $(M + \vec{p}^{\,2}/2M)$ of the intermediate states appear in the energy denominator of the Bethe-Goldstone equation (5.10) since the Pauli-blocking operator is zero for momenta below the Fermi momentum. In the so-called *continuous choice* Eq. (5.11) is used for the *whole* momentum range, hence the single-particle potentials enter also into the energy denominator. In Ref. [149] the equation of state in symmetric nuclear matter has been considered. It has been shown, that the result including three hole-lines is almost independent of the choice of the auxiliary potential. Furthermore the two-hole line result with the continuous choice comes out closer to the three hole-line result, than the two-hole line calculation with the gap choice, cf. Fig. 5.5. Another advantage of the continuous choice for intermediate spectra is that it allows for a reliable determination of the single-particle potentials including their imaginary parts [44]. Unless stated differently, all presented results in this chapter are calculated with the continuous choice.

5.2 BRUECKNER-HARTREE-FOCK APPROXIMATION

In order to investigate the properties of hyperons in nuclear matter we employ the conventional Brueckner theory at first order in the hole-line expansion, the Brueckner-Hartree-Fock approximation. We are interested in the single-particle potentials, i.e., the mean fields experienced by hyperons in nuclear matter. Our calculations are done in the particle basis and in the following we summarize the relevant formulas, based on the formalism presented in Sec. 5.1. For a more detailed derivation we refer the reader to Ref. [21] and also to Refs. [17, 18, 44, 45].

After angle-averaging of the Pauli-blocking operator and the energy denominator, the Bethe-Goldstone equation decomposes into partial waves and reads for conserved values of the total angular momentum J, total momentum $\vec{K}$ and starting energy ω:

$$\begin{aligned} &G^{\rho'' \rho', J}_{\nu'' \nu'}(k'', k'; K, \omega) \\ &= V^{\rho'' \rho', J}_{\nu'' \nu'}(k'', k') + \sum_{\rho, \nu} \int_0^\infty \frac{\mathrm{d}k\, k^2}{(2\pi)^3}\, V^{\rho'' \rho, J}_{\nu'' \nu}(k'', k) \frac{\bar{Q}_\nu(K, k)}{\bar{e}_\nu(K, k; \omega) + \mathrm{i}\epsilon} G^{\rho \rho', J}_{\nu \nu'}(k, k'; K, \omega)\,. \end{aligned} \tag{5.13}$$

As in Eq. (4.18) the symbol ρ stands for the partial waves, $\rho = (SL)$. The (coupled) two-particle channels are $\nu = (B_1 B_2)$, with the baryons B_i from the set $\{n, p, \Lambda, \Sigma^+, \Sigma^0, \Sigma^-\}$. The same potential V as in the Lippmann-Schwinger equation (4.18) for free scattering is used. Possible medium modifications of the two-meson exchange potential are not included. These represent density dependent two-body interactions arising from three-body interactions. The medium effects come, therefore, solely from the Pauli-blocking operator Q in the Bethe-Goldstone equation and the density-dependent single-particle potential in the energy denominator $e(\omega)$.

In the initial state of Eq. (5.13) the baryon B_2 is within its own Fermi sea ($|\vec{k}_2| < k_F^{(2)}$). We introduce the total and relative momenta of both baryons B_1 and B_2 by

$$\vec{K} = \vec{k}_1 + \vec{k}_2\,, \quad \vec{k} = \frac{\xi_{12}\vec{k}_1 - \vec{k}_2}{1 + \xi_{12}}\,, \quad \xi_{12} = \frac{M_2}{M_1}\,. \tag{5.14}$$

In Eq. (5.13) we have applied the standard approximation replacing Q/e by the ratio of its angle-averages $\bar{Q}/\bar{e}$. Only due to this angle-average the angular integral can be solved analytically and the total angular momentum J remains conserved. The averaged Pauli-blocking operator, involving the Fermi momenta $k_F^{(1,2)}$ of the two baryon species, is given by:

$$\begin{aligned} \bar{Q}_\nu(K, k) &= \frac{1}{2} \int_{-1}^{1} \mathrm{d}\cos\theta\; \Theta\left(|\vec{k}_1| - k_F^{(1)}\right) \Theta\left(|\vec{k}_2| - k_F^{(2)}\right) \\ &= [0|\frac{[-1|z_1|1] + [-1|z_2|1]}{2}|1]\,, \end{aligned} \tag{5.15}$$

involving an integration over the angle θ between $\vec{K}$ and $\vec{k}$. The solution is written in terms of the shorthand notation $[a|b|c] \equiv \max(a, \min(b, c))$ introduced in Ref. [44], and the arguments z_1 and z_2 are

$$\begin{aligned} z_1 &= \frac{1 + \xi_{12}}{2kK} \left\{ \left(\frac{1}{1 + \xi_{12}} K \right)^2 + k^2 - (k_F^{(1)})^2 \right\}\,, \\ z_2 &= \frac{1 + 1/\xi_{12}}{2kK} \left\{ \left(\frac{\xi_{12}}{1 + \xi_{12}} K \right)^2 + k^2 - (k_F^{(2)})^2 \right\}\,. \end{aligned} \tag{5.16}$$

The angle-averaged energy denominator takes the form

$$\bar{e}_\nu(K,k;\omega) = \omega - \frac{K^2}{2M_\nu} - \frac{k^2}{2\mu_\nu} - M_\nu - \mathrm{Re}\,U_{B_1}(\bar{k}_1) - \mathrm{Re}\,U_{B_2}(\bar{k}_2)\,, \tag{5.17}$$

with total and reduced masses, $M_\nu = M_1 + M_2$ and $\mu_\nu = M_1 M_2/(M_1+M_2)$. The angle-average is approximated and performed just for the arguments of the single particle potentials U_{B_i} of the intermediate baryons:

$$\begin{aligned}
\bar{k}_1 &= \left(\tfrac{1}{(1+\xi_{12})^2}K^2 + k^2 + 2\tfrac{1}{1+\xi_{12}}Kk\,\overline{\cos\theta}\right)^{1/2}\,,\\
\bar{k}_2 &= \left(\tfrac{\xi_{12}^2}{(1+\xi_{12})^2}K^2 + k^2 - 2\tfrac{\xi_{12}}{1+\xi_{12}}Kk\,\overline{\cos\theta}\right)^{1/2}\,,
\end{aligned} \tag{5.18}$$

with the mean directional cosine

$$\overline{\cos\theta} = \frac{\int_{-1}^{1}\mathrm{d}\cos\theta\,\cos\theta\,Q(\vec{K},\vec{k})}{\int_{-1}^{1}\mathrm{d}\cos\theta\,Q(\vec{K},\vec{k})} = \frac{1}{2}\left([-1|z_2|1] - [-1|z_1|1]\right)\,, \tag{5.19}$$

where $Q(\vec{K},\vec{k})$ is the exact Pauli-blocking operator. If two nucleons are involved, the previous expression for $\overline{\cos\theta}$ would vanish in symmetric nuclear matter, because of the equal masses, $z_1 = z_2$. Then the alternative (root mean square) angular average

$$\overline{\cos\theta} = \sqrt{\frac{\int_{-1}^{1}\mathrm{d}\cos\theta\,\cos^2\theta\,Q(\vec{K},\vec{k})}{\int_{-1}^{1}\mathrm{d}\cos\theta\,Q(\vec{K},\vec{k})}} = \frac{1}{\sqrt{3}}[0|z_1|1]\,,\quad z_1 = \frac{1}{kK}\left[\frac{K^2}{4} + k^2 - k_F^2\right], \tag{5.20}$$

is often used.

It is common practice to introduce a further simplification. The squared momenta $K^2 = K^2(\vec{k}_1,\vec{k})$ and $k_2^2 = k_2^2(\vec{k}_1,\vec{k})$ entering the Bethe-Goldstone equation are replaced by their angle averages:

$$\begin{aligned}
\bar{K}^2(k_1,k) &= \frac{\int_{|\vec{k}_2|\le k_F^{(2)}}\mathrm{d}\cos\vartheta\,K^2(k_1,k,\cos\vartheta)}{\int_{|\vec{k}_2|\le k_F^{(2)}}\mathrm{d}\cos\vartheta}\\
&= (1+\xi_{12})^2\left[k_1^2 + k^2 - k_1 k(1+[-1|x_0|1])\right]\,,\\
\bar{k}_2^2(k_1,k) &= \frac{\xi_{12}}{1+\xi_{12}}\bar{K}^2(k_1,k) + (1+\xi_{12})k^2 - \xi_{12}k_1^2\,,
\end{aligned} \tag{5.21}$$

where ϑ is the angle between $\vec{k}_1$ and $\vec{k}$, and x_0 means:

$$x_0 = \frac{\xi_{12}^2 k_1^2 + (1+\xi_{12})^2 k^2 - (k_F^{(2)})^2}{2\xi_{12}(1+\xi_{12})k_1 k}\,. \tag{5.22}$$

Note again, that the baryon B_2 in the initial state is within its Fermi sea ($|\vec{k}_2| < k_F^{(2)}$).

Finally, the single-particle potential of a baryon B_1 due to the Fermi sea of the species B_2 is calculated in the Brueckner-Hartree-Fock approximation (according to Eq. (5.11)) as follows

$$\begin{aligned}
U_{B_1}^{(B_2)}(k_1) = &\left(1 + \delta_{B_1B_2}(-1)^{L+S}\right)\frac{(1+\xi_{12})^3}{2}\sum_{J,\rho}(2J+1)\\
&\times\int_{k_{\min}}^{k_{\max}}\frac{\mathrm{d}k\,k^2}{(2\pi)^3}\,W(k_1,k)\,G^{\rho\rho,J}_{(B_1B_2)(B_1B_2)}(k,k;\bar{K},\omega_{\text{o.s.}})\,.
\end{aligned} \tag{5.23}$$

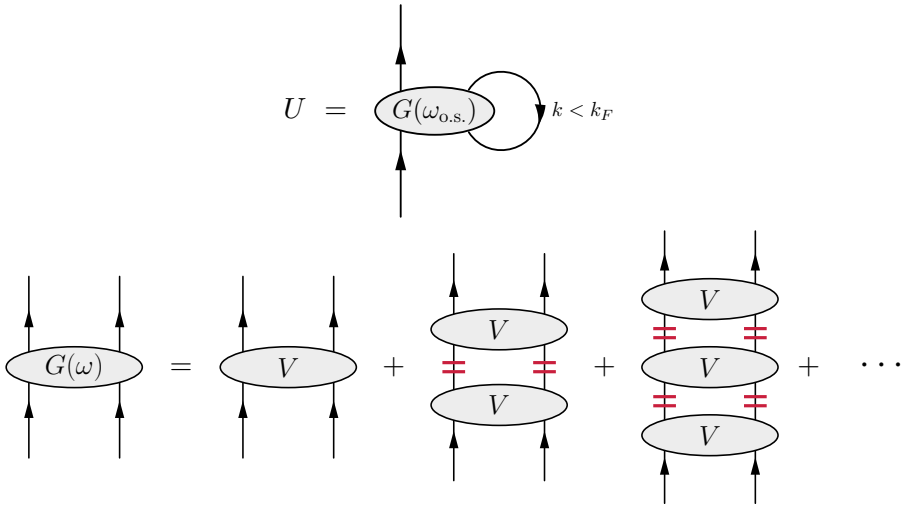

FIGURE 5.6: Graphical representation of the determination of the single-particle potential and the Bethe-Goldstone equation. The symbol $\omega_{\text{o.s}}$ denotes the on-shell starting energy.

The full single-particle potential of a baryon B_1 ($B_1 = n, p, \Lambda, \Sigma^{0,\pm}$) is then given by the sum of the contributions from all baryons B_2 ($B_2 = n, p$) in the nuclear Fermi sea. The weight function $W(k_1, k)$ has the form

$$W(k_1, k) = \frac{1}{4\pi} \int_{|\vec{k}_2| \leq k_F^{(2)}} \mathrm{d}\Omega_k = \frac{1}{2}(1 - [-1|x_0|1]) \,. \tag{5.24}$$

The lower and upper integration boundaries of the relative momentum, k_{min} and k_{max}, are determined as the solution of $W(k_1, k) = 0$, which leads to

$$k_{\text{min}} = \max\left(0, \frac{-k_F^{(2)} + \xi_{12} k_1}{1 + \xi_{12}}\right) , \qquad k_{\text{max}} = \frac{k_F^{(2)} + \xi_{12} k_1}{1 + \xi_{12}} \,. \tag{5.25}$$

The G-matrix elements in Eq. (5.23) are calculated at the on-shell starting energy

$$\begin{aligned} \omega_{\text{o.s.}} &= E_{B_1}(k_1) + E_{B_2}(\bar{k}_2) \,, \\ E_{B_i}(k_i) &= M_i + \frac{k_i^2}{2M_i} + \mathrm{Re}\, U_{B_i}(k_i) \,. \end{aligned} \tag{5.26}$$

This makes the determination of the single-particle potentials dependent on the single-particle potential itself, and, therefore, Eqs. (5.13) and (5.23) have to be solved self-consistently. In Fig. 5.6 this self-consistency is illustrated. In analogy to Fig. 2.3 the expansion of the G-matrix is depicted. The difference of the Bethe-Goldstone equation and the Lippmann-Schwinger equation stems from the factor Q/e. This medium effect on the intermediate states is denoted by a horizontal double line. The single-particle potential can be obtained pictorially by taking the on-shell G-matrix interaction and closing one of the baryon lines. When closing the other line, the total energy of the system is obtained, as can be seen in Eq. (5.12).

Λ	500	550	600	650
$\tilde{C}^{27}_{^1S_0}$	−0.1539	−0.1017	−0.0153	0.1301
$C^{27}_{^1S_0}$	2.313	2.326	2.326	2.328
$\tilde{C}^{10^*}_{^3S_1}$	−0.2100	−0.1493	0.0166	0.2059
$C^{10^*}_{^3S_1}$	0.2977	0.3139	0.5109	0.4899
$C^{10^*}_{^3S_1-{}^3D_1}$	−0.2767	−0.2896	−0.2422	−0.2234
$a_{^1S_0}$	−23.8	−23.8	−23.8	−23.7
$r_{^1S_0}$	2.81	2.75	2.68	2.62
$a_{^3S_1}$	5.42	5.43	5.42	5.43
$r_{^3S_1}$	1.81	1.76	1.72	1.67
E_d	−2.257	−2.213	−2.193	−2.145

TABLE 5.1: Contact terms and threshold parameters for the $^1S_0$ and $^3S_1$-$^3D_1$ NN partial waves for various cutoffs. The values of the $\tilde{C}$'s are in 10^4 GeV^{-2}, the ones of the C's, in 10^4 GeV^{-4}; the values of Λ in MeV. The scattering length a and the effective range r are in fm, the deuteron binding energy E_d in MeV. The empirical values are $a_{^1S_0} = -23.739$ fm, $r_{^1S_0} = 2.68$ fm, $a_{^3S_1} = 5.420$ fm, $r_{^3S_1} = 1.753$ fm [150] and $E_d = -2.224575(9)$ MeV.

5.3 HYPERON SINGLE-PARTICLE POTENTIALS IN NUCLEAR MATTER

For the description of the hyperon-nucleon interaction we use SU(3) chiral effective field theory up to next-to-leading order within the Weinberg power counting applied to the potential, as presented in Chapter 4. As stated previously, a simultaneous description of the NN and YN interactions with SU(3) symmetric LECs is not possible at NLO (the channels NN ($I = 1$) and ΣN ($I = 3/2$) are too strongly correlated through SU(3) symmetric contact terms, cf. Tab. 4.2). Therefore, we use partly different sets of LECs in the NN and YN sectors. For the YN interaction the set given in Refs. [125] and [49] is used[1], where in the latter work the contact term c^{8as} for the antisymmetric spin-orbit force in the YN interaction, allowing spin singlet-triplet transitions, is already fitted to the weak Λ-nuclear spin-orbit interaction [152, 153]. The NN interaction is based on the same meson-exchange diagrams and contact terms as given in Ref. [125], but with different LECs, compiled in Tab. 5.1. Furthermore, Tab. 5.1 reproduces the S-wave scattering lengths, the effective ranges and the deuteron binding energy, as obtained from this chiral NLO NN interaction. In Fig. 5.7 the nucleon-nucleon phase shifts in the $^1S_0$ and $^3S_1$ partial waves are shown. Note that the results are comparable to those (at NLO) in Ref. [123] where SU(2) chiral EFT was used (cf. Fig. 4 in that reference). At low energies they are in agreement with the empirical data. However, at higher energies the results of the NLO interaction become too repulsive.

In the following we present our results for the in-medium properties of hyperons, based on the YN interaction derived from chiral EFT [146]. Additionally, for the ease of comparison, the G-matrix results obtained with two phenomenological YN potentials, namely of the Jülich '04 [19] and the Nijmegen NSC97f [18] meson-exchange models, are given. Note that, like the EFT potentials, these phenomenological YN interactions produce a bound hypertriton [29]. As mentioned before, the EFT NN and YN interactions involve differ-

1 Note that in order to be consistent with the definitions in Eq. (18) of Ref. [49] the constants $C^{8_s 8_a}$ in Table 1 of Ref. [49] have to be multiplied with a factor 2.

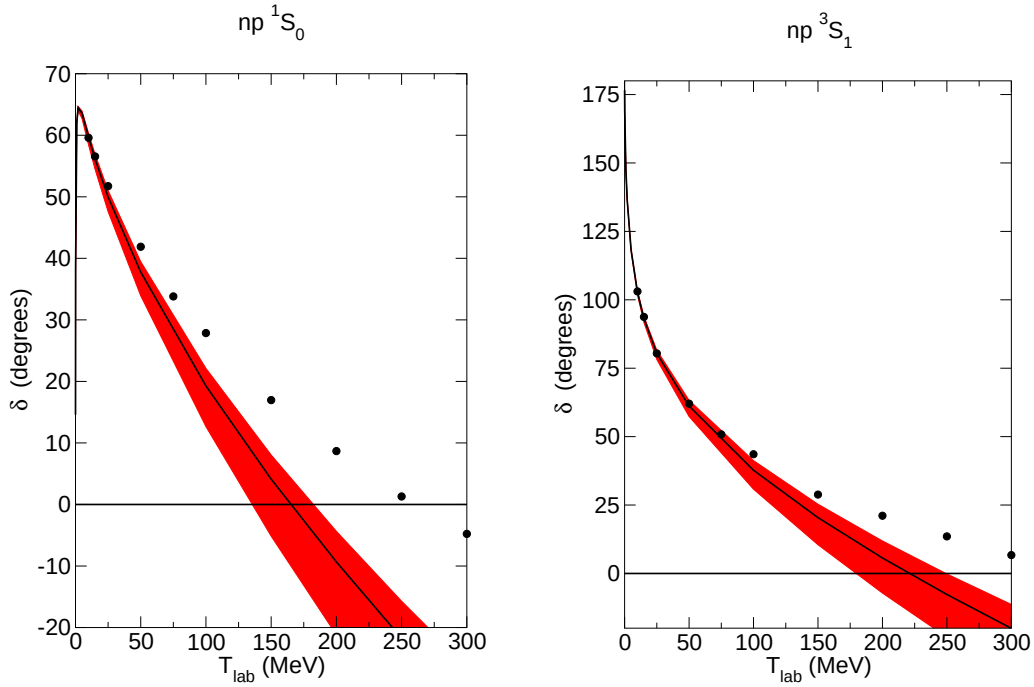

FIGURE 5.7: Nucleon-nucleon phase shifts for the $^1S_0$ and $^3S_1$ partial wave. The band represents the variation of our NLO results with the cutoff, see text. The black line is obtained with a cutoff $\Lambda = 600$ MeV. The circles denote the results from the GWU single-energy np partial wave analysis [151].

ent sets of low-energy constants. For calculations with the LO and NLO hyperon-nucleon interaction we employ as the underlying nucleon-nucleon interaction the NLO version with the same cutoff. In the case of the phenomenological YN interactions (Jülich '04 and Nijmegen NSC97f) we use for the purpose of comparison the NLO chiral NN potential with a cutoff of 600 MeV. In all calculations sums over partial waves up to J=5 are performed (see Eq. (5.23)).

First, we review the results for the nucleon single-particle potential derived from chiral effective field theory at NLO, as this is an input for our calculations of hyperons in nuclear matter. Figure 5.8 shows the real part $\mathrm{Re}\, U_N(k)$ in symmetric nuclear matter at the Fermi momenta $k_F = 1.35$ fm^{-1} and $k_F = 1.0$ fm^{-1}, corresponding to the densities $\rho = 0.166$ fm^{-3} and $\rho = 0.068$ fm^{-3}, as obtained from the chiral NN potential and from the Nijmegen 93 model [9]. According to the Hugenholtz–van-Hove theorem [154] the value at $k = k_F$ has to be $U_N(k_F) = -16$ MeV $- k_F^2/2M_N \approx -53$ MeV at saturation density ($k_F = 1.35$ fm^{-1}). The results of our calculation with the EFT interaction are consistent with this constraint. This consistency is non-trivial in view of the approximations entering the calculation. Furthermore, Fig. 5.8 shows the total binding energy per particle

$$\frac{E}{A} = \frac{\epsilon}{\rho}\,. \tag{5.27}$$

The baryon density ρ is given by a sum over the baryonic species that occupy Fermi seas,

$$\rho = \sum_B \frac{k_F^{(B)\,3}}{3\pi^2}\,, \tag{5.28}$$

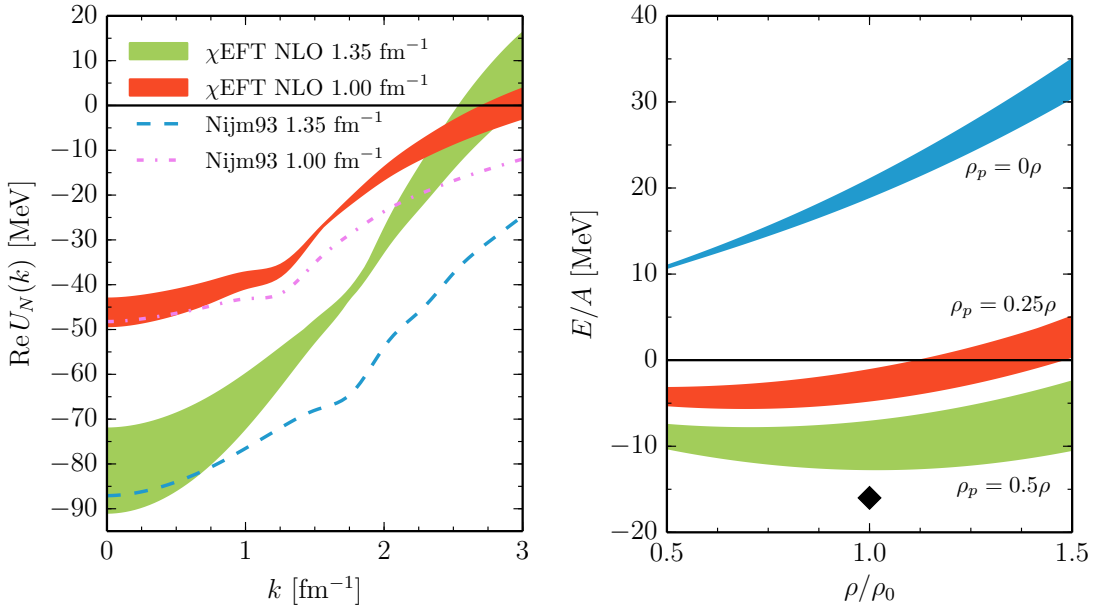

FIGURE 5.8: Nucleon single-particle potential in symmetric nuclear matter for $k_F = 1.35$ fm^{-1} and $k_F = 1.00$ fm^{-1} (left) and energy per particle of nuclear matter with different proton fractions ρ_p/ρ (right). The bands represent the variation of our results with the cutoff, see text. The diamond symbolizes the empirical saturation point of symmetric nuclear matter, with $\rho_0 = 0.16$ fm^{-3}.

and the energy density ϵ can be calculated according to Eq. (5.12) from the single-particle potential as

$$\epsilon = \sum_B \left(\frac{k_F^{(B)\,5}}{10\pi^2 M_B} + \frac{1}{2\pi^2} \int_0^{k_F^{(B)}} \mathrm{d}k\, k^2\, \mathrm{Re}\, U_B(k) \right) . \tag{5.29}$$

It is typical for non-relativistic G-matrix calculations with realistic two-body interactions, that the empirical saturation point of isospin-symmetric nuclear matter ($\rho_0 = 0.16$ fm^{-3}, $E_0/A = -16$ MeV) is not reproduced without the inclusion of three-nucleon forces [155, 156]. Note that the employed nucleon-nucleon interaction at NLO in chiral EFT becomes too repulsive for higher energies (cf. Fig. 5.7). This feature appears to be reflected in the curve for the binding energy per nucleon which saturates at lower densities than usually found in calculations using (chiral and other) nucleon-nucleon potentials [156, 157, 158, 159, 160]. But, as expected, our results still lie within the well-known Coester band [161]. In this context we want to stress that we show the nucleonic results only for illustrative purposes. Considering the recent arrival of NN interactions at fifth order in chiral EFT [162, 163] the NLO potential employed here is obviously not state-of-the-art. However, for consistency reasons we prefer to use NN and YN interactions at the same order of the chiral expansion. In any case, as we will see below, the properties of hyperons in nuclear matter do not depend strongly on the nucleon single-particle potential $U_N(k)$, and therefore the NN interaction up to NLO is certainly sufficient for our purposes.

Now we turn to the properties of hyperons in symmetric nuclear matter as they follow from SU(3) chiral effective field theory. In Tab. 5.2 values for the depth of the Λ single-particle potential $U_\Lambda(k = 0)$ at saturation density are given. In the Brueckner-Hartree-Fock approximation the binding energy of a hyperon in infinite nuclear matter is given by $B_Y(\infty) = -U_Y(k = 0)$. The results of the LO and NLO calculation are consistent

$U_\Lambda(k=0)$	$^1S_0$	$^3S_1$+$^3D_1$	$^3P_0$	$^1P_1$	$^3P_1$	$^3P_2$+$^3F_2$	Total
NLO (500) cont	−15.4	−15.7	1.0	1.8	1.5	−1.3	−28.3
NLO (550) cont	−13.9	−12.7	0.9	1.6	1.5	−1.2	−24.2
NLO (600) cont	−12.9	−13.5	0.8	1.3	1.4	−1.2	−24.4
NLO (650) cont	−12.4	−16.3	0.7	1.2	1.3	−1.2	−27.0
LO (600) gap	−12.1	−25.9	−1.7	1.5	1.7	−0.4	−37.2
LO (600) cont	−13.2	−28.0	−1.9	1.5	1.7	−0.4	−40.7
NLO (600) gap	−13.1	−13.9	0.9	1.3	1.4	−1.2	−24.8
NSC97f gap	−14.7	−24.1	0.4	2.4	4.1	−0.8	−34.1
NSC97f cont	−14.5	−25.2	0.4	2.3	3.9	−0.9	−35.5
Jülich '04 gap	−10.5	−36.5	−0.7	−0.6	0.5	−3.2	−51.7
Jülich '04 cont	−11.2	−38.0	−0.7	−0.7	0.5	−3.3	−54.2

TABLE 5.2: Λ single-particle potential $U_\Lambda(k=0)$ in symmetric nuclear matter at saturation density, $k_F = 1.35$ fm^{-1}. Values are given in MeV and decomposed into partial wave contributions.

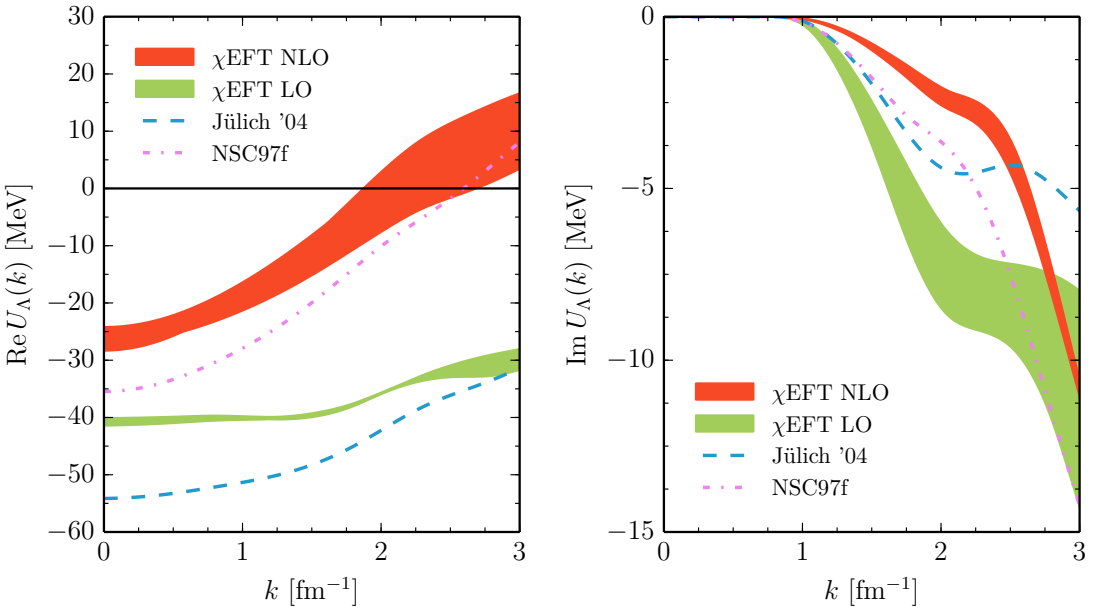

FIGURE 5.9: Momentum dependence of the real and imaginary parts of the single-particle potential of a Λ hyperon in isospin-symmetric nuclear matter at saturation density. The bands represent the variation of our results with the cutoff, see text.

with the empirical value of about $U_\Lambda(0) \approx -28$ MeV as deduced from binding energies of Λ hypernuclei [164, 165]. The results for the gap choice of intermediate spectra are similar to Ref. [49], where a phenomenological parametrization of the nucleon single-particle potential $U_N(k)$ has been used. This suggests that the results for the Λ single-particle potential do not depend strongly on those of the nucleon in nuclear matter. (Actually, using this phenomenological parametrization, we can reproduce the results of Ref. [49] which served as a test for the new code developed for the present investigation.) The differences for $U_\Lambda(0)$ between the gap choice and the continuous choice are a few MeV, comparable to what has been found, e.g., in Ref. [18] for the Nijmegen NSC97 potentials. Obviously, the two phenomenological models (Jülich '04, Nijmegen NSC97f) predict more attractive values of $U_\Lambda(0) = (-35 \ldots -50)$ MeV, where the main difference is due to the contribution in the ${}^3S_1$ partial wave. As already discussed in Ref. [49], we believe that this due to the fact that the Λp ${}^3S_1 \leftrightarrow {}^3D_1$ transition is significantly larger in the NLO chiral EFT interaction as compared to the one of the LO interaction and of the phenomenological models, whereas the diagonal (${}^3S_1 \leftrightarrow {}^3S_1$ and ${}^3D_1 \leftrightarrow {}^3D_1$) transitions are accordingly smaller.

The momentum dependence of the real and imaginary parts of the Λ single-particle potential is presented in Fig. 5.9. A marked difference between LO and NLO is, that the Λ single-particle potential at NLO turns to repulsion at fairly low momenta around $k \approx 2$ fm^{-1}. A similar behavior is also found for the NSC97f potential. The cutoff dependence at LO seems to be accidentally weak.

Corresponding results for Σ hyperons in isospin-symmetric nuclear matter at saturation density are given in Tab. 5.3 and are also graphically displayed in Fig. 5.10. The presented results are for the neutral Σ^0 hyperon. The small differences to the results for charged Σ^+ and Σ^- hyperons come solely from the mass differences of the three Σ hyperons, and is of the order of $(0.5 \ldots 1)$ MeV, where the difference between Σ^0 and $\Sigma^\pm$ is larger than the one between Σ^+ and Σ^-. According to analyses of data on (π^-, K^+) spectra related to Σ^- formation in heavy nuclei the Σ-nuclear potential is moderately repulsive in symmetric nuclear matter, see the review [166]. This feature is well reproduced in our calculation for NLO and even for LO. As stated in Chapter 4, in the course of constructing the NLO interaction it turned out that the available YN scattering data could be fitted equally well with an attractive or a repulsive interaction in the ${}^3S_1$ partial wave of the $I = 3/2$ ΣN channel [125], which is the partial wave that provides the dominant contribution to the Σ single-particle potential, cf. Tab. 5.3 and also Table 4 in Ref. [49]. For the reasons discussed above, the repulsive solution was adopted. Note that models derived within the meson-exchange framework often fail to produce a repulsive Σ-nuclear potential and the two phenomenological YN potentials considered here are exemplary for this deficiency. As visible in Fig. 5.10 the Σ potential stays repulsive for higher momenta. The imaginary part of the Σ-nuclear potential at saturation density is in good agreement with the empirical value of -16 MeV as extracted from Σ^--atom data [167]. The imaginary potential is mainly induced by the ΣN to ΛN conversion in nuclear matter. Evidently, the bands representing the cutoff dependence of the chiral potentials, become smaller when going to higher order in the chiral expansion. This feature has been also observed for the YN scattering observables in Chapter 4.

In the following we provide a more detailed view on the dependence of our in-medium results on the densities of protons and neutrons. The corresponding predictions are shown only for the chiral EFT interaction at NLO with a fixed cutoff, namely $\Lambda = 600$ MeV, for reasons of clearer presentation. However, one should keep in mind that these results

$U_\Sigma(k=0)$	$^1S_0$	$^3S_1$+$^3D_1$	$^3P_0$	$^1P_1$	$^3P_1$	$^3P_2$+$^3F_2$	Total
NLO (500) cont	−4.6	13.5	1.5	0.6	0.4	0.3	11.6
NLO (550) cont	−4.2	17.3	1.3	0.4	0.2	−0.0	14.9
NLO (600) cont	−4.7	15.4	1.2	0.2	0.0	−0.4	11.5
NLO (650) cont	−4.9	11.9	1.0	0.0	−0.1	−0.8	7.0
LO (600) gap	−1.8	25.3	−1.9	−0.2	−1.4	−1.1	18.7
LO (600) cont	−2.2	22.1	−1.9	−0.2	−1.2	−1.0	15.5
NLO (600) gap	−5.6	15.4	1.1	0.1	−0.2	−0.6	9.9
NSC97f gap	1.9	−17.3	0.4	−2.1	1.1	−2.4	−19.1
NSC97f cont	−0.5	−17.2	0.4	−2.1	1.0	−2.6	−22.0
Jülich '04 gap	−8.4	−4.0	0.4	−2.0	−1.8	−3.7	−20.1
Jülich '04 cont	−7.9	−5.6	0.4	−2.0	−2.5	−3.8	−21.9

TABLE 5.3: Σ single-particle potential $U_\Sigma(k=0)$ in symmetric nuclear matter at saturation density, $k_F = 1.35$ fm^{-1}. Values are given in MeV and decomposed into partial wave contributions.

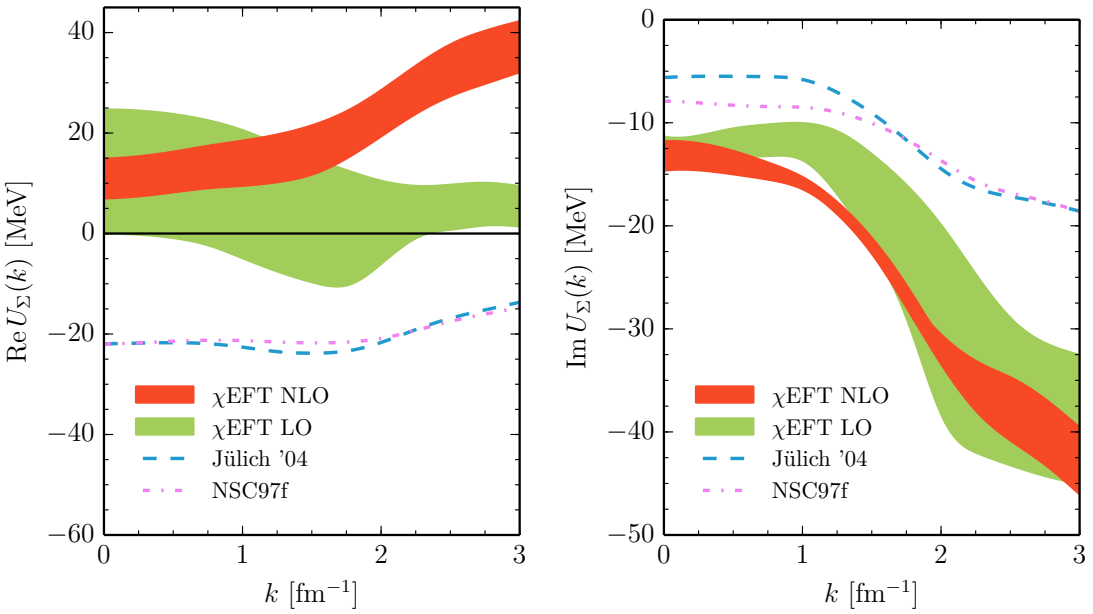

FIGURE 5.10: Momentum dependence of the real and imaginary parts of the single-particle potential of a Σ hyperon in isospin-symmetric nuclear matter at saturation density. The bands represent the variation of our results with the cutoff, see text.

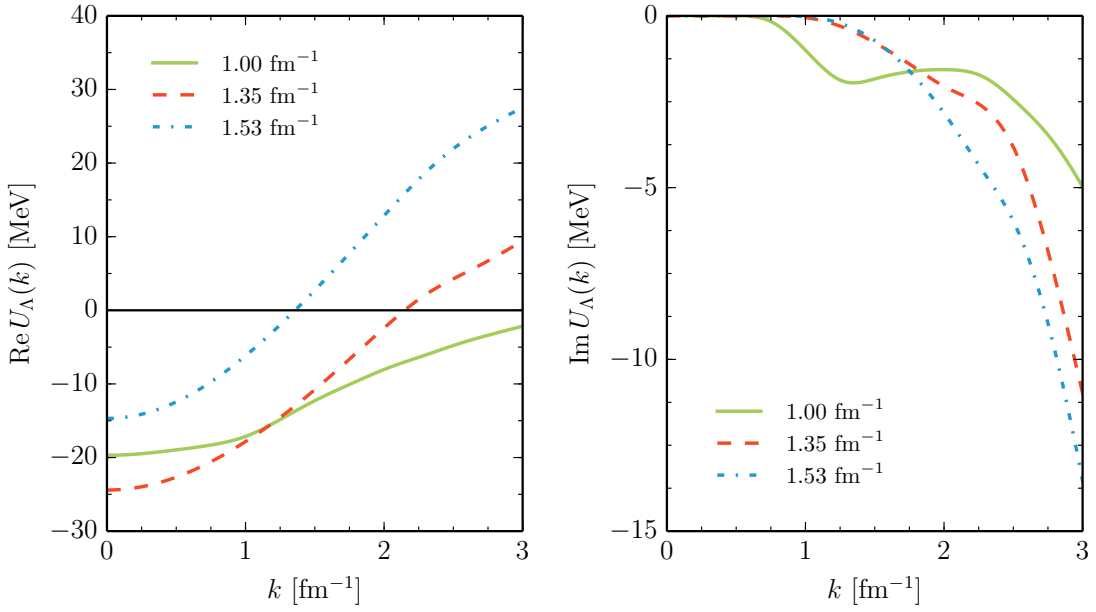

FIGURE 5.11: Momentum dependence of the real and imaginary parts of the Λ single-particle potential for different Fermi momenta $k_F = (1.00, 1.35, 1.53)\,\mathrm{fm}^{-1}$ in symmetric nuclear matter, calculated in χEFT at NLO with a cutoff $\Lambda = 600$ MeV.

are likewise subject to variations with the cutoff and, specifically, in the case of a weak dependence on the density the latter effect might be actually smaller than the cutoff dependence.

In Figs. 5.11 and 5.12 the dependence of the single-particle potential $U_Y(k)$ for Λ and Σ hyperons on the density in isospin-symmetric nuclear matter is shown. The chosen nucleon Fermi momenta $k_F = (1.00, 1.35, 1.53)\,\mathrm{fm}^{-1}$ correspond to densities of about $\rho = (0.4, 1.0, 1.5)\rho_0$ with $\rho_0 = 0.16$ fm^{-3}. The momentum dependence of the potentials is similar for different densities, but their magnitude varies strongly. Especially for the Σ hyperon the single-particle potential can even become attractive at low densities.

Pure neutron matter is another interesting environment for the in-medium behavior of hyperons. Therefore, we display in Fig. 5.13 also the density dependence of $U_Y(k)$ for Λ and Σ hyperons in pure neutron matter. The Fermi momenta of the neutrons $k_F = (1.26, 1.70, 1.92)\,\mathrm{fm}^{-1}$ correspond the same densities as selected in Figs. 5.11 and 5.12 for isospin-symmetric nuclear matter. Due to the maximal asymmetry between protons and neutrons, the single-particle potentials for the three $(\Sigma^+, \Sigma^0, \Sigma^-)$ hyperons are rather different. The Λ single-particle potential $U_\Lambda(k)$ is slightly more attractive than the one in isospin-symmetric nuclear matter at the same density, cf. Fig. 5.11, thus indicating only a weak dependence on the composition of nuclear matter. The small surplus of attraction can be understood qualitatively from the reduction of Pauli-blocking effects in pure neutron matter.

In order to get a more detailed insight into the interaction of hyperons with heavy nuclei, we consider also the strength of the Λ-nuclear spin-orbit coupling. It is experimentally well established [142, 143] that the Λ-nucleus spin-orbit force is very small. In the following

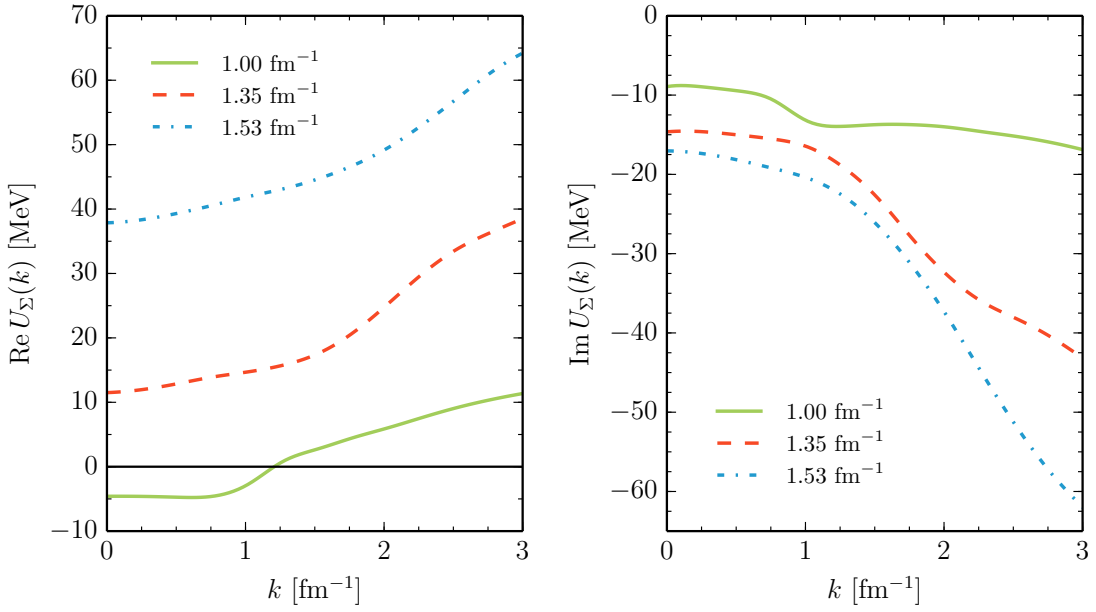

FIGURE 5.12: Momentum dependence of the real and imaginary parts of the Σ single-particle potential for different Fermi momenta $k_F = (1.00, 1.35, 1.53)\,\mathrm{fm}^{-1}$ in symmetric nuclear matter, calculated in χEFT at NLO with a cutoff $\Lambda = 600$ MeV.

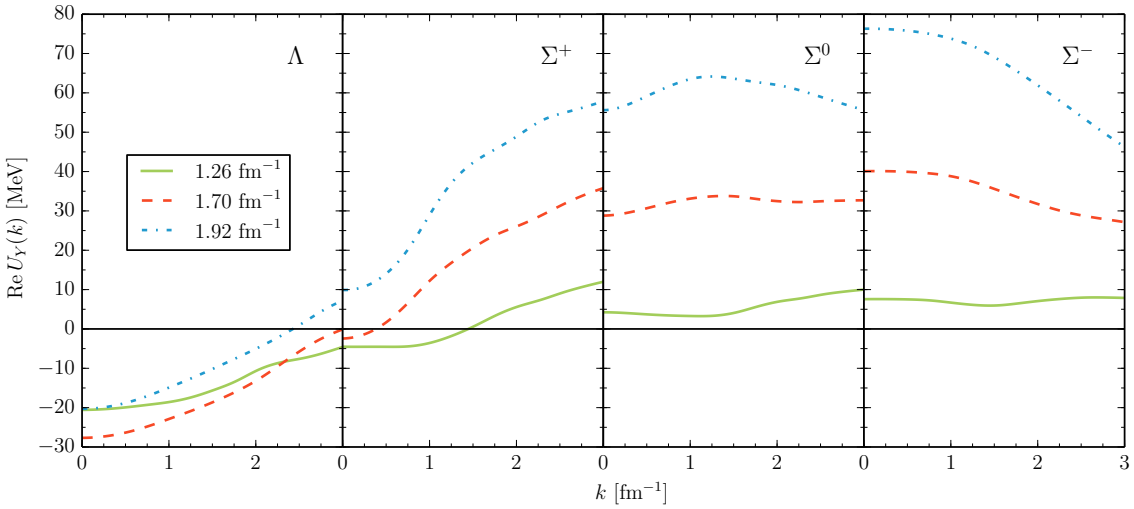

FIGURE 5.13: Momentum dependence of the real part of the single-particle potentials for hyperons in pure neutron matter for different Fermi momenta $k_F = (1.26, 1.70, 1.92)\,\mathrm{fm}^{-1}$, calculated in χEFT at NLO with a cutoff $\Lambda = 600$ MeV.

we will present results for the so-called Scheerbaum factor S_B. It quantifies the strength of the nuclear spin-orbit potential for a hyperon B, which takes the form [168]

$$U_B^{ls}(r) = -\frac{\pi}{2} S_B \frac{1}{r} \frac{\mathrm{d}\rho(r)}{\mathrm{d}r} \vec{l} \cdot \vec{\sigma} \,, \tag{5.30}$$

where $\rho(r)$ is the nucleon density distribution, $\vec{l}$ the (single-particle) orbital angular momentum operator and $\vec{\sigma}$ the hyperon spin operator. In isospin-symmetric nuclear matter with Fermi momentum k_F the Scheerbaum factor S_{B_1} is obtained from the G-matrix elements via the relation [169]

$$\begin{aligned} S_{B_1}(k_1) = &-\frac{3\pi}{4k_F^3}(1+\delta_{B_1B_2}(-1)^{L+S}) \sum_{B_2=n,p} \sum_J (2J+1)\xi_{12}(1+\xi_{12})^2 \\ &\times \int_{k_{\min}}^{k_{\max}} \frac{\mathrm{d}k}{(2\pi)^3} W(k_1,k) \,\mathrm{Re}\Big\{ \\ &\qquad (J+2)\, G^{1J+1,1J+1,J}_{(B_1B_2)(B_1B_2)}(k,k;\bar{K},\omega_{\text{o.s.}}) \\ &\qquad\quad + G^{1J,1J,J}_{(B_1B_2)(B_1B_2)}(k,k;\bar{K},\omega_{\text{o.s.}}) \\ &\qquad -(J-1)\, G^{1J-1,1J-1,J}_{(B_1B_2)(B_1B_2)}(k,k;\bar{K},\omega_{\text{o.s.}}) \\ &\quad -\sqrt{J(J+1)}\, G^{1J,0J,J}_{(B_1B_2)(B_1B_2)}(k,k;\bar{K},\omega_{\text{o.s.}}) \\ &\quad -\sqrt{J(J+1)}\, G^{0J,1J,J}_{(B_1B_2)(B_1B_2)}(k,k;\bar{K},\omega_{\text{o.s.}})\Big\} \,, \end{aligned} \tag{5.31}$$

with k_1 set to zero in the end. In Tab. 5.4 we present the Scheerbaum factor S_Λ for the Λ hyperon in symmetric nuclear matter at saturation density. The values in Tab. 5.4 are in agreement with the earlier results of Ref. [49]. The difference between the gap and the continuous choice for intermediate spectra is small. This is expected because the Scheerbaum factor involves only contributions from P-waves and higher partial waves and it is known that these are much less sensitive to the treatment of the intermediate spectra than the S-waves [18]. As stated previously, we use the same YN interaction as in Ref. [49] where the strength of the antisymmetric spin-orbit contact interaction, generating a spin singlet-triplet mixing ($^1P_1 \leftrightarrow {}^3P_1$), has been tuned to achieve $S_\Lambda \approx -3.7$ MeV fm^5, in accordance with estimates for the empirical value, which is expected to lie in the range of around -4.6 to -3.0 MeV fm^5 [170, 171]. In Tab. 5.5 we summarize our results for the Scheerbaum factor S_Σ, which are close to the values reported in Ref. [49]. As before, results are only given for Σ^0. The difference among the Scheerbaum factors for the three Σ hyperons due to their mass splitting is smaller than 0.5 MeV fm^5. In contrast to the leading-order approximation, at NLO always negative values of S_Σ are obtained, similar to the results found with the NSC97f and Jülich '04 models.

Another important quantity to characterize in-medium properties is the effective baryon mass. The ratio between the effective and the free hyperon mass in nuclear matter is usually defined as

$$\frac{M_B^*}{M_B} = \left[1 + 2M_B \left.\frac{\partial \,\mathrm{Re}\, U_B(k)}{\partial k^2}\right|_{k=0}\right]^{-1} . \tag{5.32}$$

We follow Ref. [21] where this ratio is computed as

$$\frac{M_B^*}{M_B} = \left[1 + \frac{2M_B}{k^2} \,\mathrm{Re}(U_B(k) - U_B(0))\right]^{-1} , \tag{5.33}$$

$S_\Lambda(k=0)$	$^3P_0$	$^3D_1$	$^3P_1$	$^1P_1 \leftrightarrow {}^3P_1$	$^3P_2$	$^3D_2$	$^3D_3$	Total
NLO (500) cont	−5.6	−0.6	−4.4	10.4	−3.5	0.4	0.2	−3.0
NLO (550) cont	−4.9	−0.6	−4.2	9.2	−3.2	0.4	0.2	−3.1
NLO (600) cont	−4.4	−0.6	−4.0	8.3	−3.1	0.4	0.2	−3.2
NLO (650) cont	−4.0	−0.6	−3.8	7.3	−3.1	0.4	0.2	−3.6
LO (600) gap	9.4	−0.2	−4.9	0.0	−1.1	0.4	−0.1	3.5
LO (600) cont	10.2	−0.2	−4.7	0.0	−1.2	0.4	−0.1	4.5
NLO (600) gap	−4.7	−0.6	−4.1	8.4	−3.1	0.4	0.2	−3.4
NSC97f gap	−2.2	0.5	−11.4	2.0	−2.6	1.1	−2.0	−14.2
NSC97f cont	−2.0	0.5	−10.8	1.9	−2.8	1.2	−2.0	−13.8
Jülich '04 gap	4.0	0.4	−1.4	5.1	−9.1	0.6	−1.0	−1.3
Jülich '04 cont	4.1	0.5	−1.3	5.1	−9.3	0.6	−1.1	−1.4

TABLE 5.4: Scheerbaum factor $S_\Lambda(k=0)$ in symmetric nuclear matter at saturation density, $k_F = 1.35$ fm^{-1}. Values are given in MeV fm^5 and decomposed into partial wave contributions.

$S_\Sigma(k=0)$	$^3P_0$	$^3D_1$	$^3P_1$	$^1P_1 \leftrightarrow {}^3P_1$	$^3P_2$	$^3D_2$	$^3D_3$	Total
NLO (500) cont	−7.7	0.6	−1.0	−10.6	0.9	0.1	0.1	−17.7
NLO (550) cont	−6.6	0.3	−0.6	−9.7	−0.0	0.1	0.1	−16.5
NLO (600) cont	−5.9	0.1	−0.1	−9.2	−1.0	0.1	0.0	−16.0
NLO (650) cont	−5.3	0.1	0.2	−8.3	−2.0	0.1	−0.0	−15.3
LO (600) gap	9.5	0.3	3.2	0.0	−2.8	0.1	−0.4	9.8
LO (600) cont	8.7	0.3	2.6	0.0	−2.4	0.1	−0.3	8.9
NLO (600) gap	−5.6	0.1	0.4	−10.1	−1.3	0.1	−0.1	−16.4
NSC97f gap	−2.0	0.1	−2.8	−2.7	−6.2	0.3	−1.5	−14.9
NSC97f cont	−1.8	0.0	−2.5	−2.6	−7.0	0.3	−1.6	−15.5
Jülich '04 gap	−2.2	0.1	4.5	−8.2	−9.6	0.3	−1.0	−16.4
Jülich '04 cont	−2.2	0.1	6.0	−9.8	−9.9	0.3	−1.0	−16.9

TABLE 5.5: Scheerbaum factor $S_\Sigma(k=0)$ in symmetric nuclear matter at saturation density, $k_F = 1.35$ fm^{-1}. Values are given in MeV fm^5 and decomposed into partial wave contributions.

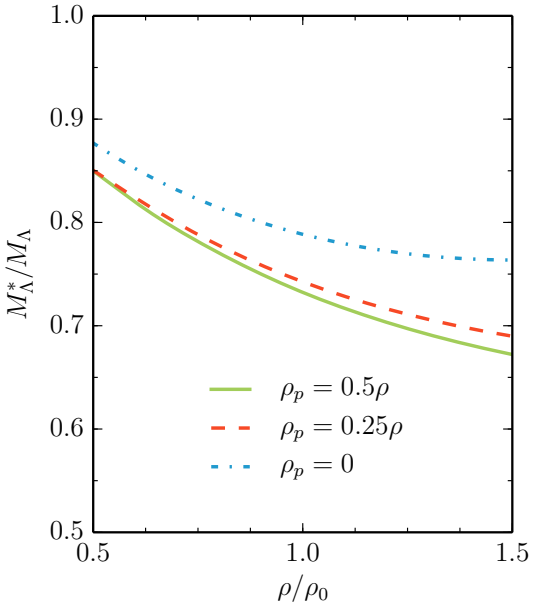

FIGURE 5.14: Density dependence of the effective mass of a Λ hyperon in (a)symmetric nuclear matter, calculated in χEFT at NLO with a cutoff $\Lambda = 600$ MeV.

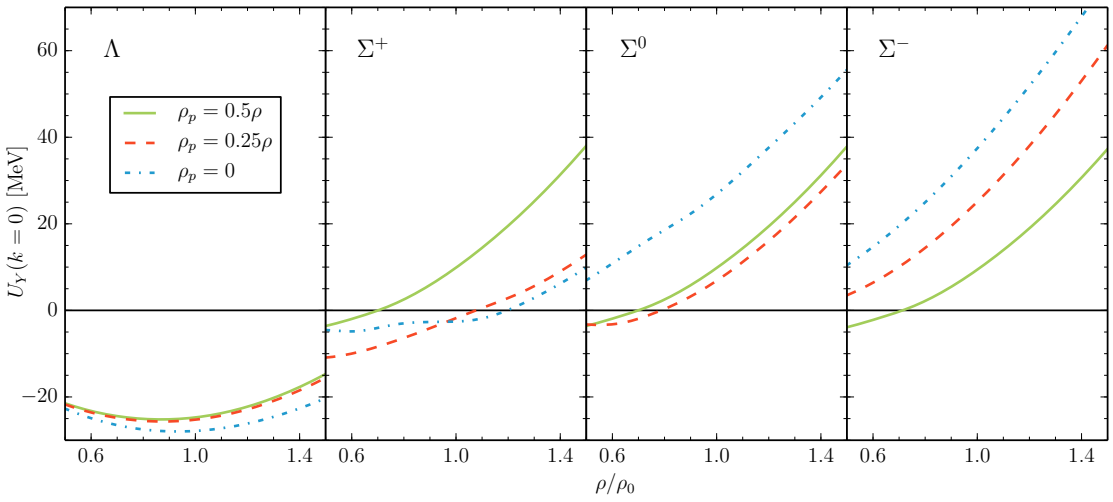

FIGURE 5.15: Density dependence of the hyperon single-particle potentials at $k = 0$ with different compositions of the nuclear matter, calculated in χEFT at NLO with a cutoff $\Lambda = 600$ MeV.

with $k \approx 1$ fm^{-1}. In some works k is even set to the Fermi momentum k_F in symmetric nuclear matter. In Fig. 5.14 the density dependence of the effective mass M^*_Λ of a Λ hyperon for different isospin asymmetries $\rho_p = (0, 0.25, 0.5)\rho$ is shown, where ρ_p is the proton density and ρ the total density. The effective Λ mass in pure neutron matter is slightly higher than the one in symmetric nuclear matter, but the shape of the curves in Fig. 5.14 does not depend on the composition of nuclear matter. Since the momentum-dependence of the Σ-nuclear potentials as obtained from the G-matrix calculations is not close to a quadratic behavior for momenta $0 \leq k \leq 3$ fm^{-1}, the effective mass does not serve as a significant quantity.

Finally, we investigate in more detail the influence of the composition and density of nuclear matter on the single-particle potentials of hyperons. In Fig. 5.15 the density dependence of the depth of the nuclear mean-field of Λ or Σ hyperons at rest ($k = 0$) is shown for isospin-symmetric nuclear matter, asymmetric nuclear matter with $\rho_p = 0.25\rho$ and pure neutron matter. The single-particle potential of the Λ hyperon is almost independent of the composition of the nuclear medium, because of its isosinglet nature. Furthermore, it is attractive over the whole considered range of density $0.5 \leq \rho/\rho_0 \leq 1.5$. The three Σ hyperons possess (up to small differences from the mass splittings) the same single-particle potential in symmetric nuclear matter. It is attractive for low densities, but turns into repulsion at $\rho \approx 0.7\rho_0$ and stays repulsive for higher densities. When introducing isospin asymmetry in the nuclear medium a splitting of the single-particle potentials occurs due to the strong isospin dependence of the ΣN interaction. The splittings among the Σ^+, Σ^0 and Σ^- potentials as obtained in our microscopic calculation have a non-linear dependence on the isospin asymmetry which goes beyond the usual (linear) parametrization in terms of an isovector Lane potential [172].

6

LEADING THREE-BARYON INTERACTION

Three-nucleon forces are an essential ingredient for a proper description of nuclei and nuclear matter with low-momentum two-body interactions. Similarly, three-baryon forces, especially the ΛNN interaction, are expected to play an important role in nuclear systems with strangeness. Their introduction in calculations of light hypernuclei seems to be required. Furthermore, the introduction of 3BF is traded as a possible solution to the hyperon puzzle (see Chapter 1). However, so far only phenomenological 3BF have been employed. In this section we derive the leading irreducible three-baryon interactions from SU(3) chiral effective field theory. We present the construction of the minimal effective Lagrangian required for the pertinent vertices. Moreover, SU(3) relations for strangeness 0 and -1 are derived. As an example, we present the ΛNN three-body interaction explicitly in the isospin basis and rederive the well-known chiral three-nucleon interaction for a check. Parts of this chapter have been previously published in Ref. [173].

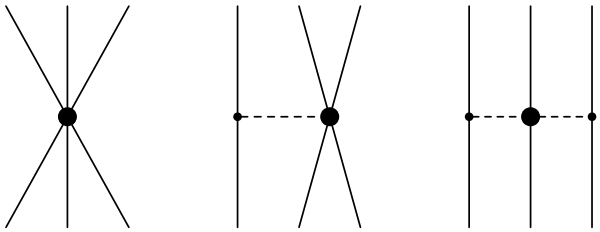

FIGURE 6.1: Leading three-baryon interactions: contact term, one-meson exchange and two-meson exchange. Filled circles and solid dots denote vertices with $\Delta_i = 1$ and $\Delta_i = 0$, respectively.

According to the power counting in Eq. (2.62) the 3BF arise formally at NNLO in the chiral expansion, as can be seen from the hierarchy of baryonic forces in Fig. 2.4. Three types of diagrams contribute: three-baryon contact terms, one-meson and two-meson exchange diagrams, cf. Fig. 6.1. Note that a two-meson exchange diagram, like in Fig. 6.1, with a (leading order) Weinberg-Tomozawa vertex in the middle, would formally be a NLO contribution. However, as in the nucleonic sector, this contribution is kinematically suppressed due to the fact that the involved meson energies are differences of baryon kinetic energies. In Chapter 7 we will show, that parts of these NNLO contributions get promoted to NLO by the introduction of intermediate decuplet baryons, so that it becomes appropriate to use these three-body interactions together with the NLO two-body interaction of Chapter 4. Note again, that we derive the irreducible contributions to the chiral potential. In three-flavor χEFT nucleons and hyperons (Λ, Σ, Ξ) are treated on equal footing. In contrast to typical phenomenological calculations, diagrams such as given in Fig. 4.10 on the left side, do not correspond to a genuine three-body potential, but to an iteration of the two-baryon potential. Such diagrams will be generated automatically when solv-

ing, e.g., the Faddeev (or Yakubovsky) equations within a coupled-channel approach. We expect, that the three-body potentials derived from SU(3) χEFT will shed light on the effect of 3BF in hypernuclear systems. In particular, their implementation in studies of light hypernuclei will be very instructive since such systems can be treated within reliable few-body techniques [29, 174].

6.1 CONTACT INTERACTION

In the following we consider the three-baryon contact interaction. We construct the minimal Lagrangian, demonstrate how to derive the antisymmetrized potentials and investigate their group-theoretical classification.

6.1.1 *Overcomplete contact Lagrangian*

As already discussed in Sec. 2.3 the terms of the effective Lagrangian have to fulfill the symmetries of quantum chromodynamics and are constructed to obey the invariances under charge conjugation, parity transformation, Hermitian conjugation and the local chiral symmetry group $\mathrm{SU}(3)_\mathrm{L} \times \mathrm{SU}(3)_\mathrm{R}$. The baryon fields are collected in a traceless matrix B, see Eq. (2.30). In order to obtain the most general contact Lagrangian in flavor SU(3), we follow the same procedure as used for the four-baryon contact terms in Chapter 3. Generalizing these construction rules straightforwardly to six-baryon contact terms, we end up with the following (largely overcomplete) set of terms for the leading covariant Lagrangian:

$$\mathscr{L} = \sum_{f=1}^{11} \sum_{a=1}^{5} t^{f,a} \mathcal{T}^{f,a} \,, \tag{6.1}$$

where the index f runs over eleven possible flavor structures. These are given by:

$$\begin{aligned}
\mathcal{T}^{1,a} &= \langle \bar{B}_\alpha \bar{B}_\beta \bar{B}_\gamma (\Gamma^{1,a} B)_\alpha (\Gamma^{2,a} B)_\beta (\Gamma^{3,a} B)_\gamma \rangle \\
&\quad + (-1)^{c_a} \langle \bar{B}_\gamma \bar{B}_\beta \bar{B}_\alpha (\Gamma^{3,a} B)_\gamma (\Gamma^{2,a} B)_\beta (\Gamma^{1,a} B)_\alpha \rangle \,, \\
\mathcal{T}^{2,a} &= \langle \bar{B}_\alpha \bar{B}_\beta (\Gamma^{1,a} B)_\alpha \bar{B}_\gamma (\Gamma^{2,a} B)_\beta (\Gamma^{3,a} B)_\gamma \rangle \\
&\quad + (-1)^{c_a} \langle \bar{B}_\gamma \bar{B}_\beta (\Gamma^{3,a} B)_\gamma \bar{B}_\alpha (\Gamma^{2,a} B)_\beta (\Gamma^{1,a} B)_\alpha \rangle \,, \\
\mathcal{T}^{3,a} &= \langle \bar{B}_\alpha \bar{B}_\beta (\Gamma^{1,a} B)_\alpha (\Gamma^{2,a} B)_\beta \bar{B}_\gamma (\Gamma^{3,a} B)_\gamma \rangle \\
&\quad + (-1)^{c_a} \langle \bar{B}_\beta \bar{B}_\alpha (\Gamma^{2,a} B)_\beta (\Gamma^{1,a} B)_\alpha \bar{B}_\gamma (\Gamma^{3,a} B)_\gamma \rangle \,, \\
\mathcal{T}^{4,a} &= \langle \bar{B}_\alpha (\Gamma^{1,a} B)_\alpha \bar{B}_\beta (\Gamma^{2,a} B)_\beta \bar{B}_\gamma (\Gamma^{3,a} B)_\gamma \rangle \\
&\quad + (-1)^{c_a} \langle \bar{B}_\gamma (\Gamma^{3,a} B)_\gamma \bar{B}_\beta (\Gamma^{2,a} B)_\beta \bar{B}_\alpha (\Gamma^{1,a} B)_\alpha \rangle \,, \\
\mathcal{T}^{5,a} &= \langle \bar{B}_\alpha \bar{B}_\beta (\Gamma^{1,a} B)_\alpha (\Gamma^{2,a} B)_\beta \rangle \, \langle \bar{B}_\gamma (\Gamma^{3,a} B)_\gamma \rangle \\
&\quad + (-1)^{c_a} \langle \bar{B}_\beta \bar{B}_\alpha (\Gamma^{2,a} B)_\beta (\Gamma^{1,a} B)_\alpha \rangle \, \langle \bar{B}_\gamma (\Gamma^{3,a} B)_\gamma \rangle \,, \\
\mathcal{T}^{6,a} &= \langle \bar{B}_\alpha (\Gamma^{1,a} B)_\alpha \bar{B}_\beta (\Gamma^{2,a} B)_\beta \rangle \, \langle \bar{B}_\gamma (\Gamma^{3,a} B)_\gamma \rangle \\
&\quad + (-1)^{c_a} \langle \bar{B}_\alpha (\Gamma^{1,a} B)_\alpha \bar{B}_\beta (\Gamma^{2,a} B)_\beta \rangle \, \langle \bar{B}_\gamma (\Gamma^{3,a} B)_\gamma \rangle \,, \\
\mathcal{T}^{7,a} &= \langle \bar{B}_\alpha \bar{B}_\beta \bar{B}_\gamma (\Gamma^{1,a} B)_\alpha \rangle \, \langle (\Gamma^{2,a} B)_\beta (\Gamma^{3,a} B)_\gamma \rangle \\
&\quad + (-1)^{c_a} \langle \bar{B}_\gamma \bar{B}_\beta \rangle \, \langle \bar{B}_\alpha (\Gamma^{3,a} B)_\gamma (\Gamma^{2,a} B)_\beta (\Gamma^{1,a} B)_\alpha \rangle \,, \\
\mathcal{T}^{8,a} &= \langle \bar{B}_\alpha \bar{B}_\beta \bar{B}_\gamma \rangle \, \langle (\Gamma^{1,a} B)_\alpha (\Gamma^{2,a} B)_\beta (\Gamma^{3,a} B)_\gamma \rangle \\
&\quad + (-1)^{c_a} \langle \bar{B}_\gamma \bar{B}_\beta \bar{B}_\alpha \rangle \, \langle (\Gamma^{3,a} B)_\gamma (\Gamma^{2,a} B)_\beta (\Gamma^{1,a} B)_\alpha \rangle \,,
\end{aligned}$$

a	c_a	$\Gamma^{1,a}$	$\Gamma^{2,a}$	$\Gamma^{3,a}$	$V^a_{ijk} = (\bar{u}\Gamma^{1,a}u)_i(\bar{u}\Gamma^{2,a}u)_j(\bar{u}\Gamma^{3,a}u)_k$
1	0	$\mathbb{1}$	$\mathbb{1}$	$\mathbb{1}$	$\mathbb{1}$
2	0	$-\mathbb{1}$	$\gamma_5\gamma^\mu$	$\gamma_5\gamma_\mu$	$\vec{\sigma}_j \cdot \vec{\sigma}_k$
3	0	$\gamma_5\gamma^\mu$	$-\mathbb{1}$	$\gamma_5\gamma_\mu$	$\vec{\sigma}_i \cdot \vec{\sigma}_k$
4	0	$\gamma_5\gamma^\mu$	$\gamma_5\gamma_\mu$	$-\mathbb{1}$	$\vec{\sigma}_i \cdot \vec{\sigma}_j$
5	1	$\gamma_5\gamma_\mu$	$-\mathrm{i}\,\sigma^{\mu\nu}$	$\gamma_5\gamma_\nu$	$\mathrm{i}\,\vec{\sigma}_i \cdot (\vec{\sigma}_j \times \vec{\sigma}_k)$

TABLE 6.1: Dirac structures $\Gamma^1, \Gamma^2, \Gamma^3$. Only structures with independent potential contributions are considered.

$$
\begin{aligned}
\mathcal{T}^{9,a} &= \langle \bar{B}_\alpha \bar{B}_\beta (\Gamma^{1,a} B)_\alpha \rangle \, \langle (\Gamma^{2,a} B)_\beta \bar{B}_\gamma (\Gamma^{3,a} B)_\gamma \rangle \\
&\quad + (-1)^{c_a} \langle \bar{B}_\beta \bar{B}_\gamma (\Gamma^{3,a} B)_\gamma \rangle \, \langle \bar{B}_\alpha (\Gamma^{2,a} B)_\beta (\Gamma^{1,a} B)_\alpha \rangle \,, \\
\mathcal{T}^{10,a} &= \langle \bar{B}_\alpha (\Gamma^{1,a} B)_\alpha \rangle \, \langle \bar{B}_\beta (\Gamma^{2,a} B)_\beta \rangle \, \langle \bar{B}_\gamma (\Gamma^{3,a} B)_\gamma \rangle \\
&\quad + (-1)^{c_a} \langle \bar{B}_\alpha (\Gamma^{1,a} B)_\alpha \rangle \, \langle \bar{B}_\beta (\Gamma^{2,a} B)_\beta \rangle \, \langle \bar{B}_\gamma (\Gamma^{3,a} B)_\gamma \rangle \,, \\
\mathcal{T}^{11,a} &= \langle \bar{B}_\alpha \bar{B}_\beta \rangle \, \langle \bar{B}_\gamma (\Gamma^{1,a} B)_\alpha \rangle \, \langle (\Gamma^{2,a} B)_\beta (\Gamma^{3,a} B)_\gamma \rangle \\
&\quad + (-1)^{c_a} \langle \bar{B}_\gamma \bar{B}_\beta \rangle \, \langle \bar{B}_\alpha (\Gamma^{3,a} B)_\gamma \rangle \, \langle (\Gamma^{2,a} B)_\beta (\Gamma^{1,a} B)_\alpha \rangle \,,
\end{aligned}
\tag{6.2}
$$

where the indices α, β, γ are Dirac indices. The index $a = 1, \ldots, 5$ in Eq. (6.1) labels the three combined Dirac structures $\Gamma^{1,a}, \Gamma^{2,a}, \Gamma^{3,a}$ that have to be inserted into each flavor structure $f = 1, \ldots, 11$. The allowed Dirac structures are given in Tab. 6.1. Note that we start with a covariant Lagrangian, but in the end are only interested in the minimal non-relativistic Lagrangian. Therefore, only Dirac structures that lead to independent (non-relativistic) spin operators are considered in Tab. 6.1. The corresponding spin-dependent potentials V^a_{ijk} (shown in the last column of Tab. 6.1) result from the Dirac structures sandwiched between Dirac spinors in spin spaces i, j and k. The overcomplete set of terms in the Lagrangian Eq. (6.1) contains 55 low-energy constants $t^{f,a}$. One observes that some combinations of Dirac and flavor structures do not even contribute at the leading order. Nevertheless, this set is a good starting point to obtain the minimal non-relativistic contact Lagrangian.

It is advantageous to rewrite the Lagrangian in the particle basis, which gives:

$$
\mathscr{L} = \sum_{f=1}^{11} \sum_{a=1}^{5} \tilde{t}^{f,a} \sum_{i,j,k,l,m,n} N^{f,a}_{\substack{ikm \\ jln}} (\bar{B}_i \Gamma^{1,a} B_j)(\bar{B}_k \Gamma^{2,a} B_l)(\bar{B}_m \Gamma^{3,a} B_n) \,. \tag{6.3}
$$

where B_i are the baryon fields in the particle basis and the indices i, j, k, l, m, n label the six occurring baryon fields, $B_i \in \{n, p, \Lambda, \Sigma^+, \Sigma^0, \Sigma^-, \Xi^0, \Xi^-\}$. The SU(3) factors N can be obtained easily by using Eq. (2.30), multiplying the respective flavor matrices and taking traces. Note that the constants $\tilde{t}^{f,a}$ are equal to $t^{f,a}$, but with an additional minus sign for $f = 1, 3, 5, 7, 8, 9, 11$, coming from the interchange of anticommuting baryon fields.

6.1.2 *Derivation of the contact potential*

Let us now consider the process $B_1 B_2 B_3 \to B_4 B_5 B_6$, where the B_i are again baryons in the particle basis. The aim is to derive a potential operator V in the threefold spin space for this process. We define the operators in spin-space 1 to act between the two-component

Pauli spinors of B_1 and B_4. Similarly, spin-space 2 belongs to B_2 and B_5, and spin-space 3 to B_3 and B_6. The potential for a fixed spin configuration is then obtained as

$$\chi^{(1)\dagger}_{B_4}\chi^{(2)\dagger}_{B_5}\chi^{(3)\dagger}_{B_6}\, V\, \chi^{(1)}_{B_1}\chi^{(2)}_{B_2}\chi^{(3)}_{B_3}\,, \tag{6.4}$$

where the superscript of a spinor denotes the spin space and the subscript denotes the baryon to which the spinor belongs.

The potential is given by $V = -\langle B_4B_5B_6|\ \mathscr{L}\ |B_1B_2B_3\rangle$, where the appropriate terms of $\mathscr{L}$ in Eq. (6.3) have to be inserted, and the 36 Wick contractions have to be performed. First, each of the 55 terms in the Lagrangian (labeled by f, a) provides six so-called direct terms,

$$\begin{aligned}
&\tilde{t}^{f,a} N^{f,a}_{\substack{456\\123}} (\bar{B}_4\Gamma^{1,a}B_1)(\bar{B}_5\Gamma^{2,a}B_2)(\bar{B}_6\Gamma^{3,a}B_3)\\
&+\tilde{t}^{f,a} N^{f,a}_{\substack{564\\231}} (\bar{B}_5\Gamma^{1,a}B_2)(\bar{B}_6\Gamma^{2,a}B_3)(\bar{B}_4\Gamma^{3,a}B_1)\\
&+\tilde{t}^{f,a} N^{f,a}_{\substack{645\\312}} (\bar{B}_6\Gamma^{1,a}B_3)(\bar{B}_4\Gamma^{2,a}B_1)(\bar{B}_5\Gamma^{3,a}B_2)\\
&+\tilde{t}^{f,a} N^{f,a}_{\substack{465\\132}} (\bar{B}_4\Gamma^{1,a}B_1)(\bar{B}_6\Gamma^{2,a}B_3)(\bar{B}_5\Gamma^{3,a}B_2)\\
&+\tilde{t}^{f,a} N^{f,a}_{\substack{654\\321}} (\bar{B}_6\Gamma^{1,a}B_3)(\bar{B}_5\Gamma^{2,a}B_2)(\bar{B}_4\Gamma^{3,a}B_1)\\
&+\tilde{t}^{f,a} N^{f,a}_{\substack{546\\213}} (\bar{B}_5\Gamma^{1,a}B_2)(\bar{B}_4\Gamma^{2,a}B_1)(\bar{B}_6\Gamma^{3,a}B_3)\,,
\end{aligned} \tag{6.5}$$

where the baryon bilinears combine the baryon pairs 1-4, 2-5 and 3-6, in the form as set up in Eq. (6.4). Keeping in mind that baryons B_1, B_2, B_3 are in spin-space 1, 2, 3, respectively, one obtains by performing the (six direct) Wick contractions the direct potential[1]

$$\begin{aligned}
V^D = -\sum_{f=1}^{11}\sum_{a=1}^{5}\tilde{t}^{f,a}\Bigg(& N^{f,a}_{\substack{456\\123}} V^a_{123} + N^{f,a}_{\substack{564\\231}} V^a_{231} + N^{f,a}_{\substack{645\\312}} V^a_{312}\\
& + N^{f,a}_{\substack{465\\132}} V^a_{132} + N^{f,a}_{\substack{654\\321}} V^a_{321} + N^{f,a}_{\substack{546\\213}} V^a_{213}\Bigg)\,.
\end{aligned} \tag{6.6}$$

The spin operators V^a_{ijk} arise from the Dirac structures $\Gamma^{1,a}\otimes\Gamma^{2,a}\otimes\Gamma^{3,a}$ and can be found in Tab. 6.1. The indices i, j, k of V^a_{ijk} denote the spin spaces of the three baryon bilinears.

One has not only these six direct Wick contractions, but in total 36 Wick contractions that contribute to the potential. This number corresponds to the $3!\times 3!$ possibilities to arrange the three initial and three final baryons into Dirac bilinears. For example a term

$$\tilde{t}^{f,a} N^{f,a}_{\substack{546\\312}} (\bar{B}_5\Gamma^{1,a}B_3)(\bar{B}_4\Gamma^{2,a}B_1)(\bar{B}_6\Gamma^{3,a}B_2) \tag{6.7}$$

gives rise to a potential contribution

$$\tilde{t}^{f,a} N^{f,a}_{\substack{546\\312}} V^a_{312}\,, \tag{6.8}$$

where the sign, reverted in comparison to Eq. (6.6), originates from the exchange of baryon fields. However, this potential is not in accordance with the form of Eq. (6.4), as baryon

1 One observes that Eq. (6.6) holds independently of whether some of the baryons are identical or not.

pairs 1-4, 2-6, 3-5 are each connected in a separate spin space. Hence, an exchange of the spin wave functions $\chi^{(2)}_{B_5}$ and $\chi^{(3)}_{B_6}$ in the final state has to be performed and this is achieved by multiplying the potential with $P^{(\sigma)}_{23}$:

$$\tilde{t}^{f,a} N^{f,a}_{\substack{546\\312}} P^{(\sigma)}_{23} V^{a}_{312}\,, \tag{6.9}$$

where $P^{(\sigma)}_{ij} = \frac{1}{2}(\mathbb{1} + \vec{\sigma}_i \cdot \vec{\sigma}_j)$ is the well-known spin-exchange operator.

Employing the above considerations to all Wick contractions, the full potential including 36 contributions is derived. For a shorter notation we express the remaining 30 contributions in terms of the six direct contributions in Eq. (6.6), with the declared replacement of the labels. The full potential is thus given by

$$\begin{aligned} V = V^D &+ P^{(\sigma)}_{23} P^{(\sigma)}_{13} \Big(V^D\Big)^{\substack{4\to5\\5\to6\\6\to4}} + P^{(\sigma)}_{23} P^{(\sigma)}_{12} \Big(V^D\Big)^{\substack{4\to6\\5\to4\\6\to5}} \\ &- P^{(\sigma)}_{23} \Big(V^D\Big)^{\substack{4\to4\\5\to6\\6\to5}} - P^{(\sigma)}_{13} \Big(V^D\Big)^{\substack{4\to6\\5\to5\\6\to4}} - P^{(\sigma)}_{12} \Big(V^D\Big)^{\substack{4\to5\\5\to4\\6\to6}}. \end{aligned} \tag{6.10}$$

The procedure described above automatically incorporates the generalized Pauli principle and leads to a fully antisymmetrized potential.

6.1.3 *Minimal contact Lagrangian*

Now we are in the position to determine a minimal and complete contact Lagrangian for the leading three-baryon contact interaction. We have derived the potential according to Eq. (6.10) and decomposed it with respect to the following operators in the three-body spin space

$$\mathbb{1}\,, \quad \vec{\sigma}_1 \cdot \vec{\sigma}_2\,, \quad \vec{\sigma}_1 \cdot \vec{\sigma}_3\,, \quad \vec{\sigma}_2 \cdot \vec{\sigma}_3\,, \quad \mathrm{i}\,\vec{\sigma}_1 \cdot (\vec{\sigma}_2 \times \vec{\sigma}_3)\,. \tag{6.11}$$

A minimal set of Lagrangian terms in the non-relativistic limit is obtained by leaving out terms until the rank of the final potential matrix matches the number of terms in the Lagrangian. Redundant terms have been deleted in such a way, that one obtains a maximal number of Lagrangian terms with a single flavor-trace. The minimal six-baryon contact Lagrangian in the non-relativistic limit is then given by

$$\begin{aligned} \mathscr{L} = &- C_1 \langle \bar{B}_a \bar{B}_b \bar{B}_c B_a B_b B_c \rangle \\ &+ C_2 \langle \bar{B}_a \bar{B}_b B_a \bar{B}_c B_b B_c \rangle \\ &- C_3 \langle \bar{B}_a \bar{B}_b B_a B_b \bar{B}_c B_c \rangle \\ &+ C_4 \langle \bar{B}_a B_a \bar{B}_b B_b \bar{B}_c B_c \rangle \\ &- C_5 \langle \bar{B}_a \bar{B}_b B_a B_b \rangle \, \langle \bar{B}_c B_c \rangle \\ &- C_6 \Big(\langle \bar{B}_a \bar{B}_b \bar{B}_c B_a (\sigma^i B)_b (\sigma^i B)_c \rangle + \langle \bar{B}_c \bar{B}_b \bar{B}_a (\sigma^i B)_c (\sigma^i B)_b B_a \rangle \Big) \\ &+ C_7 \Big(\langle \bar{B}_a \bar{B}_b B_a \bar{B}_c (\sigma^i B)_b (\sigma^i B)_c \rangle + \langle \bar{B}_c \bar{B}_b (\sigma^i B)_c \bar{B}_a (\sigma^i B)_b B_a \rangle \Big) \\ &- C_8 \Big(\langle \bar{B}_a \bar{B}_b B_a (\sigma^i B)_b \bar{B}_c (\sigma^i B)_c \rangle + \langle \bar{B}_b \bar{B}_a (\sigma^i B)_b B_a \bar{B}_c (\sigma^i B)_c \rangle \Big) \\ &+ C_9 \langle \bar{B}_a B_a \bar{B}_b (\sigma^i B)_b \bar{B}_c (\sigma^i B)_c \rangle \\ &- C_{10} \Big(\langle \bar{B}_a \bar{B}_b B_a (\sigma^i B)_b \rangle \, \langle \bar{B}_c (\sigma^i B)_c \rangle + \langle \bar{B}_b \bar{B}_a (\sigma^i B)_b B_a \rangle \, \langle \bar{B}_c (\sigma^i B)_c \rangle \Big) \end{aligned}$$

$$
\begin{aligned}
&- C_{11}\langle \bar{B}_a \bar{B}_b \bar{B}_c (\sigma^i B)_a B_b (\sigma^i B)_c \rangle \\
&+ C_{12}\langle \bar{B}_a \bar{B}_b (\sigma^i B)_a \bar{B}_c B_b (\sigma^i B)_c \rangle \\
&- C_{13}\langle \bar{B}_a \bar{B}_b (\sigma^i B)_a (\sigma^i B)_b \bar{B}_c B_c \rangle \\
&- C_{14}\langle \bar{B}_a \bar{B}_b (\sigma^i B)_a (\sigma^i B)_b \rangle \, \langle \bar{B}_c B_c \rangle \\
&- \mathrm{i}\,\epsilon^{ijk} C_{15}\langle \bar{B}_a \bar{B}_b \bar{B}_c (\sigma^i B)_a (\sigma^j B)_b (\sigma^k B)_c \rangle \\
&+ \mathrm{i}\,\epsilon^{ijk} C_{16}\langle \bar{B}_a \bar{B}_b (\sigma^i B)_a \bar{B}_c (\sigma^j B)_b (\sigma^k B)_c \rangle \\
&- \mathrm{i}\,\epsilon^{ijk} C_{17}\langle \bar{B}_a \bar{B}_b (\sigma^i B)_a (\sigma^j B)_b \bar{B}_c (\sigma^k B)_c \rangle \\
&+ \mathrm{i}\,\epsilon^{ijk} C_{18}\langle \bar{B}_a (\sigma^i B)_a \bar{B}_b (\sigma^j B)_b \bar{B}_c (\sigma^k B)_c \rangle \,. \qquad (6.12)
\end{aligned}
$$

The indices a, b, c are two-component spinor indices and the indices i, j, k are vector indices. One ends up with 18 low-energy constants $C_1 \ldots C_{18}$. The minus signs in front of some terms have been included to compensate minus signs from fermion exchange, arising from reordering baryon bilinears into the form of Eq. (6.3).

Various checks have been performed. In particular, we verified conservation of strangeness S, isospin I and isospin projection I_3 and the independence of the resulting potentials from I_3. The Lagrangian has been constructed to fulfill C and P symmetry. Time reversal symmetry follows via the CPT theorem, and we explicitly confirmed T invariance for all potentials.

6.1.4 *Group-theoretical considerations*

Let us now consider the three-baryon contact terms from a group-theoretical point of view. In flavor space the three octet baryons form the 512-dimensional tensor product $\mathbf{8} \otimes \mathbf{8} \otimes \mathbf{8}$, which decomposes into the following irreducible SU(3) representations

$$
\mathbf{8} \otimes \mathbf{8} \otimes \mathbf{8} = \mathbf{64} \oplus (\mathbf{35} \oplus \overline{\mathbf{35}})_2 \oplus \mathbf{27}_6 \oplus (\mathbf{10} \oplus \overline{\mathbf{10}})_4 \oplus \mathbf{8}_8 \oplus \mathbf{1}_2 \,, \qquad (6.13)
$$

where a subscript denotes the multiplicity of an irreducible representations. In spin space the tensor product of three doublets decomposes as

$$
\mathbf{2} \otimes \mathbf{2} \otimes \mathbf{2} = \mathbf{2}_2 \oplus \mathbf{4} \,. \qquad (6.14)
$$

Transitions are only allowed between irreducible representations of the same type. In analogy to Ref. [116] for the two-baryon sector, we determine which of the irreducible representations in Eq. (6.13) can contribute to a particular three-baryon multiplet, characterized by hypercharge $Y = S + 3$ (with strangeness S) and isospin I. Table 6.2 gives for the relevant SU(3) representations the (Y, I)-multiplets that they contain. From this table one can read off which representations are involved in the various three-baryon states, presented in Tab. 6.3. At leading order the potentials are momentum-independent and therefore only S-waves are present. Due to the Pauli principle the totally symmetric spin-quartet $\mathbf{4}$ must combine with the totally antisymmetric part of $\mathbf{8} \otimes \mathbf{8} \otimes \mathbf{8}$ in flavor space,

$$
\mathrm{Alt}_3(\mathbf{8}) = \mathbf{56}_a = \mathbf{27}_a + \mathbf{10}_a + \overline{\mathbf{10}}_a + \mathbf{8}_a + \mathbf{1}_a \,. \qquad (6.15)
$$

Therefore, these totally antisymmetric representations are present only in states with total spin 3/2. The decomposition of Eq. (6.15) is obtained by observing that one $\mathbf{1}$-plet and one $\mathbf{27}$-plet must be present. The totally symmetric part of $\mathbf{8} \otimes \mathbf{8} \otimes \mathbf{8}$ decomposes as

$$
\mathrm{Sym}_3(\mathbf{8}) = \mathbf{120}_s = \mathbf{64}_s + \mathbf{27}_s + \mathbf{10}_s + \overline{\mathbf{10}}_s + \mathbf{8}_s + \mathbf{1}_s \,, \qquad (6.16)
$$

D	allowed (Y, I)
1	$(0,0)$
8	$(1,\frac{1}{2}),(0,0),(0,1),(-1,\frac{1}{2})$
10	$(1,\frac{3}{2}),(0,1),(-1,\frac{1}{2}),(-2,0)$
$\overline{\mathbf{10}}$	$(2,0),(1,\frac{1}{2}),(0,1),(-1,\frac{3}{2})$
27	$(2,1),(1,\frac{1}{2}),(1,\frac{3}{2}),(0,0),(0,1),(0,2),(-1,\frac{1}{2}),(-1,\frac{3}{2}),(-2,1)$
35	$(2,2),(1,\frac{3}{2}),(1,\frac{5}{2}),(0,1),(0,2),(-1,\frac{1}{2}),(-1,\frac{3}{2}),(-2,0),(-2,1),(-3,\frac{1}{2})$
$\overline{\mathbf{35}}$	$(3,\frac{1}{2}),(2,0),(2,1),(1,\frac{1}{2}),(1,\frac{3}{2}),(0,1),(0,2),(-1,\frac{3}{2}),(-1,\frac{5}{2}),(-2,2)$
64	$(3,\frac{3}{2}),(2,1),(2,2),(1,\frac{1}{2}),(1,\frac{3}{2}),(1,\frac{5}{2}),(0,0),(0,1),(0,2),(0,3),$ $(-1,\frac{1}{2}),(-1,\frac{3}{2}),(-1,\frac{5}{2}),(-2,1),(-2,2),(-3,\frac{3}{2})$

TABLE 6.2: Hypercharge Y and isospin I for irreducible $SU(3)$ representations of dimension D.

states	(Y, I)	${}^2S_{1/2}$	${}^4S_{3/2}$
NNN	$(3,\frac{1}{2})$	$\overline{\mathbf{35}}$	
$\Lambda NN, \Sigma NN$	$(2,0)$	$\overline{\mathbf{10}}, \overline{\mathbf{35}}$	$\overline{\mathbf{10}}_a$
$\Lambda NN, \Sigma NN$	$(2,1)$	$\mathbf{27}, \overline{\mathbf{35}}$	$\mathbf{27}_a$
ΣNN	$(2,2)$	$\mathbf{35}$	
$\Lambda\Lambda N, \Sigma\Lambda N, \Sigma\Sigma N, \Xi NN$	$(1,\frac{1}{2})$	$\mathbf{8}, \overline{\mathbf{10}}, \mathbf{27}, \overline{\mathbf{35}}$	$\mathbf{8}_a, \overline{\mathbf{10}}_a, \mathbf{27}_a$
$\Sigma\Lambda N, \Sigma\Sigma N, \Xi NN$	$(1,\frac{3}{2})$	$\mathbf{10}, \mathbf{27}, \mathbf{35}, \overline{\mathbf{35}}$	$\mathbf{10}_a, \mathbf{27}_a$
$\Sigma\Sigma N$	$(1,\frac{5}{2})$	$\mathbf{35}$	
$\Lambda\Lambda\Lambda, \Sigma\Sigma\Lambda, \Sigma\Sigma\Sigma, \Xi\Lambda N, \Xi\Sigma N$	$(0,0)$	$\mathbf{8}, \mathbf{27}$	$\mathbf{1}_a, \mathbf{8}_a, \mathbf{27}_a$
$\Sigma\Lambda\Lambda, \Sigma\Sigma\Lambda, \Sigma\Sigma\Sigma, \Xi\Lambda N, \Xi\Sigma N$	$(0,1)$	$\mathbf{8}, \mathbf{10}, \overline{\mathbf{10}}, \mathbf{27}, \mathbf{35}, \overline{\mathbf{35}}$	$\mathbf{8}_a, \mathbf{10}_a, \overline{\mathbf{10}}_a, \mathbf{27}_a$
$\Sigma\Sigma\Lambda, \Sigma\Sigma\Sigma, \Xi\Sigma N$	$(0,2)$	$\mathbf{27}, \mathbf{35}, \overline{\mathbf{35}}$	$\mathbf{27}_a$
$\Xi\Lambda\Lambda, \Xi\Sigma\Lambda, \Xi\Sigma\Sigma, \Xi\Xi N$	$(-1,\frac{1}{2})$	$\mathbf{8}, \mathbf{10}, \mathbf{27}, \mathbf{35}$	$\mathbf{8}_a, \mathbf{10}_a, \mathbf{27}_a$
$\Xi\Sigma\Lambda, \Xi\Sigma\Sigma, \Xi\Xi N$	$(-1,\frac{3}{2})$	$\overline{\mathbf{10}}, \mathbf{27}, \mathbf{35}, \overline{\mathbf{35}}$	$\overline{\mathbf{10}}_a, \mathbf{27}_a$
$\Xi\Sigma\Sigma$	$(-1,\frac{5}{2})$	$\overline{\mathbf{35}}$	
$\Xi\Xi\Lambda, \Xi\Xi\Sigma$	$(-2,0)$	$\mathbf{10}, \mathbf{35}$	$\mathbf{10}_a$
$\Xi\Xi\Lambda, \Xi\Xi\Sigma$	$(-2,1)$	$\mathbf{27}, \mathbf{35}$	$\mathbf{27}_a$
$\Xi\Xi\Sigma$	$(-2,2)$	$\overline{\mathbf{35}}$	
$\Xi\Xi\Xi$	$(-3,\frac{1}{2})$	$\mathbf{35}$	

TABLE 6.3: Irreducible representations for three-baryon states with hypercharge Y and isospin I in partial waves.

where the decomposition follows from the observation that the highest dimensional **64**-plet and one **1**-plet must occur. Since the totally symmetric part has no totally antisymmetric counterpart in spin space, it can not contribute. This is especially true for the **64** representation, which appears only once in the decomposition $\mathbf{8} \otimes \mathbf{8} \otimes \mathbf{8}$. In Tab. 6.3 we have already included these exclusion criteria following from the generalized Pauli principle.

In the next step, we can derive the potentials for transitions between the three-baryon states, and redefine the 18 constants such that they belong to transitions between ir-

reducible representations. It is then a highly non-trivial check of our results that this redefinition fulfills the restrictions of Tab. 6.3. For example, in the NNN interaction and the $\Xi\Xi\Sigma$ $(-2,2)$ interaction the same constant associated with the $\overline{\mathbf{35}}$ representation has to be present.

In order to obtain a representation of the potentials in the isospin basis, we use the iterated Clebsch-Gordon decomposition[2]

$$\begin{aligned}
&\langle (i_4 i_5) i_{\rm out} (i_{\rm out} i_6) I_{\rm out} M_{\rm out} | \hat{\mathcal{O}} | (i_1 i_2) i_{\rm in} (i_{\rm in} i_3) I_{\rm in} M_{\rm in} \rangle \\
&= \sum_{\substack{m_1,m_2,m_3,m_{\rm in},\\ m_4,m_5,m_6,m_{\rm out}}} \delta_{m_{\rm out},m_4+m_5} \delta_{M_{\rm out},m_{\rm out}+m_6} \delta_{m_{\rm in},m_1+m_2} \delta_{M_{\rm in},m_{\rm in}+m_3} \\
&\qquad \times C^{i_4 i_5 i_{\rm out}}_{m_4 m_5 m_{\rm out}} C^{i_{\rm out} i_6 I_{\rm out}}_{m_{\rm out} m_6 M_{\rm out}} C^{i_1 i_2 i_{\rm in}}_{m_1 m_2 m_{\rm in}} C^{i_{\rm in} i_3 I_{\rm in}}_{m_{\rm in} m_3 M_{\rm in}} \\
&\qquad \times \langle i_4 m_4; i_5 m_5; i_6 m_6 | \hat{\mathcal{O}} | i_1 m_1; i_2 m_2; i_3 m_3 \rangle \,, \qquad (6.17)
\end{aligned}$$

where i stands for an isospin quantum number and the C are the Clebsch-Gordan coefficients. In order to be sign consistent with the Condon-Shortley convention for the Clebsch-Gordan coefficients, we use the baryon matrix as defined in Eq. (2.30) and make the following sign changes in the identification of the particle states $|i,m\rangle$: $\Sigma^+ = -|1,+1\rangle$, $\Xi^- = -|1/2,-1/2\rangle$. In Eq. (6.17) we have chosen to couple the isospin of the first two particles in the initial state i_1, i_2 to $i_{\rm in}$ and then to couple $i_{\rm in}$ with the isospin i_3 of the third particle to total isospin $I_{\rm in}$. The same procedure is applied to the final state. Other coupling schemes can be obtained by recoupling with the help of Racah W-coefficients or equivalently with Wigners $6j$-symbols.

It is advantageous to present the three-body potentials not only in terms of the spin operators in Eq. (6.11), but to project them also onto partial waves. For a general operator

$$\hat{\mathcal{O}} = a_1 \mathbb{1} + a_2 \vec{\sigma}_1 \cdot \vec{\sigma}_2 + a_3 \vec{\sigma}_1 \cdot \vec{\sigma}_3 + a_4 \vec{\sigma}_2 \cdot \vec{\sigma}_3 + a_5 \, \mathrm{i} \, \vec{\sigma}_1 \times \vec{\sigma}_2 \cdot \vec{\sigma}_3 \,, \qquad (6.18)$$

with coefficients a_i, the partial wave decomposition leads to the following non-vanishing transitions (between S-waves)

$$\begin{aligned}
\langle 0\ {}^2S_{1/2} | \hat{\mathcal{O}} | 0\ {}^2S_{1/2} \rangle &= a_1 - 3a_2 \,, \\
\langle 1\ {}^2S_{1/2} | \hat{\mathcal{O}} | 0\ {}^2S_{1/2} \rangle &= \sqrt{3}(-a_3 + a_4 - 2a_5) \,, \\
\langle 0\ {}^2S_{1/2} | \hat{\mathcal{O}} | 1\ {}^2S_{1/2} \rangle &= \sqrt{3}(-a_3 + a_4 + 2a_5) \,, \\
\langle 1\ {}^2S_{1/2} | \hat{\mathcal{O}} | 1\ {}^2S_{1/2} \rangle &= a_1 + a_2 - 2a_3 - 2a_4 \,, \\
\langle 1\ {}^4S_{3/2} | \hat{\mathcal{O}} | 1\ {}^4S_{3/2} \rangle &= a_1 + a_2 + a_3 + a_4 \,, \qquad (6.19)
\end{aligned}$$

where a state $|s\ {}^{2S+1}L_J\rangle$ is characterized by the total spin $S = \frac{1}{2}, \frac{3}{2}$, the angular momentum $L = 0$ and the total angular momentum $J = \frac{1}{2}, \frac{3}{2}$. Here, we have chosen to couple the spins of the first two baryons to $s = 0, 1$, and to couple this with the spin $\frac{1}{2}$ of the third baryon to S (in complete analogy to the isospin coupling in Eq. (6.17)). After this partial wave decomposition it is trivial to identify the combinations of constants belonging to the totally antisymmetric flavor representations, since these act only in the $1\ {}^4S_{3/2}$ states due to the generalized Pauli principle.

2 In order to obtain Tab. 6.4 we strictly employ Eq. (6.17), i.e., no further combinatorial factors, such as $1/\sqrt{2}$ for a ΛNN state are included. They can be included by just multiplying the corresponding row in Tab. 6.4 with that factor.

Finally, we give the SU(3) relations for the strangeness 0 and −1 sectors in Tab. 6.4. The corresponding relations for strangeness −2 are listed in Appendix A.2. The constants associated with the irreducible SU(3) representations are related to the low-energy constants of the minimal Lagrangian by:

$$
\begin{aligned}
c_{\overline{35}} &= 6(-C_4 + C_9)\,, \\
c_{35} &= 3(C_4 - C_9 + 6C_{18})\,, \\
c_{\overline{10}} &= \frac{3}{4}(2C_2 + C_3 - C_4 + C_5 - 6C_8 + C_9 - 6C_{10} \\
&\qquad - 6C_{12} + 3C_{13} + 3C_{14} + 6C_{17} - 6C_{18})\,, \\
c_{27^1} &= -\frac{37}{294}C_2 + \frac{769}{588}C_3 - \frac{473}{392}C_4 + \frac{769}{588}C_5 - \frac{74}{49}C_7 - \frac{429}{98}C_8 + \frac{473}{392}C_9 \\
&\quad - \frac{429}{98}C_{10} + \frac{185}{98}C_{12} + \frac{89}{196}C_{13} + \frac{89}{196}C_{14} + \frac{244}{49}C_{16} - \frac{207}{98}C_{17} + \frac{57}{14}C_{18}\,, \\
c_{27^2} &= \frac{1}{24}(-4C_2 - 22C_3 + 57C_4 - 22C_5 - 48C_7 - 12C_8 - 57C_9 - 12C_{10} \\
&\qquad + 60C_{12} + 78C_{13} + 78C_{14} - 96C_{16} + 60C_{17} - 252C_{18})\,, \\
c_{27^3} &= \frac{1}{8}(20C_2 - 2C_3 - 21C_4 - 2C_5 - 16C_7 + 28C_8 + 21C_9 + 28C_{10} - 44C_{12} \\
&\qquad - 22C_{13} - 22C_{14} + 32C_{16} - 76C_{17} + 12C_{18})\,, \\
c_{\overline{10}a} &= 6(-C_2 + C_3 - C_4 + C_5 - 2C_7 + 2C_8 - C_9 + 2C_{10} - C_{12} + C_{13} + C_{14})\,, \\
c_{27a} &= \frac{2}{3}(C_2 + C_3 + 3C_4 + C_5 + 2C_7 + 2C_8 + 3C_9 + 2C_{10} + C_{12} + C_{13} + C_{14})\,.
\end{aligned}
\tag{6.20}
$$

The SU(3) relations have not been obtained by group theory considerations directly, but by rewriting our results such that they fulfill the group-theoretical constraints of Tab. 6.3. The three constants C_{27^1}, C_{27^2}, C_{27^3} are associated to the irreducible representations of dimension **27**. We have chosen a particular definition for them in Eq. (6.20). Note that other linear combinations of C_{27^1}, C_{27^2}, C_{27^3} would work equally well. The SU(3) relations in Tab. 6.4 have been derived from the most general SU(3) symmetric Lagrangian. Therefore, any three-baryon potential that fulfills flavor SU(3) symmetry has to fulfill these relations. These relations provide also a valuable check for the SU(3) decomposition of the S-wave contributions from three-baryon interactions generated by one- or two-meson exchange (with all meson masses set equal).

6.2 ONE-MESON EXCHANGE COMPONENT

For the one-meson exchange diagram in Fig. 6.1 we employ the leading-order chiral Lagrangian $\mathscr{L}_{\mathrm{B}}^{(1)}$ for meson-baryon couplings, rewritten in the particle basis, see Eq. (4.7). The second vertex, necessary for the one-meson-exchange three-body interaction, involves four baryon fields and one pseudoscalar-meson field. An overcomplete set of terms for the corresponding relativistic Lagrangian can be found in Subsec. 3.2.2. In order to obtain a complete minimal set of terms in the non-relativistic limit, we consider the matrix elements of the process $B_1B_2 \to B_3B_4\phi_1$ and proceed as in Sec. 6.1. The transition matrix element is expressed in terms of spin operators

$$
\vec{\sigma}_1 \cdot \vec{q}\,, \quad \vec{\sigma}_2 \cdot \vec{q}\,, \quad \mathrm{i}\,(\vec{\sigma}_1 \times \vec{\sigma}_2) \cdot \vec{q}\,, \tag{6.21}
$$

transition	I	i_{in}	i_{out}	$V_{0^2S_{1/2}\to 0^2S_{1/2}}$	$V_{0^2S_{1/2}\to 1^2S_{1/2}}$	$V_{1^2S_{1/2}\to 0^2S_{1/2}}$	$V_{1^2S_{1/2}\to 1^2S_{1/2}}$	$V_{1^4S_{3/2}\to 1^4S_{3/2}}$
$NNN \to NNN$	$\frac{1}{2}$	0	0	0	0	0	$3c_{\overline{35}}$	0
$NNN \to NNN$	$\frac{1}{2}$	1	0	0	$-3c_{\overline{35}}$	0	0	0
$NNN \to NNN$	$\frac{1}{2}$	0	1	0	0	$-3c_{\overline{35}}$	0	0
$NNN \to NNN$	$\frac{1}{2}$	1	1	$3c_{\overline{35}}$	0	0	0	0
$\Lambda NN \to \Lambda NN$	0	$\frac{1}{2}$	$\frac{1}{2}$	$c_{\overline{10}} + c_{\overline{35}}$	$\frac{c_{\overline{10}}}{\sqrt{3}} + \frac{c_{\overline{35}}}{\sqrt{3}}$	$\frac{c_{\overline{10}}}{\sqrt{3}} + \frac{c_{\overline{35}}}{\sqrt{3}}$	$\frac{c_{\overline{10}}}{3} + \frac{c_{\overline{35}}}{3}$	$c_{\overline{10}a}$
$\Lambda NN \to \Lambda NN$	1	$\frac{1}{2}$	$\frac{1}{2}$	$c_{27^1} + \frac{12c_{27^2}}{49} + \frac{3c_{\overline{35}}}{16}$	$-\sqrt{3}c_{27^1} - \frac{12\sqrt{3}c_{27^2}}{49} - \frac{3\sqrt{3}c_{\overline{35}}}{16}$	$-\sqrt{3}c_{27^1} - \frac{12\sqrt{3}c_{27^2}}{49} - \frac{3\sqrt{3}c_{\overline{35}}}{16}$	$3c_{27^1} + \frac{36c_{27^2}}{49} + \frac{9c_{\overline{35}}}{16}$	0
$\Sigma NN \to \Sigma NN$	0	$\frac{1}{2}$	$\frac{1}{2}$	$c_{\overline{10}}$	$-\sqrt{3}c_{\overline{10}}$	$-\sqrt{3}c_{\overline{10}}$	$3c_{\overline{10}}$	0
$\Sigma NN \to \Sigma NN$	1	$\frac{1}{2}$	$\frac{1}{2}$	$c_{27^2} + \frac{c_{\overline{35}}}{48}$	$\frac{c_{27^3}}{\sqrt{3}} + \frac{\sqrt{3}c_{\overline{35}}}{16}$	$\frac{c_{27^3}}{\sqrt{3}} + \frac{\sqrt{3}c_{\overline{35}}}{16}$	$\frac{4c_{27^1}}{3} - \frac{c_{27^2}}{147} - \frac{2c_{27^3}}{3} + \frac{9c_{\overline{35}}}{16}$	c_{27a}
$\Sigma NN \to \Sigma NN$	1	$\frac{3}{2}$	$\frac{1}{2}$	$-\frac{5c_{27^2}}{4\sqrt{2}} - \frac{3c_{27^3}}{4\sqrt{2}} - \frac{c_{\overline{35}}}{6\sqrt{2}}$	$-\sqrt{\frac{3}{2}}c_{27^1} + \frac{1}{196}\sqrt{\frac{3}{2}}c_{27^2} + \frac{c_{27^3}}{4\sqrt{6}} - \frac{1}{2}\sqrt{\frac{3}{2}}c_{\overline{35}}$	$\frac{c_{27^3}}{4\sqrt{6}} - \frac{3}{4}\sqrt{\frac{3}{2}}c_{27^2}$	$\frac{c_{27^1}}{3\sqrt{2}} - \frac{c_{27^2}}{588\sqrt{2}} - \frac{11c_{27^3}}{12\sqrt{2}}$	$-\sqrt{2}c_{27a}$
$\Sigma NN \to \Sigma NN$	1	$\frac{1}{2}$	$\frac{3}{2}$	$-\frac{5c_{27^2}}{4\sqrt{2}} - \frac{3c_{27^3}}{4\sqrt{2}} - \frac{c_{\overline{35}}}{6\sqrt{2}}$	$\frac{c_{27^3}}{4\sqrt{6}} - \frac{3}{4}\sqrt{\frac{3}{2}}c_{27^2}$	$-\sqrt{\frac{3}{2}}c_{27^1} + \frac{1}{196}\sqrt{\frac{3}{2}}c_{27^2} + \frac{c_{27^3}}{4\sqrt{6}} - \frac{1}{2}\sqrt{\frac{3}{2}}c_{\overline{35}}$	$\frac{c_{27^1}}{3\sqrt{2}} - \frac{c_{27^2}}{588\sqrt{2}} - \frac{11c_{27^3}}{12\sqrt{2}}$	$-\sqrt{2}c_{27a}$
$\Sigma NN \to \Sigma NN$	1	$\frac{3}{2}$	$\frac{3}{2}$	$\frac{9c_{27^1}}{8} + \frac{38c_{27^2}}{49} + \frac{3c_{27^3}}{8} + \frac{2c_{\overline{35}}}{3}$	$-\frac{\sqrt{3}c_{27^1}}{8} + \frac{23\sqrt{3}c_{27^2}}{49} + \frac{7c_{27^3}}{8\sqrt{3}}$	$-\frac{\sqrt{3}c_{27^1}}{8} + \frac{23\sqrt{3}c_{27^2}}{49} + \frac{7c_{27^3}}{8\sqrt{3}}$	$\frac{c_{27^1}}{24} + \frac{124c_{27^2}}{147} - \frac{5c_{27^3}}{24}$	$2c_{27a}$
$\Sigma NN \to \Sigma NN$	2	$\frac{3}{2}$	$\frac{3}{2}$	$\frac{c_{35}}{2}$	$-\frac{\sqrt{3}c_{35}}{2}$	$-\frac{\sqrt{3}c_{35}}{2}$	$\frac{3c_{35}}{2}$	0
$\Lambda NN \to \Sigma NN$	0	$\frac{1}{2}$	$\frac{1}{2}$	$c_{\overline{10}} - \frac{c_{\overline{35}}}{2}$	$\frac{\sqrt{3}c_{\overline{35}}}{2} - \sqrt{3}c_{\overline{10}}$	$\frac{c_{\overline{10}}}{\sqrt{3}} - \frac{c_{\overline{35}}}{2\sqrt{3}}$	$\frac{c_{\overline{35}}}{2} - c_{\overline{10}}$	0
$\Lambda NN \to \Sigma NN$	1	$\frac{1}{2}$	$\frac{1}{2}$	$\frac{c_{27^2}}{2} + \frac{c_{27^3}}{2} - \frac{c_{\overline{35}}}{16}$	$\frac{2c_{27^1}}{\sqrt{3}} - \frac{c_{27^2}}{98\sqrt{3}} - \frac{c_{27^3}}{2\sqrt{3}} - \frac{3\sqrt{3}c_{\overline{35}}}{16}$	$-\frac{\sqrt{3}c_{27^2}}{2} - \frac{\sqrt{3}c_{27^3}}{2} + \frac{\sqrt{3}c_{\overline{35}}}{16}$	$-2c_{27^1} + \frac{c_{27^2}}{98} + \frac{c_{27^3}}{2} + \frac{9c_{\overline{35}}}{16}$	0
$\Lambda NN \to \Sigma NN$	1	$\frac{1}{2}$	$\frac{3}{2}$	$-\frac{3c_{27^1}}{2\sqrt{2}} - \frac{121c_{27^2}}{196\sqrt{2}} - \frac{c_{27^3}}{4\sqrt{2}} + \frac{c_{\overline{35}}}{2\sqrt{2}}$	$\frac{c_{27^1}}{2\sqrt{6}} - \frac{221c_{27^2}}{196\sqrt{6}} - \frac{5c_{27^3}}{4\sqrt{6}}$	$\frac{3}{2}\sqrt{\frac{3}{2}}c_{27^1} + \frac{121}{196}\sqrt{\frac{3}{2}}c_{27^2} + \frac{1}{4}\sqrt{\frac{3}{2}}c_{27^3} - \frac{1}{2}\sqrt{\frac{3}{2}}c_{\overline{35}}$	$-\frac{c_{27^1}}{2\sqrt{2}} + \frac{221c_{27^2}}{196\sqrt{2}} + \frac{5c_{27^3}}{4\sqrt{2}}$	0

TABLE 6.4: SU(3) relations of three-baryon contact terms with strangeness 0 and -1 in non-vanishing partial waves.

where $\vec{q}$ denotes the momentum of the emitted meson. The minimal Lagrangian is obtained by eliminating redundant terms until the rank of the (non-square) matrix formed by all transitions matches the number of terms in the Lagrangian. As before, redundant terms are deleted in such a way, that one obtains a maximal number of terms with a single flavor trace. The minimal non-relativistic chiral Lagrangian for the four-baryon vertex including one meson is given by

$$\begin{aligned}
\mathscr{L} = {} & D_1/f_0\langle\bar{B}_a(\nabla^i\phi)B_a\bar{B}_b(\sigma^iB)_b\rangle \\
& + D_2/f_0\Big(\langle\bar{B}_aB_a(\nabla^i\phi)\bar{B}_b(\sigma^iB)_b\rangle + \langle\bar{B}_aB_a\bar{B}_b(\sigma^iB)_b(\nabla^i\phi)\rangle\Big) \\
& + D_3/f_0\langle\bar{B}_b(\nabla^i\phi)(\sigma^iB)_b\bar{B}_aB_a\rangle \\
& - D_4/f_0\Big(\langle\bar{B}_a(\nabla^i\phi)\bar{B}_bB_a(\sigma^iB)_b\rangle + \langle\bar{B}_b\bar{B}_a(\sigma^iB)_b(\nabla^i\phi)B_a\rangle\Big) \\
& - D_5/f_0\Big(\langle\bar{B}_a\bar{B}_b(\nabla^i\phi)B_a(\sigma^iB)_b\rangle + \langle\bar{B}_b\bar{B}_a(\nabla^i\phi)(\sigma^iB)_bB_a\rangle\Big) \\
& - D_6/f_0\Big(\langle\bar{B}_b(\nabla^i\phi)\bar{B}_a(\sigma^iB)_bB_a\rangle + \langle\bar{B}_a\bar{B}_bB_a(\nabla^i\phi)(\sigma^iB)_b\rangle\Big) \\
& - D_7/f_0\Big(\langle\bar{B}_a\bar{B}_bB_a(\sigma^iB)_b(\nabla^i\phi)\rangle + \langle\bar{B}_b\bar{B}_a(\sigma^iB)_bB_a(\nabla^i\phi)\rangle\Big) \\
& + D_8/f_0\langle\bar{B}_a(\nabla^i\phi)B_a\rangle\langle\bar{B}_b(\sigma^iB)_b\rangle \\
& + D_9/f_0\langle\bar{B}_aB_a(\nabla^i\phi)\rangle\langle\bar{B}_b(\sigma^iB)_b\rangle \\
& + D_{10}/f_0\langle\bar{B}_b(\nabla^i\phi)(\sigma^iB)_b\rangle\langle\bar{B}_aB_a\rangle \\
& + \mathrm{i}\,\epsilon^{ijk}D_{11}/f_0\langle\bar{B}_a(\sigma^iB)_a(\nabla^k\phi)\bar{B}_b(\sigma^jB)_b\rangle \\
& - \mathrm{i}\,\epsilon^{ijk}D_{12}/f_0\Big(\langle\bar{B}_a(\nabla^k\phi)\bar{B}_b(\sigma^iB)_a(\sigma^jB)_b\rangle - \langle\bar{B}_b\bar{B}_a(\sigma^jB)_b(\nabla^k\phi)(\sigma^iB)_a\rangle\Big) \\
& - \mathrm{i}\,\epsilon^{ijk}D_{13}/f_0\langle\bar{B}_a\bar{B}_b(\nabla^k\phi)(\sigma^iB)_a(\sigma^jB)_b\rangle \\
& - \mathrm{i}\,\epsilon^{ijk}D_{14}/f_0\langle\bar{B}_a\bar{B}_b(\sigma^iB)_a(\sigma^jB)_b(\nabla^k\phi)\rangle\,. \qquad (6.22)
\end{aligned}$$

Here, the indices a and b are two-component spinor indices, and i, j and k are 3-vector indices. There are in total 14 low-energy constants $D_1 \ldots D_{14}$ for all five strangeness sectors $S = -4 \ldots 0$. As before, the minus signs in front of some terms have been included, in order to compensate minus signs from fermion exchange, arising from the reordering of a baryon bilinear (see Eq. (6.23) below). Let us note, that the conservation of strangeness S, isospin I and isospin projection I_3, independence of I_3, and time reversal symmetry have been checked for the $BB \to BB\phi$ transition matrix elements resulting from Eq. (6.22). Moreover, several tests employing group theoretical methods have been performed.

As done in Subsec. 6.1.1, we write the Lagrangian in the particle basis

$$\begin{aligned}
\mathscr{L} = {} & \sum_{f=1}^{10}\frac{D_f}{f_0}\sum_{i,j,k,l,m=1}^{8} N^{f\ \phi_m}_{\substack{ik\\jl}}(\bar{B}_iB_j)(\bar{B}_k\vec{\sigma}B_l)\cdot\vec{\nabla}\phi_m \\
& + \sum_{f=11}^{14}\frac{D_f}{f_0}\sum_{i,j,k,l,m=1}^{8} N^{f\ \phi_m}_{\substack{ik\\jl}}\,\mathrm{i}\,[(\bar{B}_i\vec{\sigma}B_j)\times(\bar{B}_k\vec{\sigma}B_l)]\cdot\vec{\nabla}\phi_m\,, \qquad (6.23)
\end{aligned}$$

where in each term the first bilinear comes from the summation over the spin index a and the second bilinear from the summation over the spin index b in Eq. (6.22). The indices i, j, k, l label now octet baryons.

Let us now consider the generic one-meson exchange diagram in Fig. 6.2. It involves the baryons i, j, k in the initial state, the baryons l, m, n in the final state and an exchanged

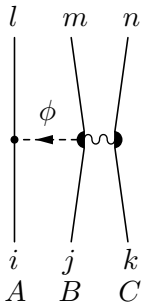

FIGURE 6.2: Generic one-meson exchange diagram. The wiggly line symbolized the four-baryon contact vertex, to illustrate the baryon bilinears.

meson ϕ. The four-baryon contact vertex is separated into two parts, in order to indicate which baryons are in the same bilinear. The indices A, B, C label the spin spaces related to the baryon bilinears.

Using standard Feynman rules for the vertices and the meson propagator one obtains the following three-body potential

$$V = \frac{1}{2f_0^2}\frac{\vec{\sigma}_A \cdot \vec{q}_{li}}{\vec{q}_{li}^{\,2} + m_\phi^2}\Big(N_1 \vec{\sigma}_C \cdot \vec{q}_{li} + N_2 \mathrm{i}\,(\vec{\sigma}_B \times \vec{\sigma}_C) \cdot \vec{q}_{li}\Big)\,, \tag{6.24}$$

with the momentum transfer $\vec{q}_{li} = \vec{p}_l - \vec{p}_i$ carried by the exchanged meson and the constants

$$\begin{aligned} N_1 &= N_{B_l B_i \phi} \sum_{f=1}^{10} D_f N^f_{\substack{mn \\ jk\ \bar{\phi}}}\,, \\ N_2 &= N_{B_l B_i \phi} \sum_{f=11}^{14} D_f N^f_{\substack{mn \\ jk\ \bar{\phi}}}\,, \end{aligned} \tag{6.25}$$

where $\bar{\phi}$ denotes the charge-conjugated meson of meson ϕ in particle basis (e.g., $\pi^+ \leftrightarrow \pi^-$).

The full one-meson exchange three-body potential for the process $B_1 B_2 B_3 \to B_4 B_5 B_6$ is obtained easily by summing up for a fixed meson the 36 permutations of initial and final baryons, shown diagrammatically in Fig. 6.3, and summing over all mesons $\phi \in \Big\{\pi^0, \pi^+, \pi^-, K^+, K^-, K^0, \bar{K}^0, \eta\Big\}$. Of course, many of these contributions will vanish for a particular process. The Feynman diagrams fall into 9 classes, where in each class the same momentum transfer $\vec{q}_{li}$ is present. In Fig. 6.3 each row corresponds to such a class and the corresponding momentum transfer is written on the left of the row. Furthermore, additional minus signs from interchanging fermions have to be included and some diagrams need to be multiplied from the left by spin exchange operators (as indicated in Fig. 6.3) in order to be in accordance with the form set up in Eq. (6.4). As before, the baryons B_1, B_2 and B_3 belong to the spin-spaces 1, 2 and 3, respectively.

6.3 TWO-MESON EXCHANGE COMPONENT

For the two-meson exchange diagram of Fig. 6.1 we need in addition to the Lagrangian in Eq. (4.7) the well-known $\mathcal{O}(q^2)$ meson-baryon Lagrangian [104]. We use the version given in Ref. [101] and display here only the terms relevant for our purpose:

$$\begin{aligned} \mathscr{L} = {} & b_D \langle \bar{B}\{\chi_+, B\}\rangle + b_F \langle \bar{B}[\chi_+, B]\rangle + b_0 \langle \bar{B}B\rangle \langle \chi_+\rangle \\ & + b_1 \langle \bar{B}[u^\mu, [u_\mu, B]]\rangle + b_2 \langle \bar{B}\{u^\mu, \{u_\mu, B\}\}\rangle \\ & + b_3 \langle \bar{B}\{u^\mu, [u_\mu, B]\}\rangle + b_4 \langle \bar{B}B\rangle \langle u^\mu u_\mu\rangle \\ & + \mathrm{i}d_1 \langle \bar{B}\{[u^\mu, u^\nu], \sigma_{\mu\nu} B\}\rangle + \mathrm{i}d_2 \langle \bar{B}[[u^\mu, u^\nu], \sigma_{\mu\nu} B]\rangle \\ & + \mathrm{i}d_3 \langle \bar{B}u^\mu\rangle \langle u^\nu \sigma_{\mu\nu} B\rangle\,, \end{aligned} \tag{6.26}$$

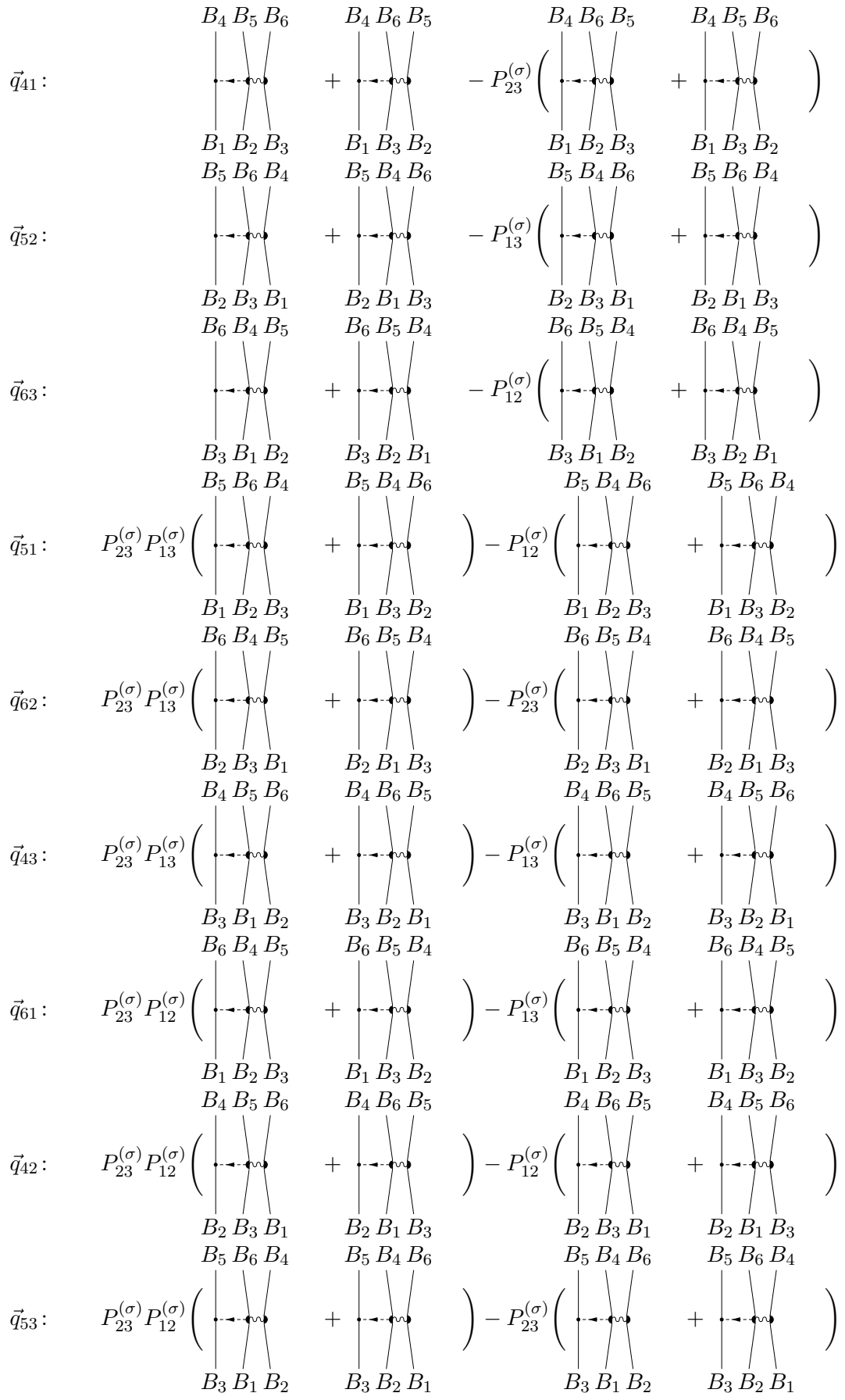

FIGURE 6.3: Feynman diagrams contributing to the one-meson exchange three-body potential for $B_1B_2B_3 \to B_4B_5B_6$.

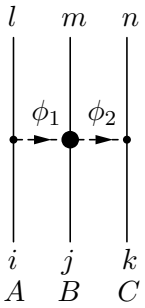

FIGURE 6.4: Generic two-meson exchange diagram.

with $u_\mu = -\frac{1}{f_0}\partial_\mu\phi + \mathcal{O}(\phi^3)$ and $\chi_+ = 2\chi - \frac{1}{4f_0^2}\{\phi,\{\phi,\chi\}\} + \mathcal{O}(\phi^4)$, where (see Eq. (4.1))

$$\chi = \begin{pmatrix} m_\pi^2 & 0 & 0 \\ 0 & m_\pi^2 & 0 \\ 0 & 0 & 2m_K^2 - m_\pi^2 \end{pmatrix} . \tag{6.27}$$

Note that the terms proportional to b_D, b_F, b_0 break explicitly SU(3) flavor symmetry, through different meson masses $m_K \neq m_\pi$. Rewriting the Lagrangian in the particle basis as in the previous sections, one obtains

$$\begin{aligned} \mathscr{L} = & - \sum_{c^f = b_D, b_F, b_0} \frac{c^f}{4f_0^2} \sum_{i,j,k,l=1}^{8} N^f_{\phi_k \, i \, j \phi_l} (\bar{B}_i B_j) \phi_k \phi_l \\ & + \sum_{c^f = b_1, b_2, b_3, b_4} \frac{c^f}{f_0^2} \sum_{i,j,k,l=1}^{8} N^f_{\phi_k \, i \, j \phi_l} (\bar{B}_i B_j) \partial_\mu \phi_k \partial^\mu \phi_l \\ & + \sum_{c^f = d_1, d_2, d_3} \frac{\mathrm{i}\, c^f}{f_0^2} \sum_{i,j,k,l=1}^{8} N^f_{\phi_k \, i \, j \phi_l} (\bar{B}_i \sigma_{\mu\nu} B_j) \partial^\mu \phi_k \partial^\nu \phi_l \, . \end{aligned} \tag{6.28}$$

Let us now consider the generic two-meson exchange diagram depicted in Fig. 6.4. It includes the baryons i, j, k in the initial state, the baryons l, m, n in the final state, and two virtual mesons ϕ_1 and ϕ_2 are exchanged. The indices A, B, C label the spin spaces related to the baryon bilinears and they are aligned with the three initial baryons. The momentum transfers carried by the virtual mesons are $\vec{q}_{li} = \vec{p}_l - \vec{p}_i$ and $\vec{q}_{nk} = \vec{p}_n - \vec{p}_k$. One obtains the following transition amplitude from the generic two-meson exchange diagram

$$V = -\frac{1}{4f_0^4} \frac{\vec{\sigma}_A \cdot \vec{q}_{li} \;\; \vec{\sigma}_C \cdot \vec{q}_{nk}}{(\vec{q}_{li}^{\,2} + m_{\phi_1}^2)(\vec{q}_{nk}^{\,2} + m_{\phi_2}^2)} \Big(N_1' + N_2' \, \vec{q}_{li} \cdot \vec{q}_{nk} + N_3' \, \mathrm{i} \, (\vec{q}_{li} \times \vec{q}_{nk}) \cdot \vec{\sigma}_B \Big) , \tag{6.29}$$

with the combinations of parameters

$$\begin{aligned} N_1' &= N_{B_l B_i \bar{\phi}_1} N_{B_n B_k \phi_2} \sum_{c^f = b_D, b_F, b_0} \frac{c^f}{4} (N^f_{\phi_1 \, m \, j \, \bar{\phi}_2} + N^f_{\bar{\phi}_2 \, m \, j \, \phi_1}) \, , \\ N_2' &= -N_{B_l B_i \bar{\phi}_1} N_{B_n B_k \phi_2} \sum_{c^f = b_1, b_2, b_3, b_4} c^f (N^f_{\phi_1 \, m \, j \, \bar{\phi}_2} + N^f_{\bar{\phi}_2 \, m \, j \, \phi_1}) \, , \\ N_3' &= N_{B_l B_i \bar{\phi}_1} N_{B_n B_k \phi_2} \sum_{c^f = d_1, d_2, d_3} c^f (N^f_{\phi_1 \, m \, j \, \bar{\phi}_2} - N^f_{\bar{\phi}_2 \, m \, j \, \phi_1}) \, . \end{aligned} \tag{6.30}$$

The complete three-body potential for a transition $B_1 B_2 B_3 \to B_4 B_5 B_6$ is finally obtained by summing up the contributions of the 18 Feynman diagrams in Fig. 6.5 and

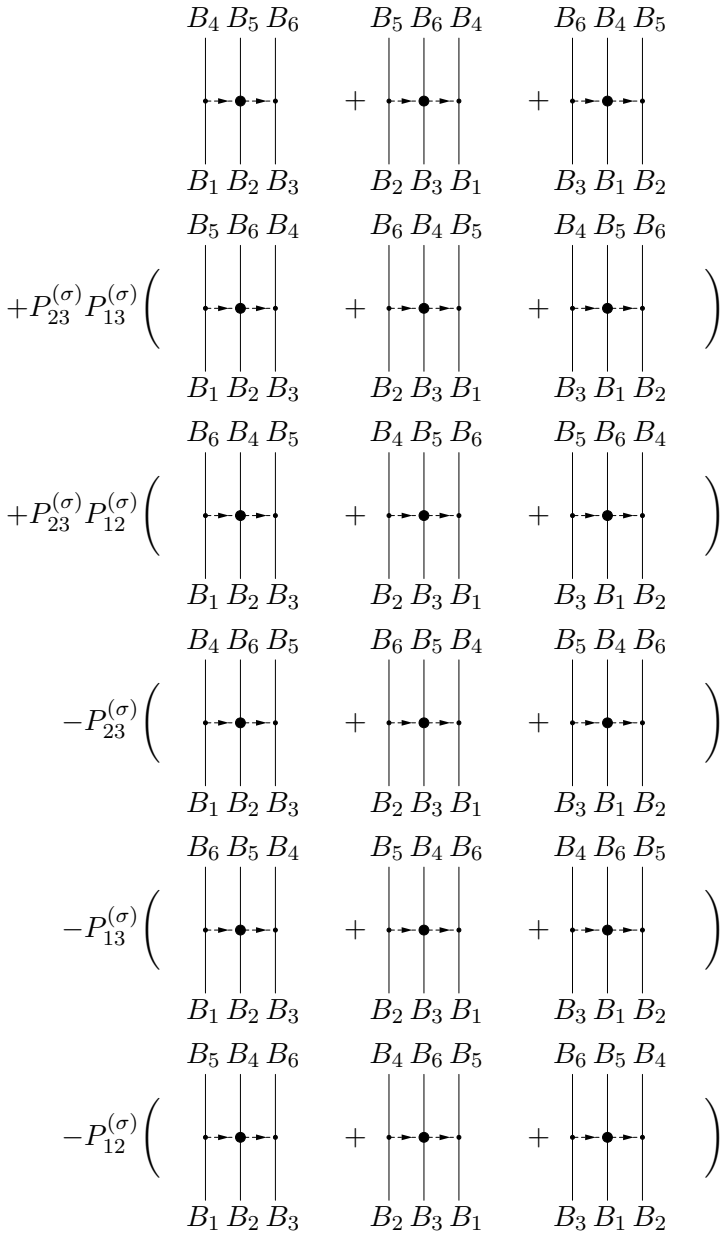

FIGURE 6.5: Feynman diagrams contributing to the two-meson exchange three-body potential for $B_1B_2B_3 \to B_4B_5B_6$.

by summing over all possible exchanged mesons. Obviously, additional (negative) spin-exchange operators need to be applied if the baryon lines are not in the configuration 1-4, 2-5 and 3-6, as illustrated in Fig. 6.5.

6.4 NNN AND ΛNN THREE-BARYON POTENTIALS

In order to give a concrete example we present in this section the explicit expression for the ΛNN three-body interaction in spin-, isospin- and momentum-space. Moreover, the leading-order chiral three-nucleon interaction is rederived, and consistency with the

conventional expression is shown. The potentials are calculated in particle basis (as shown in the previous sections) and afterwards reexpressed with isospin operators.

By adding up all 36 contributions (coming from Eqs. (6.6) and (6.10)), one obtains the following form of the three-nucleon contact potential

$$\begin{aligned} V_{\rm ct}^{NNN} = -\frac{3}{8}E\,\big[\;&(3\,\mathbb{1}-\vec\sigma_1\cdot\vec\sigma_2-\vec\sigma_1\cdot\vec\sigma_3-\vec\sigma_2\cdot\vec\sigma_3)\;\mathbb{1}\\ &+(-\mathbb{1}-\vec\sigma_1\cdot\vec\sigma_2+\vec\sigma_1\cdot\vec\sigma_3+\vec\sigma_2\cdot\vec\sigma_3)\;\vec\tau_1\cdot\vec\tau_2\\ &+(-\mathbb{1}+\vec\sigma_1\cdot\vec\sigma_2-\vec\sigma_1\cdot\vec\sigma_3+\vec\sigma_2\cdot\vec\sigma_3)\;\vec\tau_1\cdot\vec\tau_3\\ &+(-\mathbb{1}+\vec\sigma_1\cdot\vec\sigma_2+\vec\sigma_1\cdot\vec\sigma_3-\vec\sigma_2\cdot\vec\sigma_3)\;\vec\tau_2\cdot\vec\tau_3\\ &-\vec\sigma_1\times\vec\sigma_2\cdot\vec\sigma_3\;\vec\tau_1\times\vec\tau_2\cdot\vec\tau_3\,\big]\,, \end{aligned} \tag{6.31}$$

with the low-energy constant $E = 2(C_4 - C_9) = -c_{\overline{35}}/3$ and $\vec\sigma$, $\vec\tau$ denote the usual Pauli matrices in spin and isospin space. This is exactly the three-nucleon contact potential of Ref. [51] in its antisymmetrized form:

$$V_{\rm ct}^{NNN} = \frac{1}{2}E\,\mathcal{A}\sum_{j\neq k}\vec\tau_j\cdot\vec\tau_k\,, \tag{6.32}$$

where $\mathcal{A}$ denotes the three-body antisymmetrization operator, $\mathcal{A} = (\mathbb{1}-\mathcal{P}_{12})(\mathbb{1}-\mathcal{P}_{13}-\mathcal{P}_{23})$. Here, each two-particle exchange operator $\mathcal{P}_{ij} = P_{ij}^{(\sigma)}P_{ij}^{(\tau)}P_{ij}^{(p)}$ is the product of an exchange operator in spin space $P_{ij}^{(\sigma)} = \frac{1}{2}(\mathbb{1}+\vec\sigma_i\cdot\vec\sigma_j)$, in isospin space $P_{ij}^{(\tau)} = \frac{1}{2}(\mathbb{1}+\vec\tau_i\cdot\vec\tau_j)$ and in momentum space $P_{ij}^{(p)}$. Note that the leading-order $3N$ contact potential is momentum-independent, and therefore $P_{ij}^{(p)}$ has no effect. We remind that in our calculation the generalized Pauli principle is automatically built in by performing all Wick contractions.

For the ΛNN contact interaction we obtain the following expression:

$$\begin{aligned} V_{\rm ct}^{\Lambda NN} = \;&C_1'\;(\mathbb{1}-\vec\sigma_2\cdot\vec\sigma_3)(3+\vec\tau_2\cdot\vec\tau_3)\\ &+C_2'\;\vec\sigma_1\cdot(\vec\sigma_2+\vec\sigma_3)\,(\mathbb{1}-\vec\tau_2\cdot\vec\tau_3)\\ &+C_3'\;(3+\vec\sigma_2\cdot\vec\sigma_3)(\mathbb{1}-\vec\tau_2\cdot\vec\tau_3)\,, \end{aligned} \tag{6.33}$$

where the primed constants are given by

$$\begin{aligned} C_1' = -\frac{1}{48}(&2C_2-13C_3+21C_4-13C_5+24C_7+54C_8-21C_9+54C_{10}\\ &-30C_{12}-15C_{13}-15C_{14}-48C_{16}+18C_{17}-18C_{18})\,,\\ C_2' = -\frac{1}{24}(&8C_2-5C_3-3C_4-5C_5+12C_7-18C_8\\ &+15C_9-18C_{10}-3C_{13}-3C_{14}+6C_{17}-6C_{18})\,,\\ C_3' = -\frac{1}{48}(&10C_2-13C_3+21C_4-13C_5+24C_7-18C_8+3C_9-18C_{10}\\ &+18C_{12}-15C_{13}-15C_{14}-6C_{17}+6C_{18})\,. \end{aligned} \tag{6.34}$$

The constants $C_1 \ldots C_{18}$ originate from the minimal contact Lagrangian in Eq. (6.12). Note that the constant C_1' belongs exclusively to the transition with total isospin $I = 1$, whereas the constants C_2' and C_3' appear for total isospin $I = 0$. Interestingly, none of these three constants can be substituted by the constant E of the purely nucleonic sector. Thus, the strength of the ΛNN three-body contact interaction is not related to the one for NNN via SU(3) symmetry.

The one-pion exchange three-nucleon potential reads (in antisymmetrized form)

$$\begin{aligned} V_{\rm OPE}^{NNN} = & \quad (X_{123}^{456} + X_{231}^{564} + X_{312}^{645}) \\ & + P_{23}^{(\sigma)} P_{23}^{(\tau)} P_{13}^{(\sigma)} P_{13}^{(\tau)} (X_{123}^{564} + X_{231}^{645} + X_{312}^{456}) \\ & + P_{23}^{(\sigma)} P_{23}^{(\tau)} P_{12}^{(\sigma)} P_{12}^{(\tau)} (X_{123}^{645} + X_{231}^{456} + X_{312}^{564}) \,, \end{aligned} \tag{6.35}$$

where we have defined the abbreviation[3]

$$\begin{aligned} X_{ijk}^{lmn} = -\frac{g_A}{16 f_0^2} d' \frac{\vec{\sigma}_i \cdot \vec{q}_{li}}{\vec{q}_{li}^{\,2} + m_\pi^2} \Big[& (\vec{\tau}_j - \vec{\tau}_k) \cdot \vec{\tau}_i \; (\vec{\sigma}_j - \vec{\sigma}_k) \cdot \vec{q}_{li} \\ & + (\vec{\tau}_j \times \vec{\tau}_k) \cdot \vec{\tau}_i \; (\vec{\sigma}_j \times \vec{\sigma}_k) \cdot \vec{q}_{li} \Big] \,, \end{aligned} \tag{6.36}$$

with $g_A = D + F$ and $d' = 4(D_1 - D_3 + D_8 - D_{10})$. Each term in Eq. (6.35) corresponds to a complete row in Fig. 6.3. We have verified that this result is equal to the antisymmetrization of the expression given in Ref. [51],

$$V_{\rm OPE}^{NNN} = -\frac{g_A}{8 f_\pi^2} d' \mathcal{A} \sum_{i \neq j \neq k} \frac{\vec{\sigma}_j \cdot \vec{q}_j}{\vec{q}_j^{\,2} + m_\pi^2} \vec{\tau}_i \cdot \vec{\tau}_j \; \vec{\sigma}_i \cdot \vec{q}_j \,, \tag{6.37}$$

inserting the momentum transfers $\vec{q}_1 = \vec{q}_{41} = \vec{p}_4 - \vec{p}_1$, $\vec{q}_2 = \vec{q}_{52} = \vec{p}_5 - \vec{p}_2$, $\vec{q}_3 = \vec{q}_{63} = \vec{p}_6 - \vec{p}_3$. In this case the momentum part of each two-body exchange operator, $P_{ij}^{(p)}$, exchanges also the momenta in the final state.[4]

Let us continue with the ΛNN one-pion exchange three-body potentials. Many diagrams are absent due to the vanishing of the $\Lambda\Lambda\pi$-vertex (by isospin symmetry). We find the following result for the ΛNN three-body interaction mediated by one-pion exchange:

$$\begin{aligned} V_{\rm OPE}^{\Lambda NN} = -\frac{g_A}{2 f_0^2} \Bigg(& \\ & \frac{\vec{\sigma}_2 \cdot \vec{q}_{52}}{\vec{q}_{52}^{\,2} + m_\pi^2} \vec{\tau}_2 \cdot \vec{\tau}_3 \Big[(D_1' \vec{\sigma}_1 + D_2' \vec{\sigma}_3) \cdot \vec{q}_{52} \Big] \\ & + \frac{\vec{\sigma}_3 \cdot \vec{q}_{63}}{\vec{q}_{63}^{\,2} + m_\pi^2} \vec{\tau}_2 \cdot \vec{\tau}_3 \Big[(D_1' \vec{\sigma}_1 + D_2' \vec{\sigma}_2) \cdot \vec{q}_{63} \Big] \\ + P_{23}^{(\sigma)} P_{23}^{(\tau)} P_{13}^{(\sigma)} & \frac{\vec{\sigma}_2 \cdot \vec{q}_{62}}{\vec{q}_{62}^{\,2} + m_\pi^2} \vec{\tau}_2 \cdot \vec{\tau}_3 \Big[- \frac{D_1' + D_2'}{2} (\vec{\sigma}_1 + \vec{\sigma}_3) \cdot \vec{q}_{62} + \frac{D_1' - D_2'}{2} \, \mathrm{i} \, (\vec{\sigma}_3 \times \vec{\sigma}_1) \cdot \vec{q}_{62} \Big] \\ + P_{23}^{(\sigma)} P_{23}^{(\tau)} P_{12}^{(\sigma)} & \frac{\vec{\sigma}_3 \cdot \vec{q}_{53}}{\vec{q}_{53}^{\,2} + m_\pi^2} \vec{\tau}_2 \cdot \vec{\tau}_3 \Big[- \frac{D_1' + D_2'}{2} (\vec{\sigma}_1 + \vec{\sigma}_2) \cdot \vec{q}_{53} - \frac{D_1' - D_2'}{2} \, \mathrm{i} \, (\vec{\sigma}_1 \times \vec{\sigma}_2) \cdot \vec{q}_{53} \Big] \Bigg) \,, \end{aligned} \tag{6.38}$$

where we have defined the two linear combinations of constants

$$\begin{aligned} D_1' &= \frac{1}{6} (-3D_1 + D_2 + D_3 + 5D_4 + 9D_5 + D_6 - 6D_8 + D_{11} + 2D_{12} - 3D_{13}) \,, \\ D_2' &= \frac{1}{6} (D_1 + D_2 - 3D_3 + D_4 + 9D_5 + 5D_6 - 6D_{10} - D_{11} - 2D_{12} + 3D_{13}) \,. \end{aligned} \tag{6.39}$$

3 We have used the symbol d' instead of the conventional D in order to avoid confusion with the axial vector constant in Eq. (4.7).

4 For example, $P_{23}^{(p)}$ leads to the replacements $q_{41}, q_{52}, q_{63} \to q_{41}, q_{62}, q_{53}$ and $P_{12}^{(p)} P_{13}^{(p)}$ to $q_{41}, q_{52}, q_{63} \to q_{61}, q_{42}, q_{53}$.

The four lines in Eq. (6.38) correspond to the four rows in Fig. 6.3 that have no Λ hyperon at the baryon-baryon-meson vertex, i.e., the diagrams involving the momentum transfers $\vec{q}_{52}$, $\vec{q}_{63}$, $\vec{q}_{62}$, $\vec{q}_{53}$.

Finally, we obtain for the three-nucleon interaction mediated by two-pion exchange

$$\begin{aligned} V_{\rm TPE}^{NNN} = & \left(Y_{123}^{456}+Y_{231}^{564}+Y_{312}^{645}\right) \\ & +P_{23}^{(\sigma)}P_{23}^{(\tau)}P_{13}^{(\sigma)}P_{13}^{(\tau)}\left(Y_{123}^{564}+Y_{231}^{645}+Y_{312}^{456}\right) \\ & +P_{23}^{(\sigma)}P_{23}^{(\tau)}P_{12}^{(\sigma)}P_{12}^{(\tau)}\left(Y_{123}^{645}+Y_{231}^{456}+Y_{312}^{564}\right) \\ & -P_{23}^{(\sigma)}P_{23}^{(\tau)}\left(Y_{123}^{465}+Y_{231}^{654}+Y_{312}^{546}\right) \\ & -P_{13}^{(\sigma)}P_{13}^{(\tau)}\left(Y_{123}^{654}+Y_{231}^{546}+Y_{312}^{465}\right) \\ & -P_{12}^{(\sigma)}P_{12}^{(\tau)}\left(Y_{123}^{546}+Y_{231}^{465}+Y_{312}^{654}\right) , \end{aligned} \tag{6.40}$$

where the eighteen terms follow the ordering displayed in Fig. 6.5 and we have introduced the abbreviation

$$\begin{aligned} Y_{ijk}^{lmn} = \frac{g_A^2}{4f_\pi^4}\frac{\vec{\sigma}_i\cdot\vec{q}_{li}\;\vec{\sigma}_k\cdot\vec{q}_{nk}}{(\vec{q}_{li}^{\,2}+m_\pi^2)(\vec{q}_{nk}^{\,2}+m_\pi^2)}\Big[\vec{\tau}_i\cdot\vec{\tau}_k(-4c_1m_\pi^2+2c_3\vec{q}_{li}\cdot\vec{q}_{nk}) \\ + c_4\vec{\tau}_j\cdot(\vec{\tau}_i\times\vec{\tau}_k)\;\vec{\sigma}_j\cdot(\vec{q}_{li}\times\vec{q}_{nk})\Big] , \end{aligned} \tag{6.41}$$

with the constants (see also Refs. [175, 176])

$$c_1 = \frac{1}{2}(2b_0+b_D+b_F) , \quad c_3 = b_1+b_2+b_3+2b_4 , \quad c_4 = 4(d_1+d_2) . \tag{6.42}$$

Again, the result in Eq. (6.40) is equal to the antisymmetrization of the expression given in Ref. [51]:

$$V_{\rm TPE}^{NNN} = \frac{g_A^2}{8f_\pi^2}\mathcal{A}\sum_{i\neq j\neq k}\frac{\vec{\sigma}_i\cdot\vec{q}_i\;\vec{\sigma}_j\cdot\vec{q}_j}{(\vec{q}_i^{\,2}+m_\pi^2)(\vec{q}_j^{\,2}+m_\pi^2)}F_{ijk}^{\alpha\beta}\tau_i^\alpha\tau_j^\beta , \tag{6.43}$$

with

$$F_{ijk}^{\alpha\beta} = \frac{\delta^{\alpha\beta}}{f_\pi^2}(-4c_1m_\pi^2+2c_3\vec{q}_i\cdot\vec{q}_j)+\sum_\gamma\frac{c_4}{f_\pi^2}\epsilon^{\alpha\beta\gamma}\tau_k^\gamma\;\vec{\sigma}_k\cdot(\vec{q}_i\times\vec{q}_j) . \tag{6.44}$$

The ΛNN three-body interaction generated by two-pion exchange takes the form

$$\begin{aligned} V_{\rm TPE}^{\Lambda NN} = & \frac{g_A^2}{3f_0^4}\frac{\vec{\sigma}_3\cdot\vec{q}_{63}\;\vec{\sigma}_2\cdot\vec{q}_{52}}{(\vec{q}_{63}^{\,2}+m_\pi^2)(\vec{q}_{52}^{\,2}+m_\pi^2)}\vec{\tau}_2\cdot\vec{\tau}_3\Big(-(3b_0+b_D)m_\pi^2+(2b_2+3b_4)\,\vec{q}_{63}\cdot\vec{q}_{52}\Big) \\ & -P_{23}^{(\sigma)}P_{23}^{(\tau)}\frac{g_A^2}{3f_0^4}\frac{\vec{\sigma}_3\cdot\vec{q}_{53}\;\vec{\sigma}_2\cdot\vec{q}_{62}}{(\vec{q}_{53}^{\,2}+m_\pi^2)(\vec{q}_{62}^{\,2}+m_\pi^2)}\vec{\tau}_2\cdot\vec{\tau}_3\Big(-(3b_0+b_D)m_\pi^2+(2b_2+3b_4)\,\vec{q}_{53}\cdot\vec{q}_{62}\Big) . \end{aligned} \tag{6.45}$$

Note that only those two diagrams in Fig. 6.5 contribute, where the (final and initial) Λ hyperon are associated to the central baryon line. All other diagrams are simply zero due to the vanishing of the $\Lambda\Lambda\pi$ vertex.

7

THREE-BARYON FORCE THROUGH DECUPLET SATURATION

Low-energy two- and three-body interactions derived from SU(2) χEFT are used consistently in combination with each other in nuclear few- and many-body calculations. The a priori unknown low-energy constants are fitted, for example, to NN scattering data and $3N$ observables such as 3-body binding energies [51]. Some of these LECs are, however, large compared to their order of magnitude as expected from the hierarchy of nuclear forces in Fig. 2.4. This feature has its physical origin in strong couplings of the πN-system to the low-lying $\Delta(1232)$-resonance. It is therefore natural to include the $\Delta(1232)$-isobar as an explicit degree of freedom in the chiral Lagrangian (cf. Refs. [177, 178, 179]). The small mass difference between nucleons and deltas (293 MeV) introduces a small scale, which can be included consistently in the chiral power counting scheme and the hierarchy of nuclear forces. The dominant parts of the three-nucleon interaction mediated by two-pion exchange at NNLO are then promoted to NLO through the delta contributions. The appearance of the inverse mass splitting explains the large numerical values of the corresponding LECs [12, 180].

In SU(3) χEFT the situation is similar. In systems with strangeness $S = -1$ like ΛNN, resonances such as the spin-3/2 $\Sigma^*(1385)$-resonance could play a similar role as the Δ in the NNN system, as we have already depicted in Fig. 4.10 on the right side. The small decuplet-octet mass splitting (in the chiral limit), $\Delta := M_{10} - M_8$, is counted together with external momenta and meson masses as $\mathcal{O}(q)$ and thus parts of the NNLO three-baryon interaction are promoted to NLO by the explicit inclusion of the baryon decuplet, as illustrated in Fig. 7.1. It is therefore likewise compelling to treat the three-baryon interaction together with the NLO hyperon-nucleon interaction described in Chapter 4. Note that in the nucleonic sector, only the two-pion exchange diagram with an intermediate Δ-isobar is allowed. Other diagrams are forbidden due to the Pauli principle, as we will show later. For three flavors more particles are involved and, in general, also the other diagrams (contact and one-meson exchange) with intermediate decuplet baryons in Fig. 7.1 appear.

The large number of unknown LECs derived in Chapter 6 is related to the multitude of three-baryon multiplets, with strangeness ranging from 0 to -6. For selected processes only a small subset of these constants contributes as has been exemplified for the ΛNN three-body interaction. In this chapter we estimate these LECs by resonance saturation. We introduce the chiral Lagrangian for the octet to decuplet baryon transition involving a single pseudoscalar meson and we construct the necessary non-relativistic contact vertex between three octet baryons and a single decuplet baryon, B^*BBB. Finally the three leading three-baryon interaction diagrams are evaluated with decuplet-baryon resonances in the intermediate state.

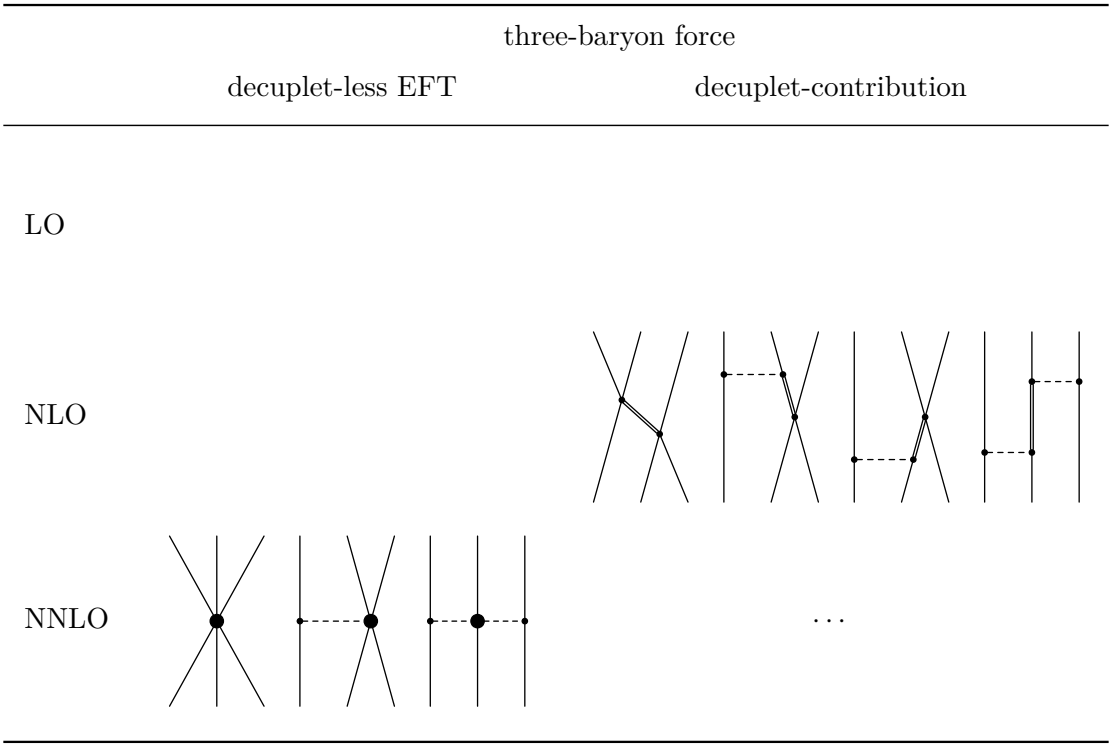

FIGURE 7.1: Hierarchy of three-baryon forces with explicit introduction of the baryon decuplet (represented by double lines).

7.1 LAGRANGIANS INCLUDING DECUPLET BARYONS

In this section, we present the minimal set of terms in the chiral Lagrangian, that are necessary for the diagrams including decuplet baryons in Fig. 7.1. The leading-order interaction Lagrangian between octet and decuplet baryons in the non-relativistic limit (see, e.g., Ref. [181]) is given by

$$\mathscr{L} = \frac{C}{f_0} \sum_{a,b,c,d,e=1}^{3} \epsilon_{abc} \left(\bar{T}_{ade} \vec{S}^{\dagger} \cdot \left(\vec{\nabla} \phi_{db} \right) B_{ec} + \bar{B}_{ce} \vec{S} \cdot \left(\vec{\nabla} \phi_{bd} \right) T_{ade} \right) , \tag{7.1}$$

where the decuplet baryons are represented by the totally symmetric three-index tensor T, cf. Eq. (2.37). The spin transition matrices $\vec{S}$ connect the two-component spinors of octet baryons with the four-component spinors of decuplet baryons, and are explicitly given in Appendix A.1. They fulfill the relation ${S_i}{S_j}^{\dagger} = \frac{1}{3}(2\delta_{ij} - \mathrm{i}\epsilon_{ijk}\sigma_k)$. Only a single LEC is present at leading order. For this constant C we use the (large-N_c) value $C = \frac{3}{4} g_A \approx 1$, which leads to a decay width $\Gamma(\Delta \to \pi N) = 110.6$ MeV that is in good agreement with the empirical value of $\Gamma(\Delta \to \pi N) = (115 \pm 5)$ MeV [178]. Rewriting the lowest-order decuplet Lagrangian Eq. (7.1) in the particle basis gives

$$\mathscr{L} = \frac{C}{f_0} \sum_{i,j,k} N_{B_i^* \phi_j B_k} \left[\bar{B}_i^* \vec{S}^{\dagger} \cdot \left(\vec{\nabla} \phi_j \right) B_k + \bar{B}_k \vec{S} \cdot \left(\vec{\nabla} \phi_j^{\dagger} \right) B_i^* \right] , \tag{7.2}$$

with SU(3) coefficients N and with the physical meson fields $\phi_i \in \{\pi^0, \pi^+, \pi^-, K^+, K^-, K^0, \bar{K}^0, \eta\}$, octet baryon fields $B_i \in \{n, p, \Lambda, \Sigma^0, \Sigma^+, \Sigma^-, \Xi^0, \Xi^-\}$ and decuplet baryon fields $B_i^* \in \{\Delta^-, \Delta^0, \Delta^+, \Delta^{++}, \Sigma^{*0}, \Sigma^{*+}, \Sigma^{*-}, \Xi^{*0}, \Xi^{*-}, \Omega^-\}$.

The other vertex with decuplet baryons that appears in Fig. 7.1 is the leading-order B^*BBB contact vertex, involving three octet and one decuplet baryon. An overcomplete set of terms for this contact Lagrangian in the non-relativistic limit takes the form

$$\mathscr{L} = \sum_{x=1}^{7} c^x \sum_{\substack{a,b,c,d,\\ e,f,g,h,i=1}}^{3} \theta^x_{abcdefghi} \left[\left(\bar{T}_{abc} \vec{S}^\dagger B_{de}\right) \cdot \left(\bar{B}_{fg} \vec{\sigma} B_{hi}\right) + \left(\bar{B}_{ed} \vec{S}\, T_{abc}\right) \cdot \left(\bar{B}_{ih} \vec{\sigma} B_{gf}\right) \right], \quad (7.3)$$

with seven different (SU(3) symmetric) flavor combinations θ^x,

$$\begin{aligned}
\theta^1_{abcdefghi} &= \epsilon_{aeg}\delta_{bd}\delta_{ch}\delta_{fi}\,, \\
\theta^2_{abcdefghi} &= \epsilon_{aeg}\delta_{bf}\delta_{ch}\delta_{di}\,, \\
\theta^3_{abcdefghi} &= \epsilon_{aei}\delta_{bd}\delta_{cf}\delta_{hg}\,, \\
\theta^4_{abcdefghi} &= \epsilon_{aei}\delta_{bh}\delta_{cf}\delta_{dg}\,, \\
\theta^5_{abcdefghi} &= \epsilon_{agi}\delta_{bf}\delta_{cd}\delta_{eh}\,, \\
\theta^6_{abcdefghi} &= \epsilon_{agi}\delta_{bh}\delta_{cd}\delta_{ef}\,, \\
\theta^7_{abcdefghi} &= \epsilon_{egi}\delta_{ad}\delta_{bf}\delta_{ch}\,,
\end{aligned} \quad (7.4)$$

and seven corresponding LECs c^x. In the particle basis the Lagrangian Eq. (7.3) reads:

$$\mathscr{L} = \sum_{x=1}^{7} c^x \sum_{i,j,k,l} N^x_{B^*_i B_j B_k B_l} \left[\left(\bar{B}^*_i \vec{S}^\dagger B_j\right) \cdot \left(\bar{B}_k \vec{\sigma} B_l\right) + \left(\bar{B}_j \vec{S}\, B^*_i\right) \cdot \left(\bar{B}_l \vec{\sigma} B_k\right) \right], \quad (7.5)$$

where i, j, k, l run now over the baryon fields in the particle basis and N are again SU(3) coefficients.

In order to get a minimal set of terms in the effective Lagrangian, we consider the process $BB \to B^*B$. The transition matrix elements arising from Eq. (7.3) are given by the Feynman diagrams

$V =$ 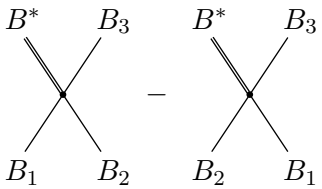

$\cdot\, P^{(\sigma)}\,,$ (7.6)

where the spin exchange operator $P^{(\sigma)} = \frac{1}{2}(\mathbb{1} + \vec{\sigma}_1 \cdot \vec{\sigma}_2)$ acts on the initial state. Making use of the (explicitly verified) identity $\vec{S}_1^\dagger \cdot \vec{\sigma}_2\, P^{(\sigma)} = \vec{S}_1^\dagger \cdot \vec{\sigma}_2$ one obtains the following expression for the transition matrix elements:

$$V = -\vec{S}_1^\dagger \cdot \vec{\sigma}_2 \sum_{x=1}^{7} c^x \left(N^x_{B^* B_1 B_3 B_2} - N^x_{B^* B_2 B_3 B_1} \right). \quad (7.7)$$

As in Chapter 6 we can obtain the minimal effective Lagrangian by eliminating redundant terms until the rank of the matrix formed by all transitions matches the number of terms in the Lagrangian. We have chosen the two independent flavor combinations θ^1 and θ^2 and obtain for the minimal non-relativistic B^*BBB Lagrangian:

$$\begin{aligned}
\mathscr{L} = \quad & G_1 \sum_{\substack{a,b,c,\\ d,e,f=1}}^{3} \epsilon_{abc} \left[\left(\bar{T}_{ade} \vec{S}^\dagger B_{db}\right) \cdot \left(\bar{B}_{fc} \vec{\sigma} B_{ef}\right) + \left(\bar{B}_{bd} \vec{S}\, T_{ade}\right) \cdot \left(\bar{B}_{fe} \vec{\sigma} B_{cf}\right) \right] \\
& + G_2 \sum_{\substack{a,b,c,\\ d,e,f=1}}^{3} \epsilon_{abc} \left[\left(\bar{T}_{ade} \vec{S}^\dagger B_{fb}\right) \cdot \left(\bar{B}_{dc} \vec{\sigma} B_{ef}\right) + \left(\bar{B}_{bf} \vec{S}\, T_{ade}\right) \cdot \left(\bar{B}_{fe} \vec{\sigma} B_{cd}\right) \right], \quad (7.8)
\end{aligned}$$

with two low-energy constants G_1 and G_2. This number of two constants can be easily understood through group theoretical considerations of the transition $BB \to B^*B$. In flavor space the two initial octet baryons form the tensor product $\mathbf{8} \otimes \mathbf{8}$, and in spin space they form the product $\mathbf{2} \otimes \mathbf{2}$. These decompose into the irreducible representations as follows:

$$\mathbf{8} \otimes \mathbf{8} = \underbrace{\mathbf{27} \oplus \mathbf{8}_s \oplus \mathbf{1}}_{\text{symmetric}} \oplus \underbrace{\mathbf{10} \oplus \mathbf{10}^* \oplus \mathbf{8}_a}_{\text{antisymmetric}}\,, \qquad \mathbf{2} \otimes \mathbf{2} = \mathbf{1}_a \oplus \mathbf{3}_s\,. \tag{7.9}$$

Similarly one finds for the final state, with a decuplet and an octet baryon, in flavor space and in spin space

$$\mathbf{10} \otimes \mathbf{8} = \mathbf{35} \oplus \mathbf{27} \oplus \mathbf{10} \oplus \mathbf{8}\,, \qquad \mathbf{4} \otimes \mathbf{2} = \mathbf{3} \oplus \mathbf{5}\,. \tag{7.10}$$

At leading order only S-waves are involved. Transitions can only occur between the same types of irreducible (flavor and spin) representations. Therefore, in spin space the representation $\mathbf{3}$ has to be chosen. Due to the Pauli principle in the initial state, the symmetric $\mathbf{3}$ in spin space combines with the antisymmetric representations $\mathbf{10}, \mathbf{10}^*, \mathbf{8}_a$ in flavor space. But only $\mathbf{10}$ and $\mathbf{8}_a$ have a counterpart in the final state flavor space. The number of two allowed transitions between irreducible representations corresponds exactly the number of two LECs in the minimal Lagrangian. A partial wave decomposition of the spin-operator $\vec{S}_1^{\,\dagger} \cdot \vec{\sigma}_2$ reveals, that indeed its only non-vanishing matrix element is given by the transition ${}^3S_1 \to {}^3S_1$.

Another interesting observation can be made from Eqs. (7.9) and (7.10). For NN states only the representations $\mathbf{27}$ and $\mathbf{10}^*$ can contribute, as can be seen, e.g., in Tab. 4.2. But these representations combine either with the wrong spin, or have no counterpart in the final state. Hence, $NN \to \Delta N$ transitions in S-waves are forbidden due to the Pauli principle.

For convenience we present also all non-vanishing transition matrix elements for the process $BB \to B^*B$ following from the minimal Lagrangian Eq. (7.8). In order to give the matrix elements in isospin basis we use (analogue to Eq. (6.17)):

$$\begin{aligned}\langle (i_3 i_4) I_{\text{out}} M_{\text{out}} | \hat{\mathcal{O}} | (i_1 i_2) I_{\text{in}} M_{\text{in}} \rangle \\ = \sum_{\substack{m_1, m_2, \\ m_3, m_4}} \delta_{M_{\text{out}}, m_3 + m_4} \delta_{M_{\text{in}}, m_1 + m_2} \\ \times C^{i_3 i_4 I_{\text{out}}}_{m_3 m_4 M_{\text{out}}} C^{i_1 i_2 I_{\text{in}}}_{m_1 m_2 M_{\text{in}}} \langle i_3 m_3; i_4 m_4 | \hat{\mathcal{O}} | i_1 m_1; i_2 m_2 \rangle\,,\end{aligned} \tag{7.11}$$

where i stands for the isospin and C are Clebsch-Gordan coefficients. The resulting matrix elements are tabulated in Tab. 7.1.

7.2 ESTIMATION OF LOW-ENERGY CONSTANTS

In this section we estimate the LECs of the leading three-baryon interaction by decuplet saturation using the diagrams shown in Fig. 7.1. At this order we can just evaluate the diagram with an intermediate decuplet baryon and compare them to the result for the diagram with the more general vertex. The resulting three-baryon potentials have the same structure and the decuplet contributions give expressions for the LECs.

S	transition	I	X
-1	$\Lambda N \to \Delta\Sigma$	$\frac{1}{2}$	$\frac{G_1+3G_2}{\sqrt{3}}$
-1	$\Lambda N \to \Sigma^* N$	$\frac{1}{2}$	$\frac{G_1+3G_2}{2\sqrt{3}}$
-1	$\Sigma N \to \Delta\Sigma$	$\frac{1}{2}$	$-\frac{G_1+3G_2}{\sqrt{3}}$
-1	$\Sigma N \to \Delta\Sigma$	$\frac{3}{2}$	$\sqrt{\frac{5}{6}}G_1$
-1	$\Sigma N \to \Delta\Lambda$	$\frac{3}{2}$	$\frac{G_1}{\sqrt{6}}$
-1	$\Sigma N \to \Sigma^* N$	$\frac{1}{2}$	$-\frac{G_1+3G_2}{2\sqrt{3}}$
-1	$\Sigma N \to \Sigma^* N$	$\frac{3}{2}$	$\frac{G_1}{\sqrt{3}}$
-2	$\Xi N \to \Delta\Xi$	1	$-\frac{2G_2}{\sqrt{3}}$
-2	$\Xi N \to \Sigma^*\Sigma$	0	$\frac{G_1+3G_2}{\sqrt{2}}$
-2	$\Xi N \to \Sigma^*\Sigma$	1	$-\frac{G_1+G_2}{\sqrt{3}}$
-2	$\Xi N \to \Sigma^*\Lambda$	1	$-\frac{G_1+3G_2}{3\sqrt{2}}$
-2	$\Xi N \to \Xi^* N$	0	$\frac{G_1+3G_2}{\sqrt{3}}$
-2	$\Xi N \to \Xi^* N$	1	$-\frac{G_1+G_2}{\sqrt{3}}$
-2	$\Sigma\Lambda \to \Delta\Xi$	1	$\frac{\sqrt{2}G_1}{3}$
-2	$\Sigma\Lambda \to \Sigma^*\Sigma$	1	$-\frac{\sqrt{2}G_1}{3}$

S	transition	I	X
-2	$\Sigma\Lambda \to \Xi^* N$	1	$-\frac{\sqrt{2}G_1}{3}$
-2	$\Sigma\Sigma \to \Delta\Xi$	1	$\frac{2(G_1+2G_2)}{\sqrt{3}}$
-2	$\Sigma\Sigma \to \Sigma^*\Sigma$	1	$\frac{2G_2}{\sqrt{3}}$
-2	$\Sigma\Sigma \to \Sigma^*\Lambda$	1	$\frac{1}{3}\sqrt{2}(G_1+3G_2)$
-2	$\Sigma\Sigma \to \Xi^* N$	1	$\frac{2G_2}{\sqrt{3}}$
-3	$\Xi\Lambda \to \Sigma^*\Xi$	$\frac{1}{2}$	$-\frac{G_1-3G_2}{2\sqrt{3}}$
-3	$\Xi\Lambda \to \Xi^*\Sigma$	$\frac{1}{2}$	$\frac{2G_1+3G_2}{2\sqrt{3}}$
-3	$\Xi\Lambda \to \Xi^*\Lambda$	$\frac{1}{2}$	$\frac{\sqrt{3}G_2}{2}$
-3	$\Xi\Lambda \to \Omega N$	$\frac{1}{2}$	$\frac{2G_1+3G_2}{\sqrt{6}}$
-3	$\Xi\Sigma \to \Sigma^*\Xi$	$\frac{1}{2}$	$-\frac{1}{2}\sqrt{3}(G_1+G_2)$
-3	$\Xi\Sigma \to \Xi^*\Sigma$	$\frac{1}{2}$	$-\frac{\sqrt{3}G_2}{2}$
-3	$\Xi\Sigma \to \Xi^*\Lambda$	$\frac{1}{2}$	$-\frac{2G_1+3G_2}{2\sqrt{3}}$
-3	$\Xi\Sigma \to \Omega N$	$\frac{1}{2}$	$-\sqrt{\frac{3}{2}}G_2$
-4	$\Xi\Xi \to \Xi^*\Xi$	0	$\frac{2G_1}{\sqrt{3}}$
-4	$\Xi\Xi \to \Omega\Lambda$	0	$\frac{2G_1}{\sqrt{3}}$

TABLE 7.1: Non-vanishing transition matrix elements $V = -X\,\vec{S}_1^{\dagger}\cdot\vec{\sigma}_2$ for the process $BB \to B^*B$.

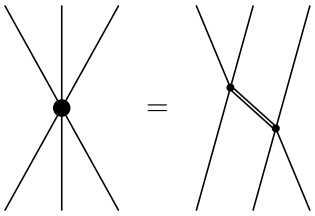

FIGURE 7.2: Saturation of the six-baryon contact interaction via decuplet resonances.

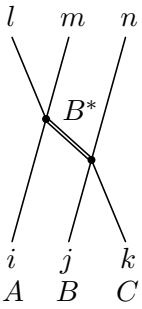

FIGURE 7.3: Generic three-body decuplet contact diagram.

In order to estimate the LECs of the six-baryon contact Lagrangian of Eq. (6.12), we consider a process $B_1B_2B_3 \to B_4B_5B_6$ and examine the diagrams in Fig. 7.2. We have already shown, how to calculate the potential on the left side of Fig. 7.2 through Eqs. (6.6) and (6.10) by performing all 36 Wick contractions. For the diagrams on right side of Fig. 7.2 the procedure is similar. For this, let us consider the generic diagram in Fig. 7.3, where the baryon pair i-l is in spin space A, j-m in spin space B and k-n in spin space C. The corresponding transition matrix element, following from standard Feynman rules, is given by

$$V^{ABC}_{\substack{lmn\\ijk}} = -\frac{1}{3\Delta}(G_1 N^1_{B^*B_mB_iB_l} + G_2 N^2_{B^*B_mB_iB_l})(G_1 N^1_{B^*B_jB_nB_k} + G_2 N^2_{B^*B_jB_nB_k}) \times (2\vec{\sigma}_A\cdot\vec{\sigma}_C - \mathrm{i}(\vec{\sigma}_A\times\vec{\sigma}_C)\cdot\vec{\sigma}_B)\,, \tag{7.12}$$

where we have used $S_aS_b^{\dagger} = \frac{1}{3}(2\delta_{ab} - \mathrm{i}\epsilon_{abc}\sigma_c)$. Since the baryons B_1, B_2, B_3 are per definition in the spin-spaces $1, 2, 3$, respectively, the assignment A, B, C is determined by

i, j, k. Thus we can drop the superscript A, B, C. The six direct Wick contractions that contribute to the process $B_1B_2B_3 \to B_4B_5B_6$ are therefore given by

$$V^D = V_{\substack{456\\123}} + V_{\substack{564\\231}} + V_{\substack{645\\312}} + V_{\substack{465\\132}} + V_{\substack{654\\321}} + V_{\substack{546\\213}} \,. \tag{7.13}$$

As in Eq. (6.10) the full potential with all 36 Wick contraction can be expressed through the direct contributions by

$$\begin{aligned} V = V^D &+ P_{23}^{(\sigma)} P_{13}^{(\sigma)} \Big(V^D\Big)_{\substack{4\to5\\5\to6\\6\to4}} + P_{23}^{(\sigma)} P_{12}^{(\sigma)} \Big(V^D\Big)_{\substack{4\to6\\5\to4\\6\to5}} \\ &- P_{23}^{(\sigma)} \Big(V^D\Big)_{\substack{4\to4\\5\to6\\6\to5}} - P_{13}^{(\sigma)} \Big(V^D\Big)_{\substack{4\to6\\5\to5\\6\to4}} - P_{12}^{(\sigma)} \Big(V^D\Big)_{\substack{4\to5\\5\to4\\6\to6}} \,. \end{aligned} \tag{7.14}$$

After summing over all intermediate decuplet baryons B^*, we can compare the full three-body potential of all possible combinations of baryons on the left side of Fig. 7.2 with the ones on the right side. The LECs of the six-baryon contact Lagrangian of Eq. (6.12) are given by:

$$\begin{aligned}
C_1 &= -\frac{7(G_1+G_2)^2}{24\Delta}\,, & C_{10} &= -\frac{25G_1^2+50G_1G_2+9G_2^2}{72\Delta}\,,\\
C_2 &= -\frac{G_1^2+18G_1G_2+9G_2^2}{36\Delta}\,, & C_{11} &= -\frac{23(G_1+G_2)^2}{72\Delta}\,,\\
C_3 &= -\frac{19G_1^2+30G_1G_2+15G_2^2}{36\Delta}\,, & C_{12} &= -\frac{13G_1^2+42G_1G_2+21G_2^2}{108\Delta}\,,\\
C_4 &= \frac{G_1^2+18G_1G_2+9G_2^2}{72\Delta}\,, & C_{13} &= -\frac{G_1^2+10G_1G_2+5G_2^2}{36\Delta}\,,\\
C_5 &= \frac{5(G_1+G_2)^2}{8\Delta}\,, & C_{14} &= \frac{5(G_1+G_2)^2}{24\Delta}\,,\\
C_6 &= \frac{17G_1^2+18G_1G_2-15G_2^2}{72\Delta}\,, & C_{15} &= -\frac{G_1^2-9G_2^2}{27\Delta}\,,\\
C_7 &= \frac{7G_1^2+6G_1G_2-9G_2^2}{108\Delta}\,, & C_{16} &= -\frac{11G_1^2+18G_1G_2+3G_2^2}{54\Delta}\,,\\
C_8 &= \frac{25G_1^2+42G_1G_2-3G_2^2}{108\Delta}\,, & C_{17} &= -\frac{2G_1(G_1+2G_2)}{9\Delta}\,,\\
C_9 &= \frac{G_1^2+18G_1G_2+9G_2^2}{72\Delta}\,, & C_{18} &= \frac{2G_1^2}{27\Delta}\,,
\end{aligned} \tag{7.15}$$

where Δ is the average decuplet-octet baryon mass splitting.

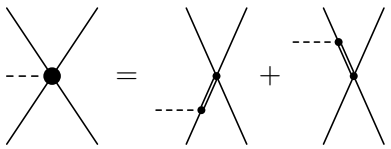

FIGURE 7.4: Saturation of the $BB \to BB\phi$ vertex via decuplet resonances.

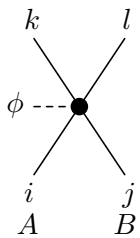

FIGURE 7.5: Generic $BB \to BB\phi$ diagram.

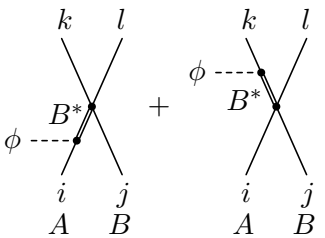

FIGURE 7.6: Generic $BB \to BB\phi$ decuplet diagrams.

Now we turn to the one-meson-exchange part of the three-baryon forces. Since we are at the leading order only tree-level diagrams are involved and we can estimate the LECs already on the level of the vertices, as depicted in Fig. 7.4. We consider the transition matrix elements of the process $B_1B_2 \to B_3B_4\phi$ and start with the left side of Fig. 7.4. In the generic diagram of Fig. 7.5 the baryon pairs i-k and j-l are in spin-space A and B, respectively. One obtains via Feynman rules the contribution

$$V_{\substack{kl\\ij}}^{AB} = \frac{\mathrm{i}}{f_0}\left(\sum_{f=1}^{10} D_f N_{\substack{kl\\ij}}^{f\ \bar{\phi}}\ \vec{\sigma}_B\cdot\vec{q} + \sum_{f=11}^{14} D_f N_{\substack{kl\\ij}}^{f\ \bar{\phi}}\ \mathrm{i}\,(\vec{\sigma}_A\times\vec{\sigma}_B)\cdot\vec{q}\right), \tag{7.16}$$

where $\vec{q}$ is the momentum of the emitted meson and N are the SU(3) coefficients given in Eq. (6.23). Since the baryon B_1 in the initial state is per definition always in the spin-space 1 and B_2 in spin-space 2, A and B are determined by i and j and therefore we drop the superscript A, B. The full transition matrix element of the process $B_1B_2 \to B_3B_4\phi$ is then given by two direct diagrams and two exchanged diagrams to which the spin-exchange operator $P^{(\sigma)} = \frac{1}{2}(\mathbb{1} + \vec{\sigma}_1\cdot\vec{\sigma}_2)$ has to be applied in the final state (in analogy to what was done in Chapter 6):

$$V = V_{\substack{34\\12}} + V_{\substack{43\\21}} - P^{(\sigma)}\left(V_{\substack{43\\12}} + V_{\substack{34\\21}}\right). \tag{7.17}$$

Let us now consider the right side of Fig. 7.4. In an analogous way, we obtain for the generic diagrams including a decuplet baryon in Fig. 7.6 the following contribution

$$\begin{aligned} V_{\substack{kl\\ij}}^{AB} = \frac{\mathrm{i}C}{3\Delta f_0}\Big[&(G_1 N^1_{B^*B_kB_jB_l} + G_2 N^2_{B^*B_kB_jB_l}) N_{B^*\bar{\phi}B_i}\left(2\vec{\sigma}_B\cdot\vec{q} - \mathrm{i}(\vec{\sigma}_A\times\vec{\sigma}_B)\cdot\vec{q}\right)\\ &+ (G_1 N^1_{B^*B_iB_lB_j} + G_2 N^2_{B^*B_iB_lB_j}) N_{B^*\phi B_k}\left(2\vec{\sigma}_B\cdot\vec{q} + \mathrm{i}(\vec{\sigma}_A\times\vec{\sigma}_B)\cdot\vec{q}\right)\Big]. \end{aligned} \tag{7.18}$$

As before the full potential is given by inserting Eq. (7.18) into Eq. (7.17) and summing over all intermediate decuplet baryons. Finally, we can compare the results for the full potential of the left and right side of Fig. 7.4 for all combinations of baryons and mesons. This leads to the following LECs of the minimal non-relativistic chiral Lagrangian for the four-baryon vertex including one meson of Eq. (6.22):

$$\begin{aligned} D_1 &= -\frac{7C(G_1+G_2)}{18\Delta}, & D_8 &= -\frac{C(5G_1-3G_2)}{18\Delta},\\ D_2 &= -\frac{C(G_1-7G_2)}{18\Delta}, & D_9 &= -\frac{C(5G_1+9G_2)}{9\Delta},\\ D_3 &= \frac{C(3G_1+11G_2)}{18\Delta}, & D_{10} &= -\frac{5C(G_1+G_2)}{6\Delta},\\ D_4 &= -\frac{C(9G_1+13G_2)}{18\Delta}, & D_{11} &= \frac{C(G_1+9G_2)}{18\Delta},\\ D_5 &= -\frac{C(G_1-3G_2)}{18\Delta}, & D_{12} &= \frac{C(2G_1+5G_2)}{9\Delta},\\ D_6 &= -\frac{C(5G_1-3G_2)}{18\Delta}, & D_{13} &= \frac{C(G_1+5G_2)}{18\Delta},\\ D_7 &= \frac{2G_2C}{9\Delta}, & D_{14} &= -\frac{C(3G_1+7G_2)}{18\Delta}. \end{aligned} \tag{7.19}$$

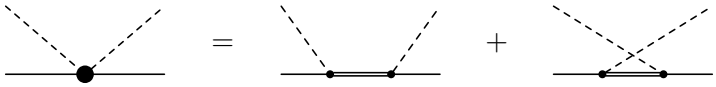

FIGURE 7.7: Saturation of the NLO baryon-meson vertex via decuplet resonances.

The last class of diagrams is the three-body interaction with two-meson exchange. As done for the one-meson exchange, we can saturate the unknown LECs directly on the level of the vertex and consider the process $B_1\phi_1 \to B_2\phi_2$, shown in Fig. 7.7. The diagram on the left side (without decuplet baryons) leads to the following transition matrix elements

$$\begin{aligned} V = & \sum_{c^f = b_D, b_F, b_0} \frac{c^f}{4f_0^2} (N^f_{\phi_1 {}^o_i \bar{\phi}_2} + N^f_{\bar{\phi}_2 {}^o_i \phi_1}) \\ & + \sum_{c^f = b_1, b_2, b_3, b_4} \frac{c^f}{f_0^2} (N^f_{\phi_1 {}^o_i \bar{\phi}_2} + N^f_{\bar{\phi}_2 {}^o_i \phi_1}) \vec{q}_1 \cdot \vec{q}_2 \\ & - \sum_{c^f = d_1, d_2, d_3} \frac{c^f}{f_0^2} (N^f_{\phi_1 {}^o_i \bar{\phi}_2} - N^f_{\bar{\phi}_2 {}^o_i \phi_1}) \, \mathrm{i} \, (\vec{q}_1 \times \vec{q}_2) \cdot \vec{\sigma} \,, \end{aligned} \tag{7.20}$$

with the SU(3) coefficients N of Eq. (6.28). For the two diagrams on the right side of Fig. 7.7 one obtains

$$V = -\frac{C^2}{3\Delta f_0^2} \big[2 (N_{B^* \phi_2 B_o} N_{B^* \phi_1 B_i} + N_{B^* \bar{\phi}_1 B_o} N_{B^* \bar{\phi}_2 B_i}) \, \vec{q}_1 \cdot \vec{q}_2 \tag{7.21}$$

$$+ (N_{B^* \phi_2 B_o} N_{B^* \phi_1 B_i} - N_{B^* \bar{\phi}_1 B_o} N_{B^* \bar{\phi}_2 B_i}) \, \mathrm{i} \, (\vec{q}_1 \times \vec{q}_2) \cdot \vec{\sigma} \big] \,. \tag{7.22}$$

A direct comparison of the transition matrix elements for all combinations of baryons and mesons after summing over all intermediate decuplet baryons B^* leads to the following contributions to the LECs of the meson-baryon Lagrangian in Eq. (6.26):

$$\begin{aligned} & b_D = 0 \,, \; b_F = 0 \,, \; b_0 = 0 \,, \\ & b_1 = \frac{7C^2}{36\Delta} \approx 0.59 \,, \; b_2 = \frac{C^2}{4\Delta} \approx 0.76 \,, \; b_3 = -\frac{C^2}{3\Delta} \approx -1.01 \,, \; b_4 = -\frac{C^2}{2\Delta} \approx -1.51 \,, \\ & d_1 = \frac{C^2}{12\Delta} \approx 0.25 \,, \; d_2 = \frac{C^2}{36\Delta} \approx 0.08 \,, \; d_3 = -\frac{C^2}{6\Delta} \approx -0.50 \,, \end{aligned} \tag{7.23}$$

where all numerical values are in GeV^{-1} and we have already inserted $\Delta \approx 300$ MeV and $C = \frac{3}{4} g_A$, with $g_A = 1.27$. The result above is in line with the well-known $\Delta(1232)$ contribution to the LECs c_1, c_3, c_4 (defined in Eq. (6.42)) in the nucleonic sector [180]:

$$c_1 = 0 \,, \qquad c_3 = -2c_4 = -\frac{g_A^2}{2\Delta} \,. \tag{7.24}$$

Using the LECs obtained via decuplet saturation, we can evaluate the constants of the ΛNN (contact interaction, one-pion and two-pion exchange) diagrams of Sec. 6.4. One obtains

$$\begin{aligned} & C_1' = C_3' = \frac{(G_1 + 3G_2)^2}{72\Delta} \,, && C_2' = 0 \,, \\ & D_1' = 0 \,, && D_2' = \frac{2C(G_1 + 3G_2)}{9\Delta} \,, \\ & 3b_0 + b_D = 0 \,, && 2b_2 + 3b_4 = -\frac{C^2}{\Delta} \,. \end{aligned} \tag{7.25}$$

transition	type	B^*
$NNN \to NNN$	$\pi\pi$	Δ
$\Lambda NN \to \Lambda NN$	ct	Σ^*
$\Lambda NN \to \Lambda NN$	π	Σ^*
$\Lambda NN \to \Lambda NN$	K	Σ^*
$\Lambda NN \to \Lambda NN$	$\pi\pi$	Σ^*
$\Lambda NN \to \Lambda NN$	πK	Σ^*
$\Lambda NN \to \Lambda NN$	KK	Σ^*
$\Lambda NN \leftrightarrow \Sigma NN$	ct	Σ^*
$\Lambda NN \leftrightarrow \Sigma NN$	π	Δ, Σ^*
$\Lambda NN \leftrightarrow \Sigma NN$	K	Σ^*
$\Lambda NN \leftrightarrow \Sigma NN$	η	Σ^*
$\Lambda NN \leftrightarrow \Sigma NN$	$\pi\pi$	Δ, Σ^*
$\Lambda NN \leftrightarrow \Sigma NN$	πK	Δ, Σ^*
$\Lambda NN \leftrightarrow \Sigma NN$	$\pi\eta$	Σ^*
$\Lambda NN \leftrightarrow \Sigma NN$	KK	Σ^*
$\Lambda NN \leftrightarrow \Sigma NN$	$K\eta$	Σ^*

transition	type	B^*
$\Sigma NN \to \Sigma NN$	ct	Σ^*
$\Sigma NN \to \Sigma NN$	π	Δ, Σ^*
$\Sigma NN \to \Sigma NN$	K	Σ^*
$\Sigma NN \to \Sigma NN$	η	Σ^*
$\Sigma NN \to \Sigma NN$	$\pi\pi$	Δ, Σ^*
$\Sigma NN \to \Sigma NN$	πK	Δ, Σ^*
$\Sigma NN \to \Sigma NN$	$\pi\eta$	Σ^*
$\Sigma NN \to \Sigma NN$	KK	Σ^*
$\Sigma NN \to \Sigma NN$	$K\eta$	Σ^*
$\Sigma NN \to \Sigma NN$	$\eta\eta$	Σ^*

TABLE 7.2: Enhanced three-body interactions through decuplet saturation for strangeness 0 and -1 systems, with the diagram types: contact term, one-meson and two-meson exchange.

Obviously, the only unknown constant here is the combination $G_1 + 3G_2$. It is also interesting to see, that the (positive) sign of the constants C_i' for the contact interaction is already fixed, independently of the values of the two LECs G_1 and G_2.

In Tab. 7.2 we illustrate, which transitions are enhanced by which decuplet resonances for the three classes of diagrams in Fig. 6.1: contact interaction, one- and two-meson exchange. The transitions for strangeness -1 are mostly saturated by the Σ^* resonance alone. For some transitions involving pions also the Δ isobar contributes. Resonances with higher strangeness can not be reached. Note that in contrast to the NNN interaction, also the contact interaction and the one-meson exchange contribution are saturated by decuplet baryons.

8

SUMMARY AND CONCLUSIONS

In this thesis we have employed SU(3) chiral effective field theory to derive the forces between octet baryons $(N, \Lambda, \Sigma, \Xi)$ at next-to-leading order. The resulting baryon-baryon interaction has been applied to hyperon-nucleon scattering and the properties of hyperons in nuclear matter. First, we have given a concise overview of quantum chromodynamics with a special focus on the low-energy regime, that is governed by confinement and spontaneous chiral symmetry breaking. The basic concepts of chiral effective field theory as a low-energy effective field theory of QCD have been introduced. Chiral EFT exhibits the same symmetries and symmetry breaking patterns as the underlying theory, QCD, but it involves the appropriate low-energy degrees of freedom, namely the hadrons. In particular, we have considered the pseudoscalar-meson octet (π, K, η), the baryon octet and the baryon decuplet $(\Delta, \Sigma^*, \Xi^*, \Omega)$ explicitly. The construction principles of the chiral effective Lagrangian and the external-field method have been presented and the Weinberg power-counting scheme has been introduced.

We have explicitly presented the construction of the chiral Lagrangian in flavor SU(3) for the baryon-number-two sector up to $\mathcal{O}(q^2)$. The pure four-baryon contact terms at leading and next-to-leading order are essential for the baryon-baryon interaction and these include SU(3) symmetric as well as SU(3) symmetry breaking contributions. Especially, the term leading to an antisymmetric spin-orbit potential has been identified. Furthermore, the Lagrangian includes all external fields and, therefore, comprises four-baryon contact terms including Goldstone bosons or electroweak gauge bosons. Such vertices are, for example, important for the construction of the leading three-baryon interactions. Within SU(3) χEFT the baryon-baryon interaction potentials have been considered at NLO. The effective potentials include contributions from the (constructed) pure four-baryon contact terms, one-meson-exchange diagrams, and two-meson-exchange diagrams at one-loop level. Following the Weinberg power counting scheme, these potentials have been inserted into a regularized Lippmann-Schwinger equation to obtain the T-matrix for hyperon-nucleon scattering. The low-energy constants of the four-baryon contact terms represent the unresolved short-distance dynamics and are fitted to YN scattering data. Due to the sparse experimental data, SU(3) flavor symmetry has been imposed on the LECs. An excellent description of the available YN data has been achieved with χEFT, comparable to the most advanced phenomenological models. A considerable improvement by going from LO to NLO has been obtained and a reduction of the cutoff dependence has been observed.

We have applied these YN potentials to study the properties of hyperons in isospin symmetric and asymmetric infinite nuclear matter. The employed Brueckner-Hartree-Fock formalism has been reviewed, and self-consistent solutions of the angle-averaged Bethe-Goldstone equation with the gap and the continuous choice for the spectrum of intermediate states have been presented. Indeed, the chiral baryon-baryon potentials at

NLO are consistent with the empirical knowledge about hyperon single-particle potentials in nuclear matter. In particular, the exceptionally weak Λ-nuclear spin-orbit force has been obtained from the contact term responsible for an antisymmetric spin-orbit interaction. A compensation between ordinary spin-orbit and antisymmetric spin-orbit components is at work. The potential depth of Λ hyperons in symmetric nuclear matter at saturation density is consistent with the empirical value of about -28 MeV. A repulsive Σ-nuclear potential has been produced, mainly by a repulsive ${}^3S_1$ ΣN ($I = 3/2$) interaction. Also the imaginary part of the Σ single-particle potential is consistent with experimental information from Σ^--atom data. Furthermore, predictions for the properties of hyperons in isospin-asymmetric nuclear matter and pure neutron matter for various densities have been presented. The Λ single-particle potential stays attractive for the considered density range $\rho/\rho_0 = 0.5 \ldots 1.5$ and is almost independent of the composition of the nuclear matter. For low densities the Σ single-particle potential can be attractive, whereas for higher densities, especially at saturation density, one obtains the required repulsion. In asymmetric nuclear matter the single-particle potentials of the $\Sigma^+, \Sigma^0, \Sigma^-$ hyperons split. The splitting as obtained in our microscopic calculation features a non-linear dependence on the isospin asymmetry, which goes beyond the usual (linear) parametrization in terms of an isovector Lane potential. Moving to higher densities and beta-stable hypernuclear matter will be an interesting future extension of our investigations. It will allow to study on the basis of the chiral YN interaction the equation of state of neutron star matter with hyperonic degrees of freedom and allow to address the hyperon puzzle (see Chapter 1).

Three-baryon forces are also often quoted as a possible solution to the hyperon puzzle. In this work we have derived the leading three-baryon forces in SU(3) χEFT, which formally start to contribute at NNLO. They consist of a three-baryon contact interaction, a one-meson exchange and a two-meson exchange component. We have established the minimal non-relativistic Lagrangian for the contact interaction, leading to 18 LECs. SU(3) relations following from group theory have been presented for the strangeness 0 and -1 sectors. Furthermore, the minimal chiral Lagrangian involving four baryon and one meson exhibits 14 LECs for the whole SU(3) sector, ranging from strangeness 0 to -6. For specific processes much fewer constants contribute. We have presented explicitly potentials for the ΛNN interaction in the spin and isospin basis. Parts of the leading order three-baryon forces involve unnaturally large LECs, which can be explained by a coupling to intermediate decuplet baryons, such as the $\Sigma^*(1385)$. The pertinent chiral Lagrangian has been constructed. Diagrams involving decuplet baryons give a three-body contribution at NLO. These diagrams can be employed to estimate the LECs of the general three-baryon forces at NNLO. One is left with only two unknown LECs for the whole SU(3) sector. We hope that these potentials will shed some light on the effect of three-baryon forces in nuclear systems with strangeness, such as hypernuclei. Future applications of our chiral potentials could include calculations of light hypernuclei through Faddeev or Yakubovsky equations as well as investigations of baryonic matter at saturation density and beta-stable neutron-star matter within the Brueckner-Hartree-Fock formalism.

In summary, we have derived the two- and three-baryon forces at next-to-leading order in SU(3) chiral effective field theory. The available YN scattering data as well as the empirical constraints on the hyperon single-particle potentials in nuclear matter can be successfully described. We can conclude, that χEFT is an excellent tool to construct the interaction among baryons in a systematic way and that lays the foundation to many promising applications in strangeness nuclear physics.

A

APPENDIX

A.1 CONVENTIONS

- We use units such that $c = \hbar = 1$.
- We use the Einstein summation convention: summation over repeated indices (lower and upper) is implicitly understood.
- The metric tensor in Minkowski space is given by $g_{\mu\nu} = g^{\mu\nu} = \mathrm{diag}\,(1, -1, -1, -1)$.
- The space-time four-vector x in Minkowski space is in its contravariant form given by $x^\mu = (t, \vec{x}\,)^\top$ and in covariant form by $x_\mu = (t, -\vec{x}\,)^\top = g_{\mu\nu} x^\nu$. The inner product is given by $a_\mu b^\mu = a_0 b_0 - \vec{a} \cdot \vec{b}$.
- The four gradient reads $\partial_\mu = \frac{\partial}{\partial x^\mu} = \left(\frac{\partial}{\partial t}, \vec{\nabla}\right)^\top$ and the four-momentum vector reads $p^\mu = \left(p^0, \vec{p}\right)^\top = (E, \vec{p}\,)^\top$.
- A commutator is defined by $[a, b] = ab - ba$, an anticommutator by $\{a, b\} = ab + ba$.
- We use the totally antisymmetric Levi-Civita tensor in three and four dimensions, ϵ_{ijk} and $\epsilon_{\mu\nu\rho\sigma}$, with the normalization $\epsilon_{123} = 1$ and $\epsilon^{0123} = -\epsilon_{0123} = 1$.
- The Lie group SU(2) is generated by $\{\mathrm{i}\sigma_i/2\}$, where σ_i are the Pauli matrices

$$\sigma_1 = \begin{pmatrix} 0 & 1 \\ 1 & 0 \end{pmatrix}, \quad \sigma_2 = \begin{pmatrix} 0 & -\mathrm{i} \\ \mathrm{i} & 0 \end{pmatrix}, \quad \sigma_3 = \begin{pmatrix} 1 & 0 \\ 0 & -1 \end{pmatrix}, \tag{A.1}$$

  which fulfill the relations

$$\sigma_i \sigma_j = \delta_{ij} + \mathrm{i}\epsilon_{ijk}\sigma_k\,, \quad [\sigma_i, \sigma_j] = 2\mathrm{i}\epsilon_{ijk}\sigma_k\,, \quad \{\sigma_i, \sigma_j\} = 2\delta_{ij}\,. \tag{A.2}$$

  In spin and isospin space, the Pauli matrices are denoted by σ_i and τ_i, respectively.
- We use $\{\mathrm{i}\lambda_i/2\}$ as generators for the Lie group SU(3) with the Gell-Mann matrices,

$$\lambda_1 = \begin{pmatrix} 0 & 1 & 0 \\ 1 & 0 & 0 \\ 0 & 0 & 0 \end{pmatrix}, \quad \lambda_2 = \begin{pmatrix} 0 & -\mathrm{i} & 0 \\ \mathrm{i} & 0 & 0 \\ 0 & 0 & 0 \end{pmatrix}, \quad \lambda_3 = \begin{pmatrix} 1 & 0 & 0 \\ 0 & -1 & 0 \\ 0 & 0 & 0 \end{pmatrix},$$
$$\lambda_4 = \begin{pmatrix} 0 & 0 & 1 \\ 0 & 0 & 0 \\ 1 & 0 & 0 \end{pmatrix}, \quad \lambda_5 = \begin{pmatrix} 0 & 0 & -\mathrm{i} \\ 0 & 0 & 0 \\ \mathrm{i} & 0 & 0 \end{pmatrix}, \quad \lambda_6 = \begin{pmatrix} 0 & 0 & 0 \\ 0 & 0 & 1 \\ 0 & 1 & 0 \end{pmatrix},$$
$$\lambda_7 = \begin{pmatrix} 0 & 0 & 0 \\ 0 & 0 & -\mathrm{i} \\ 0 & \mathrm{i} & 0 \end{pmatrix}, \quad \lambda_8 = \frac{1}{\sqrt{3}} \begin{pmatrix} 1 & 0 & 0 \\ 0 & 1 & 0 \\ 0 & 0 & -2 \end{pmatrix}. \tag{A.3}$$

Their commutator reads

$$\left[\frac{\lambda_a}{2}, \frac{\lambda_b}{2}\right] = \mathrm{i} f_{abc} \frac{\lambda_c}{2}\,, \tag{A.4}$$

where f_{abc} are the totally antisymmetric, real structure constants of SU(3). Up to permutations, the non-vanishing values are

$$f_{123} = 1,\ f_{147} = f_{165} = f_{246} = f_{257} = f_{345} = f_{376} = \frac{1}{2},\ f_{458} = f_{678} = \frac{\sqrt{3}}{2}. \tag{A.5}$$

The Gell-Mann matrices are traceless, Hermitian and trace orthogonal:

$$\mathrm{tr}\,(\lambda_a) = 0\,, \quad \lambda_a^\dagger = \lambda_a\,, \quad \mathrm{tr}\,(\lambda_a \lambda_b) = 2\delta_{ab}\,. \tag{A.6}$$

- The four gamma matrices in Dirac representation are

$$\gamma^\mu = \left(\gamma^0, \vec{\gamma}\right)^\top\,, \quad \gamma^0 = \begin{pmatrix} \mathbb{1} & 0 \\ 0 & -\mathbb{1} \end{pmatrix}\,, \quad \vec{\gamma} = \begin{pmatrix} 0 & \vec{\sigma} \\ -\vec{\sigma} & 0 \end{pmatrix}\,. \tag{A.7}$$

Additionally we define the commutator $\sigma^{\mu\nu} = \frac{\mathrm{i}}{2}\left[\gamma^\mu, \gamma^\nu\right]$ and the chirality matrix $\gamma^5 = \gamma_5 = \mathrm{i}\gamma^0\gamma^1\gamma^2\gamma^3 = -\frac{\mathrm{i}}{4!}\epsilon^{\mu\nu\rho\sigma}\gamma_\mu\gamma_\nu\gamma_\rho\gamma_\sigma = \begin{pmatrix} 0 & \mathbb{1} \\ \mathbb{1} & 0 \end{pmatrix}$. These matrices satisfy the relations

$$\begin{aligned} &\{\gamma^\mu, \gamma^\nu\} = 2g^{\mu\nu}\,, \qquad \gamma_0^\dagger = \gamma_0\,, \qquad \gamma^{i\dagger} = -\gamma^i\,, \\ &\gamma_5^\dagger = \gamma_5\,, \qquad \{\gamma^\mu, \gamma_5\} = 0\,, \qquad \gamma_5^2 = 1\,, \qquad \sigma^{\mu\nu} = -\sigma^{\nu\mu}\,. \end{aligned} \tag{A.8}$$

The 16 matrices $\{\mathbb{1}, \gamma^\mu, \gamma_5, \gamma^\mu\gamma_5, \sigma^{\mu\nu}\}$ of scalar, vector, pseudo-scalar, pseudo-vector and tensor type are basis elements for the operators involved in baryon bilinears (i.e., any Dirac matrix).

- Feynman slashed four-vectors are defined as $\not{a} = \gamma^\mu a_\mu$.
- The left- and right-handed projection operators $P_\mathrm{L} = \frac{1}{2}\left(1 - \gamma_5\right)$ and $P_\mathrm{R} = \frac{1}{2}\left(1 + \gamma_5\right)$ have the properties $P_{\mathrm{L/R}} = P_{\mathrm{L/R}}^\dagger$, $P_\mathrm{R} + P_\mathrm{L} = 1$, $P_{\mathrm{L/R}}^2 = P_{\mathrm{L/R}}$, $P_\mathrm{R} P_\mathrm{L} = P_\mathrm{L} P_\mathrm{R} = 0\,$.
- The free Dirac spinors have the form

$$u(\vec{p}, s) = \sqrt{\frac{E + M_0}{2M_0}} \begin{pmatrix} \chi_s \\ \frac{\vec{\sigma}\cdot\vec{p}}{E + M_0}\chi_s \end{pmatrix}\,, \tag{A.9}$$

with M_0 the baryon mass and the energy $E = \sqrt{M_0^2 + \vec{p}^{\,2}}\,$. For $\vec{p} \parallel \vec{e}_z$ the two-component helicity spinors are given by

$$\chi_{s=+\frac{1}{2}} = \begin{pmatrix} 1 \\ 0 \end{pmatrix}\,, \quad \chi_{s=-\frac{1}{2}} = \begin{pmatrix} 0 \\ 1 \end{pmatrix}\,. \tag{A.10}$$

The Dirac spinors fulfill the normalization (with $\bar{u}(\vec{p}, s) = u^\dagger(\vec{p}, s)\gamma^0$)

$$u^\dagger(\vec{p}, s) u(\vec{p}, s') = \frac{E}{M_0}\delta_{ss'}\,, \quad \bar{u}(\vec{p}, s) u(\vec{p}, s') = \delta_{ss'}\,. \tag{A.11}$$

- An expansion of baryon bilinears in the inverse large baryon mass results in:

$$
\begin{aligned}
\bar{u}(\vec{p}\,',s')\,\mathbb{1}\,u(\vec{p},s) &\approx 1 \;+\; \frac{p^2+p'^2}{8M_0^2} - \frac{\vec{\sigma}\cdot\vec{p}\,'\;\vec{\sigma}\cdot\vec{p}}{4M_0^2}\,, \\
\bar{u}(\vec{p}\,',s')\,\gamma^0\,u(\vec{p},s) &\approx 1 \;+\; \frac{p^2+p'^2}{8M_0^2} + \frac{\vec{\sigma}\cdot\vec{p}\,'\;\vec{\sigma}\cdot\vec{p}}{4M_0^2}\,, \\
\bar{u}(\vec{p}\,',s')\,\vec{\gamma}\,u(\vec{p},s) &\approx \vec{0} \;+\; \frac{(\vec{p}+\vec{p}\,')+\mathrm{i}(\vec{p}-\vec{p}\,')\times\vec{\sigma}}{2M_0}\,, \\
\bar{u}(\vec{p}\,',s')\,\gamma_5\,u(\vec{p},s) &\approx 0 \;+\; \frac{\vec{\sigma}\cdot(\vec{p}-\vec{p}\,')}{2M_0}\,, \\
\bar{u}(\vec{p}\,',s')\,\gamma^0\gamma_5\,u(\vec{p},s) &\approx 0 \;+\; \frac{\vec{\sigma}\cdot(\vec{p}+\vec{p}\,')}{2M_0}\,, \\
\bar{u}(\vec{p}\,',s')\,\vec{\gamma}\gamma_5\,u(\vec{p},s) &\approx \vec{\sigma} + \frac{p^2+p'^2}{8M_0^2}\vec{\sigma} + \frac{\vec{\sigma}\cdot\vec{p}\,'\;\vec{\sigma}\;\vec{\sigma}\cdot\vec{p}}{4M_0^2}\,, \\
\bar{u}(\vec{p}\,',s')\,\sigma^{0l}\,u(\vec{p},s) &\approx 0 \;+\; \mathrm{i}\frac{(p^l-p'^l)+\mathrm{i}\epsilon^{lmn}(p^m+p'^m)\sigma^n}{2M_0}\,, \\
\bar{u}(\vec{p}\,',s')\,\sigma^{kl}\,u(\vec{p},s) &\approx \epsilon^{klm}\sigma^m \;+\; \epsilon^{klm}\frac{p^2+p'^2}{8M_0^2}\sigma^m - \epsilon^{klm}\frac{\vec{\sigma}\cdot\vec{p}\,'\;\sigma^m\;\vec{\sigma}\cdot\vec{p}}{4M_0^2}\,.
\end{aligned}
\tag{A.12}
$$

  where we have dropped the Pauli spinors $\chi^\dagger_{s'}$ and χ_s to the left and right of the spin-operator.

- The spin $\frac{1}{2}$ to $\frac{3}{2}$ transition operators $\vec{S}$ are defined by [182]:

$$
\langle \tfrac{3}{2}m'|\vec{S}^\dagger|\tfrac{1}{2}m\rangle = \sum_{\lambda=-1}^{1} C^{1\frac{1}{2}\frac{3}{2}}_{\lambda m m'}\hat{e}^*_\lambda\,,
\tag{A.13}
$$

  where $*$ denotes the complex conjugate and C are the Clebsch-Gordon coefficients. The spherical basis vectors read

$$
\hat{e}_{+1} = -\frac{1}{\sqrt{2}}\begin{pmatrix}1\\ \mathrm{i}\\ 0\end{pmatrix}\,,\quad \hat{e}_0 = \begin{pmatrix}0\\0\\1\end{pmatrix}\,,\quad \hat{e}_{-1} = \frac{1}{\sqrt{2}}\begin{pmatrix}1\\ -\mathrm{i}\\ 0\end{pmatrix}\,.
\tag{A.14}
$$

  This leads to the explicit form of the 2×4 transition matrices

$$
\begin{aligned}
S_1 &= \begin{pmatrix} -\frac{1}{\sqrt{2}} & 0 & \frac{1}{\sqrt{6}} & 0 \\ 0 & -\frac{1}{\sqrt{6}} & 0 & \frac{1}{\sqrt{2}} \end{pmatrix}, \\
S_2 &= \begin{pmatrix} -\frac{i}{\sqrt{2}} & 0 & -\frac{i}{\sqrt{6}} & 0 \\ 0 & -\frac{i}{\sqrt{6}} & 0 & -\frac{i}{\sqrt{2}} \end{pmatrix}, \\
S_3 &= \begin{pmatrix} 0 & \sqrt{\frac{2}{3}} & 0 & 0 \\ 0 & 0 & \sqrt{\frac{2}{3}} & 0 \end{pmatrix}.
\end{aligned}
\tag{A.15}
$$

  They fulfill the relation $S_i {S_j}^\dagger = \frac{1}{3}(2\delta_{ij} - \mathrm{i}\epsilon_{ijk}\sigma_k)$.

A.2 THREE-BARYON SU(3) RELATIONS FOR $S = -2$

In this section, we extend Tab. 6.4 of Subsec. 6.1.4 to strangeness -2. The SU(3) relations for non-vanishing partial wave amplitudes of three baryons can be found in Tab. A.1. The full redefinition of the 18 LECs of the minimal contact Lagrangian Eq. (6.12) into constants associated to transitions between irreducible representations is given by

$$
\begin{aligned}
c_{\overline{35}} &= -6(C_4 - C_9)\,, \\
c_{35} &= 3(C_4 - C_9 + 6C_{18})\,, \\
c_{10} &= 3(C_2 - C_3 + C_4 + C_5 - 6C_7 + 6C_8 - C_9 - 6C_{10} \\
&\quad + 3C_{12} - 3C_{13} + 3C_{14} + 6C_{16} + 6C_{17} - 6C_{18})\,, \\
c_{\overline{10}} &= -\frac{3}{4}(-2C_2 - C_3 + C_4 - C_5 + 6C_8 - C_9 + 6C_{10} + 6C_{12} - 3C_{13} - 3C_{14} - 6C_{17} + 6C_{18})\,, \\
c_{27^1} &= -\frac{37}{294}C_2 + \frac{769}{588}C_3 - \frac{473}{392}C_4 + \frac{769}{588}C_5 - \frac{74}{49}C_7 - \frac{429}{98}C_8 + \frac{473}{392}C_9 - \frac{429}{98}C_{10} \\
&\quad + \frac{185}{98}C_{12} + \frac{89}{196}C_{13} + \frac{89}{196}C_{14} + \frac{244}{49}C_{16} - \frac{207}{98}C_{17} + \frac{57}{14}C_{18}\,, \\
c_{27^2} &= -\frac{1}{24}(4C_2 + 22C_3 - 57C_4 + 22C_5 + 48C_7 + 12C_8 + 57C_9 + 12C_{10} \\
&\quad - 60C_{12} - 78C_{13} - 78C_{14} + 96C_{16} - 60C_{17} + 252C_{18})\,, \\
c_{27^3} &= -\frac{1}{8}(-20C_2 + 2C_3 + 21C_4 + 2C_5 + 16C_7 - 28C_8 - 21C_9 - 28C_{10} \\
&\quad + 44C_{12} + 22C_{13} + 22C_{14} - 32C_{16} + 76C_{17} - 12C_{18})\,, \\
c_{8^1} &= -\frac{3}{2}C_1 - 9C_{10} - \frac{1}{96}(-252C_2 - 48C_3 + 405C_4 - 176C_5 + 288C_6 + 312C_7 + 288C_8 - 405C_9 \\
&\quad - 720C_{11} + 444C_{12} - 144C_{13} - 336C_{14} + 864C_{15} - 1464C_{16} + 336C_{17} - 1206C_{18})\,, \\
c_{8^2} &= -\frac{1}{6}(9C_2 + 3C_3 - 36C_4 + 11C_5 - 6C_7 - 18C_8 + 36C_9 - 18C_{10} - 21C_{12} + 9C_{13} \\
&\quad - 15C_{14} - 108C_{15} + 78C_{16} + 6C_{17} + 99C_{18})\,, \\
c_{8^3} &= -\frac{1}{48}(-96C_1 - 216C_2 - 84C_3 + 1449C_4 - 116C_5 + 384C_6 + 96C_7 + 504C_8 \\
&\quad - 1449C_9 + 696C_{10} - 96C_{11} + 552C_{12} - 252C_{13} - 348C_{14} \\
&\quad + 5328C_{15} - 2112C_{16} - 2616C_{17} - 3906C_{18})\,, \\
c_{8^4} &= -\frac{1}{296}(48C_1 - 114C_2 - 69C_3 + 108C_4 - 53C_5 - 192C_6 - 48C_7 + 414C_8 - 108C_9 + 318C_{10} \\
&\quad + 48C_{11} + 390C_{12} - 207C_{13} - 159C_{14} - 1608C_{16} + 642C_{17} - 1377C_{18})\,, \\
c_{8^5} &= -\frac{9}{368}(24C_1 + 12C_2 - 15C_4 + 8C_5 - 96C_6 - 24C_7 + 15C_9 - 48C_{10} + 24C_{11} \\
&\quad - 12C_{12} + 24C_{14} + 24C_{16} - 208C_{17} - 102C_{18})\,, \\
c_{8^6} &= -\frac{1}{384}(-24C_1 - 12C_2 + 27C_4 - 8C_5 + 96C_6 + 24C_7 - 27C_9 + 48C_{10} - 24C_{11} \\
&\quad + 12C_{12} - 24C_{14} - 24C_{16} - 48C_{17} - 162C_{18})\,, \\
c_{\overline{10}a} &= 6(-C_2 + C_3 - C_4 + C_5 - 2C_7 + 2C_8 - C_9 + 2C_{10} - C_{12} + C_{13} + C_{14})\,, \\
c_{10a} &= 6(C_2 - C_3 - C_4 + C_5 + 2C_7 - 2C_8 - C_9 + 2C_{10} + C_{12} - C_{13} + C_{14})\,, \\
c_{8a} &= -3(C_1 + 3C_4 + 2C_5 + 2C_6 + 3C_9 + 4C_{10} + C_{11} + 2C_{14})\,, \\
c_{27a} &= \frac{2}{3}(C_2 + C_3 + 3C_4 + C_5 + 2C_7 + 2C_8 + 3C_9 + 2C_{10} + C_{12} + C_{13} + C_{14})\,, \\
c_{1a} &= \frac{9}{2}(5C_4 + 3C_5 + 5C_9 + 6C_{10} + 3C_{14})\,.
\end{aligned}
\tag{A.16}
$$

As in Eq. (6.20) this definition is not unique. Linear combinations of the c_{8^i} and c_{27^i} constants (associated to representations of the same type) work equally well. Note that in Tab. 6.3 the representations **8** always appear together with **27**, hence, it is not possible to distinguish between them uniquely.

TABLE A.1: SU(3) relations of three-baryon contact terms with strangeness -2 in non-vanishing partial waves.

transition	I	i_{in}	i_{out}	$V_{0^2S_{1/2}\to 0^2S_{1/2}}$	$V_{0^2S_{1/2}\to 1^2S_{1/2}}$	$V_{1^2S_{1/2}\to 0^2S_{1/2}}$	$V_{1^2S_{1/2}\to 1^2S_{1/2}}$	$V_{1^4S_{3/2}\to 1^4S_{3/2}}$
$\Lambda\Lambda N \to \Lambda\Lambda N$	$\frac{1}{2}$	0	0	$c_{\overline{10}} + \frac{79c_{27^1}}{128} + \frac{61c_{27^2}}{49} - \frac{43c_{27^3}}{128} + \frac{7c_{\overline{35}}}{16} + c_{8^1}$	0	0	0	0
$\Lambda\Sigma N \to \Lambda\Sigma N$	$\frac{1}{2}$	1	1	$\frac{55c_{27^1}}{128} - \frac{27c_{27^2}}{49} - \frac{51c_{27^3}}{128} + \frac{c_{\overline{35}}}{4} + c_{8^1} + c_{8^2}$	$\frac{23\sqrt{3}c_{27^1}}{256} - \frac{71\sqrt{3}c_{27^2}}{392} - \frac{51\sqrt{3}c_{27^3}}{256} + \frac{\sqrt{3}c_{\overline{35}}}{8} - \frac{\sqrt{3}c_{8^2}}{8} + \frac{\sqrt{3}c_{8^3}}{148} - \frac{22c_{8^4}}{23\sqrt{3}} + \frac{c_{8^5}}{3\sqrt{3}} - 8\sqrt{3}c_{8^6}$	$\frac{23\sqrt{3}c_{27^1}}{256} - \frac{71\sqrt{3}c_{27^2}}{392} - \frac{51\sqrt{3}c_{27^3}}{256} + \frac{\sqrt{3}c_{\overline{35}}}{8} - \frac{\sqrt{3}c_{8^2}}{8} + \frac{\sqrt{3}c_{8^3}}{148} - \frac{22c_{8^4}}{23\sqrt{3}} + \frac{c_{8^5}}{3\sqrt{3}} - 8\sqrt{3}c_{8^6}$	$\frac{c_{\overline{10}}}{3} - \frac{35c_{27^1}}{128} + \frac{13c_{27^2}}{28} - \frac{17c_{27^3}}{128} + \frac{7c_{\overline{35}}}{48} + \frac{c_{8^2}}{4} + \frac{3c_{8^3}}{74} + \frac{16c_{8^4}}{69} - \frac{7c_{8^5}}{9} + 8c_{8^6}$	$\frac{c_{\overline{10}a}}{4} - \frac{3c_{27a}}{4} - \frac{c_{8a}}{3}$
$\Lambda\Sigma N \to \Lambda\Sigma N$	$\frac{3}{2}$	1	1	$\frac{c_{10}}{8} + \frac{25c_{27^1}}{128} + \frac{129c_{27^2}}{392} - \frac{45c_{27^3}}{128} + \frac{7c_{35}}{32} + \frac{c_{\overline{35}}}{8}$	$-\frac{c_{10}}{8\sqrt{3}} - \frac{15\sqrt{3}c_{27^1}}{128} + \frac{25\sqrt{3}c_{27^2}}{196} + \frac{11\sqrt{3}c_{27^3}}{128} + \frac{13c_{35}}{32\sqrt{3}} - \frac{\sqrt{3}c_{\overline{35}}}{8}$	$-\frac{c_{10}}{8\sqrt{3}} - \frac{15\sqrt{3}c_{27^1}}{128} + \frac{25\sqrt{3}c_{27^2}}{196} + \frac{11\sqrt{3}c_{27^3}}{128} + \frac{13c_{35}}{32\sqrt{3}} - \frac{\sqrt{3}c_{\overline{35}}}{8}$	$\frac{c_{10}}{24} + \frac{27c_{27^1}}{128} + \frac{57c_{27^2}}{392} + \frac{9c_{27^3}}{128} + \frac{47c_{35}}{96} + \frac{3c_{\overline{35}}}{8}$	$\frac{c_{10a}}{8} + \frac{9c_{27a}}{8}$
$\Sigma\Sigma N \to \Sigma\Sigma N$	$\frac{1}{2}$	0	0	$\frac{c_{\overline{10}}}{3} + \frac{459c_{27^1}}{128} - \frac{15c_{27^2}}{98} + \frac{297c_{27^3}}{128} - \frac{c_{\overline{35}}}{48} + \frac{c_{8^1}}{3} + \frac{41c_{8^2}}{6} + c_{8^3}$	0	0	0	0
$\Sigma\Sigma N \to \Sigma\Sigma N$	$\frac{1}{2}$	1	0	0	0	$-\sqrt{\frac{2}{3}}c_{\overline{10}} + \frac{15}{32}\sqrt{\frac{3}{2}}c_{27^1} - \frac{123}{49}\sqrt{\frac{3}{2}}c_{27^2} - \frac{11}{32}\sqrt{\frac{3}{2}}c_{27^3} + \frac{c_{\overline{35}}}{8\sqrt{6}} - \sqrt{\frac{2}{3}}c_{8^1} + \frac{17c_{8^2}}{2\sqrt{6}} + \frac{21}{37}\sqrt{\frac{3}{2}}c_{8^3} + \frac{38}{23}\sqrt{\frac{2}{3}}c_{8^4} - \frac{13c_{8^5}}{\sqrt{6}} - 12\sqrt{6}c_{8^6}$	0	0

. . . continues on next page

TABLE A.1: (... continued)

transition	I	i_{in}	i_{out}	$V_{0^2S_{1/2}\to 0^2S_{1/2}}$	$V_{0^2S_{1/2}\to 1^2S_{1/2}}$	$V_{1^2S_{1/2}\to 0^2S_{1/2}}$	$V_{1^2S_{1/2}\to 1^2S_{1/2}}$	$V_{1^4S_{3/2}\to 1^4S_{3/2}}$
$\Sigma\Sigma N \to \Sigma\Sigma N$	$\frac{1}{2}$	0	1	0	$-\sqrt{\frac{2}{3}}c_{\overline{10}} + \frac{15}{32}\sqrt{\frac{3}{2}}c_{27^1} - \frac{123}{49}\sqrt{\frac{3}{2}}c_{27^2} - \frac{11}{32}\sqrt{\frac{3}{2}}c_{27^3} + \frac{c_{\overline{35}}}{8\sqrt{6}} - \sqrt{\frac{2}{3}}c_{8^1} + \frac{17c_{8^2}}{2\sqrt{6}} + \frac{21}{37}\sqrt{\frac{3}{2}}c_{8^3} + \frac{38}{23}\sqrt{\frac{2}{3}}c_{8^4} - \frac{13c_{8^5}}{\sqrt{6}} - 12\sqrt{6}c_{8^6}$	0	0	0
$\Sigma\Sigma N \to \Sigma\Sigma N$	$\frac{1}{2}$	1	1	0	0	0	$2c_{\overline{10}} - \frac{77c_{27^1}}{64} - \frac{13c_{27^2}}{7} - \frac{95c_{27^3}}{64} - \frac{c_{\overline{35}}}{8} + 2c_{8^1} + 2c_{8^2} + \frac{12c_{8^3}}{37} - \frac{56c_{8^4}}{23} - \frac{10c_{8^5}}{3} - 48c_{8^6}$	$-6c_{27a} - 2c_{8a}$
$\Sigma\Sigma N \to \Sigma\Sigma N$	$\frac{3}{2}$	1	1	0	0	0	$\frac{c_{10}}{4} + \frac{121c_{27^1}}{64} + \frac{5c_{27^2}}{196} - \frac{77c_{27^3}}{64} + \frac{7c_{35}}{16} + \frac{c_{\overline{35}}}{4}$	$\frac{3c_{10a}}{4} + \frac{3c_{27a}}{4}$
$\Sigma\Sigma N \to \Sigma\Sigma N$	$\frac{3}{2}$	2	1	0	$\frac{1}{4}\sqrt{\frac{5}{3}}c_{10} - \frac{33\sqrt{15}c_{27^1}}{64} + \frac{3\sqrt{15}c_{27^2}}{49} + \frac{5\sqrt{15}c_{27^3}}{64} + \frac{\sqrt{15}c_{35}}{16} - \frac{1}{4}\sqrt{\frac{5}{3}}c_{\overline{35}}$	0	0	0
$\Sigma\Sigma N \to \Sigma\Sigma N$	$\frac{3}{2}$	1	2	0	0	$\frac{1}{4}\sqrt{\frac{5}{3}}c_{10} - \frac{33\sqrt{15}c_{27^1}}{64} + \frac{3\sqrt{15}c_{27^2}}{49} + \frac{5\sqrt{15}c_{27^3}}{64} + \frac{\sqrt{15}c_{35}}{16} - \frac{1}{4}\sqrt{\frac{5}{3}}c_{\overline{35}}$	0	0
$\Sigma\Sigma N \to \Sigma\Sigma N$	$\frac{3}{2}$	2	2	$\frac{5c_{10}}{12} + \frac{135c_{27^1}}{64} + \frac{285c_{27^2}}{196} + \frac{45c_{27^3}}{64} + \frac{11c_{35}}{48} + \frac{5c_{\overline{35}}}{12}$	0	0	0	0

... continues on next page

TABLE A.1: (... continued)

transition	I	i_{in}	i_{out}	$V_{0^2S_{1/2}\to 0^2S_{1/2}}$	$V_{0^2S_{1/2}\to 1^2S_{1/2}}$	$V_{1^2S_{1/2}\to 0^2S_{1/2}}$	$V_{1^2S_{1/2}\to 1^2S_{1/2}}$	$V_{1^4S_{3/2}\to 1^4S_{3/2}}$
$\Sigma\Sigma N \to \Sigma\Sigma N$	$\frac{5}{2}$	2	2	$2c_{35}$	0	0	0	0
$\Xi NN \to \Xi NN$	$\frac{1}{2}$	0	0	$-\frac{105c_{27^1}}{256} + \frac{39c_{27^2}}{56} - \frac{51c_{27^3}}{256} + \frac{c_{\overline{35}}}{8} + \frac{c_{8^1}}{2} + \frac{c_{8^2}}{2} + \frac{3c_{8^3}}{37} + c_{8^4}$	$-\frac{119\sqrt{3}c_{27^1}}{256} + \frac{23\sqrt{3}c_{27^2}}{56} + \frac{19\sqrt{3}c_{27^3}}{256} - \frac{\sqrt{3}c_{8^1}}{2} + \frac{\sqrt{3}c_{8^3}}{37} + \frac{20\sqrt{3}c_{8^4}}{23} - \sqrt{3}c_{8^5}$	$-\frac{119\sqrt{3}c_{27^1}}{256} + \frac{23\sqrt{3}c_{27^2}}{56} + \frac{19\sqrt{3}c_{27^3}}{256} - \frac{\sqrt{3}c_{8^1}}{2} + \frac{\sqrt{3}c_{8^3}}{37} + \frac{20\sqrt{3}c_{8^4}}{23} - \sqrt{3}c_{8^5}$	$\frac{2c_{\overline{10}}}{3} + \frac{517c_{27^1}}{256} + \frac{151c_{27^2}}{392} - \frac{89c_{27^3}}{256} - \frac{c_{\overline{35}}}{12} + \frac{3c_{8^1}}{2} + \frac{c_{8^2}}{2} - \frac{3c_{8^3}}{37} - \frac{143c_{8^4}}{69} + 2c_{8^5}$	$\frac{c_{\overline{10}a}}{8} - \frac{3c_{27a}}{8} - \frac{c_{8a}}{6}$
$\Xi NN \to \Xi NN$	$\frac{1}{2}$	1	0	$\frac{189\sqrt{3}c_{27^1}}{256} - \frac{3\sqrt{3}c_{27^2}}{56} + \frac{15\sqrt{3}c_{27^3}}{256} - \frac{c_{\overline{35}}}{4\sqrt{3}} + \frac{c_{8^1}}{2\sqrt{3}} - \frac{c_{8^2}}{\sqrt{3}} - \frac{3\sqrt{3}c_{8^3}}{37} - \frac{106c_{8^4}}{23\sqrt{3}} + \sqrt{3}c_{8^5}$	$-\frac{2c_{\overline{10}}}{3} - \frac{279c_{27^1}}{256} + \frac{171c_{27^2}}{392} + \frac{51c_{27^3}}{256} + \frac{c_{\overline{35}}}{12} - \frac{c_{8^1}}{2} - \frac{c_{8^2}}{2} + \frac{c_{8^3}}{37} + \frac{c_{8^4}}{3}$	$\frac{105c_{27^1}}{256} - \frac{39c_{27^2}}{56} + \frac{51c_{27^3}}{256} - \frac{c_{\overline{35}}}{8} - \frac{c_{8^1}}{2} - \frac{c_{8^2}}{2} - \frac{3c_{8^3}}{37} - c_{8^4}$	$\frac{119\sqrt{3}c_{27^1}}{256} + \frac{23\sqrt{3}c_{27^2}}{56} - \frac{19\sqrt{3}c_{27^3}}{256} + \frac{\sqrt{3}c_{8^1}}{2} - \frac{\sqrt{3}c_{8^3}}{37} - \frac{20\sqrt{3}c_{8^4}}{23} + \sqrt{3}c_{8^5}$	$-\frac{\sqrt{3}c_{\overline{10}a}}{8} + \frac{3\sqrt{3}c_{27a}}{8} + \frac{c_{8a}}{2\sqrt{3}}$
$\Xi NN \to \Xi NN$	$\frac{1}{2}$	0	1	$\frac{189\sqrt{3}c_{27^1}}{256} - \frac{3\sqrt{3}c_{27^2}}{56} + \frac{15\sqrt{3}c_{27^3}}{256} - \frac{c_{\overline{35}}}{4\sqrt{3}} + \frac{c_{8^1}}{2\sqrt{3}} - \frac{c_{8^2}}{\sqrt{3}} - \frac{3\sqrt{3}c_{8^3}}{37} - \frac{106c_{8^4}}{23\sqrt{3}} + \sqrt{3}c_{8^5}$	$\frac{105c_{27^1}}{256} - \frac{39c_{27^2}}{56} + \frac{51c_{27^3}}{256} - \frac{c_{\overline{35}}}{8} - \frac{c_{8^1}}{2} - \frac{c_{8^2}}{2} - \frac{3c_{8^3}}{37} - c_{8^4}$	$-\frac{2c_{\overline{10}}}{3} - \frac{279c_{27^1}}{256} + \frac{171c_{27^2}}{392} + \frac{51c_{27^3}}{256} + \frac{c_{\overline{35}}}{12} - \frac{c_{8^1}}{2} - \frac{c_{8^2}}{2} + \frac{c_{8^3}}{37} + \frac{c_{8^4}}{3}$	$\frac{119\sqrt{3}c_{27^1}}{256} + \frac{23\sqrt{3}c_{27^2}}{56} - \frac{19\sqrt{3}c_{27^3}}{256} + \frac{\sqrt{3}c_{8^1}}{2} - \frac{\sqrt{3}c_{8^3}}{37} - \frac{20\sqrt{3}c_{8^4}}{23} + \sqrt{3}c_{8^5}$	$-\frac{\sqrt{3}c_{\overline{10}a}}{8} + \frac{3\sqrt{3}c_{27a}}{8} + \frac{c_{8a}}{2\sqrt{3}}$
$\Xi NN \to \Xi NN$	$\frac{1}{2}$	1	1	$\frac{2c_{\overline{10}}}{3} - \frac{99c_{27^1}}{256} - \frac{129c_{27^2}}{392} - \frac{81c_{27^3}}{256} + \frac{c_{\overline{35}}}{12} + \frac{c_{8^1}}{6} + \frac{7c_{8^2}}{6} + \frac{5c_{8^3}}{37} + \frac{63c_{8^4}}{23} - 2c_{8^5}$	$-\frac{189\sqrt{3}c_{27^1}}{256} + \frac{3\sqrt{3}c_{27^2}}{56} - \frac{15\sqrt{3}c_{27^3}}{256} + \frac{c_{\overline{35}}}{4\sqrt{3}} - \frac{c_{8^1}}{2\sqrt{3}} + \frac{c_{8^2}}{\sqrt{3}} + \frac{3\sqrt{3}c_{8^3}}{37} + \frac{106c_{8^4}}{23\sqrt{3}} - \sqrt{3}c_{8^5}$	$-\frac{189\sqrt{3}c_{27^1}}{256} + \frac{3\sqrt{3}c_{27^2}}{56} - \frac{15\sqrt{3}c_{27^3}}{256} + \frac{c_{\overline{35}}}{4\sqrt{3}} - \frac{c_{8^1}}{2\sqrt{3}} + \frac{c_{8^2}}{\sqrt{3}} + \frac{3\sqrt{3}c_{8^3}}{37} + \frac{106c_{8^4}}{23\sqrt{3}} - \sqrt{3}c_{8^5}$	$-\frac{105c_{27^1}}{256} + \frac{39c_{27^2}}{56} - \frac{51c_{27^3}}{256} + \frac{c_{\overline{35}}}{8} + \frac{c_{8^1}}{2} + \frac{c_{8^2}}{2} + \frac{3c_{8^3}}{37} + c_{8^4}$	$\frac{3c_{\overline{10}a}}{8} - \frac{9c_{27a}}{8} - \frac{c_{8a}}{2}$
$\Xi NN \to \Xi NN$	$\frac{3}{2}$	1	1	$\frac{c_{10}}{12} + \frac{27c_{27^1}}{64} + \frac{57c_{27^2}}{196} + \frac{9c_{27^3}}{64} + \frac{7c_{35}}{48} + \frac{c_{\overline{35}}}{12}$	$-\frac{c_{10}}{4\sqrt{3}} - \frac{27\sqrt{3}c_{27^1}}{64} - \frac{57\sqrt{3}c_{27^2}}{196} - \frac{9\sqrt{3}c_{27^3}}{64} - \frac{7c_{35}}{16\sqrt{3}} - \frac{c_{\overline{35}}}{4\sqrt{3}}$	$-\frac{c_{10}}{4\sqrt{3}} - \frac{27\sqrt{3}c_{27^1}}{64} - \frac{57\sqrt{3}c_{27^2}}{196} - \frac{9\sqrt{3}c_{27^3}}{64} - \frac{7c_{35}}{16\sqrt{3}} - \frac{c_{\overline{35}}}{4\sqrt{3}}$	$\frac{c_{10}}{4} + \frac{81c_{27^1}}{64} + \frac{171c_{27^2}}{196} + \frac{27c_{27^3}}{64} + \frac{7c_{35}}{16} + \frac{c_{\overline{35}}}{4}$	0

... continues on next page

TABLE A.1: (... continued)

transition	I	i_{in}	i_{out}	$V_{0^2S_{1/2}\to 0^2S_{1/2}}$	$V_{0^2S_{1/2}\to 1^2S_{1/2}}$	$V_{1^2S_{1/2}\to 0^2S_{1/2}}$	$V_{1^2S_{1/2}\to 1^2S_{1/2}}$	$V_{1^4S_{3/2}\to 1^4S_{3/2}}$
$\Lambda\Lambda N \to \Lambda\Sigma N$	$\frac{1}{2}$	0	1	$-\frac{453c_{27^1}}{256} - \frac{225c_{27^2}}{392} - \frac{39c_{27^3}}{256} + \frac{3c_{\overline{35}}}{8} - c_{8^1} + \frac{c_{8^2}}{8} + \frac{15c_{8^3}}{148} + \frac{188c_{8^4}}{69} - \frac{19c_{8^5}}{9} + 8c_{8^6}$	$-\frac{c_{\overline{10}}}{\sqrt{3}} + \frac{137\sqrt{3}c_{27^1}}{256} + \frac{131\sqrt{3}c_{27^2}}{392} + \frac{147\sqrt{3}c_{27^3}}{256} + \frac{11c_{\overline{35}}}{16\sqrt{3}} + \frac{\sqrt{3}c_{8^2}}{8} - \frac{\sqrt{3}c_{8^3}}{148} - \frac{82c_{8^4}}{69\sqrt{3}} + \frac{43c_{8^5}}{18\sqrt{3}} - \frac{4c_{8^6}}{\sqrt{3}}$	0	0	0
$\Lambda\Lambda N \to \Sigma\Sigma N$	$\frac{1}{2}$	0	0	$\frac{c_{\overline{10}}}{\sqrt{3}} - \frac{37\sqrt{3}c_{27^1}}{64} - \frac{89\sqrt{3}c_{27^2}}{196} - \frac{23\sqrt{3}c_{27^3}}{64} - \frac{5c_{\overline{35}}}{16\sqrt{3}} - \frac{c_{8^1}}{\sqrt{3}} - \frac{7c_{8^2}}{4\sqrt{3}} - \frac{3\sqrt{3}c_{8^3}}{74} - \frac{16c_{8^4}}{23\sqrt{3}} - \frac{16c_{8^5}}{3\sqrt{3}}$	0	0	0	0
$\Lambda\Lambda N \to \Sigma\Sigma N$	$\frac{1}{2}$	0	1	0	$-\sqrt{2}c_{\overline{10}} - \frac{171c_{27^1}}{64\sqrt{2}} - \frac{9c_{27^2}}{98\sqrt{2}} - \frac{105c_{27^3}}{64\sqrt{2}} + \frac{5c_{\overline{35}}}{8\sqrt{2}} + \sqrt{2}c_{8^1} - \frac{c_{8^2}}{\sqrt{2}} - \frac{3\sqrt{2}c_{8^3}}{37} - \frac{106\sqrt{2}c_{8^4}}{69} - \frac{5c_{8^5}}{9\sqrt{2}} - 4\sqrt{2}c_{8^6}$	0	0	0
$\Lambda\Lambda N \to \Xi N N$	$\frac{1}{2}$	0	0	$-\frac{69c_{27^1}}{32\sqrt{2}} + \frac{33\sqrt{2}c_{27^2}}{49} + \frac{9c_{27^3}}{32\sqrt{2}} - \frac{3c_{\overline{35}}}{8\sqrt{2}} + \frac{c_{8^1}}{\sqrt{2}} + \frac{c_{8^2}}{4\sqrt{2}} + \frac{3c_{8^3}}{74\sqrt{2}} + \frac{53c_{8^4}}{69\sqrt{2}} + \frac{5c_{8^5}}{36\sqrt{2}} + \sqrt{2}c_{8^6}$	$-\sqrt{\frac{2}{3}}c_{\overline{10}} + \frac{197}{128}\sqrt{\frac{3}{2}}c_{27^1} - \frac{67}{196}\sqrt{\frac{3}{2}}c_{27^2} - \frac{25}{128}\sqrt{\frac{3}{2}}c_{27^3} + \frac{c_{\overline{35}}}{4\sqrt{6}} - \sqrt{\frac{3}{2}}c_{8^1} + \frac{\sqrt{6}c_{8^3}}{37} + \frac{323c_{8^4}}{69\sqrt{6}} - \frac{157c_{8^5}}{36\sqrt{6}} + 7\sqrt{\frac{2}{3}}c_{8^6}$	0	0	0

... continues on next page

TABLE A.1: (... continued)

transition	I	i_{in}	i_{out}	$V_{0^2S_{1/2}\to 0^2S_{1/2}}$	$V_{0^2S_{1/2}\to 1^2S_{1/2}}$	$V_{1^2S_{1/2}\to 0^2S_{1/2}}$	$V_{1^2S_{1/2}\to 1^2S_{1/2}}$	$V_{1^4S_{3/2}\to 1^4S_{3/2}}$
$\Lambda\Lambda N \to \Xi NN$	$\frac{1}{2}$	0	1	$\sqrt{\frac{2}{3}}c_{\overline{10}} - \frac{13}{128}\sqrt{\frac{3}{2}}c_{27^1} - \frac{109}{196}\sqrt{\frac{3}{2}}c_{27^2} + \frac{1}{128}\sqrt{\frac{3}{2}}c_{27^3} + \frac{c_{\overline{35}}}{2\sqrt{6}} + \frac{c_{8^1}}{\sqrt{6}} - \frac{c_{8^2}}{2\sqrt{6}} - \frac{3}{37}\sqrt{\frac{3}{2}}c_{8^3} - \frac{143c_{8^4}}{23\sqrt{6}} + \frac{49c_{8^5}}{12\sqrt{6}} - 3\sqrt{6}c_{8^6}$	$\frac{69c_{27^1}}{32\sqrt{2}} - \frac{33\sqrt{2}c_{27^2}}{49} - \frac{9c_{27^3}}{32\sqrt{2}} + \frac{3c_{\overline{35}}}{8\sqrt{2}} - \frac{c_{8^1}}{\sqrt{2}} - \frac{c_{8^2}}{4\sqrt{2}} - \frac{3c_{8^3}}{74\sqrt{2}} - \frac{53c_{8^4}}{69\sqrt{2}} - \frac{5c_{8^5}}{36\sqrt{2}} - \sqrt{2}c_{8^6}$	0	0	0
$\Lambda\Sigma N \to \Sigma\Sigma N$	$\frac{1}{2}$	1	0	$\frac{117\sqrt{3}c_{27^1}}{256} + \frac{197\sqrt{3}c_{27^2}}{392} + \frac{55\sqrt{3}c_{27^3}}{256} - \frac{c_{\overline{35}}}{8\sqrt{3}} + \frac{c_{8^1}}{\sqrt{3}} - \frac{7c_{8^2}}{8\sqrt{3}} - \frac{19\sqrt{3}c_{8^3}}{148} - \frac{100c_{8^4}}{23\sqrt{3}} + \frac{5c_{8^5}}{\sqrt{3}} + 24\sqrt{3}c_{8^6}$	0	$-\frac{c_{\overline{10}}}{3} - \frac{177c_{27^1}}{256} + \frac{393c_{27^2}}{392} - \frac{75c_{27^3}}{256} - \frac{c_{\overline{35}}}{48} - \frac{9c_{8^2}}{8} - \frac{23c_{8^3}}{148} + \frac{62c_{8^4}}{69} + \frac{c_{8^5}}{2} - 12c_{8^6}$	0	0
$\Lambda\Sigma N \to \Sigma\Sigma N$	$\frac{1}{2}$	1	1	0	$\frac{77c_{27^1}}{128\sqrt{2}} + \frac{47c_{27^2}}{28\sqrt{2}} + \frac{127c_{27^3}}{128\sqrt{2}} + \frac{c_{\overline{35}}}{4\sqrt{2}} - \sqrt{2}c_{8^1} - \frac{5c_{8^2}}{4\sqrt{2}} - \frac{3c_{8^3}}{74\sqrt{2}} + \frac{22\sqrt{2}c_{8^4}}{23} - \frac{\sqrt{2}c_{8^5}}{3} + 24\sqrt{2}c_{8^6}$	0	$\sqrt{\frac{2}{3}}c_{\overline{10}} + \frac{47}{128}\sqrt{\frac{3}{2}}c_{27^1} - \frac{13}{196}\sqrt{\frac{3}{2}}c_{27^2} + \frac{21}{128}\sqrt{\frac{3}{2}}c_{27^3} + \frac{c_{\overline{35}}}{8\sqrt{6}} - \frac{1}{4}\sqrt{\frac{3}{2}}c_{8^2} - \frac{7}{74}\sqrt{\frac{3}{2}}c_{8^3} + \frac{2\sqrt{6}c_{8^4}}{23} + 2\sqrt{\frac{2}{3}}c_{8^5}$	$-3\sqrt{\frac{3}{2}}c_{27a} - \sqrt{\frac{2}{3}}c_{8a}$
$\Lambda\Sigma N \to \Sigma\Sigma N$	$\frac{3}{2}$	1	1	0	$-\frac{c_{10}}{4\sqrt{2}} + \frac{55c_{27^1}}{64\sqrt{2}} + \frac{29c_{27^2}}{196\sqrt{2}} - \frac{67c_{27^3}}{64\sqrt{2}} - \frac{7c_{35}}{16\sqrt{2}} - \frac{c_{\overline{35}}}{4\sqrt{2}}$	0	$\frac{c_{10}}{4\sqrt{6}} - \frac{33}{64}\sqrt{\frac{3}{2}}c_{27^1} + \frac{3}{49}\sqrt{\frac{3}{2}}c_{27^2} + \frac{5}{64}\sqrt{\frac{3}{2}}c_{27^3} - \frac{13c_{35}}{16\sqrt{6}} + \frac{1}{4}\sqrt{\frac{3}{2}}c_{\overline{35}}$	$\frac{3}{4}\sqrt{\frac{3}{2}}c_{27a} - \frac{1}{4}\sqrt{\frac{3}{2}}c_{10a}$

... continues on next page

TABLE A.1: (... continued)

transition	I	i_{in}	i_{out}	$V_{0^2S_{1/2}\to 0^2S_{1/2}}$	$V_{0^2S_{1/2}\to 1^2S_{1/2}}$	$V_{1^2S_{1/2}\to 0^2S_{1/2}}$	$V_{1^2S_{1/2}\to 1^2S_{1/2}}$	$V_{1^4S_{3/2}\to 1^4S_{3/2}}$
$\Lambda\Sigma N\to\Sigma\Sigma N$	$\frac{3}{2}$	1	2	$-\frac{1}{4}\sqrt{\frac{5}{6}}c_{10}-\frac{15}{64}\sqrt{\frac{15}{2}}c_{27^1}+\frac{25}{98}\sqrt{\frac{15}{2}}c_{27^2}+\frac{11}{64}\sqrt{\frac{15}{2}}c_{27^3}-\frac{1}{16}\sqrt{\frac{15}{2}}c_{35}+\frac{1}{4}\sqrt{\frac{5}{6}}c_{\overline{35}}$	0	$\frac{1}{12}\sqrt{\frac{5}{2}}c_{10}+\frac{27}{64}\sqrt{\frac{5}{2}}c_{27^1}+\frac{57}{196}\sqrt{\frac{5}{2}}c_{27^2}+\frac{9}{64}\sqrt{\frac{5}{2}}c_{27^3}-\frac{1}{48}\sqrt{\frac{5}{2}}c_{35}-\frac{1}{4}\sqrt{\frac{5}{2}}c_{\overline{35}}$	0	0
$\Lambda\Sigma N\to\Xi NN$	$\frac{1}{2}$	1	0	$-\frac{39c_{27^1}}{128\sqrt{2}}-\frac{45c_{27^2}}{49\sqrt{2}}-\frac{93c_{27^3}}{128\sqrt{2}}-\frac{c_{\overline{35}}}{4\sqrt{2}}-\frac{c_{8^1}}{\sqrt{2}}+\frac{c_{8^2}}{2\sqrt{2}}+\frac{3\sqrt{2}c_{8^3}}{37}+\frac{83c_{8^4}}{23\sqrt{2}}-\frac{3c_{8^5}}{\sqrt{2}}$	$-\frac{121}{128}\sqrt{\frac{3}{2}}c_{27^1}-\frac{19}{49}\sqrt{\frac{3}{2}}c_{27^2}-\frac{3}{128}\sqrt{\frac{3}{2}}c_{27^3}+\sqrt{\frac{3}{2}}c_{8^1}+\frac{1}{2}\sqrt{\frac{3}{2}}c_{8^2}-\frac{\sqrt{6}c_{8^3}}{37}-\frac{83c_{8^4}}{23\sqrt{6}}+\sqrt{\frac{3}{2}}c_{8^5}$	$\frac{91}{128}\sqrt{\frac{3}{2}}c_{27^1}+\frac{1}{7}\sqrt{\frac{3}{2}}c_{27^2}+\frac{25}{128}\sqrt{\frac{3}{2}}c_{27^3}-\frac{1}{8}\sqrt{\frac{3}{2}}c_{\overline{35}}+\frac{1}{4}\sqrt{\frac{3}{2}}c_{8^2}+\frac{1}{74}\sqrt{\frac{3}{2}}c_{8^3}-\frac{22}{23}\sqrt{\frac{2}{3}}c_{8^4}+\frac{31c_{8^5}}{12\sqrt{6}}-\sqrt{6}c_{8^6}$	$\frac{\sqrt{2}c_{\overline{10}}}{3}-\frac{17c_{27^1}}{32\sqrt{2}}+\frac{97c_{27^2}}{196\sqrt{2}}+\frac{13c_{27^3}}{32\sqrt{2}}-\frac{c_{\overline{35}}}{12\sqrt{2}}-\frac{c_{8^2}}{2\sqrt{2}}-\frac{23c_{8^5}}{36\sqrt{2}}-7\sqrt{2}c_{8^6}$	$-\frac{c_{\overline{10}a}}{4\sqrt{2}}-\frac{3c_{27a}}{4\sqrt{2}}-\frac{c_{8a}}{3\sqrt{2}}$
$\Lambda\Sigma N\to\Xi NN$	$\frac{1}{2}$	1	1	$\frac{147}{128}\sqrt{\frac{3}{2}}c_{27^1}+\sqrt{\frac{3}{2}}c_{27^2}+\frac{65}{128}\sqrt{\frac{3}{2}}c_{27^3}+\frac{c_{\overline{35}}}{2\sqrt{6}}-\frac{c_{8^1}}{\sqrt{6}}-\frac{5c_{8^2}}{2\sqrt{6}}-\frac{\sqrt{6}c_{8^3}}{37}-\frac{83c_{8^4}}{23\sqrt{6}}+\sqrt{\frac{3}{2}}c_{8^5}$	$\frac{39c_{27^1}}{128\sqrt{2}}+\frac{45c_{27^2}}{49\sqrt{2}}+\frac{93c_{27^3}}{128\sqrt{2}}+\frac{c_{\overline{35}}}{4\sqrt{2}}+\frac{c_{8^1}}{\sqrt{2}}-\frac{c_{8^2}}{2\sqrt{2}}-\frac{3\sqrt{2}c_{8^3}}{37}-\frac{83c_{8^4}}{23\sqrt{2}}+\frac{3c_{8^5}}{\sqrt{2}}$	$-\frac{\sqrt{2}c_{\overline{10}}}{3}-\frac{57c_{27^1}}{64\sqrt{2}}-\frac{153c_{27^2}}{196\sqrt{2}}-\frac{51c_{27^3}}{64\sqrt{2}}+\frac{c_{\overline{35}}}{3\sqrt{2}}-\frac{c_{8^3}}{37\sqrt{2}}+\frac{44\sqrt{2}c_{8^4}}{69}-\frac{13c_{8^5}}{12\sqrt{2}}+9\sqrt{2}c_{8^6}$	$-\frac{91}{128}\sqrt{\frac{3}{2}}c_{27^1}-\frac{1}{7}\sqrt{\frac{3}{2}}c_{27^2}-\frac{25}{128}\sqrt{\frac{3}{2}}c_{27^3}+\frac{1}{8}\sqrt{\frac{3}{2}}c_{\overline{35}}-\frac{1}{4}\sqrt{\frac{3}{2}}c_{8^2}-\frac{1}{74}\sqrt{\frac{3}{2}}c_{8^3}+\frac{22}{23}\sqrt{\frac{2}{3}}c_{8^4}-\frac{31c_{8^5}}{12\sqrt{6}}+\sqrt{6}c_{8^6}$	$\frac{1}{4}\sqrt{\frac{3}{2}}c_{\overline{10}a}+\frac{3}{4}\sqrt{\frac{3}{2}}c_{27a}+\frac{c_{8a}}{\sqrt{6}}$

... continues on next page

TABLE A.1: (... continued)

transition	I	i_{in}	i_{out}	$V_{0^2S_{1/2}\to 0^2S_{1/2}}$	$V_{0^2S_{1/2}\to 1^2S_{1/2}}$	$V_{1^2S_{1/2}\to 0^2S_{1/2}}$	$V_{1^2S_{1/2}\to 1^2S_{1/2}}$	$V_{1^4S_{3/2}\to 1^4S_{3/2}}$
$\Lambda\Sigma N \to \Xi NN$	$\frac{3}{2}$	1	1	$-\frac{c_{10}}{4\sqrt{6}} + \frac{15}{64}\sqrt{\frac{3}{2}}c_{27^1} - \frac{25}{98}\sqrt{\frac{3}{2}}c_{27^2} - \frac{11}{64}\sqrt{\frac{3}{2}}c_{27^3} + \frac{1}{16}\sqrt{\frac{3}{2}}c_{35} + \frac{c_{\overline{35}}}{4\sqrt{6}}$	$\frac{c_{10}}{4\sqrt{2}} - \frac{45c_{27^1}}{64\sqrt{2}} + \frac{75c_{27^2}}{98\sqrt{2}} + \frac{33c_{27^3}}{64\sqrt{2}} - \frac{3c_{35}}{16\sqrt{2}} - \frac{c_{\overline{35}}}{4\sqrt{2}}$	$\frac{c_{10}}{12\sqrt{2}} - \frac{27c_{27^1}}{64\sqrt{2}} - \frac{57c_{27^2}}{196\sqrt{2}} - \frac{9c_{27^3}}{64\sqrt{2}} + \frac{17c_{35}}{48\sqrt{2}} - \frac{c_{\overline{35}}}{4\sqrt{2}}$	$-\frac{c_{10}}{4\sqrt{6}} + \frac{27}{64}\sqrt{\frac{3}{2}}c_{27^1} + \frac{57}{196}\sqrt{\frac{3}{2}}c_{27^2} + \frac{9}{64}\sqrt{\frac{3}{2}}c_{27^3} - \frac{17c_{35}}{16\sqrt{6}} + \frac{1}{4}\sqrt{\frac{3}{2}}c_{\overline{35}}$	0
$\Sigma\Sigma N \to \Xi NN$	$\frac{1}{2}$	0	0	$-\frac{63}{64}\sqrt{\frac{3}{2}}c_{27^1} - \frac{3}{7}\sqrt{\frac{3}{2}}c_{27^2} - \frac{69}{64}\sqrt{\frac{3}{2}}c_{27^3} + \frac{c_{\overline{35}}}{8\sqrt{6}} - \frac{c_{8^1}}{\sqrt{6}} - \frac{19c_{8^2}}{4\sqrt{6}} - \frac{15}{74}\sqrt{\frac{3}{2}}c_{8^3} - \frac{43c_{8^4}}{23\sqrt{6}} - \frac{19c_{8^5}}{4\sqrt{6}} + 3\sqrt{6}c_{8^6}$	$-\frac{\sqrt{2}c_{\overline{10}}}{3} + \frac{243c_{27^1}}{128\sqrt{2}} + \frac{477c_{27^2}}{196\sqrt{2}} + \frac{321c_{27^3}}{128\sqrt{2}} + \frac{c_{\overline{35}}}{12\sqrt{2}} + \frac{c_{8^1}}{\sqrt{2}} + \frac{c_{8^2}}{\sqrt{2}} - \frac{\sqrt{2}c_{8^3}}{37} - \frac{157c_{8^4}}{69\sqrt{2}} + \frac{59c_{8^5}}{12\sqrt{2}} + 21\sqrt{2}c_{8^6}$	0	0	0
$\Sigma\Sigma N \to \Xi NN$	$\frac{1}{2}$	1	0	0	0	$-\frac{69c_{27^1}}{64} + \frac{33c_{27^2}}{49} - \frac{39c_{27^3}}{64} - \frac{c_{\overline{35}}}{8} + c_{8^1} - \frac{5c_{8^2}}{4} - \frac{15c_{8^3}}{74} - \frac{39c_{8^4}}{23} + \frac{5c_{8^5}}{12} + 6c_{8^6}$	$\frac{2c_{\overline{10}}}{\sqrt{3}} + \frac{29\sqrt{3}c_{27^1}}{128} + \frac{17\sqrt{3}c_{27^2}}{196} + \frac{47\sqrt{3}c_{27^3}}{128} - \frac{c_{\overline{35}}}{4\sqrt{3}} - \sqrt{3}c_{8^1} + \frac{2\sqrt{3}c_{8^3}}{37} + \frac{83c_{8^4}}{23\sqrt{3}} - \frac{13c_{8^5}}{12\sqrt{3}} + 14\sqrt{3}c_{8^6}$	$-\frac{3\sqrt{3}c_{27a}}{2} - \frac{c_{8a}}{\sqrt{3}}$

... continues on next page

TABLE A.1: (... continued)

transition	I	i_{in}	i_{out}	$V_{0^2S_{1/2}\to 0^2S_{1/2}}$	$V_{0^2S_{1/2}\to 1^2S_{1/2}}$	$V_{1^2S_{1/2}\to 0^2S_{1/2}}$	$V_{1^2S_{1/2}\to 1^2S_{1/2}}$	$V_{1^4S_{3/2}\to 1^4S_{3/2}}$
$\Sigma\Sigma N\to\Xi NN$	$\frac{1}{2}$	0	1	$\frac{\sqrt{2}c_{\overline{10}}}{3}+\frac{9c_{27^1}}{128\sqrt{2}}-\frac{309c_{27^2}}{196\sqrt{2}}-\frac{45c_{27^3}}{128\sqrt{2}}-\frac{c_{\overline{35}}}{6\sqrt{2}}-\frac{c_{8^1}}{3\sqrt{2}}+\frac{13c_{8^2}}{6\sqrt{2}}+\frac{17c_{8^3}}{37\sqrt{2}}+\frac{81c_{8^4}}{23\sqrt{2}}-\frac{7c_{8^5}}{4\sqrt{2}}-27\sqrt{2}c_{8^6}$	$\frac{63}{64}\sqrt{\frac{3}{2}}c_{27^1}+\frac{3}{7}\sqrt{\frac{3}{2}}c_{27^2}+\frac{69}{64}\sqrt{\frac{3}{2}}c_{27^3}-\frac{c_{\overline{35}}}{8\sqrt{6}}+\frac{c_{8^1}}{\sqrt{6}}+\frac{19c_{8^2}}{4\sqrt{6}}+\frac{15}{74}\sqrt{\frac{3}{2}}c_{8^3}+\frac{43c_{8^4}}{23\sqrt{6}}+\frac{19c_{8^5}}{4\sqrt{6}}-3\sqrt{6}c_{8^6}$	0	0	0
$\Sigma\Sigma N\to\Xi NN$	$\frac{1}{2}$	1	1	0	0	$-\frac{2c_{\overline{10}}}{\sqrt{3}}+\frac{63\sqrt{3}c_{27^1}}{128}-\frac{15\sqrt{3}c_{27^2}}{28}+\frac{5\sqrt{3}c_{27^3}}{128}+\frac{c_{\overline{35}}}{2\sqrt{3}}+\frac{c_{8^1}}{\sqrt{3}}+\frac{5c_{8^2}}{2\sqrt{3}}+\frac{3\sqrt{3}c_{8^3}}{37}-\frac{5c_{8^4}}{23\sqrt{3}}+\frac{c_{8^5}}{4\sqrt{3}}-18\sqrt{3}c_{8^6}$	$\frac{69c_{27^1}}{64}-\frac{33c_{27^2}}{49}+\frac{39c_{27^3}}{64}+\frac{c_{\overline{35}}}{8}-c_{8^1}+\frac{5c_{8^2}}{4}+\frac{15c_{8^3}}{74}+\frac{39c_{8^4}}{23}-\frac{5c_{8^5}}{12}-6c_{8^6}$	$\frac{9c_{27a}}{2}+c_{8a}$
$\Sigma\Sigma N\to\Xi NN$	$\frac{3}{2}$	1	1	0	0	$\frac{c_{10}}{4\sqrt{3}}+\frac{33\sqrt{3}c_{27^1}}{64}-\frac{3\sqrt{3}c_{27^2}}{49}-\frac{5\sqrt{3}c_{27^3}}{64}-\frac{\sqrt{3}c_{35}}{16}-\frac{c_{\overline{35}}}{4\sqrt{3}}$	$-\frac{c_{10}}{4}-\frac{99c_{27^1}}{64}+\frac{9c_{27^2}}{49}+\frac{15c_{27^3}}{64}+\frac{3c_{35}}{16}+\frac{c_{\overline{35}}}{4}$	0
$\Sigma\Sigma N\to\Xi NN$	$\frac{3}{2}$	2	1	$\frac{\sqrt{5}c_{10}}{12}-\frac{27\sqrt{5}c_{27^1}}{64}-\frac{57\sqrt{5}c_{27^2}}{196}-\frac{9\sqrt{5}c_{27^3}}{64}+\frac{\sqrt{5}c_{35}}{48}+\frac{\sqrt{5}c_{\overline{35}}}{12}$	$-\frac{1}{4}\sqrt{\frac{5}{3}}c_{10}+\frac{27\sqrt{15}c_{27^1}}{64}+\frac{57\sqrt{15}c_{27^2}}{196}+\frac{9\sqrt{15}c_{27^3}}{64}-\frac{1}{16}\sqrt{\frac{5}{3}}c_{35}-\frac{1}{4}\sqrt{\frac{5}{3}}c_{\overline{35}}$	0	0	0

BIBLIOGRAPHY

[1] S. Aoki, *et al.*, "Lattice quantum chromodynamical approach to nuclear physics," *Prog. Theor. Exp. Phys.* **2012** (2012) 01A105.

[2] S. R. Beane, W. Detmold, K. Orginos, and M. J. Savage, "Nuclear physics from lattice QCD," *Prog. Part. Nucl. Phys.* **66** (2011) 1–40.

[3] S. R. Beane, *et al.*, "Hyperon-Nucleon Interactions from Quantum Chromodynamics and the Composition of Dense Nuclear Matter," *Phys. Rev. Lett.* **109** (2012) 172001.

[4] S. Weinberg, "Nonlinear Realizations of Chiral Symmetry," *Phys. Rev.* **166** (1968) 1568–1577.

[5] S. Weinberg, "Phenomenological Lagrangians," *Physica* **96A** (1979) 327–340.

[6] J. Gasser and H. Leutwyler, "Chiral perturbation theory to one loop," *Ann. Phys.* **158** (1984) 142–210.

[7] J. Gasser, M. E. Sainio, and A. Svarc, "Nucleons with chiral loops," *Nucl. Phys. B* **307** (1988) 779–853.

[8] V. Bernard, N. Kaiser, and U.-G. Meißner, "Chiral Dynamics in Nucleons and Nuclei," *Int. J. Mod. Phys. E* **04** (1995) 193–344.

[9] V. G. J. Stoks, R. A. M. Klomp, C. P. F. Terheggen, and J. J. de Swart, "Construction of high-quality NN potential models," *Phys. Rev. C* **49** (1994) 2950–2962.

[10] R. Wiringa, V. G. J. Stoks, and R. Schiavilla, "Accurate nucleon-nucleon potential with charge-independence breaking," *Phys. Rev. C* **51** (1995) 38–51.

[11] R. Machleidt, "High-precision, charge-dependent Bonn nucleon-nucleon potential," *Phys. Rev. C* **63** (2001) 024001.

[12] E. Epelbaum, H.-W. Hammer, and U.-G. Meißner, "Modern Theory of Nuclear Forces," *Rev. Mod. Phys.* **81** (2009) 1773–1825.

[13] R. Machleidt and D. R. Entem, "Chiral effective field theory and nuclear forces," *Phys. Rep.* **503** (2011) 1–75.

[14] D. B. Kaplan, M. J. Savage, and M. B. Wise, "A new expansion for nucleon-nucleon interactions," *Phys.Lett.* **B424** (1998) 390–396.

[15] A. Nogga, R. Timmermans, and U. van Kolck, "Renormalization of one-pion exchange and power counting," *Phys.Rev.* **C72** (2005) 054006.

[16] B. Holzenkamp, K. Holinde, and J. Speth, "A meson exchange model for the hyperon-nucleon interaction," *Nucl. Phys. A* **500** (1989) 485–528.

[17] A. G. Reuber, K. Holinde, and J. Speth, "Meson-exchange hyperon-nucleon interactions in free scattering and nuclear matter," *Nucl. Phys. A* **570** (1994) 543–579.

[18] T. A. Rijken, V. G. J. Stoks, and Y. Yamamoto, "Soft-core hyperon-nucleon potentials," *Phys. Rev. C* **59** (1999) 21–40.

[19] J. Haidenbauer and U.-G. Meißner, "Jülich hyperon-nucleon model revisited," *Phys. Rev. C* **72** (2005) 044005.

[20] T. A. Rijken, M. M. Nagels, and Y. Yamamoto, "Baryon-Baryon Interactions," *Prog. Theor. Phys. Suppl.* **185** (2010) 14–71.

[21] M. Kohno, Y. Fujiwara, T. Fujita, C. Nakamoto, and Y. Suzuki, "Hyperon single-particle potentials calculated from quark-model baryon-baryon interactions," *Nucl. Phys. A* **674** (2000) 229–245.

[22] Y. Fujiwara, Y. Suzuki, and C. Nakamoto, "Baryon-baryon interactions in the SU(6) quark model and their applications to light nuclear systems," *Prog. Part. Nucl. Phys.* **58** (2007) 439–520.

[23] M. J. Savage and M. B. Wise, "Hyperon masses in nuclear matter," *Phys. Rev. D* **53** (1996) 349–354.

[24] C. Korpa, A. Dieperink, and R. Timmermans, "Hyperon-nucleon scattering and hyperon masses in the nuclear medium," *Phys.Rev.* **C65** (2002) 015208.

[25] H. Polinder, J. Haidenbauer, and U.-G. Meißner, "Hyperon-nucleon interactions - a chiral effective field theory approach," *Nucl. Phys. A* **779** (2006) 244–266.

[26] H. Polinder, J. Haidenbauer, and U.-G. Meißner, "Strangeness S=-2 baryon-baryon interactions using chiral effective field theory," *Phys. Lett. B* **653** (2007) 29–37.

[27] J. Haidenbauer and U.-G. Meißner, "Predictions for the strangeness S=-3 and S=-4 baryon-baryon interactions in chiral effective field theory," *Phys. Lett. B* **684** (2010) 275–280.

[28] A. Nogga, H. Kamada, and W. Glöckle, "The hypernuclei ${}^{4}_{\Lambda}He$ and ${}^{4}_{\Lambda}H$: challenges for modern hyperon-nucleon forces.," *Phys. Rev. Lett.* **88** (2002) 172501.

[29] A. Nogga, "Light Hypernuclei Based on Chiral Interactions at Next-to-Leading Order," *Few-Body Syst.* **55** (2014) 757–760.

[30] S. Gandolfi, F. Pederiva, S. Fantoni, and K. E. Schmidt, "Quantum Monte Carlo Calculations of Symmetric Nuclear Matter," *Phys. Rev. Lett.* **98** (2007) 102503.

[31] S. Gandolfi, A. Y. Illarionov, K. E. Schmidt, F. Pederiva, and S. Fantoni, "Quantum Monte Carlo calculation of the equation of state of neutron matter," *Phys. Rev. C* **79** (2009) 054005.

[32] D. Lonardoni, F. Pederiva, and S. Gandolfi, "Accurate determination of the interaction between Lambda hyperons and nucleons from auxiliary field diffusion Monte Carlo calculations," *Phys. Rev. C* **89** (2014) 014314.

[33] B. Borasoy, E. Epelbaum, H. Krebs, D. Lee, and U.-G. Meißner, "Lattice simulations for light nuclei: Chiral effective field theory at leading order," *Eur. Phys. J. A* **31** (2007) 105–123.

[34] E. Epelbaum, H. Krebs, D. Lee, and U.-G. Meißner, "Ab Initio Calculation of the Hoyle State," *Phys. Rev. Lett.* **106** (2011) 192501.

[35] U.-G. Meißner, "A New Tool in Nuclear Physics: Nuclear Lattice Simulations," *Nucl. Phys. News* **24** (2014) 11–15.

[36] J. W. Holt, N. Kaiser, and W. Weise, "Nuclear chiral dynamics and thermodynamics," *Prog. Part. Nucl. Phys.* **73** (2013) 35–83.

[37] L. Coraggio, J. W. Holt, N. Itaco, R. Machleidt, L. E. Marcucci, and F. Sammarruca, "Nuclear-matter equation of state with consistent two- and three-body perturbative chiral interactions," *Phys. Rev. C* **89** (2014) 044321.

[38] F. Sammarruca, L. Coraggio, J. W. Holt, N. Itaco, R. Machleidt, and L. E. Marcucci, "Toward order-by-order calculations of the nuclear and neutron matter equations of state in chiral effective field theory," *Phys. Rev. C* **91** (2015) 054311.

[39] N. Kaiser and W. Weise, "Chiral SU(3) dynamics and Lambda hyperons in the nuclear medium," *Phys. Rev. C* **71** (2005) 015203.

[40] N. Kaiser, "Chiral dynamics of Sigma hyperons in the nuclear medium," *Phys. Rev. C* **71** (2005) 068201.

[41] K. Brueckner, C. A. Levinson, and H. Mahmoud, "Two-Body Forces and Nuclear Saturation. I. Central Forces," *Phys. Rev.* **95** (1954) 217–228.

[42] K. Brueckner and C. A. Levinson, "Approximate Reduction of the Many-Body Problem for Strongly Interacting Particles to a Problem of Self-Consistent Fields," *Phys. Rev.* **97** (1955) 1344–1352.

[43] B. D. Day, "Elements of the Brueckner-Goldstone Theory of Nuclear Matter," *Rev. Mod. Phys.* **39** (1967) 719–744.

[44] H.-J. Schulze, M. Baldo, U. Lombardo, J. Cugnon, and A. Lejeune, "Hyperonic nuclear matter in Brueckner theory," *Phys. Rev. C* **57** (1998) 704–713.

[45] I. Vidaña, A. Polls, A. Ramos, M. Hjorth-Jensen, and V. G. J. Stoks, "Strange nuclear matter within Brueckner-Hartree-Fock theory," *Phys. Rev. C* **61** (2000) 025802.

[46] M. Baldo, G. F. Burgio, and H.-J. Schulze, "Hyperon stars in the Brueckner-Bethe-Goldstone theory," *Phys. Rev. C* **61** (2000) 055801.

[47] H.-J. Schulze, A. Polls, A. Ramos, and I. Vidaña, "Maximum mass of neutron stars," *Phys. Rev. C* **73** (2006) 058801.

[48] H.-J. Schulze and T. A. Rijken, "Maximum mass of hyperon stars with the Nijmegen ESC08 model," *Phys. Rev. C* **84** (2011) 035801.

[49] J. Haidenbauer and U.-G. Meißner, "A study of hyperons in nuclear matter based on chiral effective field theory," *Nucl. Phys. A* **936** (2015) 29–44.

[50] S. C. Pieper and R. Wiringa, "Quantum Monte Carlo Calculations of Light Nuclei," *Annu. Rev. Nucl. Part. Sci.* **51** (2001) 53–90.

[51] E. Epelbaum, A. Nogga, W. Glöckle, H. Kamada, U.-G. Meißner, and H. Witala, "Three-nucleon forces from chiral effective field theory," *Phys. Rev. C* **66** (2002) 064001.

[52] B. H. J. McKellar and R. Rajaraman, "Three-Body Forces in Nuclear Matter," *Phys. Rev. Lett.* **21** (1968) 450–453.

[53] S. A. Coon, M. D. Scadron, and B. R. Barrett, "The three-body force, off-shell πN scattering and binding energies in nuclear matter," *Nucl. Phys. A* **242** (1975) 467–480.

[54] H. T. Coelho, T. K. Das, and M. R. Robilotta, "Two-pion-exchange three-nucleon force and the 3H and 3He nuclei," *Phys. Rev. C* **28** (1983) 1812–1828.

[55] B. S. Pudliner, V. R. Pandharipande, J. Carlson, S. C. Pieper, and R. Wiringa, "Quantum Monte Carlo calculations of nuclei with $A \leq 7$," *Phys. Rev. C* **56** (1997) 1720–1750.

[56] S. C. Pieper, V. R. Pandharipande, R. Wiringa, and J. Carlson, "Realistic models of pion-exchange three-nucleon interactions," *Phys. Rev. C* **64** (2001) 014001.

[57] S. Weinberg, "Nuclear forces from chiral lagrangians," *Phys. Lett. B* **251** (1990) 288–292.

[58] S. Weinberg, "Effective chiral lagrangians for nucleon-pion interactions and nuclear forces," *Nucl. Phys. B* **363** (1991) 3–18.

[59] S. Weinberg, "Three-body interactions among nucleons and pions," *Phys. Lett. B* **295** (1992) 114–121.

[60] U. van Kolck, "Few-nucleon forces from chiral Lagrangians," *Phys. Rev. C* **49** (1994) 2932–2941.

[61] S. Ishikawa and M. R. Robilotta, "Two-pion exchange three-nucleon potential: O(q**4) chiral expansion," *Phys. Rev. C* **76** (2007) 014006.

[62] V. Bernard, E. Epelbaum, H. Krebs, and U.-G. Meißner, "Subleading contributions to the chiral three-nucleon force: Long-range terms," *Phys. Rev. C* **77** (2008) 064004.

[63] V. Bernard, E. Epelbaum, H. Krebs, and U.-G. Meißner, "Subleading contributions to the chiral three-nucleon force. II. Short-range terms and relativistic corrections," *Phys. Rev. C* **84** (2011) 054001.

[64] H. Krebs, A. Gasparyan, and E. Epelbaum, "Chiral three-nucleon force at N^4LO: Longest-range contributions," *Phys. Rev. C* **85** (2012) 054006.

[65] H. Krebs, A. Gasparyan, and E. Epelbaum, "Chiral three-nucleon force at N^4LO. II. Intermediate-range contributions," *Phys. Rev. C* **87** (2013) 054007.

[66] R. Bhaduri, B. Loiseau, and Y. Nogami, "Effect of three-body ΛNN long-range potential in nuclear matter," *Nucl. Phys. B* **3** (1967) 380–386.

[67] R. Bhaduri, B. Loiseau, and Y. Nogami, "Effects of three-body ΛNN forces in light hypernuclei," *Ann. Phys.* **44** (1967) 57–73.

[68] A. Gal, J. Soper, and R. Dalitz, "A shell-model analysis of Λ binding energies for the p-shell hypernuclei. I. Basic formulas and matrix elements for ΛN and ΛNN forces," *Ann. Phys.* **63** (1971) 53–126.

[69] A. Gal, J. Soper, and R. Dalitz, "A shell-model analysis of Λ binding energies for the p-shell hypernuclei II. Numerical Fitting, Interpretation, and Hypernuclear Predictions," *Ann. Phys.* **72** (1972) 445–488.

[70] A. Gal, J. Soper, and R. Dalitz, "A shell-model analysis of Λ binding energies for the p-shell hypernuclei III. Further analysis and predictions," *Ann. Phys.* **113** (1978) 79–97.

[71] A. Bodmer and Q. Usmani, "Binding energies of the s-shell hypernuclei and the Λ well depth," *Nucl. Phys. A* **477** (1988) 621–651.

[72] A. A. Usmani, "Three-baryon Lambda N N potential," *Phys. Rev. C* **52** (1995) 1773–1777.

[73] D. Lonardoni, S. Gandolfi, and F. Pederiva, "Effects of the two-body and three-body hyperon-nucleon interactions in Λ hypernuclei," *Phys. Rev. C* **87** (2013) 041303.

[74] P. B. Demorest, T. T. Pennucci, S. M. Ransom, M. S. E. Roberts, and J. W. T. Hessels, "A two-solar-mass neutron star measured using Shapiro delay.," *Nature* **467** (2010) 1081–3.

[75] J. Antoniadis et al., "A Massive Pulsar in a Compact Relativistic Binary," *Science* **340** (2013) 1233232.

[76] K. Hebeler, J. M. Lattimer, C. J. Pethick, and A. Schwenk, "Constraints on Neutron Star Radii Based on Chiral Effective Field Theory Interactions," *Phys. Rev. Lett.* **105** (2010) 161102.

[77] T. Hell and W. Weise, "Dense baryonic matter: Constraints from recent neutron star observations," *Phys. Rev. C* **90** (2014) 045801.

[78] A. W. Steiner, J. M. Lattimer, and E. F. Brown, "Neutron Star Radii, Universal Relations, and the Role of Prior Distributions," *Eur. Phys. J. A* **52** (2016) 18.

[79] I. Vidaña, "Hyperons in Neutron Stars," *J. Phys. Conf. Ser.* **668** (2016) 012031.

[80] H. Djapo, B.-J. Schaefer, and J. Wambach, "Appearance of hyperons in neutron stars," *Phys. Rev. C* **81** (2010) 035803.

[81] S. Weissenborn, D. Chatterjee, and J. Schaffner-Bielich, "Hyperons and massive neutron stars: The role of hyperon potentials," *Nucl. Phys. A* **881** (2012) 62–77.

[82] S. Weissenborn, D. Chatterjee, and J. Schaffner-Bielich, "Hyperons and massive neutron stars: Vector repulsion and SU(3) symmetry," *Phys. Rev. C* **85** (2012) 065802.

[83] Y. Yamamoto, T. Furumoto, N. Yasutake, and T. A. Rijken, "Hyperon mixing and universal many-body repulsion in neutron stars," *Phys. Rev. C* **90** (2014) 045805.

[84] T. Takatsuka, S. Nishizaki, and R. Tamagaki, "Three-Body Force as an "Extra Repulsion" Suggested from Hyperon-Mixed Neutron Stars," *Prog. Theor. Phys. Suppl.* **174** (2008) 80–83.

[85] I. Vidaña, D. Logoteta, C. Providência, A. Polls, and I. Bombaci, "Estimation of the effect of hyperonic three-body forces on the maximum mass of neutron stars," *Europhys. Lett.* **94** (2011) 11002.

[86] D. Lonardoni, A. Lovato, S. Gandolfi, and F. Pederiva, "Hyperon Puzzle: Hints from Quantum Monte Carlo Calculations," *Phys. Rev. Lett.* **114** (2015) 092301.

[87] A. W. Thomas and W. Weise, *The Structure of the Nucleon*. Wiley-VCH Verlag, Berlin, 2001.

[88] S. Scherer and M. Schindler, "A Primer for Chiral Perturbation Theory," *Lect. Notes Phys.* **830** (2012) 1–338.

[89] C. A. Baker, *et al.*, "An Improved Experimental Limit on the Electric-Dipole Moment of the Neutron," *Phys. Rev. Lett.* **97** (2006) 131801.

[90] S. L. Adler, "Axial-Vector Vertex in Spinor Electrodynamics," *Phys. Rev.* **177** (1969) 2426–2438.

[91] J. S. Bell and R. Jackiw, "A PCAC Puzzle: $\pi^0 \to \gamma\gamma$ in the σ-Model," *Nuovo Cim. A* **60** (1969) 47–61.

[92] J. Gasser and H. Leutwyler, "Chiral perturbation theory: Expansions in the mass of the strange quark," *Nucl. Phys. B* **250** (1985) 465–516.

[93] H. Leutwyler, "On the Foundations of Chiral Perturbation Theory," *Ann. Phys.* **235** (1994) 165–203.

[94] S. L. Adler and R. F. Dashen, *Current algebras and applications to particle physics*. Benjamin, New York, 1968.

[95] S. Coleman, J. Wess, and B. Zumino, "Structure of Phenomenological Lagrangians. I," *Phys. Rev.* **177** (1969) 2239–2247.

[96] C. G. Callan, S. Coleman, J. Wess, and B. Zumino, "Structure of Phenomenological Lagrangians. II," *Phys. Rev.* **177** (1969) 2247–2250.

[97] E. Jenkins and A. V. Manohar, "Baryon chiral perturbation theory using a heavy fermion lagrangian," *Phys. Lett. B* **255** (1991) 558–562.

[98] H. Georgi, *Weak Interactions and Modern Particle Theory.* Benjamin / Cummings, Reading, MA, 1984.

[99] H. W. Fearing and S. Scherer, "Extension of the chiral perturbation theory meson Lagrangian to order p**6," *Phys. Rev. D* **53** (1996) 315–348.

[100] J. Bijnens, G. Colangelo, and G. Ecker, "The Mesonic Chiral Lagrangian of Order p**6," *J. High Energy Phys.* **1999** (1999) 020.

[101] J. A. Oller, M. Verbeni, and J. Prades, "Meson-baryon effective chiral Lagrangians to O(q**3)," *J. High Energy Phys.* **2006** (2006) 079.

[102] M. Frink and U.-G. Meißner, "On the chiral effective meson-baryon Lagrangian at third order," *Eur. Phys. J. A* **29** (2006) 255–260.

[103] S. Petschauer and N. Kaiser, "Relativistic SU(3) chiral baryon-baryon Lagrangian up to order q**2," *Nucl. Phys. A* **916** (2013) 1–29.

[104] A. Krause, "Baryon Matrix Elements of the Vector Current in Chiral Perturbation Theory," *Helv. Phys. Acta* **63** (1990) 3–70.

[105] M. Gell-Mann, R. J. Oakes, and B. Renner, "Behavior of Current Divergences under SU(3)xSU(3)," *Phys. Rev.* **175** (1968) 2195–2199.

[106] N. Kaiser and S. Petschauer, "Radiative corrections to the charged pion-pair production process $\pi^-\gamma \to \pi^+\pi^-\pi^-$ at low energies," *Eur. Phys. J. A* **49** (2013) 159.

[107] C. Adolph et al. (COMPASS Collaboration), "First Measurement of Chiral Dynamics in $\pi^-\gamma \to \pi^-\pi^-\pi^+$," *Phys. Rev. Lett.* **108** (2012) 192001.

[108] N. Kaiser, "Chiral corrections to $\pi^-\gamma \to 3\pi$ processes at low energies," *Nucl. Phys. A* **848** (2010) 198–217.

[109] N. Kaiser, "Radiative corrections to neutral pion-pair production," *Eur. Phys. J. A* **46** (2010) 373–378.

[110] R. Mertig, M. Böhm, and A. Denner, "Feyn Calc – Computer-algebraic calculation of Feynman amplitudes," *Comput. Phys. Commun.* **64** (1991) 345–359.

[111] T. Hahn and M. Pérez-Victoria, "Automated one-loop calculations in four and D dimensions," *Comput. Phys. Commun.* **118** (1999) 153–165.

[112] N. Fettes, U.-G. Meißner, M. Mojzis, and S. Steininger, "The Chiral Effective Pion-Nucleon Lagrangian of Order p**4," *Ann. Phys.* **283** (2000) 273–307.

[113] L. Girlanda, S. Pastore, R. Schiavilla, and M. Viviani, "Relativity constraints on the two-nucleon contact interaction," *Phys. Rev. C* **81** (2010) 034005.

[114] Z. Hong-Hao, Y. Wen-Bin, and L. Xue-Song, "Trace Formulae of Characteristic Polynomial and Cayley-Hamilton's Theorem, and Applications to Chiral Perturbation Theory and General Relativity," *Commun. Theor. Phys.* **49** (2008) 801–808.

[115] S. Iwao, "Baryon-baryon interactions and unitary symmetry," *Nuovo Cim.* **34** (1964) 1167–1183.

[116] C. B. Dover and H. Feshbach, "Unitary symmetry in baryon-baryon scattering," *Ann. Phys.* **198** (1990) 321–357.

[117] C. B. Dover and H. Feshbach, "Unitary symmetry in baryon-baryon scattering, II," *Ann. Phys.* **217** (1992) 51–65.

[118] E. Epelbaum, W. Glöckle, and U.-G. Meißner, "The two-nucleon system at next-to-next-to-next-to-leading order," *Nucl. Phys. A* **747** (2005) 362–424.

[119] J. Haidenbauer, U.-G. Meißner, and S. Petschauer, "Do Xi-Xi bound states exist?," *Eur. Phys. J. A* **51** (2015) 17.

[120] S. Petschauer, *Chiral SU(3)-Dynamics and Baryon-Baryon Interactions.* Diploma thesis, TU München, 2011.

[121] N. Kaiser, R. Brockmann, and W. Weise, "Peripheral nucleon-nucleon phase shifts and chiral symmetry," *Nucl. Phys. A* **625** (1997) 758–788.

[122] E. Epelbaum, W. Glöckle, and U.-G. Meißner, "Nuclear forces from chiral Lagrangians using the method of unitary transformation (I): Formalism," *Nucl. Phys. A* **637** (1998) 107–134.

[123] E. Epelbaum, W. Glöckle, and U.-G. Meißner, "Nuclear forces from chiral Lagrangians using the method of unitary transformation II: The two-nucleon system," *Nucl. Phys. A* **671** (2000) 295–331.

[124] D. R. Entem and R. Machleidt, "Accurate charge-dependent nucleon-nucleon potential at fourth order of chiral perturbation theory," *Phys. Rev. C* **68** (2003) 041001.

[125] J. Haidenbauer, S. Petschauer, N. Kaiser, U.-G. Meißner, A. Nogga, and W. Weise, "Hyperon-nucleon interaction at next-to-leading order in chiral effective field theory," *Nucl. Phys. A* **915** (2013) 24–58.

[126] C. M. Vincent and S. Phatak, "Accurate momentum-space method for scattering by nuclear and Coulomb potentials," *Phys. Rev. C* **10** (1974) 391–394.

[127] R. J. Furnstahl, D. R. Phillips, and S. Wesolowski, "A recipe for EFT uncertainty quantification in nuclear physics," *J. Phys. G* **42** (2015) 034028.

[128] E. Epelbaum, H. Krebs, and U.-G. Meißner, "Improved chiral nucleon-nucleon potential up to next-to-next-to-next-to-leading order," *Eur. Phys. J. A* **51** (2015) 53.

[129] R. J. Furnstahl, N. Klco, D. R. Phillips, and S. Wesolowski, "Quantifying truncation errors in effective field theory," *Phys. Rev. C* **92** (2015) 024005.

[130] B. Sechi-Zorn, B. Kehoe, J. Twitty, and R. A. Burnstein, "Low-Energy Lambda-Proton Elastic Scattering," *Phys. Rev.* **175** (1968) 1735–1740.

[131] G. Alexander, *et al.*, "Study of the Lambda-N System in Low-Energy Lambda-p Elastic Scattering," *Phys. Rev.* **173** (1968) 1452–1460.

[132] R. Engelmann, H. Filthuth, V. Hepp, and E. Kluge, "Inelastic $\Sigma^- p$-interactions at low momenta," *Phys. Lett.* **21** (1966) 587–589.

[133] F. Eisele, H. Filthuth, W. Föhlisch, V. Hepp, and G. Zech, "Elastic $\Sigma^{\pm} p$ scattering at low energies," *Phys. Lett. B* **37** (1971) 204–206.

[134] V. Hepp and H. Schleich, "A New Determination of the Capture Ratio $r_c = (\Sigma^- p \to \Sigma^0 n)/((\Sigma^- p \to \Sigma^0 n) + (\Sigma^- p \to \Lambda^0 n))$, the Λ^0-Lifetime and $\Sigma^- \Lambda^0$ Mass Difference," *Z. Phys.* **214** (1968) 71–77.

[135] D. Stephen, PhD thesis, University of Massachusetts, 1970.

[136] J. Kadyk, G. Alexander, J. Chan, P. Gaposchkin, and G. Trilling, "Lambda-p interactions in momentum range 300 to 1500 MeV/c," *Nucl. Phys. B* **27** (1971) 13–22.

[137] J. Hauptman, J. Kadyk, and G. Trilling, "Experimental study of Λp and $\Xi^0 p$ interactions in the range 1 - 10 GeV/c," *Nucl. Phys. B* **125** (1977) 29–51.

[138] Y. Kondo, *et al.*, "$\Sigma^- p$ elastic-scattering in the region of $400 < p_{\Sigma^-} < 700$ MeV/c with a scintillating-fiber active target," *Nucl. Phys. A* **676** (2000) 371–387.

[139] J. Ahn, *et al.*, "$\Sigma^+ p$ elastic scattering in the region of $300 \leq p_\Sigma \leq 600$ MeV/c with a scintillating fiber target," *Nucl. Phys. A* **648** (1999) 263–279.

[140] J. Ahn, *et al.*, "$\Sigma^+ p$ elastic scattering cross sections in the region of $350 \leq P_{\Sigma^+} \leq 750$ MeV/c with a scintillating fiber active target," *Nucl. Phys. A* **761** (2005) 41–66.

[141] A. Nogga, "Light hypernuclei based on chiral and phenomenological interactions," *Nucl. Phys. A* **914** (2013) 140–150.

[142] S. Ajimura, *et al.*, "Observation of Spin-Orbit Splitting in Lambda Single-Particle States," *Phys. Rev. Lett.* **86** (2001) 4255–4258.

[143] H. Akikawa, *et al.*, "Hypernuclear Fine Structure in ${}^{9}_{\Lambda}Be$," *Phys. Rev. Lett.* **88** (2002) 082501.

[144] M. Baldo, *Nuclear methods and the nuclear equation of state*, vol. 8 of *International Review of Nuclear Physics*. World Scientific Publishing Co. Pte. Ltd., 1999.

[145] A. L. Fetter and J. D. Walecka, *Quantum Theory of Many-Particle Systems*. Dover Books on Physics. Dover Publications, 2003.

[146] S. Petschauer, J. Haidenbauer, N. Kaiser, U.-G. Meißner, and W. Weise, "Hyperons in nuclear matter from SU(3) chiral effective field theory," *Eur. Phys. J. A* **52** (2016) 15.

[147] J. Goldstone, "Derivation of the Brueckner Many-Body Theory," *Proc. Roy. Soc. A* **239** (1957) 267–279.

[148] H. A. Bethe, B. H. Brandow, and A. G. Petschek, "Reference Spectrum Method for Nuclear Matter," *Phys. Rev.* **129** (1963) 225–264.

[149] H. Q. Song, M. Baldo, G. Giansiracusa, and U. Lombardo, "Bethe-Brueckner-Goldstone Expansion in Nuclear Matter," *Phys. Rev. Lett.* **81** (1998) 1584–1587.

[150] V. G. J. Stoks, R. A. M. Klomp, M. C. M. Rentmeester, and J. J. de Swart, "Partial-wave analysis of all nucleon-nucleon scattering data below 350 MeV," *Phys. Rev. C* **48** (1993) 792–815.

[151] R. A. Arndt, I. I. Strakovsky, and R. L. Workman, "Updated analysis of NN elastic scattering data to 1.6 GeV," *Phys. Rev. C* **50** (1994) 2731–2741. SAID partial wave analysis online service, http://gwdac.phys.gwu.edu.

[152] A. Gal, "Strangeness Nuclear Physics - 2010," *Prog. Theor. Phys. Suppl.* **186** (2010) 270–281.

[153] E. Botta, T. Bressani, and G. Garbarino, "Strangeness nuclear physics: a critical review on selected topics," *Eur. Phys. J. A* **48** (2012) 41.

[154] N. Hugenholtz and L. van Hove, "A theorem on the single particle energy in a Fermi gas with interaction," *Physica* **24** (1958) 363–376.

[155] J. Jeukenne, A. Lejeune, and C. Mahaux, "Many-body theory of nuclear matter," *Phys. Rep.* **25** (1976) 83–174.

[156] Z. H. Li, U. Lombardo, H.-J. Schulze, W. Zuo, L. W. Chen, and H. R. Ma, "Nuclear matter saturation point and symmetry energy with modern nucleon-nucleon potentials," *Phys. Rev. C* **74** (2006) 047304.

[157] S. Bogner, A. Schwenk, R. J. Furnstahl, and A. Nogga, "Is nuclear matter perturbative with low-momentum interactions?," *Nucl. Phys. A* **763** (2005) 59–79.

[158] S. Krewald, E. Epelbaum, U.-G. Meißner, and P. Saviankou, "Effective field theory approach to nuclear matter," *Prog. Part. Nucl. Phys.* **67** (2012) 322–326.

[159] R. Machleidt, P. Liu, D. R. Entem, and E. Ruiz Arriola, "Renormalization of the leading-order chiral nucleon-nucleon interaction and bulk properties of nuclear matter," *Phys. Rev. C* **81** (2010) 024001.

[160] A. Carbone, A. Polls, and A. Rios, "Symmetric nuclear matter with chiral three-nucleon forces in the self-consistent Green's functions approach," *Phys. Rev. C* **88** (2013) 044302.

[161] F. Coester, S. D. Cohen, B. D. Day, and C. M. Vincent, "Variation in Nuclear-Matter Binding Energies with Phase-Shift-Equivalent Two-Body Potentials," *Phys. Rev. C* **1** (1970) 769–776.

[162] E. Epelbaum, H. Krebs, and U.-G. Meißner, "Precision Nucleon-Nucleon Potential at Fifth Order in the Chiral Expansion," *Phys. Rev. Lett.* **115** (2015) 122301.

[163] D. R. Entem, N. Kaiser, R. Machleidt, and Y. Nosyk, "Peripheral nucleon-nucleon scattering at fifth order of chiral perturbation theory," *Phys. Rev. C* **91** (2015) 014002.

[164] D. J. Millener, C. B. Dover, and A. Gal, "Lambda-nucleus single-particle potentials," *Phys. Rev. C* **38** (1988) 2700–2708.

[165] Y. Yamamoto, H. Bandō, and J. Zofka, "On the Lambda-Hypernuclear Single Particle Energies," *Prog. Theor. Phys.* **80** (1988) 757–761.

[166] E. Friedman and A. Gal, "In-medium nuclear interactions of low-energy hadrons," *Phys. Rep.* **452** (2007) 89–153.

[167] C. B. Dover, D. J. Millener, and A. Gal, "On the production and spectroscopy of Sigma hypernuclei," *Phys. Rep.* **184** (1989) 1–97.

[168] R. R. Scheerbaum, "Spin-orbit splitting in nuclei near closed shells," *Nucl. Phys. A* **257** (1976) 77–108.

[169] Y. Fujiwara, M. Kohno, T. Fujita, C. Nakamoto, and Y. Suzuki, "Single-particle spin-orbit strengths of the nucleon and hyperons by quark-model," *Nucl. Phys. A* **674** (2000) 493–514.

[170] M. Kohno, "Comparative study of hyperon-nucleon interactions in a quark model and in chiral effective field theory by low-momentum equivalent interactions and G matrices," *Phys. Rev. C* **81** (2010) 014003.

[171] M. Kohno, *private communication.*

[172] J. Dabrowski, "Isospin dependence of the single-particle potential of the Sigma hyperon in nuclear matter," *Phys. Rev. C* **60** (1999) 025205.

[173] S. Petschauer, N. Kaiser, J. Haidenbauer, U.-G. Meißner, and W. Weise, "Leading three-baryon forces from SU(3) chiral effective field theory," *Phys. Rev. C* **93** (2016) 014001.

[174] R. Wirth, D. Gazda, P. Navrátil, A. Calci, J. Langhammer, and R. Roth, "Ab Initio Description of p -Shell Hypernuclei," *Phys. Rev. Lett.* **113** (2014) 192502.

[175] M. Frink and U.-G. Meißner, "Chiral extrapolations of baryon masses for unquenched three-flavor lattice simulations," *J. High Energy Phys.* **0407** (2004) 028–028.

[176] M. Mai, P. Bruns, B. Kubis, and U.-G. Meißner, "Aspects of meson-baryon scattering in three- and two-flavor chiral perturbation theory," *Phys. Rev. D* **80** (2009) 094006.

[177] V. Bernard, N. Kaiser, and U.-G. Meißner, "Aspects of chiral pion-nucleon physics," *Nucl. Phys. A* **615** (1997) 483–500.

[178] N. Kaiser, S. Gerstendörfer, and W. Weise, "Peripheral NN-scattering: role of delta-excitation, correlated two-pion and vector meson exchange," *Nucl.Phys.* **A637** (1998) 395–420.

[179] H. Krebs, E. Epelbaum, and U.-G. Meißner, "Nuclear forces with Δ excitations up to next-to-next-to-leading order, part I: Peripheral nucleon-nucleon waves," *Eur. Phys. J. A* **32** (2007) 127–137.

[180] E. Epelbaum, H. Krebs, and U.-G. Meißner, "Δ-excitations and the three-nucleon force," *Nucl. Phys. A* **806** (2008) 65–78.

[181] K. Sasaki, E. Oset, and M. J. V. Vacas, "Scalar ΛN and $\Lambda\Lambda$ interaction in a chiral unitary approach," *Phys. Rev. C* **74** (2006) 064002.

[182] T. E. O. Ericson and W. Weise, *Pions and Nuclei*. Clarendon Press, Oxford, 1988.

ACKNOWLEDGMENTS

In the first place, I would like to express my gratitude to my supervisor Prof. Dr. Norbert Kaiser for his guidance, his support and for many enlightening discussions on technical problems. I am thankful to Prof. Dr. Wolfram Weise for giving me the opportunity to write my thesis in his group T39 and for many stimulating and motivating conversations concerning strangeness nuclear physics. I also thank them for giving me the chance to participate in various workshops and conferences all over the world.

Special thanks go to Dr. Johann Haidenbauer for the very pleasant and successful working together on various topics and for many helpful discussions. Moreover, I am glad to thank Dr. Andreas Nogga and Prof. Dr. Ulf-G. Meißner for their fruitful cooperation.

For financial support, I would like to thank the Sino-German CRC 110 "Symmetries and the Emergence of Structure in QCD" by DFG and NSFC, the BMBF, the Excellence cluster "Origin and Structure of the Universe", the TUM Graduate School and the Wilhelm und Else Heraeus-Stiftung.

It is a pleasure to thank all my current and former colleagues at T39, in particular Michael Altenbuchinger, Nino Bratovic, Matthias Drews, Maximilian Duell, Salvatore Fiorilla, Lisheng Geng, Thomas Hell, Jeremy Holt, Bertram Klein, Robert Lang, Alexander Laschka, Paul Springer and Corbinian Wellenhofer for the enjoyable working atmosphere and for the shared hours outside the office.

Last but not least, I am deeply grateful to my family for their permanent support during all these years.